Simplifying Cast-In-Place Joint Design Using ABC Pocket Connection Details in High Seismic Regions

June 2021

Disclaimer

TECHNICAL REPORT DOCUMENTATION PAGE

1. Report No. 494-18-803	2. Government Accession No.	3. Recipient's Catalog No.
4. Title and Subtitle SIMPLIFYING CAST-IN-PLACE JOINT DESIGN USING ABC POCKET CONNECTION DETAILS IN HIGH SEISMIC REGIONS		5. Report Date Month 01, 2020
		6. Performing Organization Code
7. Author(s) Taylor Schwartz, M. Saiid Saiidi, and Mohamed Moustafa		8. Performing Organization Report No. CCEER 20-01
9. Performing Organization Name and Address University of Nevada, Reno Reno, NV 89557		10. Work Unit No.
		11. Contract or Grant No. P494-18-803
12. Sponsoring Agency Name and Address Nevada Department of Transportation 1263 South Stewart Street Carson City, NV 89712		13. Type of Report and Period Covered Final Report
		14. Sponsoring Agency Code
15. Supplementary Notes		

16. Abstract

Accelerated bridge construction (ABC) utilizes precast members to minimize on-site construction time, making it an appealing alternative to conventional cast-in-place (CIP) construction. The connections between these precast members are crucial as they must maintain structural integrity, and in regions of moderate and high seismic activity, ensure the ductile behavior of bridge columns. Recent research has demonstrated that pocket/socket connections meet these requirements while simplifying the construction of joints. Pocket connections allow precast members to be inserted into adjacent members.   To form a pocket connection between a column and cap beam, the longitudinal reinforcement in the cap beam must be bundled outside the pocket to allow the precast column to extend into the pocket uninhibited. Earthquake-resistant CIP column-cap beam joints are difficult to construct because the column reinforcement must be threaded through the reinforcement of the cap beam. Additional reinforcement is also necessary within the joint, which can lead to rebar congestion. The primary goal of this study was to adapt ABC pocket connection details for use in CIP column-cap beam joint construction to avoid steel congestion and simplify construction.

   To achieve this goal, a CIP emulating ABC pocket connection detail was developed, implemented in a large-scale test model, and evaluated under seismic loading on a shake table. Summary design recommendations for the connection based on the results of the shake table testing were then developed. This project consisted of an experimental study, analytical studies, and development of detailing recommendations. The experimental study involved shake table testing of a 1/3 scale CIP model of a column and cap beam which incorporated a novel CIP pocket connection. The specimen was subjected to multiple runs of simulated, scaled versions of the 1994 Northridge earthquake event recorded at the Sylmar Converter Station. Results from the experimental study showed the column reached a drift ratio of 7.8 percent, and the connection was effective in forming the plastic hinge in the column while keeping the joint and cap beam free of damage. The cap beam behaved as a capacity-protected member and met the seismic performance objective of both CIP and ABC bridges. Analytical models were developed before testing to estimate the response of the specimen. After testing, the models were refined, and the calculated results were compared with the measured results. These studies revealed that relatively simple analytical models could estimate the global response of the specimen under dynamic loading with reasonable accuracy. Finally, design recommendations for CIP pocket column-cap beam connections emulating ABC were developed based on the performance of joint reinforcement during the testing.

17. Key Words Accelerated bridge construction, analytical models, pocket connections, socket connections, reinforcement congestion, shake table testing	18. Distribution Statement No restrictions. This document is available through the: National Technical Information Service Springfield, VA 22161		
19. Security Classif. (of this report) Unclassified	20. Security Classif. (of this page) Unclassified	21. No. of Pages 215	22. Price

Form DOT F 1700.7 (8-72)   Reproduction of completed page authorized

Report No. CCEER 20-01

Simplifying Cast-in-Place Joint Design Using ABC Pocket Connection Details in High Seismic Regions

Taylor Schwartz
M. Saiid Saiidi
and
Mohamed Moustafa

Center for Civil Engineering Earthquake Research

University of Nevada, Reno
Department of Civil and Environmental Engineering, MS 258
1664 N. Virginia St.
Reno, NV 89557

January 2020

Abstract

Accelerated bridge construction (ABC) utilizes precast members to minimize on-site construction time, making it an appealing alternative to conventional cast-in-place (CIP) construction. The connections between these precast members are crucial as they must maintain structural integrity, and in regions of moderate and high seismic activity, ensure the ductile behavior of bridge columns. Recent research has demonstrated that pocket (socket) connections meet these requirements while simplifying the construction of joints. Pocket connections allow precast members to be inserted into adjacent members. To form a pocket connection between a column and cap beam, the longitudinal reinforcement in the cap beam must be bundled outside the pocket to allow the precast column to extend into the pocket uninhibited. Earthquake-resistant CIP column-cap beam joints are difficult to construct because the column reinforcement must be threaded through the reinforcement of the cap beam. Additional reinforcement is also necessary within the joint, which can lead to rebar congestion. The primary goal of this study was to adapt ABC pocket connection details for use in CIP column-cap beam joint construction to avoid steel congestion and simplify construction.

To achieve this goal, a CIP emulating ABC pocket connection detail was developed, implemented in a large-scale test model, and evaluated under seismic loading on a shake table. Summary design recommendations for the connection based on the results of the shake table testing were then developed. This project consisted of an experimental study, analytical studies, and development of detailing recommendations. The experimental study involved shake table testing of a 1/3 scale CIP model of a column and cap beam which incorporated a novel CIP pocket connection. The specimen was subjected to multiple runs of simulated, scaled versions of the 1994 Northridge earthquake event recorded at the Sylmar Converter Station. Results from the experimental study showed the column reached a drift ratio of 7.8 percent, and the connection was effective in forming the plastic hinge in the column while keeping the joint and cap beam free of damage. The cap beam behaved as a capacity-protected member, and met the seismic performance objective of both CIP and ABC bridges. Analytical models were developed before testing to estimate the response of the specimen. After testing, the models were refined, and calculated results were compared with the measured results. These studies revealed that relatively simple analytical models could estimate the global response of the specimen under dynamic loading with reasonable accuracy. Finally, design recommendations for CIP pocket column-cap beam connections emulating ABC were developed based on the performance of joint reinforcement during the testing.

i

Acknowledgments

Table of Contents

List of Tables

List of Figures

Chapter 1.   Introduction

1.1. Background

Accelerated bridge construction (ABC) is preferable in many instances to conventional cast-in-place (CIP) concrete construction because of the reduction in on-site construction time. ABC utilizes precast members that reduce the need for on-site formwork, shoring, casting, and curing of concrete. The elimination of these time-consuming processes leads to a reduction in traffic delays and road closures. Low seismic regions have embraced the use of ABC because of its ability to expedite the construction process. The joints between precast members are a concern for bridge designers. These joints are critical because they must maintain structural integrity, and in regions of moderate and high seismic activity, ensure the ductile performance of columns. Recent research has examined the applicability of ABC for use in areas of moderate and high seismic activity [[1]-[4]]. Several types of ABC connections have been developed to satisfy these performance criteria. Studies conducted by Tazarv and Saiidi [1], Mohebbi et al. [2], and Mehrsoroush et al. [3] have shown that one of these connections, pocket (socket) connection types, significantly improve the construction of joints while ensuring ductile behavior in bridge columns. Pocket connections allow precast members to be inserted into adjacent members and are then secured with high strength grout.

In contrast with ABC pocket connections, the construction and design of CIP cap beam-column joints can be significantly more difficult and time-consuming. In CIP joint construction, the column reinforcement must extend into the joint and is required to thread through the cap beam reinforcement. Additional joint reinforcement is also required to resist principle stresses that develop in the joint. This additional reinforcement can lead to rebar congestion within the joint. Adapting the design guidelines for ABC pocket connections for use in CIP has the potential to simplify the design and construction of CIP joints.

1.2. Literature Review

A literature review of previous research that investigated the seismic performance of pocket connections was conducted. A summary of the design methods and recommendations utilized in the designing of these connections is presented.

ABC pocket connections allow reinforced concrete columns to be inserted into adjacent members, such as footings or cap beams. Pocket connections can be utilized with precast columns, partially-cast columns, or columns made of fiber-reinforced polymer composite tube materials. The column and adjoining member are then joined with concrete or high-strength non-shrink grout. Pocket connections may form full moment connections or hinge connections. Recent research has shown that pocket connections allow for ductile behavior in the column while limiting damage in the joint and adjacent members during strong earthquakes.

1

1.2.1. Pocket Connections with Partially-Cast Columns

Pocket connections with partially-cast columns have been the subject of several research projects. A column that is partially-cast will typically be precast until the section that extends into the joint. The partially cast column will have reinforcement extending into the joint area that will then be cast with the joint. Matsumoto et al. [5] investigated pocket connections between precast pier caps and partially-cast columns. Two 0.42-scale column-pier cap pocket connections were tested and the performance was compared to a reference CIP pier model under quasi-static cyclic loading. One connection in the model was designed to have low ductility and the other high ductility. In the high ductility model, stirrups and hoops were included around the joint region. Both pockets were formed with corrugated steel pipes and cast with conventional concrete. The column longitudinal bars extended the same length into the pocket in both connections. The column longitudinal bars had to be threaded through the cap beam longitudinal reinforcement because this reinforcement was not bundled. The high ductility pocket formed a plastic hinge in the column, while the low ductility connection experienced joint shear cracking and deformation in addition to forming a plastic hinge in the column.

Mehraein and Saiidi [6] also investigated pocket connections with partially-cast columns and precast cap beams. This research involved shake table testing of two 0.27-scale two-column bents. One column was precast in each test model while the other was CIP. The precast column was only partially cast with column longitudinal reinforcement extending into the pocket. The pocket area was filled with self-consolidating concrete (SCC). The longitudinal reinforcement in the cap beam was bundled and placed outside of the pocket to avoid interference with the column reinforcement. A spiral was included around the lower one-third of the pocket depth to provide confinement. The specimens were subjected to several runs of the 1994 Northridge earthquake at increasing amplitudes. The columns formed plastic hinges while the precast cap beam remained elastic and incurred no damage. Similar performance was observed in the CIP and precast columns.

1.2.2. Pocket Connections with Composite Columns

Pocket connections have also been investigated for use with columns made of fiber-reinforced polymer composite tube materials. Zhu et al. [7] tested three 1/6-scale columns made of concrete-filled fiber reinforced polymer tubes (CFFT) connected to precast footings. The specimens consisted of a CIP CFFT column with steel starter bars (CIP-CFFT), a precast CFFT column with steel starter bars extending out of the footing and into column grouted ducts (GD-CFFT), and a precast CFFT column with a post-tensioned connection (PT-CFFT). All columns were connected to the footings through a pocket connection, which was formed with a Sonotube. All models were subjected to quasi-static cyclic loading. It was found that all precast columns performed better than the reference CIP column model.

Motaref et al. [8] utilized one composite column in the testing of a 0.3-scale two column bent which incorporated two precast columns, a precast footing, and a precast cap beam. Pocket connections were used between the columns and footing. One column was made of conventional concrete with engineered cementitious material in the plastic hinge (RC-ECC). The other

was made of a glass fiber reinforced polymer (GFRP) tube filled with concrete. The pocket connection openings in the footing were octagonal shaped and filled with grout. The bent was tested on a shake table simulating successive runs of the 1994 Northridge earthquake at Sylmar. The tests showed that the RC-ECC column formed a plastic hinge above the footing while the GFRP failed due to tube rupture above the footing. No damage was visible in the footing or in either connection.

1.2.3. Pocket Connections with Fully Precast Columns

Fully precast columns are precast for the entire length of the column including the length that extends into the joint. Research involving the use of pocket connections with fully precast columns has also been conducted. Three 0.42-scale column to footing pocket connections were tested under quasi-static loading by Haraldsson et al. [9]. A precast column to CIP footing connection was utilized in two of the models. These models had the same overall geometry, but one had a lower longitudinal steel ratio to improve constructability. The third model was designed with a thinner footing to force the connection to fail within the footing. The column sections extending into the footing were octagonal. The surface of the parts of the column to be embedded in the pockets were roughened. The models with the same geometry performed in a manner comparable to a CIP connection with the failure mode being the crushing of concrete in the plastic hinge region. The model with the thin footing failed in the connection due to buckling of column longitudinal reinforcement and punching shear.

Larosche et al. [10] tested four full-scale exterior pile to bent cap pocket connections under quasi-static cyclic loading. The models included one reference model to represent current design practices, two connections intended to act as moment connections, and one connection intended to act as a hinge. One of the moment connections used an embedment depth of 1.44 times the pile width and relatively high reinforcement ratio in the cap beam. The other moment connection used an embedment depth of 1.22 times the pile width and longer bent cap overhang. Test results showed that both moment connections failed due to the formation of a plastic hinge within the piles and had superior performance compared to the reference model which failed under prying action.

After conducting an extensive literature search examining the seismic performance of cap beams with pocket connections, Tazarv and Saiidi [1] developed a preliminary design guideline for pocket connections between columns and cap beams. The guideline specified that the pocket should be formed with a helical lock-seam corrugated steel pipe and included an equation for determining the minimum thickness of the pipe. To allow a precast column to extend into the pocket uninhibited, the guideline recommended that the bottom layer of cap beam longitudinal reinforcement be bundled and placed outside the pocket area per Section 5.10 of AASHTO [11]. The guideline also dictated that transverse hoops or spirals of the same volumetric ratio as the column spiral be included in the lower half of the cap beam.

Two 0.28-scale models were tested under static loading by Tran and Stanton [12] to study the performance of pocket connections between precast columns and drilled shafts. The design of the two shafts was identical except that the transverse reinforcement ratio was decreased in one shaft. The portion of the column that extended into the pocket had an octagonal shape with roughened surface. A plastic hinge was formed in the column that was connected to the shaft with the higher transverse

reinforcement ratio. The shaft was essentially undamaged under static loading. The other column failed due to prying action in the shaft, indicating that lower shaft transverse reinforcement can cause the failure mechanism to shift from the column to the connection.

Mohebbi et al. [2] evaluated the performance of precast bridge columns with pocket connections. A 0.33-scale square column model and a pier model were evaluated through shake table testing. The square column model utilized a pocket connection between the column and the footing. The pier model utilized pocket connections between square columns and a cap beam. The connections performed well in the shake table tests and structural integrity of the joint was maintained throughout both tests. Design methods for pocket connections with square columns were then developed based on the experimental results. The method recommended bundling cap beam longitudinal reinforcement and including additional longitudinal reinforcement outside of the pocket area to address temperature and shrinkage cracks. This reinforcement would be designed per Section 5.10.6 of AASHTO [11]. Diagonal reinforcement around the square pocket was recommended to address tensile stresses at the corners of the pocket.

Mehrsoroush et al. [3] tested a 1/3 scale pier model on a shake table that utilized full moment pocket connections between the column and the footing. The pockets were formed with corrugated steel pipes and filled with high-strength non-shrink grout. The pockets in the footing were successful in maintaining structural integrity under high drift ratios during shake table testing.

1.3. Objectives and Scope

The main objectives of this study were to: (1) develop and evaluate a CIP emulating ABC pocket connection subjected to simulated seismic loading on a shake table, and (2) develop design recommendations for the connection based on the results of shake table testing. This CIP pocket connection would take advantage of the simplification in the design and construction of joints that is offered through the use of ABC pocket connections but without the requirement that the column or cap beam be precast elements.

To achieve the first objective, design recommendations for ABC pocket connections were adapted to develop a CIP pocket connection. Details such as the bundling of cap beam longitudinal reinforcement and the addition of transverse hoops to provide confinement were utilized. Additional reinforcement not typical to the design of CIP joints or ABC pocket connections was also included to address prying forces. One test model which included a column and cap beam was designed and constructed. The dimensions and reinforcement in the test model were based on a prototype bridge to ensure the model had a realistic design. The column longitudinal reinforcement ratio in the test model was increased from that of the prototype to place more demand on the connection. The focus of the study was on the out-of-plane performance of the specimen because no information on the seismic performance pocket connections under out-of-plane loading was available. The out-of-plane response could be more critical because there is less material surrounding the joint to contribute to the strength of the joint. A parallel study focused on the in-plane response of ABC-emulating CIP cap beam-column joints.

To evaluate performance of the connection, the specimen was instrumented with strain gauges, displacement transducers, and accelerometers. The strain in the column, cap beam, and joint reinforcement was measured to determine if a plastic hinge was formed in the column and that the cap beam and joint remained capacity-protected. Measuring displacement of the column was also crucial to ensure the specimen was tested to high drift levels and adequate demand was placed on the connection. The scope of the project also involved developing analytical models before and after shake table testing to estimate the response of the specimen and compare with the measured results.

To achieve the second objective, i.e. develop design recommendations for the connection, the performance of joint reinforcement was evaluated to determine if the design of the CIP pocket connection was adequate. The strains in the transverse hoops and additional joint reinforcement were monitored to ensure they were engaged in providing confinement and addressing prying action, respectively. Damage in the column and cap beam was tracked to evaluate the ability of the connection to concentrate ductility in the column plastic hinge zone and limit damage elsewhere. The column and cap beam longitudinal reinforcement strains were measured to determine if yielding is limited to the column plastic hinge and not in of the cap beam. Detailed design recommendations for CIP pocket connections were described based on the specimen performance.

1.4. Report Outline

This report is organized into seven chapters. Chapter 1 provides an introduction, problem statement and research objectives, and a literature review. The design and construction of the test specimen are described in Chapter 2. Chapter 3 discusses the pre-test analytical studies. Details about the experimental study and instrumentation are described in Chapter 4, and measured results from testing are reported and analyzed in Chapter 5. Chapter 6 presents further analytical studies and design recommendations. Finally, Chapter 7 provides a summary and conclusions of the study.

Chapter 2.   Specimen Description

2.1. Introduction

One large-scale laboratory specimen was built to evaluate the feasibility of designing and constructing an accelerated bridge construction (ABC) column-to-cap beam pocket connection for use in cast-in-place (CIP) bridge construction. The out-of-plane seismic performance of this connection was the primary focus of the study. A unique joint reinforcement design was developed to meet the requirements of this study. The out-of-plane seismic loading required the specimen members to have a distinct configuration that included an element representing the cap beam. This chapter describes the configuration, design, and construction of the specimen.

2.2. Specimen Configuration

A specimen consisting primarily of a 1/3-scale column and cap beam was designed and constructed for out-of-plane shake table testing. Figure 2.1 shows the elevation views of the specimen. The column and cap beam were arranged in an inverted T configuration to simplify testing the connection. A loading head was located on the top of the column so the specimen could be attached to the mass rig in the shake table setup. Two end blocks were attached to each end of the cap beam so the specimen could be attached to the shake table while allowing the cap beam to twist under the out-of-plane loading. These blocks simulated the restrain that the bridge longitudinal girders would impose on the cap beam. The column was tested in a cantilever configuration, i.e. single curvature, as the end of the column with the loading head effectively behaves as a free end and the column-to-cap beam connection behaves as a moment connection.

2.2.1. Prototype Bridge

Before designing the specimen, a prototype bridge was developed by bridge designers at the Nevada Department of Transportation (NDOT). This prototype was based on an actual bridge located in Carson City, Nevada at the intersection of US 395 and Clearview Drive. This location was later used to determine the seismic design response spectrum for the specimen. The prototype was a box-girder bridge with an integral bent cap. Figure 2.2 shows a typical cross-section of the prototype. The dimensions of prototype members were scaled down to determine the dimensions of members of the specimen. The longitudinal and transverse reinforcement ratios of the prototype bridge columns were used as starting points for determining the reinforcement ratios of the specimen column.

The axial load index (ALI) for the prototype bridge was calculated. ALI is the ratio of axial compressive force due to dead load to the product of the column gross cross-sectional area and the nominal compressive strength of concrete. The ALI for the prototype bridge columns was 8.3 percent. The compressive force for the specimen column based on an ALI of 8.3 percent was 67 kips (298 kN).

2.3. Design

2.3.1. Dimensions

The specimen represented a 1/3-scale model of components of a prototype bridge. The dimensions of the specimen are shown in Figure 2.3. The column utilized a circular cross-section, the same shape as the prototype column. The cap beam utilized an I-shaped cross-section to better represent the prototype integral cap beam with soffit and deck slabs contributions. Many studies involving column and cap beam testing use a rectangular cross-section for the cap beam, despite the fact that integral cap beams in box-girder bridges can be effectively represented as an I-shaped cross-section to account for soffit and deck slab contributions. Using an I-shaped cap beam cross-section in the specimen allowed the specimen to have a behavior more realistic to integral cap beams. In most bridge designs the upper flange of the cap beam cross-section, i.e. deck slab, is slightly thicker than the lower flange, i.e. soffit slab. This difference was neglected to simplify the construction of the cap beam. The flange thickness in the specimen slightly exceeded the scaled thickness to ensure that the reinforcement in the flange would have an adequate concrete cover.

Dimensions for the loading head were based on the test setup requirements and the dimensions of loading heads used in previous studies, in which shake table testing of columns in single curvature was conducted. The end block width was based on the need to allow the specimen to align with the strong tie-down locations on the shake table. It was also necessary that the end blocks have enough length to capture four tie-down points to prevent overturning of the specimen. Figure 2.4 shows the specimen oriented on the shake table with the end blocks capturing the appropriate tie-down locations. The red holes in the figure indicate the strong tie-down points (with a limit of 30 kips (133 kN)) and the green holes indicate the weak tie-down points (with a limit of 10 kips (44 kN)). The height of the end blocks was based on the need to have the cap beam centered within the block height, with sufficient gap between the bottom of the cap beam and the shake table surface to allow the cap beam to twist during shake table testing without bearing directly on the table.

2.3.2. Reinforcement Details

2.3.2.1. Column

The column was the first member of the test specimen to be designed. Figure 2.5 shows the column cross-section and Table 2.1 lists the design properties of the column. The longitudinal reinforcement ratio of the prototype bridge columns (1.1 percent), was initially used as a target for the amount of longitudinal reinforcement used in the specimen column. This reinforcement ratio is near the minimum longitudinal steel ratio in bridge columns, which is 1 percent. The relatively small steel ratio places relatively small demand on the connection. To truly assess the performance of the connection under more realistic conditions, the target longitudinal reinforcement ratio was raised to 1.6 percent to increase the moment and shear demand on the connection. This reinforcement ratio was achieved with the use of 16-#4 (Ø13 mm) bars in the column cross-section, which corresponded to 1.59 percent steel ratio. The transverse reinforcement ratio of the prototype bridge column was 0.7 percent,

7

which would have required the specimen column to have a relatively large spiral pitch to match this ratio. The target column transverse reinforcement ratio was increased to 1.25 percent to provide sufficient displacement ductility for the column specimen with an increased longitudinal reinforcement ratio from 1.1 to 1.59 percent. This was achieved with a #3 (Ø9.5 mm) spiral at a pitch of 2.25 in. (57 mm). The effect of this increase is reflected in moment curvature analysis of the column section that is discussed subsequently.

2.3.2.1.1. Moment-Curvature Analysis

A moment-curvature analysis of the final column cross-section was conducted to determine the plastic moment capacity of the column. The guidelines followed for conducting this analysis are outlined in Section 8.5 of the AASHTO Guide Specifications for LRFD Seismic Bridge Design [13]. The moment-curvature analysis of the column was conducted in both OpenSEES [14] and SAP2000 [15] to increase confidence in the results of the analysis. Table 2.2 and Table 2.3 show the results of the analysis from both programs. Percent difference was calculated for the results from the two programs and showed good correlation between the OpenSEES and SAP2000 results. The moment-curvature analysis was conducted with a compressive axial load of 67 kips (298 kN) and with no axial load. The moment-curvature analysis results with an axial load of 67 kips (298 kN) and the idealized curve is shown in Figure 2.6. The result for the case with no axial load and the idealized curve is shown in Figure 2.7. The analysis with no axial load was conducted because there would be no axial load applied to the specimen during the shake table testing to avoid inducing unrealistic moments in the cap beam. The overstrength moment of capacity-protected members was calculated from the moment-curvature analysis of the column with the axial load. The overstrength moment was used when designing the reinforcement of capacity-protected members. Using the results from the moment-curvature analysis with axial load rather than that with no axial load ensured that the cap beam and joint region would have a representative and realistic design.

2.3.2.2. Cap Beam

The cap beam was designed as a capacity-protected member to resist positive and negative moments, shear, and torsion forces. A typical cross-section of the cap beam reinforcement outside of the joint region is shown in Figure 2.8. To resist positive and negative moments the cap beam was reinforced with 10-#5 (Ø16 mm) in both the top and bottom faces of the cap beam. In the top layer of cap beam reinforcement (would be the bottom layer in a real bridge), the longitudinal bars were bundled to allow the column reinforcement cage extend into the cap beam joint. This requirement did not apply to the bottom layer of cap beam reinforcement, so the longitudinal bars were evenly distributed. Because of the bundling of longitudinal bars in the upper face, 2-#3 (Ø9.5 mm) longitudinal bars were added to the cap beam cross-section outside of the joint region to resist shrinkage and temperature cracking. Torsion forces were resisted with additional 8-#5 (Ø16 mm) longitudinal bars distributed evenly on the side faces of the cap beam web. Torsion controlled the design of the transverse reinforcement within the cap beam. A #3 (Ø9.5 mm) stirrup and horizontal tie at 4 in. (102 mm) were used to resist torsion in the cap beam section. Two #3 (Ø9.5 mm) vertical ties were included in the section to resist shear forces at a spacing of 4 in. (102 mm). A straight #3 (Ø9.5 mm) bar

was used in both the top and bottom faces of the cap beam to support the longitudinal bars in the flanges. Transverse reinforcement around the column to cap beam joint was adjusted to accommodate the pocket connection. These adjustments are described in the next section.

2.3.2.2.1. Pocket Connection

Reinforcement details of the pocket connection are shown in Figure 2.9 to Figure 2.13. Design of the pocket connection began with a CIP connection detail provided by NDOT bridge designers. In CIP connections, column and cap beam bars intersect, which is a source of steel congestion and construction difficulties. However, to mimic ABC connection details, transverse reinforcement within the pocket itself would need to be limited to allow the column reinforcement cage to extend into the cap beam uninhibited with no intersecting bars. The bars that were eliminated within the joint were the #3 (Ø9.5 mm) horizontal ties, which acted to close the stirrup surrounding the cap beam longitudinal bars. The #3 (Ø9.5 mm) straight bars in the upper face of the cap beam were also eliminated within the joint. These straight bars acted to support the longitudinal bars in the cap beam upper flange. Figure 2.11 shows the column to cap beam joint where some of the transverse reinforcement was eliminated. Additional reinforcement was included adjacent to the pocket to resist joint stresses. Two #3 (Ø9.5 mm) horizontal ties were placed adjacent to the pocket on each side of the column to address any prying forces. The placement of the ties can be seen in Figure 2.10. Five #3 (Ø9.5 mm) transverse hoops spaced at 1.5 in. (38 mm) were placed in the upper half of the joint and one #3 (Ø9.5 mm) hoop was centered in the lower half of the joint. The placement of the hoops is shown in Figure 2.11 and Figure 2.12. The transverse reinforcement volumetric ratio of the upper hoops was the same as that of the column transverse reinforcement ratio per the design recommendations for pocket connections proposed by Tazarv and Saiidi [1]. This recommendation only applies to the upper half of the pocket (would be lower half in a real bridge). Meeting this recommendation ensures the pocket has adequate confinement. Figure 2.13 shows the cap beam transverse reinforcement layout away from the joint, adjacent to the joint, and within the joint.

Because the cap beam was not precast, the design recommendations for depth and width of the pocket proposed by Tazarv and Saiidi [1] were not appropriate for determining the spacing between the column reinforcement cage and cap beam reinforcement. The column reinforcement cage extended 15 in. (381 mm) into the cap beam, which provided adequate development for the longitudinal bars. There was no specific required amount of spacing between the column reinforcement cage and the cap beam transverse reinforcement, but sufficient space was provided so that concrete could flow between the reinforcement. The clearance between the column reinforcement cage and the cap beam reinforcement is shown in Figure 2.9. To allow the column reinforcement cage to freely extend into the cap beam, the cap beam longitudinal bars were bundled and placed outside of the pocket at the upper face of the cap beam so that no bars would need to be threaded through the column reinforcement cage. The bundled cap beam longitudinal bars are shown in Figure 2.8, Figure 2.10, and Figure 2.11. Principle stresses for this moment resisting joint were then calculated to satisfy AASHTO requirements in section 8.13.2 [13].

2.3.2.3. Loading Head and End Blocks

The details of the reinforcement in the loading head are shown in Figure 2.14 and Figure 2.15. The purpose of the loading head was to allow the specimen to be attached to a mass rig through a rigid link. When testing a column in single curvature, a single link system is used, and the link is attached directly to the specimen. Rotation of the loading head was not restrained by the rigid link due to the pin at the end of the link, so the loading head did not behave as a moment joint and hence, required only minimal reinforcement. An offset at the ends of several of the column longitudinal bars was necessary to accommodate the placement of four 2.25 in. (57 mm) diameter PVC pipes in the loading head, which were necessary for passing threaded rods for link connection.

Reinforcement details for the end blocks are shown in Figure 2.16 to Figure 2.18. The end blocks allowed the specimen to be anchored to the shake table and acted as fixed supports at the ends of the cap beam. Because there was clearance between the bottom of the cap beam and surface of the shake table, the cap beam was allowed to twist between the end blocks. Four threaded rods each post-tensioned to 30 kips (133 kN) clamped each end block to the shake table. Moment, shear, and bearing demands were checked. The cap beam longitudinal bars were extended into the end blocks to meet the development length requirements described in Section 25.4 of the ACI 318-14 [16]. The ends of some of the cap beam longitudinal bars were bent to 90 degrees to accommodate the placement of four 2.25 in. (57 mm) diameter PVC pipes in each end block.

2.4. Construction

The specimen was constructed at the University of Nevada, Reno from March 2019 to April 2019. All reinforcement was A706 Grade 60. First, forms for the end blocks and cap beam were constructed. Then the reinforcement for the cap beam and end blocks were tied and placed in the forms. The cap beam and end block reinforcement is shown in Figure 2.19. Note the opening left in the middle of the cap beam reinforcement to serve as a pocket. The pocket connection reinforcement is shown in Figure 2.20. The lower half of the column reinforcement cage was then assembled and placed in the pocket area of the cap beam as shown in Figure 2.21. The clearance between the column reinforcement cage and the cap beam reinforcement is shown in Figure 2.22. Because the cap beam joint reinforcement was arranged to form a pocket, there was no need to thread the column longitudinal and transverse reinforcement through cap beam reinforcement. The column reinforcement cage was simply placed and centered within the pocket. Lifting anchors were attached to the end block forms at specific locations so that the specimen could be lifted with a forklift and moved into the lab for testing. Four 2.25 in. (57 mm) diameter PVC pipes were also placed in each end block so that threaded rods could pass through the end blocks, allowing the specimen to be anchored to the shake table. Lifting anchors and the placement of the PVC pipes are shown in Figure 2.23 and Figure 2.24, respectively. Once these elements were in place, concrete with a specified 28-day compressive strength of 4,500 psi (31.0 MPa) was poured in the cap beam and end block forms. The concrete was consolidated using a mechanical vibrator. Figure 2.25 through Figure 2.29 show the concrete casting, vibration, and finishing for the cap beam and end blocks.

After allowing the concrete for the cap beam and end blocks to cure for one week, the forms were stripped. The cap beam and end blocks after the removal of formwork are shown in Figure 2.30. The remaining length of the column cage was tied and a Sonotube was placed around the column reinforcement cage. The loading head reinforcement cage was then assembled and the form for the loading head was constructed. The specimen with the Sonotube and loading head form in place is shown in Figure 2.31. Four 2.25 in. (57 mm) diameter PVC pipes were placed in the loading head to allow threaded rods to pass through and attach to the mass rig link. Four 5/16-in. (8-mm) diameter threaded rods were run through the column Sonotube so that Novatechnik displacement transducers could later be attached to the column during testing. The threaded rods for the Novatechniks are shown in Figure 2.32. Concrete was then placed to the same specifications as those described for the cap beam and end blocks. Casting, vibrating, and finishing of the concrete for the column and the loading head is shown in Figure 2.33 through Figure 2.35. Figure 2.36 shows the specimen after all formwork was stripped.

Two minor construction errors were noted after the forms were stripped from the specimen. One was bulging of the formwork for the cap beam web due to fluid concrete pressure. This resulted in the width of the cap beam web increasing by about 0.75 in. (19 mm) on one side, and 0.5 in. (13 mm) on the other side at mid-depth of the cap beam but tapering down to near zero at the junction with the flanges. The deformed area of the cap beam web on one side is shown in Figure 2.37. This bulging occurred only on the mid and lower portion of the web. Therefore, it was determined that it would not have a significant effect on the behavior of the cap beam. The other error was a warping of a lower portion of the column Sonotube. This caused a deformation at the base of the column which is shown in Figure 2.38. While this deformation was within the plastic hinge zone, it was not in the direction of loading and its effect was considered negligible. Patching of this area of the column was considered for aesthetic reasons, but was ultimately not performed because it would have delayed testing.

Chapter 3.   Pre-test Analytical Studies

3.1. Introduction

Static and dynamic nonlinear analysis of the specimen was conducted in OpenSEES [14]. These analytical models had varying levels of sophistication. The goal of this simulation was to predict the specimen response under earthquake loading and determine a loading protocol which would apply sufficient demand associated with different limit states on the model.

3.2. Analytical Modeling

3.2.1. Pushover Analysis

A nonlinear static analysis, commonly referred to as pushover analysis, of the model was conducted to develop an estimate of the lateral load behavior and capacity of the specimen. This analysis produces a pushover curve, which is calculated by pushing the model laterally to a desired drift level, in this case, 10 percent. Fiber sections representing the members of the specimen were defined. The fibers within these sections represent the reinforcement and the confined and unconfined concrete material. The first step in a pushover analysis is to apply a gravity load. The only gravity load imposed on the model was the self-weight of the column and loading head and one-half of the weight of the mass rig link, which was estimated at 2 kips (8.9 kN). Once the gravity load is applied, stresses in the fiber sections are calculated over the member length for each displacement increment until the user-defined drift level is reached at the control node. Initially, a two-dimensional model of the specimen was developed and a pushover analysis of this model was conducted. This model was expected to capture the majority of lateral displacement that the specimen would undergo and it provided an idea about what to expect before the more complex model of the cap beam was added. A more sophisticated three-dimensional model of the specimen was subsequently developed, and the model was analyzed under both static and dynamic loading. Details of these models and their analyses are discussed in the following sections.

3.2.1.1. Two-Dimensional Model

The two-dimensional analytical model of the specimen represented a fixed-base cantilever column. The column was composed of a fiber section applied to a force-based beam/column element with five Gauss-Lobatto integration points. The fiber section was composed of two patches and one circular layer. The patch sections represented the concrete material, both confined and unconfined. The circular layer represented the longitudinal reinforcement. There is no mechanism for directly defining transverse reinforcement in fiber elements, which is why it is necessary to separately define the behavior of confined concrete to account for the transverse reinforcement confinement effects indirectly. Details for the two-dimensional analytical model are shown in Figure 3.1. OpenSEES offers many different uniaxial material models to represent concrete and reinforcing steel. Concrete01 material model, which neglects tensile properties of concrete, was selected to model both confined and unconfined

concrete. The stress-strain relationship for Concrete01 material is shown in Figure 3.2. This material model was appropriate because the user-defined material properties can be adjusted to account for confined and unconfined concrete behavior. The material model ReinforcingSteel was used to represent the longitudinal steel in the column. The stress-strain relationship for the ReinforcingSteel material is shown in Figure 3.3. This material model offers a more sophisticated stress-strain relationship than the alternative bilinear material model for reinforcement. Instead of a bilinear relationship, ReinforcingSteel material model allows the user to define the yield plateau, strain hardening, and strain softening sections of the stress-strain curve. Because the analytical models were developed before the construction of the actual specimen, the expected material properties from AASHTO [13] were used in the analysis. The Mander et al. [17] model was used to calculate confined concrete properties. Table 3.1 and Table 3.2 list the reinforcement and concrete properties used in the pre-test two-dimensional analytical model. Note that negative numbers in Table 3.2 indicate compressive stresses and strains.

The two-dimensional fixed-base analytical model does not account for torsional and flexural flexibility of the cap beam because the column is fixed at the connection to the cap beam. To account for the effect of cap beam flexibility, a hand calculation for the additional displacement due to cap beam twist was added to the results of the pushover analysis. Flexural deformation of the cap beam was not expected to affect horizontal displacement because of symmetry. Displacement due to cap beam twist was calculated by first determining the angle of twist based on the applied torque and multiplying this angle by the length of the column. Angle of twist was calculated using Equation 3-1.

$$\varphi = \frac{TL_{beam}}{JG} \tag{3-1}$$

where,

φ = angle of twist

T = torque applied to cap beam, equivalent to moment at column base

L_{beam} = length of cap beam

J = cracked polar moment of inertia

G = shear modulus of cap beam

The cracked cross-section dimensions were used to calculate polar moment of inertia of the cap beam. The cracked section accounted for only the area enclosed by the outermost stirrup in the cap beam and was considered to be a conservative assumption. Because the cap beam was expected to behave as a capacity-protected member, the nominal compressive strength of concrete was used when determining the shear modulus of the section. The results of the pushover analysis with and without the cap beam twisting effect are shown in Figure 3.4. When accounting for twisting of the cap beam, the initial stiffness of the

13

model decreases slightly because of the added flexibility of the cap beam. The lateral force capacity is unaffected because it is controlled by yielding of the longitudinal reinforcement in the column. To better account for the effect of cap beam twist on the behavior of the specimen, a three-dimensional model of the specimen was created. This model is discussed in the next section.

3.2.1.2. Three-Dimensional Model

A three-dimensional analytical model representing the column and cap beam was created in OpenSEES and a pushover analysis of this model was performed. Figure 3.5 shows the details for the three-dimensional analytical model. The ends of the cap beam element were modeled as fixed to mimic the behavior of the end blocks of the test model. During shake table testing, the end blocks would clamp the specimen to the shake table while still allowing the cap beam to twist due to out-of-plane loading. A fiber section and force-based beam/column element were used to model the behavior of the cap beam. While the cap beam was designed as a capacity-protected member and expected to remain elastic during testing, a nonlinear force-based beam/column element was used to capture any nonlinear behavior that could potentially occur in the cap beam. The I-shaped cross-section of the cap beam was also better represented through the use of a fiber section. Using a fiber section allowed for the evaluation of strains in the cap beam reinforcement to ensure there was no significant yielding and section remains essentially elastic.

Several patches and layers were necessary to define the cap beam fiber section due to its unique geometry and reinforcement layout. Concrete01 was used to model the confined and unconfined concrete, and ReinforcingSteel was used to model the reinforcement. The material properties used for steel and concrete are listed in Table 3.3 and Table 3.4, respectively. Because this was a capacity-protected element, the nominal values for concrete and reinforcement strengths were used. Confined concrete properties were calculated using Mander's model [17]. Because a fiber section cannot account for the torsional effects, it was necessary to use the section aggregator command to explicitly define torsional stiffness with the fiber section. The column member in this model had the same properties as the column in the two-dimensional model.

A pushover analysis of the three-dimensional model was conducted in the out-of-plane of the test model and compared to the two-dimensional model with a fixed base and the two-dimensional model with the beam twist hand calculation. Figure 3.6 shows the results of this analysis. The three-dimensional model had a significantly lower initial stiffness and lateral force capacity than the two-dimensional model. The decrease in initial stiffness is due to the added flexibility that the cap beam contributes to the model. The decrease in lateral force capacity is due to the spread of column plasticity into the cap beam. In the two-dimensional model, yielding is limited to the fixed base of the column through the plastic hinge zone, but in the three-dimensional model column reinforcement yielding extends into the cap beam. The column element length was increased in three-dimensional model. The column started at the face of the cap beam in the two-dimensional model, but in the three-dimensional model it started at the cap beam center-line. This effectively increased the moment arm for the lateral force acting at the top of the column. Because the column plastic moment capacity is the same between the two models, a larger moment arm dictates a decrease in the lateral force capacity in the three-dimensional model.

The stress-strain response for the extreme tensile bar at different points along the length of the column is shown in Figure 3.7. The stress-strain response for two longitudinal bars at the center of the cap beam is shown in Figure 3.8. These stress-strain relationships demonstrate the inelastic response of the column reinforcement and the elastic response of the cap beam bars. With the more sophisticated three-dimensional model, it could be confirmed that the plastic hinge was formed in the column while the cap beam remained essentially elastic. The three-dimensional model was used in subsequent analyses as it provided the most realistic representation of the specimen behavior.

3.2.2. Dynamic Analysis

After conducting the nonlinear static analysis and developing a suitable three-dimensional analytical model of the specimen, a dynamic analysis was conducted. The purpose of the dynamic analysis was to determine the earthquake acceleration record and the loading protocol to be used during the shake table testing. A damping ratio of 2 percent was applied to the model using Rayleigh damping. Nine earthquake records were evaluated for potential simulation in shake table testing. The ground motion records were obtained from the NGA-West2 ground motion database developed by the Pacific Earthquake Engineering Research (PEER) Center [18].

When searching the PEER database, the seismic design response spectrum is needed to compare to the response spectra of the earthquakes being considered. The seismic design response spectrum for the prototype bridge location was determined for this purpose. The prototype was located in Carson City, Nevada at the intersection of US 395 and Clearview Drive. This location has seismic parameters $S_{DS} = 1.25$ g and $S_{D1} = 0.5$ g, where S_{DS} is the design spectral acceleration at 0.2-sec period and S_{D1} is the design spectral acceleration at 1-sec period. The seismic design response spectrum for this location is shown in Figure 3.9. Once the seismic design response spectrum was determined, the period of the specimen was calculated. Assuming the specimen is a single-degree-of-freedom system, the period was calculated from Equation 3-2.

$$\text{T} = 2\pi\sqrt{M\ /K_{tot}} \tag{3-2}$$

where,

M = mass due to dead load

K_{tot} = stiffness of system T

= period of system

To determine the lateral stiffness of the specimen in the out-of-plane direction, the flexibility of the column and the torsional flexibility of the cap beam need to be combined. The specimen, column, and cap beam stiffness can be determined by combining the flexibility of the column and cap beam using Equations 3-3 through 3-5 because the two elements work in series.

$$\frac{1}{K_{tot}} = \frac{1}{K_{col}} + \frac{1}{K_{beam}} \qquad (3\text{-}3)$$

$$K_{col} = \frac{3EI_{cr}}{L^3} \qquad (3\text{-}4)$$

$$K_{beam} = \left(\frac{J_{cr}G}{L_b}\right)/L^2 \qquad (3\text{-}5)$$

where,

EI_{cr} = cracked rigidity of column, determined from the idealized moment-curvature analysis L = length of column

J_{cr} = cracked polar moment of inertia for cap beam

G = shear modulus of cap beam concrete

L_b = length of cap beam

Equation 3-4 is based on the assumption that the column acts as a fixed-base cantilever and Equation 3-5 is idealizing the cap beam torsional stiffness as a rotational spring at the base of the column. The estimated period of the specimen was 0.575 seconds. This was close to the period calculated from the OpenSEES model (0.408 seconds). The OpenSEES model could not account for the cracked stiffness of the column or cap beam; consequently, this model underestimated the specimen period.

The period of the prototype was determined by dividing the specimen period (0.575 sec) by the square root of the specimen geometric scale factor (1/3). The estimated prototype period was 0.995 seconds. The spectral design acceleration of the bridge specimen for the design level earthquake event is then found for this period. After inputting the prototype period and seismic design response spectrum in the PEER database, the database was searched for earthquake records with the appropriate scale factors to match the specified spectral design acceleration.

When determining the design level earthquake, the specimen period rather than prototype period was plotted on the seismic design response spectrum in error. This gave a different spectral acceleration that was not equivalent to the 100 percent design earthquake for the prototype. The scale factors determined from the PEER search tool to scale the earthquake response spectra to match the seismic design response spectrum were also incorrect. This error was noted after shake table testing and the design level earthquake was redefined to address the error. However, most of the scale factors determined from the PEER database for the specimen period were close to the factors that would have corresponded to the prototype period. Because the differences were insignificant, the results from the pre-test analyses still provided a valuable insight into the demands placed on

the specimen during shake table testing. Note that the overall goal of the shake table test was to subject the specimen to different limit states. This was accomplished in the course of the tests.

3.2.2.1. Northridge Earthquake at Sylmar Converter Station, H1 Component

The ground motion selected for simulation in the shake table testing was the Northridge event recorded at the Sylmar Converter Station in 1994. There are three components to this earthquake record, two horizontal and a vertical component. The first horizontal component, H1, was selected for the tests input signal in the out-of-plane direction of the specimen, i.e. uniaxial testing was sought. This record was selected because of its symmetric acceleration history that would impose comparable displacements in the positive and negative directions and potentially small residual displacements. The symmetric acceleration history helped to ensure the demand on the connection would also be symmetric. The record is a well-known seismic event which has been simulated in many shake table tests for past research projects. The unscaled and uncompressed acceleration histories of the record are shown in Figure 3.10. Figure 3.11 shows the response spectrum for this record.

A nonlinear dynamic analysis was conducted using the acceleration history for this event. The time axis of the acceleration history was compressed to account for similitude requirements. This was accomplished by multiplying the time step of the acceleration history by the square root of the specimen geometric scale factor. The acceleration was also multiplied by a scale factor to amplify the record to match the design response spectrum in defining the 100 percent design earthquake level. Because the specimen period was mistakenly used to determine the scale factor instead of the prototype period, a scale factor of 0.41 was applied to the record. The correct scale factor would have been 0.37. The compressed and scaled acceleration history, based on a factor of 0.41, used in the dynamic analysis is shown in Figure 3.12. The dynamic response of the specimen for this ground motion is illustrated in the hysteretic force-displacement relationship (Figure 3.13) and the displacement history at the top of the column (Figure 3.14). It can be seen that the estimated displacement response under the Northridge Sylmar ground motion led to a reasonable drift level that is normally expected of structures subjected to design earthquakes. The demand in the push and pull directions was fairly symmetric as well although some residual displacement occurred. This indicates that demand on the connection would also be symmetric. Based on this initial analysis, a loading protocol was developed. The loading protocol involved the acceleration record being applied in successive motions at increasing scales of the design earthquake.

3.2.2.2. Additional earthquake records considered

Nine earthquake records were applied to the model in the pre-test analysis phase before Northridge Sylmar H1 was ultimately selected. The dynamic responses of the model for each ground motion were compared so that an appropriate ground motion would be identified for simulation on the shake table. The records described in this section were not ultimately selected for use in shake table testing because of one or more of the following reasons: (1) they did not produce symmetric response in the column; (2) did not place sufficient demand on the column with reasonable scale factors; or (3) caused a relatively large

residual displacement in the column. Details for all nine earthquake records that were used in the analyses are listed in Table 3.5. For six of the nine records, the discrepancy between the specimen and prototype scale factors was small. Therefore, this error did not significantly impact the results of the pretest analytical studies. The earthquake records which were ultimately not used in shake table testing and the analytical results are briefly discussed. Three of the nine events are not discussed because there was a large difference between scale factors. The amplitudes and the time axes of all acceleration histories shown are unscaled, but the records that were applied in the analysis were scaled and compressed using the previously described method.

3.2.2.2.1. 1940 Imperial Valley-02 at El Centro Array #9

The acceleration history for this event is shown in Figure 3.15. This record was a suitable candidate for shake table testing because it has a fairly symmetric acceleration history and is a historically significant earthquake record. The hysteresis loops produced from the dynamic analysis are shown in Figure 3.16 and the displacement history at the top of the column is shown in Figure 3.17. The results of this dynamic analysis showed a symmetric response in displacement demands and yielding of the columns. The Imperial Valley event was initially considered for use in shake table testing and a loading protocol for this record was developed. However, when this ground motion was applied at higher amplitudes, higher drift levels could not be reached without significantly amplifying the accelerations.

3.2.2.2.2. 1952 Kern County at Taft Lincoln School

The acceleration history for this event is shown in Figure 3.18. The hysteresis loops and displacement history are shown in Figure 3.19 and Figure 3.20, respectively. This earthquake event was not well-known, and the ground motion did not place symmetric displacement demands on the column, therefore, it was not selected for use in shake table testing.

3.2.2.2.3. 1954 Northern California-03 at Ferndale City Hall

The acceleration history for this event is shown in Figure 3.21. The hysteresis loops and displacement history are shown in Figure 3.22 and Figure 3.23, respectively. The Northern California ground motion placed a large demand on the column for a design level event. Having the column reach large displacements early in the loading protocol would have limited the drift levels which could be reached in the later runs, and could cause the column to fail early during the shake table tests. For this reason, the Northern California event was not selected.

3.2.2.2.4. 1971 San Fernando at LA – Hollywood Stor. FF

The acceleration history for this event is shown in Figure 3.24. The hysteresis loops and displacement history are shown in Figure 3.25 and Figure 3.26, respectively. Based on the analysis, this record did not place a symmetric demand on the column and also caused a residual displacement which would have the potential to propagate with further testing. For these reasons, this ground motion was not selected for use in shake table testing.

3.2.2.2.5. 1994 Northridge at Sylmar Converter Station, H2 Component

The acceleration history for this component is shown in Figure 3.27. The H2 component of Sylmar is more frequently simulated in shake table testing. This component had a slightly asymmetric acceleration history, so it was not ideal for the testing purposes, but it reached a larger peak ground acceleration (PGA) than the H1 component. The hysteresis loops and displacement history for this event are shown in Figure 3.28 and Figure 3.29, respectively. Based on the pre-test analysis, this record causes a residual displacement and an asymmetric displacement demand on the column, therefore it was not selected for use in the shake table testing.

3.2.2.3. Loading Protocol

A loading protocol was developed based on the analysis of the test specimen under the Northridge event recorded at the Sylmar Converter Station in the H1 component. Successive scaled versions of this ground motion were stitched together at varying amplification factors of the design earthquake. The spliced acceleration history for this loading protocol is shown in Figure 3.30. Because the scale factor used when determining the design level earthquake was based on the specimen period and not the prototype period, describing each run in terms of percent of design earthquake does not accurately reflect the demand placed on the specimen. Instead of referencing these percentages for each run, the runs are described in terms of the specimen drift level to the nearest half percent. The loading protocol consisted of seven runs which were estimated to impose 1, 1.5, 2.5, 3, 4.5, 6.5, and 9 percent drift in the column. Before each earthquake motion and after the last motion, white noise motions with an amplitude of approximately 0.05g were applied to estimate the period and damping ratio of the specimen.

Table 3.6 lists details of the loading protocol. The factor listed in Table 3.6 was used to amplify the acceleration record simulated in shake table testing. This factor represents the scale factor determined from PEER multiplied by the percentage of the design level earthquake each run was meant to represent. If this loading protocol did not place sufficient demand on the specimen, additional runs at larger scales of the design earthquake would be simulated on the shake table until the specimen reached high drift levels with substantial damage or failure.

3.2.2.3.1. Estimated Response

The pushover curve with the predicted maximum displacement for each run is shown in Figure 3.31. The specific loading protocol described above was selected to capture different limit states that cover the entire pushover curve. The one percent drift run captures the elastic region of the curve, and ensuing runs capture the nonlinear portion of the curve. The displacement history at the top of the column (Figure 3.32) showed the column was subjected to minimal residual displacements, even when reaching 4.5 and 6.5 percent drift, which was promising for the actual shake table testing. In the last run, when the column reached about nine percent drift, a large residual drift was observed.

Table 3.7 lists the predicted maximum column displacement and base shear for each run. The predicted force-displacement relationship for each run is shown in Figure 3.33 through Figure 3.39. The envelopes of the hysteresis loops for the push and pull sides were determined and averaged to develop an envelope which was compared with the pushover curve. This comparison is shown in Figure 3.40. There is good correlation between the two curves, with the hysteresis envelope having a slightly smaller base shear capacity than the pushover curve.

Chapter 4.   Experimental Studies

4.1. Introduction

Shake table testing was used to evaluate the performance of the novel ABC-inspired column-to-cap beam connection design under out-of-plane seismic loading. Testing was conducted on a biaxial shake table in the Earthquake Engineering Laboratory (EEL) at the University of Nevada, Reno (UNR). Specimen material properties and the experimental setup are described in this chapter. The instrumentation to capture the specimen response during testing is also discussed.

4.2. Measured Material Properties

Samples of the materials used in the specimen were taken to determine properties of interest. This was necessary to ensure that the materials met the required specified properties that are representative of those used in typical bridges. These properties were also used to update the material models in the post-test analysis. The sampled materials consisted of concrete and reinforcing steel. The compressive strength of concrete was determined at 7 and 28 days after casting. In addition, the compressive strength of concrete was measured on the day of shake table testing. The shake table tests were conducted over two days. The test-day strengths were determined on the second day of shake table testing.

Standard 6 in (152 mm) diameter by 12 in (305 mm) tall concrete cylinders were sampled during construction. The specimens were cast in two separate concrete pours. Therefore, it was necessary to sample concrete from both batches. The end blocks and cap beam were cast in the first casting, and the column and loading head were cast in the second. Nine cylinders were taken from each batch. The average compressive strengths for all members at 7-day, 28-day, and test-day are listed in Table 4.1.

Reinforcing steel for each bar size used in the specimen was sampled and tested at UNR. The bars were tested to the ASTM A370 standard [19]. Yield stress, ultimate stress, yield strain, strain at hardening, and ultimate strain were determined from the measured stress-strain relationships. The modulus of elasticity for all samples was taken as 29,000 ksi (200 GPa). The measured stress-strain plots for each bar size are shown in Figure 4.1 through Figure 4.3. When testing the second sample for both #3 (Ø9.5 mm) and #4 (Ø13 mm) bar sizes, the laser extensometer malfunctioned; consequently, the results for these samples were not used in the determination of material properties. The jagged regions of the stress-strain relationship for bar size #3 (Ø9.5 mm) (Figure 4.1) were the result of the bar samples slipping during testing. This slippage did not affect the test results for these bars. Table 4.2 lists the relevant stresses and strains determined from the measured results.

4.3. Experimental Setup

The shake table test setup is shown in Figure 4.4 and Figure 4.5. The specimen was tested in the out-of-plane direction, which was the north-south orientation in the laboratory. The specimen was placed on the shake table with a 1.5 in. (38 mm) gap

between the top of the shake table and the bottom of the end blocks. This gap allowed non-shrink grout to be placed around both end blocks, which ensured the specimen would be placed on a level surface. The grout was allowed to cure and then the specimen was anchored to the shake table through eight threaded rods. The rods passed through the PVC pipes located in each end block, and each rod was tensioned to 30 kips (133 kN).

The loading head of the specimen was then connected to a mass rig, which would provide inertial mass during the dynamic tests. The mass rig provided 60 kips (267 kN) of inertial mass, which was achieved by placing two 20 kip (89 kN) concrete blocks on the rig. The mass rig itself weighs an additional 20 kips (89 kN), but because it is supported on a mechanism with hinges at base, its entire inertial force from mass is transferred to the top of the specimen through the rigid link that was connected to the specimen. The link system included a load cell that measured the lateral force applied at the top of the column. The column and cap beam were covered with a white-wash solution to make cracks that developed during testing more visible. After each run, new visible cracks in the column and cap beam would be marked to highlight the damage and help keep track of the earthquake level under which the damage occurred. Figure 4.6 shows a photo of the experimental setup.

Cameras were placed on and around the specimen to capture the response of the specimen during testing. GoPro cameras were aimed at the plastic hinge zone of the column from the north, south, east, and west directions. The movement in the north and south sides of the cap beam was also captured with GoPro cameras. Two video cameras were set up on the east and west sides of the shake table to record the overall response of the specimen. The location of all recording devices is shown in Figure 4.7. In addition to the videos taken during testing, photos of the observed damage were taken after each run.

4.4. Instrumentation

The specimen was instrumented to measure its response during shake table testing. Data was continuously recorded from 130 data acquisition channels throughout each run of testing. Strain gauges, displacement transducers, string potentiometers, and accelerometers were used to collect data. In addition to these instruments, the shake table actuators are instrumented to either measure or calculate displacement, velocity, acceleration, and force.

4.4.1. Strain Gauges

Strain gauges were attached to column and cap beam reinforcement to measure local changes in reinforcement length. The strain gauges were manufactured by Tokyo Measuring Instruments Laboratory Co., Ltd. The gauge type was YEFLA-5 with a gauge length of 0.20 in. (5 mm). Figure 4.8 to Figure 4.10 show the locations of the 104 strain gauges that were placed on the column and cap beam reinforcement. All strain gauges were attached following the manufacturer's recommendations.

The column longitudinal reinforcement was instrumented with gauges placed at six heights (layers) as illustrated in Figure 4.8. Four layers of gauges were located above the cap beam, with the first layer at the face of the beam, and other layers spaced at 6 in. (152 mm). The gauges located above the cap beam captured the yielding of reinforcement within the plastic hinge zone. Two layers of gauges, spaced at 4.5 in. (114 mm) below the top beam face, were located on the column reinforcement that

22

extended into the cap beam pocket. These gauges measured the spread of yielding in the cap beam. For redundancy, three bars on the north and south sides of the column were instrumented in each layer. Gauges were also attached to the column spiral at the same heights as those of the longitudinal gauges. A gauge was placed on the north, south, east, and west sides of the column spiral at each layer. These gauges measured the maximum spiral strains due to confinement and shear. The strain gauges placed on the longitudinal and transverse reinforcement in the column are shown in Figure 4.8.

Strain gauges were also placed at multiple locations of the cap beam around the pocket connection to determine whether the novel connection design still allows the cap beam to remain essentially elastic and prevent significant yielding of cap beam reinforcement. The hoops that encircled the pocket were instrumented in two layers (Figure 4.8) to measure the confinement they provided. Transverse horizontal and vertical ties adjacent to the pocket and on stirrups throughout the cap beam length were instrumented to measure the extent to which this reinforcement was engaged during out-of-plane loading. The locations of these gauges are shown in Figure 4.9 and Figure 4.10. Strain gauges were attached to the cap beam longitudinal reinforcement to determine if that the cap beam remained elastic during testing (Figure 4.10). Since the cap beam would act mainly in torsion during testing, these gauges were located on the longitudinal skin bars.

4.4.2. Displacement Transducers

Four pairs of TR-75 and TR-100 Novatechnik displacement transducers were spaced along the length of the column plastic hinge zone to calculate curvature (Figure 4.11). These instruments have a stroke of 2.95 in. (75 mm) and 3.94 in. (100 mm), respectively. The transducers were placed on 5/16-in (8-mm) diameter threaded rods, which had been inserted through the column during construction. A pair of TR-100 transducers were also attached to the cap beam bottom flanges to measure cap beam twist due to the out-of-plane loading of the test specimen. The geometry of the cap beam allowed these instruments to be directly attached to the flanges without the need for a threaded rod. The location and spacing of the column and cap beam displacement transducers are shown in Figure 4.11. The distance between pairs of instruments and the actual gauge length was measured after the instruments were attached.

4.4.3. String Potentiometers and Accelerometers

Six string potentiometers were used to measure the horizontal displacement of the column and cap beam (Figure 4.11). Four instruments were attached to the north face of the loading head, with one instrument at each corner. The displacement of the column was determined as the average of the measurements from the four instruments on the loading head. The other two instruments were attached to the midpoints of the upper and lower flanges on the south side of the cap beam. These were used to measure the horizontal displacement of the cap beam in the out-of-plane direction and also as a redundant means of measuring cap beam twist.

The accelerometer locations are shown in Figure 4.12. Three tri-axial accelerometers measured accelerations at different points on the specimen. An accelerometer was located on top of the loading head to measure accelerations at the top of the

column. To measure the accelerations in the cap beam, an accelerometer was centered on the north side of the cap beam web. For redundancy in measuring the shake table accelerations, an accelerometer was also placed on the bottom of the cap beam, centered along the length.

Chapter 5.   Experimental Results

5.1. Introduction

The specimen was tested in the out-of-plane direction on a shake table in EEL at UNR. The H1 component of the 1994 Northridge Sylmar event was used as input signal for testing. Shake table testing was conducted on May 20 and 21, 2019. While the initial loading protocol specified seven runs at increasing scales of the design earthquake, these runs did not achieve high levels of drift. It was necessary to include four additional runs at higher accelerations to cause larger drifts in the column. Thus, a total of 11 runs of earthquake excitation were completed: four on May 20, and seven on May 21. The observed and measured seismic performance of the specimen are discussed in this chapter.

5.2. Observed Damage

GoPro video cameras and camcorders were used to record the movements and damage progression of the specimen. Shrinkage cracks and other construction flaws were marked on the specimen with a black crayon and denoted with the run number zero to indicate damage that was in place before testing was conducted. After each earthquake motion, the new cracks were marked with a new color and the run number was written adjacent to the crack to track the damage associated with each run. Photos were then taken at areas of interest on the specimen. Damage in the column plastic hinge zone and the pocket connection area of the cap beam was documented. Photos of the overall specimen were taken from the north, south, east and west directions. Any unexpected damage was also documented.

The runs described in this section reference the drift level reached. Because displacement was measured at the top and bottom of the loading head, the effective column height was taken as the column clear height plus one-half of the loading head height. The effective column height was 90 in. (2286 mm). Drift ratio was calculated by dividing the column displacement by the effective height of the column.

Several shrinkage cracks were noted along the length of the cap beam before testing (Figure 5.1). In the initial runs of testing, the shake table achieved significantly lower PGA than expected. The specimen did not experience significant damage during these runs. Figure 5.2 shows the minimal cracking in the column and cap beam, which was observed after run two when the column reached 0.5 percent drift ratio. Small transverse cracks appeared in the cap beam, and minor flexural cracking was noted in the column plastic hinge zone after run two. During run three the column reached 2.1 percent drift ratio, and significantly more flexural cracks were noted in the column plastic hinge (Figure 5.3). Some minor shear and torsion cracks were observed on the north side of the cap beam web as well as shown in Figure 5.4.

After runs four and five, the large flexural cracks that developed in run three extended and widened. Figure 5.5 shows the column flexural cracks after run five, where the column reached a drift ratio of 3.7 percent. A few small torsion and shear cracks were observed on the top face of the cap beam after run five as well (Figure 5.6). Minor concrete spalling on the south side of the column was noted after run six (Figure 5.7), where the column reached a drift ratio of 4.3 percent. Concrete spalling

continued to expand at the base of the south side of the column after runs seven and eight. Figure 5.8 shows the spalling of concrete on the south side of the column after the column reached 5.1 percent drift ratio during run eight. Small torsion cracks were observed in the cap beam flanges after runs seven and eight (Figure 5.9 and Figure 5.10). The column flexural cracks continued to expand and widen through runs six, seven, eight, and nine.

Some thin shear cracks were observed at the end of flexural cracks in the column after run nine (Figure 5.11), where the column reached a drift ratio of 5.6 percent. During run 10 the column reached 5.8 percent drift. The cover concrete on the north side of the column spalled during run 10 (Figure 5.12), and flexural cracks on the south side of the column widened significantly due to a residual drift in the column (Figure 5.13). The area of concrete spalling on the north and south sides of the column expanded after run eleven, the final run, where the column drift ratio reached 7.8 percent. Additional shear cracks formed after this final run and the flexural cracks on the column south side widened due to a propagation of the residual drift that was imposed after run 10. The concrete spalling on the north and south sides of the column after the final run is shown in Figure 5.14 and Figure 5.15, respectively. The widening of flexural cracks on the column south side is shown in Figure 5.16, and the shear cracks on the south side of the column are shown in Figure 5.17. No new damage was observed in the cap beam after runs nine, ten, and eleven.

The photos show that damage in the specimen was essentially concentrated in the plastic hinge region of the column with only minor cracking elsewhere. Large flexural cracks formed in the column in the later runs, when the column reached high drift levels. Cover concrete began to spall at the base of the column in the direction of loading, but no transverse or longitudinal reinforcement was exposed. No buckling of rebar or bar rupture was observed in the column reinforcement.

5.3. Measured Performance

5.3.1. Shake Table

The actual shake table achieved motions were different than the target motions due to the shake table mass and dynamics and the shake table-specimen interaction. The shake table consistently achieved lower PGAs compared to the PGAs in the loading protocol, which was used in the pre-test dynamic analyses. Table 5.1 lists the target and achieved PGA values for each run, and the percent difference. In the initial runs, the shake table achieved significantly smaller accelerations than the target. The difference between the target and achieved PGA values improved as the runs progressed, but never became less than 12 percent. The predicted and achieved spectral accelerations (S_a), i.e. acceleration at the top of the specimen representing a single-degree-of-freedom vibrating system, were also compared (Table 5.2). The error between predicted and achieved S_a for the initial runs was also high, but decreased in the later runs. The achieved shake table motions were used to generate response spectra. Figure 5.18 to Figure 5.28 show the target and achieved response spectra for each earthquake run. The period of the specimen was estimated using frequency response factors (FRF) as well as Fast Fourier Transform (FFT) from the measured specimen accelerations during the white noise runs. This period was plotted with the target and achieved response spectra for each run to determine the target and achieved spectral accelerations. It can be seen that there was generally good correlation between the

shape of the target and achieved response spectra during run three and after. The achieved response spectra for all runs were compared with the seismic design response spectrum for the specimen as well (Figure 5.29).

5.3.2. Force-Displacement Relationship

The lateral force-displacement relationship is an important indicator of seismic performance of structures. The hysteretic force-displacement relationships help track when yielding occurs, indicate the amount of dissipated energy, and are used to determine lateral force and displacement capacities. To measure the displacement of the column, the data from the four string potentiometers attached to the loading head was averaged and filtered to remove high-frequency noise. The shake table displacement in the direction of motion (recorded by the internal instruments attached to the shake table actuators) was subtracted from this displacement at the top of the column to find the relative displacement of the column during testing. The force applied at the top of the column was measured through the load cell embedded in the link to the mass rig. This force was the same as the column base shear because the mass rig was a four-hinge mechanism that does not transfer force to its base. Hence, the entire inertia force was transferred to the specimen.

The measured force-displacement relationships for each of the 11 test runs are shown in Figure 5.30 to Figure 5.40, respectively. The negative displacements indicate the column displacing to the north. In the first run, very little energy is dissipated and the response is linear, indicating that no reinforcement had yielded (Fig. 5.30). In run two, the initial response was slightly softer than the initial response during run one, but was still essentially linear with little energy dissipation (Figure 5.31). During run three, the response became nonlinear, indicating that some of the column longitudinal reinforcement had yielded (Figure 5.32). The response started to become slightly asymmetric in run three, with the column reaching higher displacements to the south. Runs four and five showed a similar response to run three, with the column reaching larger displacements with subsequent runs. Figure 5.33 and Figure 5.34 show the response for runs four and five, respectively. The hysteresis loops for runs four and five are wider, and the column response is asymmetric. The effective stiffness of the column keep reducing with each run, which is expected as damage progressed. The force-displacement response during runs six, seven, and eight (Figure 5.35 to Figure 5.37) showed hysteresis loops continuing to widen and the displacement response continuing to be asymmetric, with the column reaching slightly higher displacements to the south.

Figure 5.38 shows the force-displacement response for run nine. During this run, the column response became more symmetric, and a small residual displacement occurred toward the north. The residual displacement toward the north became larger after run 10, and the column response during this run was symmetric, shown in Figure 5.39. During run 11eleven, the residual displacement to the north continued to increase and a large residual displacement was observed in the column after the run was completed (Figure 5.40). The column response became highly asymmetric due to this residual displacement.

The specimen force-displacement relationship showed wide hysteresis loops for runs three through 11, which indicates good energy dissipation. While the response was slightly asymmetric, the column was able to reach high displacements in both loading directions. The residual displacement in the column was small until run 11. The high residual displacement after run

11 was not an issue because the column had reached high levels of displacement in previous runs. The dissipated energy in each run is listed in

Table 5.3. Energy dissipation was determined by calculating the area inside the hysteresis loops for each run.

The envelope of cumulative hysteresis curves was determined to capture the maximum response of the specimen in both the north and south directions (Figure 5.41). The envelopes for both directions were averaged to find the "effective experimental pushover" curve for the specimen, which was used to determine the lateral load and displacement/drift capacity. The average curve was then idealized by an elasto-plastic curve. The elastic portion of the idealized curve was formed by passing a line through the origin to the point where yielding of column longitudinal reinforcement first occurred. The plastic portion of the curve was formed by balancing the areas under the actual pushover curve. The idealized and actual pushover curves are shown in Figure 5.42. The effective yield point was at 15.21 kips (67.7 kN) and 1.56 in. (39.6 mm). The maximum measured displacement reached in the tests was 6.97 in. (177 mm), which corresponds to a drift ratio of 7.75 percent.

5.3.3. Displacement and Drift Ratios

The column displacement history for runs one through five and runs six through 11 are shown in Figure 5.43 and Figure 5.44, respectively. Table 5.4 lists the residual displacement reached in the column after each run. Note that positive displacements correspond to southward movements. The displacement histories for the column show that while a large residual displacement was observed in the later runs, the residual displacement was not cumulative throughout all the tests because it changed direction. In runs two through seven, the column reached a small residual displacement of about 0.25 in. (6.4 mm) to the south. The residual displacement was recovered during run eight. After run nine, the column started to experience residual displacements to the north and at a higher magnitude. This is evidence that the specimen did not reach a high level of displacement only through the propagation of residual displacements over the course of several runs, but instead was tested to high levels of displacement in both directions. Thus, cyclic demand was placed on the column and cap beam connection during testing.

The maximum value of absolute (regardless of the sign) column displacement relative to the base, base shear, and drift ratio for each run are listed in Table 5.5. Displacement was measured at the top and bottom of the loading head to coincide with the effective column height, which was taken as the column clear height plus one-half of the loading head height. The effective column height was 90 in (2286 mm). Drift ratio was calculated by dividing the column displacement by the effective height of the column.

The string potentiometers attached to the top and bottom cap beam flanges measured movement of the beam in the out-of-plane direction (the loading direction). The data between the two devices was totaled and filtered. The out-of-plane displacement history for the cap beam is shown in Figure 5.45 and Figure 5.46. Based on the displacement history recorded by the cap beam string potentiometers, the cap beam provided very little contribution to the overall displacement in the column. However, string potentiometers do not provide a high level of accuracy for very small levels of displacement. To address this issue, Novatechnik displacement transducers were also attached to the cap beam to capture a more accurate level of cap beam displacement during testing.

To determine the effect of cap beam torsional flexibility on the overall displacement of the column, the angle of twist for the cap beam was calculated. The cap beam twist was determined by subtracting the measurements from the vertical displacement transducers attached to the opposite edges of the cap beam bottom flange and dividing by the distance between the two instruments, 36 in. (914 mm). The distance between the cap beam center of rotation and the effective column height, 99 in. (2515 mm), was multiplied by the angle of twist to determine displacement due to cap beam torsional flexibility. Figure 5.47 and Figure 5.48 show the displacement history due to cap beam twist. The absolute maximum displacement due to cap beam twist was calculated for each run and is listed in Table 5.6. These values were compared to the overall displacement of the column to determine the proportion of overall displacement that was due to the twisting of the cap beam. Table 5.6 shows that the contribution of cap beam twist to overall column displacement was significant in the initial runs, but decreased as the column reached higher drift levels. As the column reinforcement yielded, the cap beam twist contributed less to the overall displacement. The yielding of column reinforcement provided the main source of ductility in the specimen, while the cap beam remained elastic as expected from a capacity-protected element and illustrated in the next section using the strain data. Only about 4 percent of the maximum displacement was due to cap beam twist in the later runs.

5.3.4. Strains

The maximum and minimum strains recorded by all gauges in each run are listed in Table 5.7 to Table 5.17. The locations of all strain gauges are shown in Figs. 4.7 through 4.9. Negative values indicate tension. Bolded values indicate strains that are at or beyond the yield strain. All strain values are reported as microstrain. Dashes indicate strain gauges that were damaged or malfunctioned during testing.

The strains in the column longitudinal reinforcement are shown in Table 5.7 through Table 5.9. No yielding occurred in the first two runs. During run three, column longitudinal reinforcement yielded in both directions. Yielding during run three was limited to sections of reinforcement within the plastic hinge zone. During run four, the column longitudinal reinforcement inside the cap beam pocket also yielded. The maximum tensile strains throughout the length of the column in the southern longitudinal bars are shown in Figure 5.49 through Figure 5.51. The highest strains in column longitudinal reinforcement were reached in the plastic hinge region above the cap beam face. However, yielding also extended into the cap beam in later runs.

Table 5.10 through Table 5.12 list the column transverse reinforcement strains. It can be seen that the column spiral did not yield during shake table testing. Figure 5.52 and Figure 5.53 show the maximum strains due to confinement (in the north-south plane) and shear (in the east-west plane) for each run, respectively. The column spiral experienced slightly higher strains to due confinement than due to shear.

The strains in cap beam longitudinal reinforcement are shown in

Table 5.17. No cap beam longitudinal reinforcement yielded. The maximum measured tensile strain was 616 microstrain, which is 36 percent of the yield strain, indicating that the beam remained elastic throughout testing. Note that in a more realistic bidirectional loading conditions, the cap beam would be subjected to flexure as well as torsion and would experience higher strains in the longitudinal reinforcement.

The cap beam transverse reinforcement strains are listed in Table 5.13 to

Table 5.16. There was no yielding of cap beam transverse reinforcement during shake table testing. The hoops encircling the pocket connection reached about 30 percent of yield strain, indicating that these hoops were engaged in providing confinement for the pocket. The #3 (Ø9.5 mm) horizontal ties placed adjacent to the pocket appeared to play a role in addressing prying as they reached 47 percent of yield strain. The maximum strains in the stirrups along the cap beam length are shown in Figure 5.54 and Figure 5.55. See Figs. 4.8 and 4.9 for the locations of the gauges. The maximum stirrup tensile strain, about 40 percent of yield, was reached in the stirrups that were within or directly adjacent to the pocket connection region. The #3 (Ø9.5 mm) vertical ties reached about 20 percent of yield strain, indicating there was low shear demand placed on the cap beam and the connection. If the specimen had been subjected to bidirectional loading, the cap beam would have experienced higher flexure and shear demands, which would have led to higher strains in the transverse reinforcement.

5.3.5. Curvature

Curvatures in the plastic hinge region of the column were determined for the direction of loading using data recorded by the Novatechnik displacement transducers. Curvatures were calculated over the lower 21 in. (533 mm) of the column. Four pairs of displacement transducers were used to measure curvature at four sections along the plastic hinge zone of the column. Curvature for each pair of Novatechniks was calculated using Equation 5-1.

$$\phi_i = \frac{\frac{\Delta_{i,1}}{l_{i,1}} - \frac{\Delta_{i,2}}{l_{i,2}}}{x_{i,1} + D + x_{i,2}} \tag{5-1}$$

where,

ϕ_i = average curvature at section i
$\Delta_{i,1}$, $\Delta_{i,2}$ = measured displacements from Novatechnik at section i
$l_{i,1}$, $l_{i,2}$ = gauge lengths at section i
$x_{i,1}$, $x_{i,2}$ = distance from column face to Novatechnik at section i
D = column diameter

The column curvature profiles for runs one through five and runs six through 11 are shown in Figure 5.56 and Figure 5.57, respectively. The profiles show that the plastic hinge is formed at the base of the column, with higher curvatures observed at the base, and a decrease in curvature away from the cap beam.

5.3.6. Accelerations

Acceleration was measured at three locations on the specimen during testing. The data were measured along the X (north-south), Y (east-west), and Z (vertical) axes at each location. The peak accelerations recorded along the Y and Z axes were 0.002g and 0.035g, respectively; hence, these accelerations were deemed negligible. The small accelerations in these directions indicate that the test setup was properly aligned as intended.

Shake table accelerations were recorded under the cap beam for redundancy in measuring the input ground motion. Figure 5.58 and Figure 5.59 show the comparison of these accelerations and the accelerations recorded by shake table internal instruments. There was good correlation between the measurements at the two locations, indicating that the shake table internal instruments were a reliable source of input ground motion

acceleration data. Accelerometers were also located at the north side of the cap beam web and the top of the loading head. Figure 5.60 and Figure 5.61 show the acceleration history for the cap beam at the web, and Figure 5.62 and Figure 5.63 show the acceleration history for the column. Table 5.18 lists the peak accelerations at each location for each run. The accelerometer on the cap beam web reached very similar peak accelerations as the accelerometer on the table surface. By comparison, the top of the column experienced smaller accelerations in the later runs because, once the column reinforcement yielded, it softened and could no longer transfer high accelerations from the table to the top of the column.

5.3.7. White Noise

In addition to the 11 earthquake runs simulated on the shake table, white noise motions with an amplitude of approximately 0.05g were applied before each earthquake motion and after the last motion. Because testing was conducted over two days, a white noise motion was conducted after run four on day one of testing (WN 5), and before run five on day two of testing (WN 5a). The specimen response during the white noise motions was used to estimate its fundamental period and damping ratio.

A FFT of the acceleration data at the top of the column was used to estimate the fundamental period. The single-sided Fourier amplitude spectrum of the column acceleration data was plotted for each white noise run. These plots showed noticeable peaks with characteristics of possible fundamental frequencies. The fundamental frequency and period were estimated from the peaks in these plots. The half-power bandwidth method was used to estimate the inherent damping ratio from these plots as well. Table 5.19 lists the fundamental period and damping ratio from each white noise test. The estimated period of the specimen in the early runs of testing showed good correlation with the hand calculation for cracked period of the specimen determined during the pre-test analysis (0.575 seconds). The damping ratios listed in Table 5.19 are lower than the damping ratio values typically used to model concrete bridge structures (e.g. 5 percent). This is because the test specimen was only a subassembly that excluded many bridge components that could contribute to the inherent damping.

Chapter 6.   Analytical   Studies   and   Design Recommendations

6.1. Introduction

Extensive analytical studies were conducted after shake table testing to determine the ability of analytical models to estimate the response of the specimen under seismic loading. The analytical model used in the post-test studies was the OpenSEES [14] three-dimensional model that was initially developed for the pre-test analysis. Modifications were made to the analytical model to reflect measured material properties and calibrate against testing results. The analytical results were compared with the measured shake table test data to assess adequacy of the modeling. Another objective of this phase of the study was to determine if the method to design the test model led to satisfactory performance and identify any necessary refinement of the method. This chapter presents recommendations for the design of CIP pocket connections in addition to the analytical studies.

6.2. Description of Analytical Models

The measured material properties discussed in Chapter 4 were used to update the constitutive properties for the Concrete01 and ReinforcingSteel material models used in the analysis. Tables 4.1 and 4.2 list the measured material properties for concrete and reinforcement. The input ground motion for the dynamic analysis was the filtered achieved acceleration data measured by the shake table internal sensors. The acceleration histories for each run were spliced together and 10 seconds of no motion was added after each run to allow for free vibration and for the motion to damp out to avoid one earthquake run affecting the response during the next earthquake. This reflects the actual testing program in which at least 15 minutes' pause existed between successive runs. Figure 6.1 shows the filtered achieved acceleration history that was applied in the post-test dynamic analysis.

The strain gauges attached to the cap beam longitudinal reinforcement revealed that this reinforcement did not yield during shake table testing. Because the cap beam remained elastic, i.e. capacity-protected, it was possible to simplify the cap beam element in the model. The cap beam was modeled as an elastic beam/column element instead of using a nonlinear fiber section in conjunction with a force-based element. The properties required for defining an elastic element in OpenSEES are: area, elastic and shear moduli, moment of inertia about the local y and z axes, and torsional moment of inertia. Changing the cap beam to an elastic element simplified the model for the post-test analysis.

Two versions of the model were developed to determine the effects of bond-slip at the base of the column on the calculated response of the specimen. One version of the model included the effects of bond-slip, and the other version did not. Both versions incorporated the modifications described above. Figure 6.2 shows the model used that did not include bond-slip effects, and Figure 6.3 shows the model that did include these effects. To include the effect of bond-slip in the model, the elastic modulus of column longitudinal reinforcement was reduced using the method described by Tazarv and Saiidi [20]. A new column fiber section was created that incorporated the reinforcement material model with reduced elastic modulus. The new column fiber section was applied only at the base of the column where bond-slip is expected. Dynamic analyses of both versions of the model were

conducted, and the results from these analyses were compared with the measured results from shake table testing.

6.3. Analytical Results

6.3.1. Comparison with Measured Results

The calculated displacement histories and peak responses for both versions of the model were compared to the measured results. The envelopes of the measured and calculated hysteresis curves were also compared. These envelopes present a measure of the pushover response of the structure under dynamic cyclic loads.

The calculated and measured displacement histories for each run are shown in Figure 6.4 through Figure 6.14. In the initial runs, where input accelerations were very low, both versions of the model overestimated the column top lateral displacement, shown in Figure 6.4 and Figure 6.5. However, by run three both versions of the model became much more accurate at predicting column response, and this trend continued through the remaining runs (Figure 6.6 through Figure 6.14). Figure 6.13 and Figure 6.14 show that the model with bond-slip effects underestimated the residual displacement in the column after runs 10 and 11. The model without bond-slip effects is able to better capture the residual displacement after runs 10 and 11. However, this version of the model also ultimately underestimated the residual displacement after run eleven.

The maximum measured and calculated displacement and base shear for each run were compared. Table 6.1 shows the comparison of measured and calculated displacements for both versions of the model. During runs one and two, both versions of the model overestimate the displacement in the column. The model with bond-slip effects had a softer initial stiffness which led to higher displacements in these runs. The percent difference between measured and calculated displacements for runs three through ten is reasonably low in both versions of the model. There was especially good correlation with the measured displacements during runs nine and ten for the version of the model with bond-slip effects. However, because the model without bond-slip effects was able to better estimate the residual displacement after run 10, this model led to significantly better correlation with the measured data in run eleven.

The measured and calculated base shears for both versions of the model are compared in

Table 6.2. The correlation trends in the base shears were similar to those of the displacements. In the first two runs, both versions of the model overestimated the base shear in the column. The percent difference between the measured and calculated data decreases in runs three through eleven. The differences in calculated base shears between the two versions of the model are smaller than the differences in calculated displacements because bond-slip does not affect lateral force capacity.

The envelopes for the measured and calculated data from both versions of the model were determined. The envelopes were calculated by averaging the envelopes of the hysteresis curves in the positive and negative displacement sides of the cumulative hysteresis loops. The measured and calculated envelopes are shown in Figure 6.15. There is good correlation among the three curves which all share a similar overall shape. The initial stiffness and peak base shears for the three curves are very similar. The model without the bond-slip effect has the largest initial stiffness, while the model with bond-slip has the lowest initial stiffness. The curve for the measured data has an initial stiffness that falls between these two versions of the model. The measured curve reaches the highest level of displacement, while the model with bond-slip effects reaches the lowest level of displacement. Because neither version of the model captured the large residual displacement after run 11, the maximum calculated displacement was lower than the measured peak displacement.

6.4. Design Recommendations

There were no design guidelines for the type of column-to-cap beam connection proposed and tested in this study. For this reason, the design was developed from a combination of the ABC pocket connections design recommendations proposed by Tazarv and Saiidi [1] and the AASHTO Guide Specifications for LRFD Seismic Bridge Design [13]. Some recommendations from the existing design guidelines had to be modified because the connection was different from typical ABC and CIP connections. Additionally, one design recommendation is unique to CIP pocket connections mimicking ABC pocket connection details. In light of the shake table performance of the test model, the connection design method was evaluated and summary design recommendations for CIP pocket connections mimicking ABC were developed. The key differences between the CIP pocket connection and a standard CIP joint were: (1) the bundling of cap beam longitudinal reinforcement, (2) the elimination of vertical joint reinforcement within the joint, and (3) the addition of transverse reinforcement adjacent to and near the joint.

The cap beam longitudinal reinforcement was bundled and placed outside of the joint area (Fig. 2.7), which allowed the column reinforcement to extend into the joint uninhibited. The bundled bars followed the requirements for bundled rebar described in Section 5.10.3.1.5 of the AASHTO LRFD Bridge Design Specification [11]. Because longitudinal reinforcement was bundled, additional bars were included to prevent the formation of temperature and shrinkage cracks (Fig. 2.7). These additional bars were designed in accordance with Section 5.10.6 of AASHTO [11] and terminated before the pocket connection. The test data showed that the bundled bars and the temperature and shrinkage reinforcement led to satisfactory performance with the former ensuring capacity-protected behavior for the beam and the latter controlling cracks.

Vertical bars normally used in CIP to resist shear forces were eliminated within the joint. Eliminating these ties improved constructability of the joint by removing bars that

36

would normally be threaded through the column reinforcement cage. The vertical ties adjacent to the joint did not experience a significant increase in demand due to the elimination of the vertical ties within the joint. The maximum tensile strain in the vertical ties adjacent to the joint was 488 microstrains, which is only 20 percent of yield strain. In addition to eliminating vertical ties within the joint, the horizontal ties used to enclose column stirrups where also removed to allow the column reinforcement cage to extend into the joint. The vertical and horizontal reinforcement that were eliminated within the joint are shown in Fig. 2.12. No overstressing of these bars was observed in the tests as indicated by the relatively small strains in these bars.

Because reinforcement was eliminated or bundled to accommodate the column reinforcement cage, additional transverse reinforcement was added around the pocket connection (Figs. 2.8 and 2.12). Transverse hoops encircling the pocket connection were added to provide confinement to the joint (Fig. 2.8). These hoops were only necessary in the upper half of the joint in the test model (would be over the lower half in a real bridge). The transverse reinforcement ratio of the hoops was the same as the column transverse reinforcement ratio per the design recommendations for pocket connections proposed by Tazarv and Saiidi [1]. The hoops reached a maximum tensile strain of 732 microstrains during testing, which is 30 percent of yield strain, indicating that these hoops were engaged in providing confinement to the joint and they are necessary. Horizontal ties perpendicular to the cap beam length were added in several layers adjacent to the joint as well (Fig. 2.12). The addition of these ties is not typical to the design of ABC pocket connections or CIP joints, but were included to address any prying forces. The horizontal ties were designed to match the same bar size, spacing, and number of bars as the vertical ties. The ties were placed in two layers on either side of the pocket. The maximum measured tensile strain in these ties was 1160 microstrains, which is 47 percent of yield. The relatively high strains in these bars confirm that they were engaged during testing and played a significant role in maintaining the structural integrity of the joint.

Some of the guidelines for the design of ABC pocket connections proposed by Tazarv and Saiidi [1] were not implemented because they did not apply to members that were not precast. The recommendations for depth and width of the pocket were not appropriate for determining the spacing between the column reinforcement cage and cap beam reinforcement because the cap beam was not precast. The column reinforcement cage was extended into the cap beam to provide adequate development for the longitudinal bars and to satisfy joint principle stress requirements. The embedment depth for the column reinforcement cage was 15 in. (381 mm), which is equivalent to 30 times bar diameter. There was also no specific required amount of spacing between the column reinforcement cage and the cap beam transverse reinforcement, but sufficient space was provided so that concrete could flow between the reinforcement. An opening above the cap beam pocket was not included because the pocket was not filled with grout. It was simply cast with conventional concrete during casting of the cap beam. The pocket was formed by arranging the cap beam reinforcement so that it did not interfere with the column reinforcement as it extended into the pocket. For this reason, it was also not necessary to form the pocket with a helical, lock-seam, corrugated steel pipe.

Chapter 7.   Summary and Conclusions

7.1. Summary

ABC allows the construction of bridges to be expedited for faster project delivery through the use of precast members. Joints between precast members are of particular interest to bridge designers because of the need to ensure structural integrity. The joints in bridges in moderate and high seismic areas have to also ensure ductile behavior of bridge columns in addition to maintaining structural integrity. Previous research has shown that ABC is a viable alternative to conventional bridge construction in areas of moderate and high seismic activity. Several types of ABC connections between precast members have been developed. Among these, pocket connections have been proven to meet these requirements while also substantially simplifying the design and construction of the bridge. In CIP bridge construction, cap beam to column joints can be difficult to construct because the beam reinforcement has to pass through the column reinforcement, and additional bars are required for the joint, which leads to congestion of reinforcement within the joint. This congestion can make construction difficult and time-consuming.

The main objective of this study was to adapt the design and detailing guidelines for ABC cap beam to column pocket connections for use in CIP bridge construction, with the ultimate objective of simplifying the design and construction of CIP joints. One large-scale laboratory specimen was built to evaluate the feasibility of designing and constructing an ABC column to cap beam pocket connection for use in CIP bridge construction and to investigate its seismic performance on a shake table. Because of a lack of past research data on out-of-plane seismic performance of pocket connections, the study was focused on the out-of-plane behavior of the CIP connections that emulate ABC connections.

A literature review was first conducted to compare the design of column to cap beam joints for CIP construction and the design of ABC column to cap beam pocket connections. A novel design for a CIP pocket connection was developed and incorporated in a 1/3 scale specimen representing components of a prototype bridge. The prototype was a CIP box girder bridge with an integral bent cap located in Carson City, Nevada. The CIP pocket connection details were developed by adapting preliminary guidelines for the design of ABC pocket connections. These guidelines are yet to be codified because the studies on ABC connections on seismic areas are still in progress. The specimen was composed of a column and cap beam arranged in an inverted T configuration. Inverting the column and cap beam simplified the out-of-plane testing. End blocks were attached to the cap beam to simulate the fixity provided by the longitudinal girders of the bridge superstructure. The bottom of the cap beam was clear from the shake table to allow for the cap beam to twist without bearing on the shake table.

Before finalizing the test specimen, an analytical model of the specimen was developed to estimate its response under dynamic loading. Several earthquake records were applied to the model to determine a loading protocol that would subject the specimen to high levels of demand leading to its eventual failure. The 1994 Northridge event recorded at the Sylmar Converter Station in the H1 component was selected for simulation in shake table testing. The specimen was subjected to eleven runs at increasing percentages of the design earthquake. The performance of the specimen was evaluated through strain, displacement, force, and acceleration data collected by 130 instruments during testing.

Subsequent to the tests and processing and interpretation of the data, the analytical model was updated, and extensive analytical studies were conducted to compare with the measured data from testing. Design recommendations for CIP pocket connections were developed based on the performance of joint reinforcement during seismic loading.

7.2. Conclusions

The following conclusions were drawn based on the results of this study:

1) The constructability of a CIP joint is improved by bundling cap beam longitudinal reinforcement and removing joint reinforcement to form a pocket. The CIP pocket connection allows the column reinforcement cage to extend into the joint without the need to thread column reinforcement through cap beam reinforcement. There is also no congestion of reinforcement because select cap beam transverse reinforcement is eliminated within the joint.

2) CIP emulating ABC pocket connections perform well under out-of-plane seismic loading and produce a similar response to traditional CIP connections. The large scale test model column reached high drift levels during shake table tests while the cap beam and joint remained capacity-protected. Ductility was provided through column reinforcement yielding in the plastic hinge zone.

3) The method used to design the CIP pocket connection leads to satisfactory performance in out-of-plane seismic loading and no refinement is necessary. Out-of-plane behavior is potentially more critical than in-plane behavior. Hence, the in-plane behavior is expected to be satisfactory as well. The following design recommendations are proposed to utilize in the design of CIP pocket connections:

    a) The cap beam bottom longitudinal reinforcement is bundled and placed outside the joint area. The bundled bars are designed according to the AASHTO LRFD Bridge Design Specifications. Additional longitudinal reinforcement is included outside the joint area to prevent temperature and shrinkage cracks. This temperature/shrinkage reinforcement is designed per the AASHTO LRFD Bridge Design Specifications.

    b) Select transverse reinforcement normally used within CIP cap beam-column joints is removed to allow the column reinforcement cage to extend into the joint uninhibited. The bars removed are vertical shear ties and horizontal ties used to enclose stirrups. The measured data showed that eliminating the joint bars did not place any additional demand on the vertical ties adjacent to the joint.

    c) Transverse reinforcement is added adjacent to and near the joint region. Transverse hoops that encircle the pocket connection are included in the design. These hoops have the same transverse reinforcement ratio as the column transverse reinforcement ratio and are only necessary in the lower half of the cap beam. Horizontal ties perpendicular to the axis of the cap beam are added adjacent to the joint. These bars are included to resist prying forces and are added in two layers on either side of the joint. The horizontal ties match the same bar size, spacing, and number of bars as the vertical shear ties.

    d) No specific recommendations are needed for depth and width of the pocket because the cap beam is not precast. The column reinforcement extends into the joint to provide adequate embedment and satisfy principal stress requirements. There is no specific required spacing between the column reinforcement cage and cap beam

reinforcement, but sufficient space is provided so that concrete can flow between the reinforcement.

e) Corrugated steel pipes or other types are not needed to form the pocket because the pocket is formed by arranging the cap beam reinforcement so that it does not interfere with the column reinforcement.

4) Relatively simple analytical models can adequately estimate the response of the specimen under seismic loading. The column should be modeled as a force-based element while the cap beam can be idealized as an elastic element. Including bond-slip effects in the analytical model improves the accuracy of the model when residual displacement is low.

References

[1]   Tazarv, M., Saiidi, M. (2015) "Design and Construction of Precast Bent Caps with Pocket Connections for High Seismic Regions." Center for Civil Engineering Earthquake Research, Department of Civil and Environmental Engineering, University of Nevada, Reno, Report No. CCEER 15-06.

[2]   Mohebbi, A., Saiidi, M., and Itani, A. (2017). "Development and Seismic Evaluation of Pier Systems w/Pocket Connections, CFRP Tendons, and ECC/UHPC Columns." Center for Civil Engineering Earthquake Research, Department of Civil and Environmental Engineering, University of Nevada, Reno, Report No. CCEER-17-02.

[3]   Mehrsoroush, A., Saiidi, M., and Ryan, K. (2017). "Development of Earthquake-Resistant Precast Pier Systems for Accelerated Bridge Construction in Nevada." Center for Civil Engineering Earthquake Research, Department of Civil and Environmental Engineering, University of Nevada, Reno, Report No. CCEER-17-03.

[4]   Haber, Z., Saiidi, M., and Sanders, D. (2013). "Precast Column-Footing Connections for Accelerated Bridge Construction in Seismic Zones." Center for Civil Engineering Earthquake Research, Department of Civil and Environmental Engineering, University of Nevada, Reno, Report No. CCEER-13-08.

[5]   Matsumoto, E. E., Waggoner, M. C., Sumen, G., and Kreger, M. E. (2001). "Development of a Precast Bent Cap System." Center for Transportation Research, University of Texas at Austin, Report No. FHWA/TX-0-1748-2.

[6]   Mehraein, M., Saiidi, M. (2016) "Seismic Performance of Bridge Column-Pile-Shaft Pin Connections for Application in Accelerated Bridge Construction." Center for Civil Engineering Earthquake Research, Department of Civil and Environmental Engineering, University of Nevada, Reno, Report No. CCEER 16-01.

[7]   Zhu, Z., Ahmad, I., and Mirmiran, A. (2006). "Seismic Performance of Concrete-Filled FRP Tube Columns for Bridge Substructure." Journal of Bridge Engineering, 11(3), 359-370.

[8]   Motaref, S., Saiidi, M., and Sanders, D. (2011) "Seismic Response of Precast Bridge Columns with Energy Dissipating Joints." Center for Civil Engineering Earthquake Research, Department of Civil and Environmental Engineering, University of Nevada, Reno, Report No. CCEER 11-01.

[9]   Haraldsson, O. S., Janes, T. M., Eberhard, M. O., and Stanton, J. F. (2013). "Seismic Resistance of Socket Connection between Footing and Precast Column." Journal of Bridge Engineering, 18(9), 910-919.

[10]   Larosche, A., Cukrov, M., Sanders, D., and Ziehl, P. (2013). "Prestressed Pile to Bent Cap Connections: Seismic Performance of a Full-Scale Three-Pile Specimen." Journal of Bridge Engineering, 19(3), 04013012.

[11] American Association of State Highway and Transportation Officials (AASHTO) (2017). "AASHTO LRFD Bridge Design Specifications (8th Ed.)," Washington, D.C.

[12] Tran, H. V., and Stanton, J. F. (2015). "Drilled Shaft Socket Connections for Precast Columns in Seismic Regions (Doctoral dissertation)". Retrieved from ProQuest Dissertations and Theses database. (UMI No. 3688978)

[13] American Association of State Highway and Transportation Officials (AASHTO) (2011). "AASHTO Guide Specifications for LRFD Seismic Bridge Design (2nd Ed.)," Washington, D.C.

[14] OpenSees (2016) [Computer software]. Berkeley, CA, Pacific Earthquake Engineering Research Center, Univ. of California–Berkeley.

[15] SAP2000, CSI Computer & Structures Inc. Linear and nonlinear static and dynamic analysis of three-dimensional structures. Berkeley (CA): Computer & Structures, Inc., V18.1.1, 2018.

[16] ACI Committee 318 (2014). "Building Code Requirements for Structural Concrete (ACI 318-14) and Commentary (ACI 318R-14)," American Concrete Institute, Farmington Hills, MI.

[17] Mander, J. B., Priestley, M. J. N., and Park, R. (1988). Theoretical stress strain model for confined concrete. Journal of Structural Engineering, 114(8), 1804–1826.

[18] PEER. (2014). Pacific Earthquake Engineering Research Center (PEER) Ground Motion Database. Retrieved from https://ngawest2.berkeley.edu/

[19] ASTM International, (2017) "Standard Test Methods and Definitions for Mechanical Testing of Steel Products." A370-17a, West Conshohocken, PA.

[20] Tazarv, M., Saiidi, M. (2014) "Next Generation of Bridge Columns for Accelerated Bridge Construction in High Seismic Zones." Center for Civil Engineering Earthquake Research, Department of Civil and Environmental Engineering, University of Nevada, Reno, Report No. CCEER 14-06.

Chapter 2 Tables

Table 2.1 Column design properties

Scale Factor	1/3
Column diameter, inch (mm)	16 (406)
Column clear height, inch (mm)	80 (2032)
Cover, inch (mm)	0.75 (19)
Column longitudinal bar, US size (mm)	16 - #4 (Ø13)
Column long. steel ratio	1.59%
Column transverse steel, US size, inch (mm)	#3 @ 2.25 (Ø9.5 @ 57)
Column transverse steel ratio	1.35%

Table 2.2 Moment-curvature results with axial load

	SAP2000	OpenSEES	Difference, %
M_y, kip-in (kN-mm)	1196 (135119)	1190 (134395)	0.5
φ_y, rad/in (rad/mm)	0.00025679 (0.0000101)	0.00027138 (0.0000107)	5.7
M_p, kip-in (kN-mm)	1685 (190097)	1703 (192216)	1.1
φ_p, rad/in (rad/mm)	0.000362 (0.0000142)	0.000389 (0.0000153)	7.4

Table 2.3 Moment-curvature results without axial load

	SAP2000	OpenSEES	Difference, %
M_y, kip-in (kN-mm)	868 (97978)	890 (100478)	2.5
φ_y, rad/in (rad/mm)	0.000232 (0.00000912)	0.000239 (0.00000943)	3.3
M_p, kip-in (kN-mm)	1421 (160357)	1428 (161169)	0.5
φ_p, rad/in (rad/mm)	0.000379 (0.0000149)	0.000384 (0.0000151)	1.3

Chapter 3 Tables

Table 3.1 Column reinforcing steel properties

f_y, ksi	68
(MPa)	(469)
f_u, ksi	95
(MPa)	(655)
E_s, ksi	29000
(MPa)	(199948)
ε_{sh}	0.015
ε_{su}	0.12

Table 3.2 Column concrete properties

	Confined	Unconfined
f'_c, ksi	-7.84	-5.2
(MPa)	(-54.1)	(-36.9)
ε_{c0}	-0.0073	-0.002
f'cu, ksi	-6.96	0
(MPa)	(-48.0)	(0)
ε_{cu}	-0.0174	-0.005

Table 3.3 Cap beam reinforcing steel properties

f_y, ksi	60
(MPa)	(414)
f_u, ksi	90
(MPa)	(621)
E_s, ksi	29000
(MPa)	(199948)
ε_{sh}	0.015
ε_{su}	0.12

Table 3.4 Cap beam concrete properties

	Confined	Unconfined
f'_c, ksi	-5.67	-4.5
(MPa)	(-39.1)	(-31.0)
ε_{c0}	-0.006	-0.002
f'cu, ksi	-3.20	0
(MPa)	(-22.1)	(0)
ε_{cu}	-0.015	-0.005

Table 3.5 Earthquake records considered in pre-test analysis

Event Name	Station Name	Year	Component	Scale Factor Used	Correct Scale Factor
Hollister-01	Hollister City Hall	1961	H1	2.42	4.09
Imperial Valley-02	El Centro Array #9	1940	H1	1.02	1.06
Kern County	Taft Lincoln School	1952	H1	2.14	2.80
Lytle Creek	Wrightwood - 6074 Park Dr	1970	H1	2.30	5.23
San Fernando	LA - Hollywood Stor FF	1971	H1	2.14	2.02
Northern Calif-03	Ferndale City Hall	1954	H1	1.67	1.89
Northridge-01	Sylmar - Converter Sta	1994	H1	0.41	0.37
Northridge-01	Sylmar - Converter Sta	1994	H2	0.41	0.36
Loma Prieta	Gilroy - Gavilan Coll	1989	H1	1.30	2.07

Table 3.6 Loading protocol details

Run #	Test Type	PGA (g)	Factor	Drift (%)
WN 1	White Noise			
1	Sylmar - H1	0.06	0.08	0.85
WN 1	White Noise			
2	Sylmar - H1	0.13	0.20	1.71
WN 1	White Noise			
3	Sylmar - H1	0.25	0.41	2.35
WN 1	White Noise			
4	Sylmar - H1	0.38	0.61	2.85
WN 1	White Noise			
5	Sylmar - H1	0.51	0.81	4.48
WN 1	White Noise			
6	Sylmar - H1	0.63	1.02	6.60
WN 1	White Noise			
7	Sylmar - H1	0.76	1.22	8.89
WN 1	White Noise			

Table 3.7 Predicted maximum displacement and base shear

Run #	Test Type	Drift, %	Max. Disp., in (mm)	Base Shear at Max. Disp., kips (kN)
1	Sylmar - H1	0.85	0.68 (17)	10.14 (45)
2	Sylmar - H1	1.71	1.37 (35)	14.38 (64)
3	Sylmar - H1	2.35	1.88 (48)	14.73 (66)
4	Sylmar - H1	2.85	2.28 (58)	15.48 (69)
5	Sylmar - H1	4.48	3.58 (91)	17.24 (77)
6	Sylmar - H1	6.60	5.28 (134)	17.55 (78)
7	Sylmar - H1	8.89	7.11 (181)	17.66 (79)

Chapter 4 Tables

Table 4.1 Concrete test results

	7-day, ksi (MPa)	28-day, ksi (MPa)	Test day, ksi (MPa)	Test day age, days
Cap Beam and End Blocks	3.83 (26.4)	4.75 (32.8)	5.81 (40.1)	57
Column and Loading Head	3.94 (27.2)	5.20 (35.9)	6.18 (42.6)	46

Table 4.2 Reinforcement test results

Bar Size	f_y , ksi (MPa)	f_u , ksi (MPa)	ε_y , in/in	ε_{sh} , in/in	ε_u , in/in
#3	63.1 (435)	89.1 (614)	0.00246	0.0123	0.1292
#4	69.0 (476)	96.7 (667)	0.00292	0.0100	0.1298
#5	64.3 (444)	106.8 (737)	0.00171	0.0058	0.1006

Chapter 5 Tables

Table 5.1 Target and achieved peak ground accelerations

Run No.	Peak Ground Acceleration, PGA, g		Difference, %
	Target	Achieved	
Run 1	0.05	0.03	45.64
Run 2	0.13	0.09	32.42
Run 3	0.25	0.21	14.36
Run 4	0.38	0.31	18.41
Run 5	0.51	0.44	13.48
Run 6	0.63	0.55	12.87
Run 7	0.76	0.66	13.76
Run 8	0.89	0.76	14.61
Run 9	1.14	0.93	18.15
Run 10	1.39	1.17	15.93
Run 11	1.65	1.45	12.16

Table 5.2 Predicted and achieved spectral accelerations

Run No.	Spectral Acceleration, S_a, g		Difference, %
	Predicted	Achieved	
Run 1	0.13	0.05	58.56
Run 2	0.28	0.10	62.53
Run 3	0.31	0.29	5.72
Run 4	0.30	0.34	13.71
Run 5	0.48	0.34	28.74
Run 6	0.59	0.43	27.47
Run 7	0.71	0.51	29.12
Run 8	0.83	0.59	28.65
Run 9	1.07	0.77	28.33
Run 10	1.31	0.92	29.48
Run 11	1.55	1.09	29.29

Table 5.3 Measured energy dissipation

Run No.	Energy Dissipation, k-in (kN-m)
Run 1	0.45 (0.05)
Run 2	3.08 (0.35)
Run 3	32.08 (3.62)
Run 4	85.44 (9.65)
Run 5	138.98 (15.70)
Run 6	203.84 (23.03)
Run 7	279.75 (31.61)
Run 8	368.82 (41.67)
Run 9	491.85 (55.57)
Run 10	647.63 (73.17)
Run 11	843.81 (95.34)

Table 5.4 Column residual displacement

Run No.	Residual Displacement, in (mm)
Run 1	0.01 (0.4)
Run 2	0.02 (0.5)
Run 3	0.20 (5.1)
Run 4	0.25 (6.4)
Run 5	0.12 (3.0)
Run 6	0.21 (5.2)
Run 7	0.22 (5.6)
Run 8	0.06 (1.5)
Run 9	-0.48 (-12.1)
Run 10	-1.73 (-43.8)
Run 11	-4.42 (-112.3)

Table 5.5 Measured maximum drifts, displacements, and forces

Run No.	Max. Drift Ratio, %	Max. Column Disp, in. (mm)	Max. Base Shear, kips (kN)
Run 1	0.11	0.10 (2.5)	2.12 (9.4)
Run 2	0.49	0.44 (11.2)	5.12 (22.8)
Run 3	2.07	1.86 (47.3)	14.24 (63.3)
Run 4	3.12	2.81 (71.3)	15.88 (70.6)
Run 5	3.65	3.29 (83.5)	15.74 (70.0)
Run 6	4.34	3.91 (99.3)	16.16 (71.9)
Run 7	4.79	4.31 (109.6)	16.29 (72.4)
Run 8	5.11	4.60 (116.7)	16.14 (71.8)
Run 9	5.61	5.04 (128.1)	16.11 (71.7)
Run 10	5.81	5.23 (132.7)	15.85 (70.5)
Run 11	7.75	6.97 (177.1)	16.57 (73.7)

Table 5.6 Cap beam twist contribution to column displacement

Run No.	Column Displacement, in (mm)		Cap Beam Twist Contribution, Percent
	Due to Cap Beam Twist	Overall	
Run 1	0.01 (0.3)	0.10 (2.5)	11.38
Run 2	0.03 (0.7)	0.44 (11.2)	6.38
Run 3	0.11 (2.7)	1.86 (47.3)	5.69
Run 4	0.15 (3.8)	2.81 (71.3)	5.31
Run 5	0.16 (4.2)	3.29 (83.5)	5.01
Run 6	0.18 (4.7)	3.91 (99.3)	4.68
Run 7	0.20 (5.0)	4.31 (109.6)	4.56
Run 8	0.20 (5.2)	4.60 (116.7)	4.44
Run 9	0.21 (5.4)	5.04 (128.1)	4.21
Run 10	0.22 (5.7)	5.23 (132.7)	4.29
Run 11	0.27 (6.7)	6.97 (177.1)	3.81

Table 5.7 Column longitudinal reinforcement strain data (values reported in microstrains)

Location	Column, 9" (229 mm) Inside Cap Beam										
Gauge No.	SG 1		SG 2		SG 3		SG 4		SG 5		SG 6	
Bar Type	Longitudinal		Longitudinal		Longitudinal		Longitudinal		Longitudinal		Longitudinal	
Run No.	Max	Min	Max	Min	Max	Min	Max	Min	Max	Min	Max	Min
Run 1	32.1	-38.5	-6.4	-121.9	32.1	-57.8	47.5	-33.9	40.7	-40.7	47.5	-27.1
Run 2	77.0	-103.0	160.0	-629.0	270.0	-995.0	88.2	-129.0	74.6	-95.0	81.4	-74.6
Run 3	962.0	-1460.0	1050.0	-2430.0	1010.0	-2170.0	753.0	-1310.0	746.0	-1130.0	726.0	-1020.0
Run 4	1320.0	-1920.0	1580.0	-2790.0	1450.0	-2500.0	1230.0	-1860.0	1180.0	-1720.0	1130.0	-1570.0
Run 5	1390.0	-2190.0	1870.0	**-3050.0**	1700.0	-2730.0	-	-	1420.0	-1930.0	1330.0	-1780.0
Run 6	1490.0	-2320.0	2100.0	**-3360.0**	1880.0	-2860.0	-	-	1530.0	-2050.0	1420.0	-1880.0
Run 7	1570.0	-2420.0	2820.0	**-6010.0**	2040.0	**-2960.0**	-	-	1550.0	-2150.0	1450.0	-1970.0
Run 8	6400.0	-	2840.0	**-13100.0**	2160.0	**-3230.0**	-	-	-	-	-	-
Run 9	19500.0	-	2110.0	**-14500.0**	2380.0	**-4110.0**	-	-	-	-	-	-
Run 10	27500.0	-	2890.0	-	-	-	-	-	-	-	-	-
Run 11	-	-	-	-	-	-	-	-	-	-	-	-

Location	Column, 4.5" (114 mm) Inside Cap Beam										
Gauge No.	SG 15		SG 16		SG 17		SG 18		SG 19		SG 20	
Bar Type	Longitudinal		Longitudinal		Longitudinal		Longitudinal		Longitudinal		Longitudinal	
Run No.	Max	Min	Max	Min	Max	Min	Max	Min	Max	Min	Max	Min
Run 1	77.0	-89.8	44.9	-186.2	-	-	-	-	94.9	-67.8	54.2	-94.9
Run 2	244.0	-520.0	257.0	-783.0	-	-	-	-	264.0	-400.0	210.0	-413.0
Run 3	1480.0	-2480.0	1370.0	-2880.0	-	-	-	-	1140.0	-1940.0	1040.0	-2140.0
Run 4	1950.0	-2710.0	2140.0	**-4400.0**	-	-	-	-	1650.0	-2360.0	1480.0	-2510.0
Run 5	2720.0	**-7330.0**	2020.0	**-13600.0**	-	-	-	-	1950.0	-2550.0	1730.0	-2690.0
Run 6	2450.0	**-8860.0**	1590.0	**-15200.0**	-	-	-	-	2180.0	-2700.0	1860.0	-2790.0
Run 7	-738.0	-2860.0	1690.0	**-16200.0**	-	-	-	-	-	-	-	-
Run 8	-	-	1710.0	**-17000.0**	-	-	-	-	-	-	-	-
Run 9	-	-	-	-	-	-	-	-	-	-	-	-
Run 10	-	-	-	-	-	-	-	-	-	-	-	-
Run 11	-	-	-	-	-	-	-	-	-	-	-	-

Table 5.8 (continued) Column longitudinal reinforcement strain data (values reported in microstrains)

Location	Column, At Cap Beam Face											
Gauge No.	SG 29		SG 30		SG 31		SG 32		SG 33		SG 34	
Bar Type	Longitudinal		Longitudinal		Longitudinal		Longitudinal		Longitudinal		Longitudinal	
Run No.	Max	Min	Max	Min	Max	Min	Max	Min	Max	Min	Max	Min
Run 1	224.7	-487.9	192.5	-615.9	-	-	-	-	94.9	-67.8	54.2	-94.9
Run 2	526.0	-1530.0	430.0	-1480.0	-	-	-	-	264.0	-400.0	210.0	-413.0
Run 3	725.0	**-4350.0**	648.0	**-17000.0**	-	-	-	-	1140.0	-1940.0	1040.0	-2140.0
Run 4	424.0	-1640.0	**-4090.0**	**-20100.0**	-	-	-	-	1650.0	-2360.0	1480.0	-2510.0
Run 5	398.0	-1620.0	**-4710.0**	**-26200.0**	-	-	-	-	1950.0	-2550.0	1730.0	-2690.0
Run 6	334.0	-1680.0	**-5430.0**	**-30500.0**	-	-	-	-	2180.0	-2700.0	1860.0	-2790.0
Run 7	295.0	-1770.0	**-6770.0**	**-33900.0**	-	-	-	-	-	-	-	-
Run 8	212.0	-1770.0	**-7370.0**	**-37300.0**	-	-	-	-	-	-	-	-
Run 9	160.0	-1930.0	**-8620.0**	**-42900.0**	-	-	-	-	-	-	-	-
Run 10	128.0	-2100.0	-	-	-	-	-	-	-	-	-	-
Run 11	38.5	-2200.0	-	-	-	-	-	-	-	-	-	-

Location	Column, 6" (152 mm) Above Cap Beam											
Gauge No.	SG 39		SG 40		SG 41		SG 42		SG 43		SG 44	
Bar Type	Longitudinal		Longitudinal		Longitudinal		Longitudinal		Longitudinal		Longitudinal	
Run No.	Max	Min	Max	Min	Max	Min	Max	Min	Max	Min	Max	Min
Run 1	89.9	-205.4	115.5	-186.2	96.3	-186.3	-	-	169.5	-101.7	162.6	-128.7
Run 2	334.0	-1440.0	424.0	-1550.0	321.0	-1400.0	-	-	447.0	-1290.0	413.0	-1270.0
Run 3	693.0	**-13400.0**	790.0	**-18700.0**	597.0	**-18700.0**	-	-	1150.0	**-12400.0**	1630.0	**-3440.0**
Run 4	372.0	**-8810.0**	-1440.0	**-21200.0**	**-2990.0**	**-20100.0**	-	-	1550.0	**-17200.0**	2130.0	**-19800.0**
Run 5	533.0	**-5030.0**	-2140.0	**-26400.0**	**-3260.0**	**-23400.0**	-	-	217.0	**-20200.0**	-1110.0	**-19500.0**
Run 6	1750.0	**-3330.0**	-2730.0	**-30500.0**	**-3290.0**	**-26000.0**	-	-	-664.0	**-22200.0**	-1730.0	**-20900.0**
Run 7	-	-	**-3910.0**	**-34000.0**	**-3980.0**	**-28200.0**	-	-	-1790.0	**-24900.0**	-2440.0	**-23300.0**
Run 8	-	-	**-4670.0**	**-36900.0**	**-4470.0**	**-30400.0**	-	-	-2450.0	**-27400.0**	**-3300.0**	**-26300.0**
Run 9	-	-	**-4900.0**	**-39400.0**	**-4800.0**	**-34500.0**	-	-	**-3920.0**	**-31800.0**	**-4800.0**	**-32700.0**
Run 10	-	-	-	-	**-5590.0**	**-36700.0**	-	-	**-4550.0**	**-35200.0**	**-8080.0**	**-40700.0**
Run 11	-	-	-	-	**-5060.0**	**-36100.0**	-	-	**-11400.0**	**-49800.0**	-	**-51600.0**

Table 5.9 (continued) Column longitudinal reinforcement strain data (values reported in microstrains)

Location	Column, 12" (305 mm) Above Cap Beam											
Gauge No.	SG 49		SG 50		SG 51		SG 52		SG 53		SG 54	
Bar Type	Longitudinal		Longitudinal		Longitudinal		Longitudinal		Longitudinal		Longitudinal	
Run No.	Max	Min	Max	Min	Max	Min	Max	Min	Max	Min	Max	Min
Run 1	-	-	89.9	-353.2	83.4	-269.6	162.7	-122.0	155.9	-142.3	162.6	-162.6
Run 2	-	-	462.0	-1520.0	347.0	-1270	386.0	-1190.0	413.0	-1320.0	400.0	-1270.0
Run 3	-	-	815.0	**-17200**	956.0	**-12500**	220000.0	**-224000**	1060.0	**-7630**	1400.0	**-3270.0**
Run 4	-	-	-2720.0	**-19500**	-1940.0	**-15100**	220000.0	**-224000**	1690.0	**-14700**	1780.0	**-3420.0**
Run 5	-	-	-2850.0	**-19900**	-1950.0	**-14800**	-2170.0	**-6560**	-1090.0	**-14200**	2070.0	**-3690.0**
Run 6	-	-	-2740.0	**-21900**	-1950.0	**-15900**	**-3010.0**	**-9480**	-1380.0	**-13600**	2260.0	**-3920.0**
Run 7	-	-	-2730.0	**-23800**	-1620.0	**-16600**	**-4100.0**	**-26900**	-1900.0	**-14600**	2540.0	**-4950.0**
Run 8	-	-	-2420.0	**-25000**	-1120.0	**-17300**	**-6570.0**	**-38600**	-1270.0	**-16100**	2490.0	**-12400.0**
Run 9	-	-	-1980.0	**-27600**	-777.0	**-18600**	**-4280.0**	**-120000**	-2630.0	**-22300**	-	-
Run 10	-	-	-1910.0	**-28700**	-597.0	**-19000**	-	-	-	-	-	-
Run 11	-	-	-1860.0	**-27600**	-430.0	**-18500**	-	-	-	-	-	-

Location	Column, 18" (457 mm) Above Cap Beam			
Gauge No.	SG 59		SG 60	
Bar Type	Longitudinal		Longitudinal	
Run No.	Max	Min	Max	Min
Run 1	102.7	-102.7	-	-
Run 2	270.0	-995.0	-	-
Run 3	777.0	**-3160.0**	-	-
Run 4	674.0	**-12600.0**	-	-
Run 5	**-3720.0**	**-13000.0**	-	-
Run 6	**-4050.0**	**-14300.0**	-	-
Run 7	**-4510.0**	**-14900.0**	-	-
Run 8	**-4620.0**	**-15300.0**	-	-
Run 9	**-4320.0**	**-15700.0**	-	-
Run 10	**-3930.0**	**-15500.0**	-	-
Run 11	**-3590.0**	**-14300.0**	-	-

Table 5.10 Column transverse reinforcement strain data (values reported in microstrains)

Location	Column, 9" (229 mm) Inside Cap Beam							
Gauge No.	SG 7		SG 8		SG 9		SG 10	
Bar Type	Transverse		Transverse		Transverse		Transverse	
Run No.	Max	Min	Max	Min	Max	Min	Max	Min
Run 1	25.66	-25.66	12.83	-44.90	-	-	13.56	-33.90
Run 2	25.70	-25.70	6.41	-57.70	-	-	20.30	-54.20
Run 3	25.70	-128.00	0.00	-128.00	-	-	13.60	-149.00
Run 4	-25.70	-205.00	-38.50	-186.00	-	-	-33.90	-203.00
Run 5	-64.20	-282.00	-64.10	-378.00	-	-	-74.60	-251.00
Run 6	-77.00	-372.00	-	-	-	-	-	-
Run 7	-89.80	-456.00	-	-	-	-	-	-
Run 8	-103.00	-545.00	-	-	-	-	-	-
Run 9	-	-	-	-	-	-	-	-
Run 10	-	-	-	-	-	-	-	-
Run 11	-	-	-	-	-	-	-	-

Location	Column, 4.5" (114 mm) Inside Cap Beam							
Gauge No.	SG 21		SG 22		SG 23		SG 24	
Bar Type	Transverse		Transverse		Transverse		Transverse	
Run No.	Max	Min	Max	Min	Max	Min	Max	Min
Run 1	6.77	-33.87	38.48	-25.65	13.55	-33.88	0.00	-47.43
Run 2	6.77	-40.60	38.50	-32.10	13.60	-47.40	6.78	-81.30
Run 3	0.00	-196.00	25.70	-224.00	20.30	-196.00	-6.78	-278.00
Run 4	-61.00	-278.00	-19.20	-430.00	-74.50	-285.00	-13.60	-373.00
Run 5	-40.60	-332.00	-	-1440.00	-94.90	-339.00	-74.50	-481.00
Run 6	-	-332.00	-	-	-81.30	-373.00	-122.00	-549.00
Run 7	-	-	-	-	-74.50	-386.00	-	-
Run 8	-	-	-	-	-67.80	-400.00	-	-
Run 9	-	-	-	-	-	-	-	-
Run 10	-	-	-	-	-	-	-	-
Run 11	-	-	-	-	-	-	-	-

Table 5.11 (continued) Column transverse reinforcement strain data (values reported in microstrains)

Location	Column, At Cap Beam Face							
Gauge No.	SG 35		SG 36		SG 37		SG 38	
Bar Type	Transverse		Transverse		Transverse		Transverse	
Run No.	Max	Min	Max	Min	Max	Min	Max	Min
Run 1	0.00	-47.41	25.67	-44.92	-6.77	-67.71	0.00	-54.19
Run 2	-6.77	-115.00	25.70	-109.00	-20.30	-122.00	0.00	-183.00
Run 3	-40.60	-433.00	19.20	-411.00	-40.60	-460.00	20.30	-393.00
Run 4	-33.90	-481.00	51.30	-654.00	-88.00	-724.00	-20.30	-427.00
Run 5	-	-	70.60	-2180.00	-67.70	-745.00	-54.20	-379.00
Run 6	-	-	-	-	-47.40	-704.00	-67.70	-386.00
Run 7	-	-	-	-	-54.20	-664.00	-	-
Run 8	-	-	-	-	-33.90	-623.00	-	-
Run 9	-	-	-	-	13.50	-576.00	-	-
Run 10	-	-	-	-	-	-	-	-
Run 11	-	-	-	-	-	-	-	-

Location	Column, 6" (152 mm) Above Cap Beam							
Gauge No.	SG 45		SG 46		SG 47		SG 48	
Bar Type	Transverse		Transverse		Transverse		Transverse	
Run No.	Max	Min	Max	Min	Max	Min	Max	Min
Run 1	27.10	-27.10	19.26	-38.51	6.42	-51.34	-20.34	-81.37
Run 2	13.50	-108.00	6.42	-141.00	0.00	-116.00	-27.10	-258.00
Run 3	-40.60	-203.00	0.00	-295.00	-44.90	-154.00	-108.00	-448.00
Run 4	-115.00	-406.00	-19.30	-514.00	-64.20	-327.00	-136.00	-617.00
Run 5	-196.00	-535.00	-25.70	-732.00	-160.00	-379.00	-251.00	-692.00
Run 6	-237.00	-549.00	-64.20	-1030.00	-193.00	-411.00	-258.00	-692.00
Run 7	-217.00	-617.00	-57.80	-1140.00	-218.00	-443.00	-217.00	-773.00
Run 8	-176.00	-623.00	-83.40	-1170.00	-237.00	-590.00	-190.00	-861.00
Run 9	-176.00	-766.00	-96.30	-1290.00	-250.00	-847.00	-190.00	-1040.00
Run 10	-156.00	-908.00	-96.30	-1330.00	-205.00	-995.00	-156.00	-1240.00
Run 11	-210.00	-881.00	-96.30	-1280.00	-122.00	-975.00	-170.00	-1290.00

Table 5.12 (continued) Column transverse reinforcement strain data (values reported in microstrains)

Location	Column, 12" (305 mm) Above Cap Beam							
Gauge No.	SG 55		SG 56		SG 57		SG 58	
Bar Type	Transverse		Transverse		Transverse		Transverse	
Run No.	Max	Min	Max	Min	Max	Min	Max	Min
Run 1	13.55	-33.88	6.42	-57.80	51.32	-12.83	13.54	-47.39
Run 2	6.78	-136.00	12.80	-270.00	57.70	-89.80	6.77	-102.00
Run 3	-54.20	-325.00	-77.10	-315.00	25.70	-237.00	-67.70	-203.00
Run 4	-136.00	-400.00	-83.50	-244.00	-70.60	-417.00	-88.00	-250.00
Run 5	-203.00	-501.00	-64.20	-206.00	-141.00	-398.00	-47.40	-257.00
Run 6	-210.00	-603.00	-32.10	-206.00	-148.00	-443.00	-47.40	-298.00
Run 7	-230.00	-705.00	25.70	-225.00	-135.00	-539.00	-40.60	-325.00
Run 8	-230.00	-806.00	77.10	-231.00	-115.00	-597.00	-33.80	-379.00
Run 9	-230.00	-820.00	135.00	-276.00	-83.40	-622.00	0.00	-494.00
Run 10	-217.00	-827.00	186.00	-366.00	-44.90	-603.00	20.30	-508.00
Run 11	-136.00	-922.00	180.00	-520.00	-32.10	-699.00	27.10	-420.00

Table 5.13 Hoops encircling pocket connection strain data (values reported in microstrains)

Location	Cap Beam, 9" (229 mm) Inside Beam							
Gauge No.	SG 11		SG 12		SG 13		SG 14	
Bar Type	Transverse		Transverse		Transverse		Transverse	
Run No.	Max	Min	Max	Min	Max	Min	Max	Min
Run 1	-128.87	-176.34	19.24	-32.06	40.67	-6.78	0.00	-47.45
Run 2	-129.00	-176.00	19.20	-44.90	47.40	-6.78	6.78	-54.20
Run 3	-129.00	-244.00	19.20	-128.00	40.70	-47.50	0.00	-115.00
Run 4	-156.00	-312.00	-12.80	-192.00	20.30	-298.00	-33.90	-149.00
Run 5	-183.00	-380.00	-38.50	-192.00	-88.10	-461.00	-47.40	-169.00
Run 6	-210.00	-515.00	-57.70	-205.00	-129.00	-563.00	-61.00	-197.00
Run 7	-244.00	-577.00	-83.40	-244.00	-156.00	-664.00	-67.80	-230.00
Run 8	-265.00	-624.00	-103.00	-276.00	-183.00	-732.00	-88.10	-251.00
Run 9	-	-	-	-	-	-	-	-
Run 10	-	-	-	-	-	-	-	-
Run 11	-	-	-	-	-	-	-	-

Location	Cap Beam, 4.5" (114 mm) Inside Beam							
Gauge No.	SG 25		SG 26		SG 27		SG 28	
Bar Type	Transverse		Transverse		Transverse		Transverse	
Run No.	Max	Min	Max	Min	Max	Min	Max	Min
Run 1	-	-	51.38	0.00	-	-	6.78	-40.68
Run 2	-	-	51.40	-6.42	-	-	6.78	-61.00
Run 3	-	-	51.40	-193.00	-	-	-6.78	-305.00
Run 4	-	-	0.00	-366.00	-	-	-108.00	-468.00
Run 5	-	-	-	-	-	-	-156.00	-495.00
Run 6	-	-	-	-	-	-	-	-
Run 7	-	-	-	-	-	-	-	-
Run 8	-	-	-	-	-	-	-	-
Run 9	-	-	-	-	-	-	-	-
Run 10	-	-	-	-	-	-	-	-
Run 11	-	-	-	-	-	-	-	-

Table 5.14 Cap beam transverse reinforcement strain data (values reported in microstrains)

Location	Cap Beam														
Gauge No.	SG 61		SG 62		SG 63		SG 64		SG 65		SG 66		SG 67		SG 68	
Bar Type	Transverse		Transverse		Transverse		Transverse		Transverse		Transverse		Transverse		Transverse	
Run No.	Max	Min	Max	Min	Max	Min	Max	Min	Max	Min	Max	Min	Max	Min	Max	Min
Run 1	32.1	-19.3	34.1	-13.6	51.4	-19.3	27.1	-27.1	38.5	-19.3	0.0	-40.7	6.4	-51.4	13.5	-33.9
Run 2	64.2	-19.3	40.9	-13.6	129.0	-32.2	47.4	-20.3	89.8	-19.3	27.1	-40.7	12.8	-57.8	20.3	-40.6
Run 3	167.0	-44.9	81.7	-40.9	514.0	-161.0	203.0	-33.9	308.0	-225.0	190.0	-40.7	96.3	-38.5	94.8	-102.0
Run 4	135.0	-180.0	34.1	-81.7	572.0	-225.0	163.0	-60.9	340.0	-321.0	156.0	-47.4	96.3	-57.8	115.0	-156.0
Run 5	44.9	-257.0	-6.8	-95.3	482.0	-276.0	122.0	-74.5	270.0	-366.0	129.0	-47.4	89.9	-83.5	135.0	-176.0
Run 6	32.1	-308.0	-40.9	-129.0	469.0	-334.0	94.8	-108.0	244.0	-391.0	108.0	-54.2	83.5	-89.9	129.0	-203.0
Run 7	25.7	-347.0	-61.3	-157.0	437.0	-386.0	81.3	-142.0	212.0	-417.0	108.0	-67.8	77.0	-116.0	108.0	-224.0
Run 8	19.3	-385.0	-81.7	-170.0	399.0	-431.0	81.3	-163.0	160.0	-449.0	122.0	-61.0	57.8	-128.0	81.3	-244.0
Run 9	-6.4	-430.0	-88.5	-204.0	360.0	-489.0	88.0	-176.0	128.0	-481.0	149.0	-74.5	19.3	-167.0	54.2	-312.0
Run 10	-25.7	-494.0	-109.0	-245.0	244.0	-521.0	74.5	-196.0	38.5	-488.0	136.0	-102.0	-38.5	-193.0	13.5	-528.0
Run 11	-57.8	-552.0	-191.0	-286.0	32.1	-527.0	33.9	-196.0	-116.0	-456.0	74.5	-142.0	-77.0	-238.0	-40.6	-996.0

Location	Cap Beam														
Gauge No.	SG 69		SG 70		SG 71		SG 72		SG 73		SG 74		SG 75		SG 76	
Bar Type	Transverse		Transverse		Transverse		Transverse		Transverse		Transverse		Transverse		Transverse	
Run No.	Max	Min	Max	Min	Max	Min	Max	Min	Max	Min	Max	Min	Max	Min	Max	Min
Run 1	32.1	-25.7	0.0	-47.4	0.0	-51.3	13.6	-33.9	40.7	-6.8	44.9	-12.8	-	-	20.3	-27.1
Run 2	32.1	-25.7	0.0	-54.2	0.0	-51.3	13.6	-33.9	40.7	-6.8	44.9	-12.8	-	-	27.1	-27.1
Run 3	64.2	-19.3	20.3	-88.1	-6.4	-83.4	40.7	-33.9	47.4	-6.8	51.4	-44.9	-	-	74.5	-94.9
Run 4	89.9	-12.8	27.1	-94.9	0.0	-103.0	33.9	-40.7	40.7	-27.1	25.7	-180.0	-	-	74.5	-149.0
Run 5	103.0	-12.8	40.7	-88.1	-38.5	-122.0	27.1	-40.7	33.9	-67.8	-32.1	-295.0	-	-	108.0	-156.0
Run 6	96.3	-25.7	40.7	-102.0	-44.9	-122.0	20.3	-54.2	13.6	-210.0	-64.2	-469.0	-	-	102.0	-183.0
Run 7	96.3	-38.5	33.9	-115.0	-57.8	-135.0	20.3	-54.2	-33.9	-352.0	-89.9	-616.0	-	-	81.3	-224.0
Run 8	96.3	-51.4	33.9	-122.0	-57.8	-141.0	13.6	-61.0	-67.8	-447.0	-103.0	-693.0	-	-	74.5	-264.0
Run 9	103.0	-64.2	27.1	-149.0	-57.8	-148.0	6.8	-67.8	-102.0	-535.0	-116.0	-803.0	-	-	67.8	-359.0
Run 10	103.0	-70.6	27.1	-183.0	-64.2	-160.0	0.0	-94.9	-136.0	-610.0	-135.0	-828.0	-	-	27.1	-583.0
Run 11	103.0	-70.6	0.0	-217.0	-77.0	-160.0	-6.8	-108.0	-190.0	-664.0	-167.0	-835.0	-	-	-13.6	-881.0

Location	Cap Beam															
Gauge No.	SG 77		SG 78		SG 79		SG 80		SG 81		SG 82		SG 83		SG 84	
Bar Type	Transverse		Transverse		Transverse		Transverse		Transverse		Transverse		Transverse		Transverse	
Run No.	Max	Min	Max	Min	Max	Min	Max	Min	Max	Min	Max	Min	Max	Min	Max	Min
Run 1	51.4	-19.3	20.3	-27.1	-	-	-	-	32.1	-19.3	27.1	-27.1	45.0	-12.8	27.1	-20.3
Run 2	51.4	-19.3	20.3	-27.1	-	-	-	-	44.9	-19.3	27.1	-27.1	45.0	-25.7	27.1	-20.3
Run 3	38.5	-64.2	40.6	-33.9	-	-	-	-	96.3	-44.9	81.3	-40.7	83.5	-70.7	47.4	-20.3
Run 4	25.7	-173.0	20.3	-33.9	-	-	-	-	135.0	-89.8	94.9	-81.3	83.5	-122.0	33.9	-40.7
Run 5	-32.1	-244.0	13.5	-40.6	-	-	-	-	141.0	-128.0	115.0	-108.0	89.9	-116.0	40.7	-47.4
Run 6	-51.4	-315.0	6.8	-47.4	-	-	-	-	135.0	-160.0	108.0	-115.0	89.9	-128.0	33.9	-54.2
Run 7	-57.8	-334.0	6.8	-54.2	-	-	-	-	135.0	-193.0	115.0	-129.0	89.9	-122.0	33.9	-61.0
Run 8	-64.2	-366.0	0.0	-67.7	-	-	-	-	135.0	-199.0	115.0	-142.0	89.9	-122.0	27.1	-61.0
Run 9	-77.1	-411.0	-6.8	-88.1	-	-	-	-	148.0	-218.0	108.0	-156.0	83.5	-128.0	13.6	-54.2
Run 10	-96.3	-450.0	-13.5	-224.0	-	-	-	-	154.0	-225.0	102.0	-163.0	64.2	-141.0	6.8	-67.8
Run 11	-96.3	-488.0	-61.0	-420.0	-	-	-	-	148.0	-225.0	74.6	-230.0	38.5	-154.0	-6.8	-258.0
Location	Cap Beam															
Gauge No.	SG 85		SG 86		SG 87		SG 88		SG 89		SG 90		SG 91		SG 92	
Bar Type	Transverse		Transverse		Transverse		Transverse		Transverse		Transverse		Transverse		Transverse	
Run No.	Max	Min	Max	Min	Max	Min	Max	Min	Max	Min	Max	Min	Max	Min	Max	Min
Run 1	32.1	-19.3	33.9	-13.5	19.3	-38.5	20.3	-33.9	32.1	-19.3	-	-	38.5	-19.3	20.3	-27.1
Run 2	32.1	-25.7	33.9	-13.5	12.8	-38.5	20.3	-33.9	32.1	-25.7	-	-	38.5	-19.3	20.3	-27.1
Run 3	32.1	-32.1	33.9	-142.0	38.5	-38.5	74.5	-74.5	32.1	-70.6	-	-	32.1	-25.7	20.3	-61.0
Run 4	25.7	-83.5	-20.3	-386.0	38.5	-77.0	88.1	-196.0	25.7	-51.4	-	-	32.1	-180.0	-6.8	-346.0
Run 5	-6.4	-116.0	-54.2	-508.0	44.9	-109.0	74.5	-251.0	-12.8	-77.1	-	-	-51.4	-327.0	-88.1	-454.0
Run 6	-12.8	-160.0	-60.9	-630.0	32.1	-148.0	67.7	-291.0	-19.3	-89.9	-	-	-109.0	-488.0	-129.0	-508.0
Run 7	-38.5	-218.0	-81.3	-745.0	32.1	-180.0	74.5	-318.0	-25.7	-96.3	-	-	-167.0	-629.0	-156.0	-556.0
Run 8	-70.6	-270.0	-94.8	-840.0	38.5	-218.0	54.2	-352.0	-25.7	-103.0	-	-	-238.0	-719.0	-183.0	-623.0
Run 9	-103.0	-321.0	-115.0	-928.0	44.9	-250.0	47.4	-406.0	-25.7	-96.3	-	-	-289.0	-815.0	-203.0	-752.0
Run 10	-122.0	-366.0	-129.0	-968.0	51.4	-270.0	33.9	-474.0	-32.1	-103.0	-	-	-340.0	-912.0	-224.0	-908.0
Run 11	-154.0	-424.0	-149.0	-941.0	44.9	-270.0	6.8	-535.0	-25.7	-96.3	-	-	-411.0	-1160.0	-257.0	-1100.0

Table 5.16 (continued) Cap beam transverse reinforcement strain data (values reported in microstrains)

Location																
Gauge No.	SG 93		SG 94		SG 95		SG 96		SG 97		SG 98		SG 99		SG 100	
Bar Type	Transverse		Transverse		Transverse		Transverse		Transverse		Transverse		Transverse		Transverse	
Run No.	Max	Min	Max	Min	Max	Min	Max	Min	Max	Min	Max	Min	Max	Min	Max	Min
Run 1	19.3	-38.5	33.9	-13.5	6.4	-38.5	27.1	-27.1	-	-	-115.2	-155.8	19.3	-38.5	20.4	-27.1
Run 2	19.3	-38.5	47.4	-20.3	12.8	-45.0	27.1	-33.9	-	-	-142.0	-190.0	19.3	-44.9	27.1	-40.7
Run 3	38.5	-148.0	74.5	-74.5	25.7	-51.4	47.4	-54.2	-	-	-217.0	-285.0	38.5	-64.2	67.8	-109.0
Run 4	12.8	-218.0	88.0	-108.0	45.0	-51.4	47.4	-60.9	-	-	-298.0	-549.0	32.1	-77.0	54.3	-136.0
Run 5	12.8	-257.0	94.8	-108.0	38.5	-38.5	81.3	-54.2	-	-	20.3	-312.0	6.4	-89.9	27.1	-156.0
Run 6	12.8	-295.0	94.8	-108.0	32.1	-45.0	60.9	-81.3	-	-	6.8	-373.0	12.8	-83.4	20.4	-163.0
Run 7	0.0	-308.0	88.0	-108.0	25.7	-64.2	60.9	-108.0	-	-	40.6	-406.0	6.4	-83.4	20.4	-170.0
Run 8	6.4	-302.0	94.8	-115.0	19.3	-96.3	60.9	-129.0	-	-	47.4	-447.0	6.4	-83.4	27.1	-176.0
Run 9	19.3	-295.0	94.8	-108.0	6.4	-109.0	54.2	-176.0	-	-	54.2	-569.0	6.4	-89.9	27.1	-183.0
Run 10	12.8	-282.0	88.0	-108.0	0.0	-128.0	47.4	-237.0	-	-	33.9	-705.0	0.0	-96.3	27.1	-170.0
Run 11	32.1	-270.0	81.3	-108.0	6.4	-148.0	20.3	-311.0	-	-	13.5	-840.0	-6.4	-96.3	33.9	-163.0

Table 5.17 Cap beam longitudinal reinforcement strain data (values reported in microstrains)

Location	Cap Beam							
Gauge No.	SG 101		SG 102		SG 103		SG 104	
Bar Type	Longitudinal		Longitudinal		Longitudinal		Longitudinal	
Run No.	Max	Min	Max	Min	Max	Min	Max	Min
Run 1	-19.3	-70.6	96.3	38.5	-	-	-6.8	-54.2
Run 2	-25.7	-89.9	103.0	32.1	-	-	-13.5	-81.3
Run 3	-19.3	-161.0	109.0	-57.8	-	-	-13.5	-224.0
Run 4	-25.7	-186.0	89.9	-64.2	-	-	-67.7	-271.0
Run 5	-32.1	-180.0	-167.0	-340.0	-	-	-67.7	-251.0
Run 6	-64.2	-244.0	-199.0	-385.0	-	-	-88.0	-278.0
Run 7	-103.0	-295.0	-212.0	-430.0	-	-	-102.0	-318.0
Run 8	-128.0	-340.0	-218.0	-449.0	-	-	-108.0	-339.0
Run 9	-148.0	-366.0	-231.0	-494.0	-	-	-115.0	-373.0
Run 10	-173.0	-392.0	-238.0	-546.0	-	-	-122.0	-400.0
Run 11	-186.0	-443.0	-250.0	-616.0	-	-	-129.0	-406.0

Table 5.18 Maximum accelerations at different locations

Absolute Maximum Accelerations, g			
Shake Table	Cap Beam (underside)	Cap Beam (web)	Column
0.03	0.04	0.05	0.05
0.09	0.10	0.08	0.12
0.21	0.23	0.19	0.32
0.31	0.32	0.31	0.38
0.44	0.43	0.37	0.39
0.55	0.53	0.48	0.41
0.66	0.64	0.59	0.43
0.76	0.75	0.71	0.44
0.93	0.95	0.90	0.46
1.17	1.23	1.17	0.60
1.45	1.46	1.41	0.69

Table 5.19 Periods and damping determined from white noise motions

Run No.	Period, sec	Damping, %
Run 1	0.533	0.77
Run 2	0.579	0.42
Run 3	0.800	1.22
Run 4	1.008	1.00
Run 5	1.103	1.05
Run 6	1.103	1.06
Run 7	1.103	1.09
Run 8	1.103	1.10
Run 9	1.103	1.10
Run 10	1.103	1.05
Run 11	1.103	1.07

Chapter 6 Tables

Table 6.1 Comparison of measured and calculated peak displacement

Run No.	Peak Displacement, in (mm)			Percent Difference, No Bond-Slip	Percent Difference, Bond-Slip
	Measured	Calculated, No Bond-Slip	Calculated, Bond-Slip		
Run 1	0.10 (2.5)	0.29 (7.5)	0.32 (8.2)	203.48	234.67
Run 2	0.44 (11.2)	0.75 (19.1)	0.95 (24.1)	70.33	115.84
Run 3	1.86 (47.3)	1.76 (44.7)	2.01 (51.0)	5.48	7.82
Run 4	2.81 (71.3)	2.43 (61.8)	2.49 (63.3)	13.27	11.16
Run 5	3.29 (83.5)	2.98 (75.7)	2.92 (74.1)	9.32	11.27
Run 6	3.91 (99.3)	3.60 (91.5)	3.58 (91.0)	7.81	8.33
Run 7	4.31 (109.6)	3.98 (101.1)	4.06 (103.1)	7.75	5.87
Run 8	4.60 (116.7)	4.18 (106.3)	4.40 (111.9)	8.95	4.17
Run 9	5.04 (128.1)	4.63 (117.7)	4.99 (126.6)	8.18	1.17
Run 10	5.23 (132.7)	5.52 (140.3)	5.18 (131.6)	5.70	0.82
Run 11	6.97 (177.1)	6.78 (172.2)	5.93 (150.6)	2.79	15.00

Table 6.2 Comparison of measured and calculated peak base shear

Run No.	Peak Base Shear, kips (kN)			Percent Difference, No Bond-Slip	Percent Difference, Bond-Slip
	Measured	Calculated, No Bond-Slip	Calculated, Bond-Slip		
Run 1	2.12 (9.4)	3.54 (15.7)	3.51 (15.6)	65.46	66.82
Run 2	5.12 (22.8)	8.74 (38.9)	9.81 (43.6)	91.45	70.57
Run 3	14.24 (63.3)	13.46 (59.9)	13.66 (60.8)	4.07	5.44
Run 4	15.88 (70.6)	14.56 (64.8)	14.42 (64.2)	9.17	8.31
Run 5	15.74 (70.0)	14.99 (66.7)	14.63 (65.1)	7.02	4.75
Run 6	16.16 (71.9)	15.55 (69.2)	15.39 (68.5)	4.75	3.75
Run 7	16.29 (72.4)	15.68 (69.8)	15.75 (70.1)	3.28	3.71
Run 8	16.14 (71.8)	15.57 (69.3)	15.80 (70.3)	2.14	3.54
Run 9	16.11 (71.7)	15.33 (68.2)	15.65 (69.6)	2.89	4.85
Run 10	15.85 (70.5)	15.74 (70.0)	15.26 (67.9)	3.75	0.74
Run 11	16.57 (73.7)	16.22 (72.2)	15.76 (70.1)	4.90	2.09

Chapter 2 Figures

LOADING DIRECTION

Loading Head

Column

End Block

Cap Beam

Loading Head

Column

End Block

Cap Beam

End Block
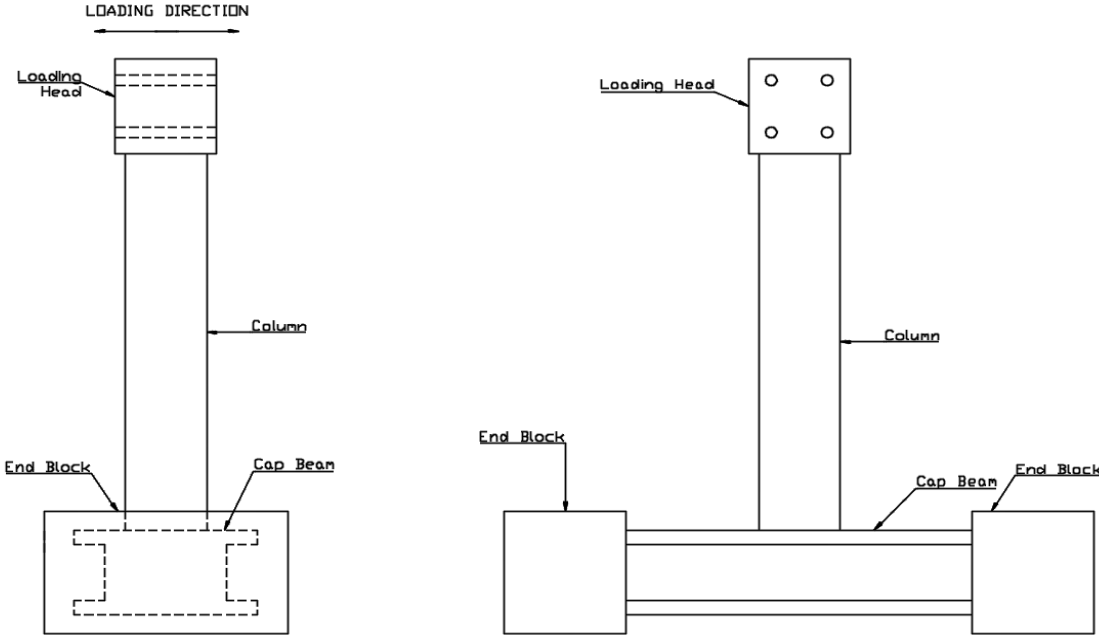
Figure 2.1 Specimen configuration

TYPICAL SECTION

Figure 2.2 Prototype bridge typical cross-section
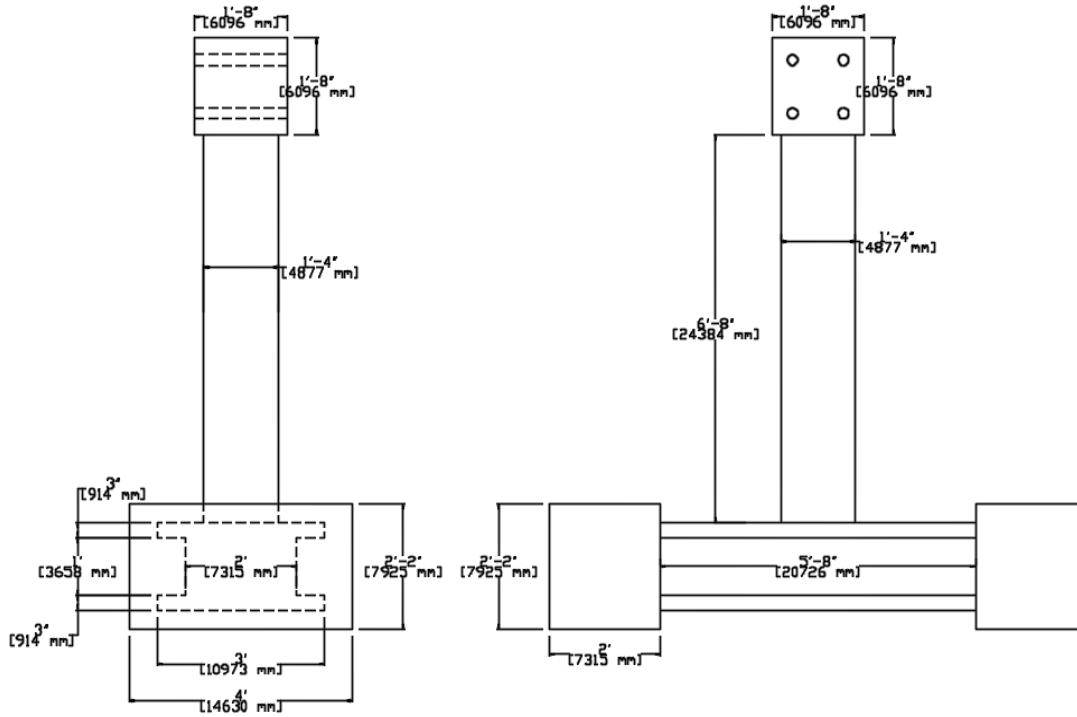
Figure 2.3 Specimen dimensions

SOUTH ← → NORTH
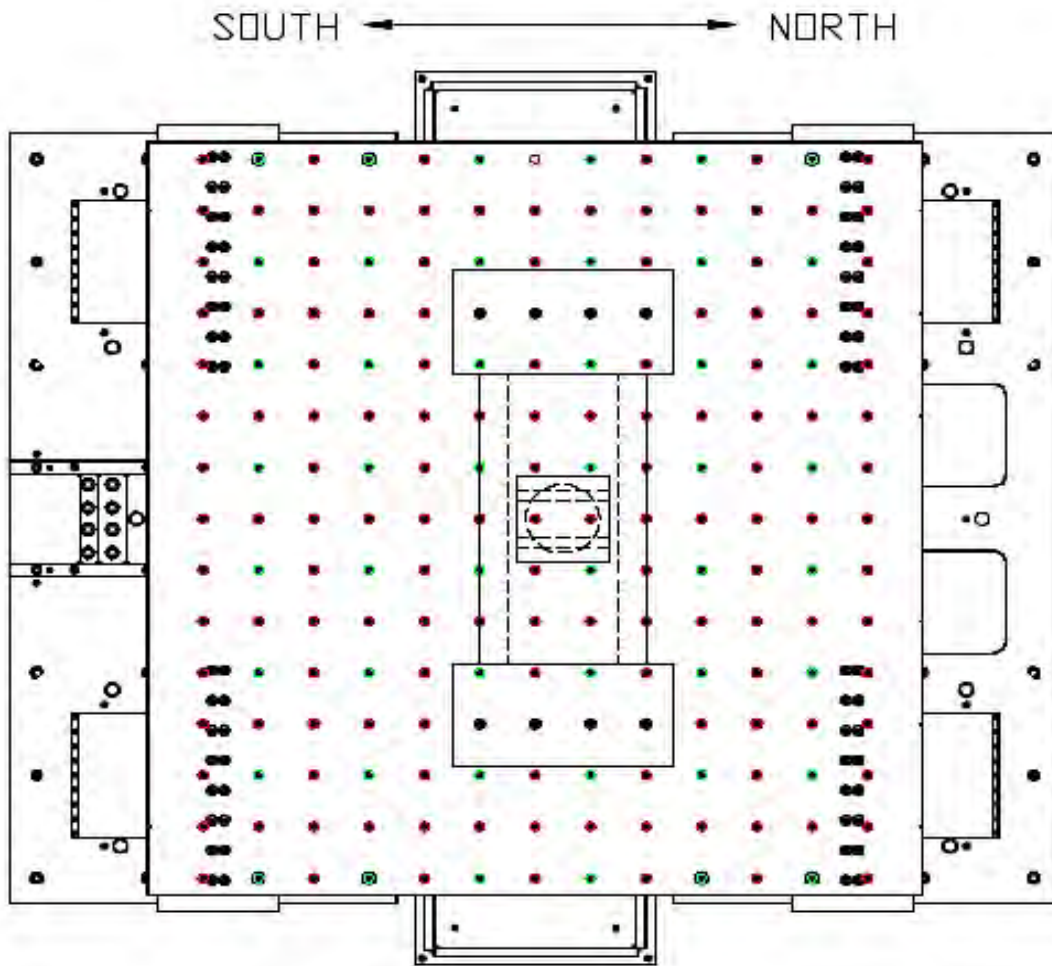
Figure 2.4 Specimen on the shake table

Ø1'-4"
[Ø406 mm]

16-#4 column long

0.75"
[19 mm]
CC

#3 spiral @ 2.25" pitch
[57 mm]
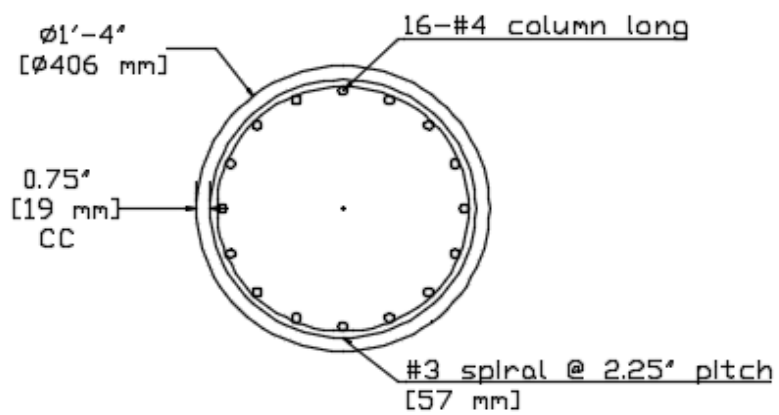
Figure 2.5 Column cross-section

71
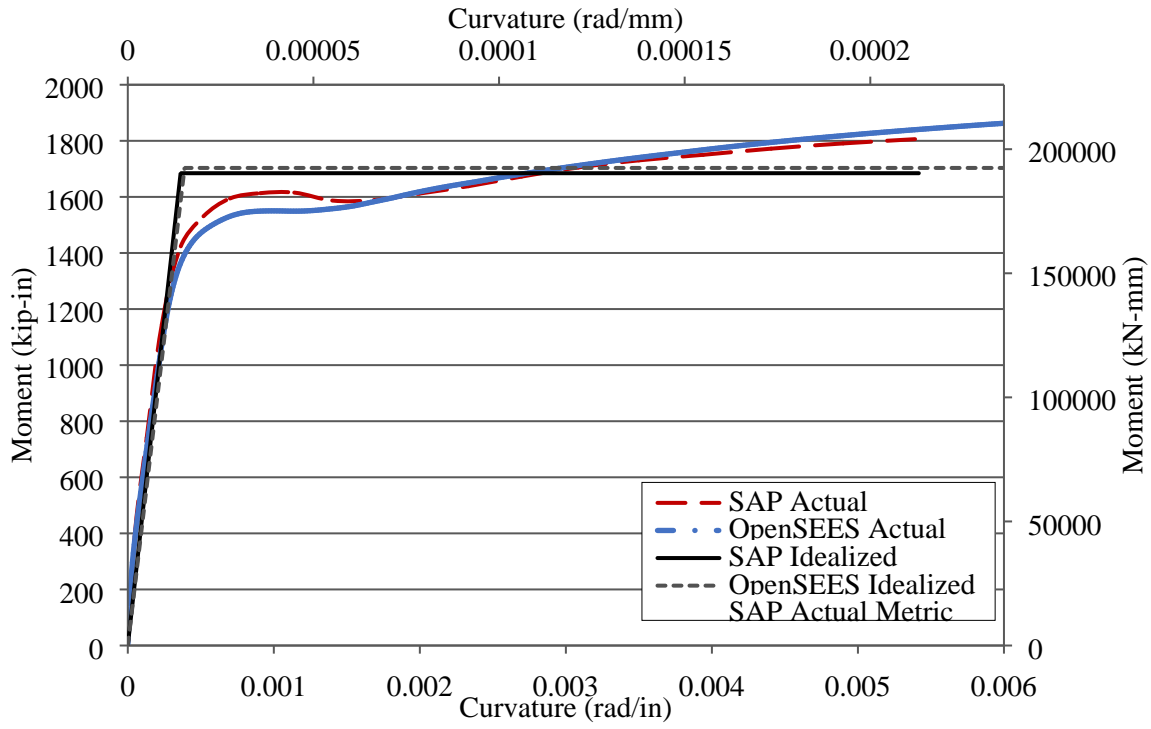
Figure 2.6 Moment-curvature analysis with axial load
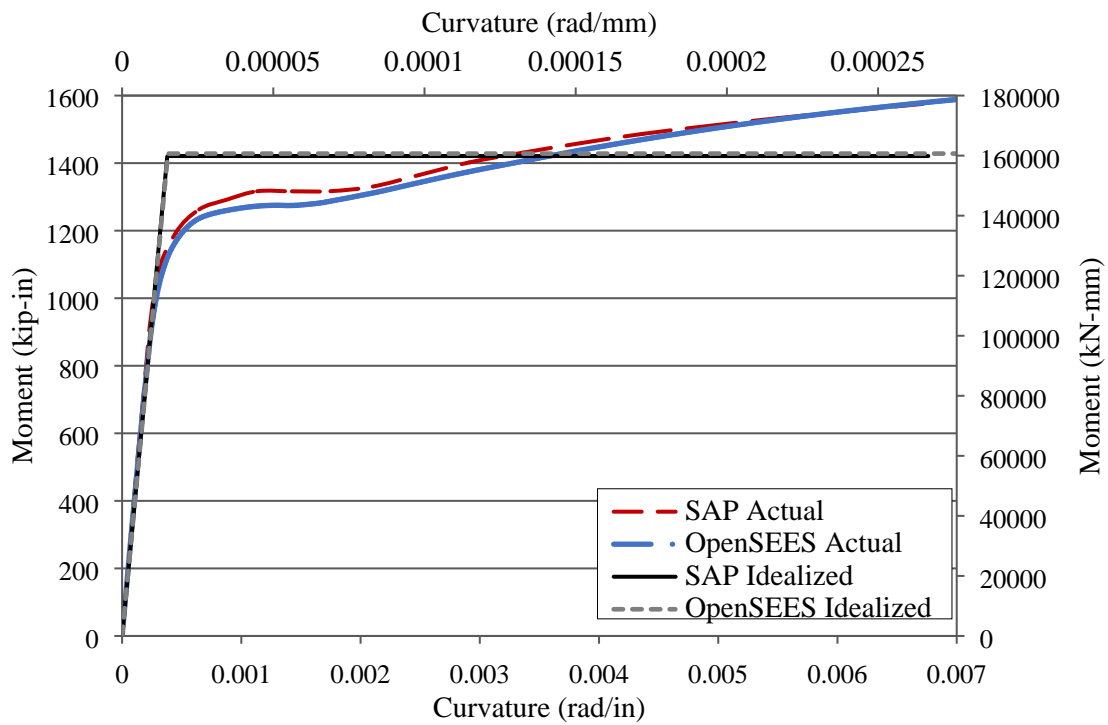
Figure 2.7 Moment-curvature analysis without axial load
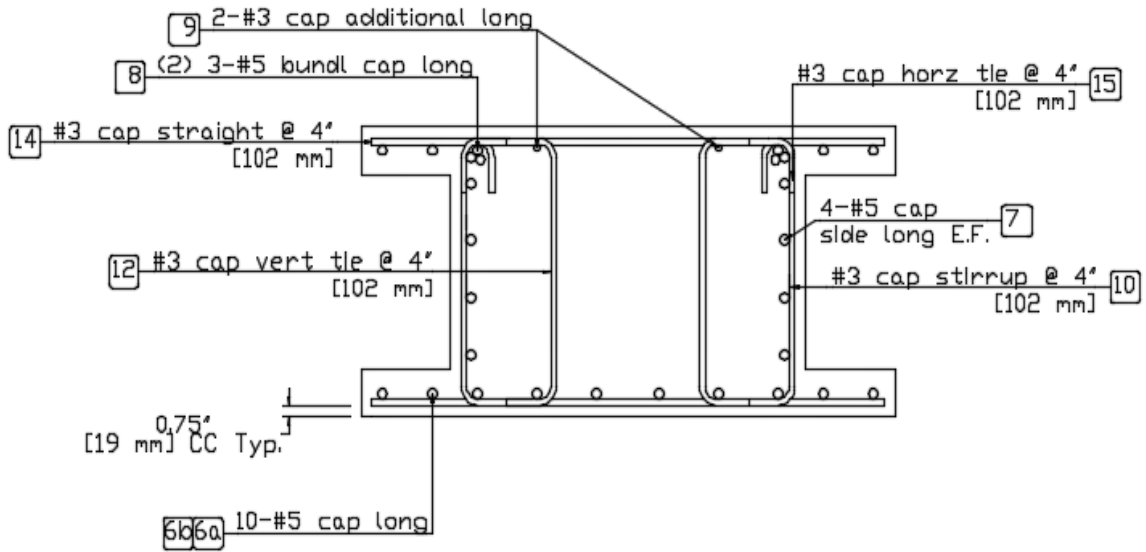
Figure 2.8 Cap Beam cross-section outside of joint region
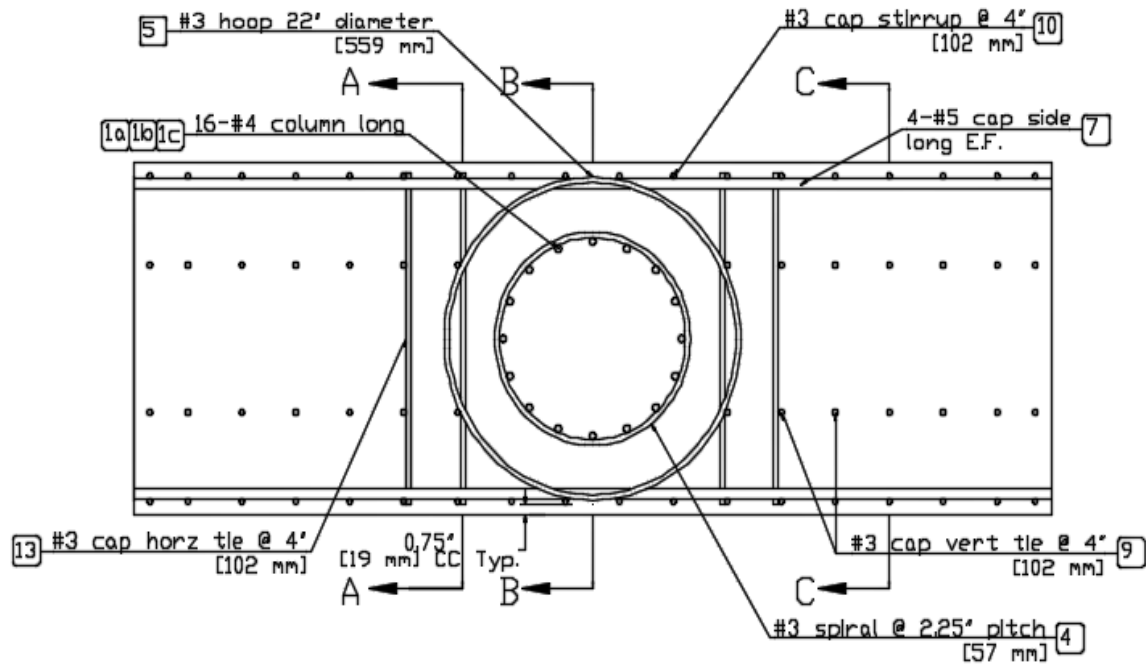
Figure 2.9 Plan View of cap beam joint, flanges not shown for clarity

73
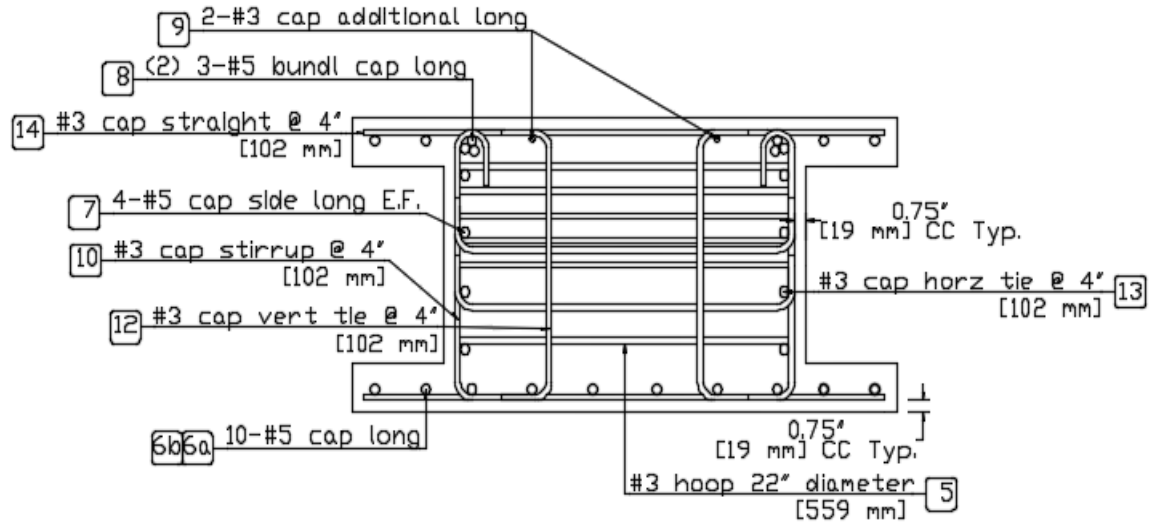
Figure 2.10 Section of cap beam adjacent to joint
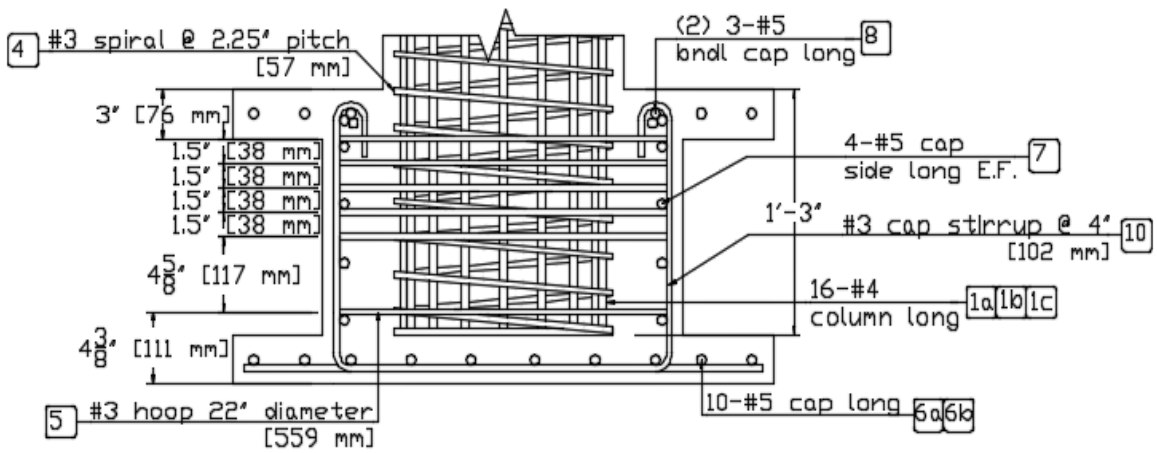
Figure 2.11 Section of cap beam to column joint

74
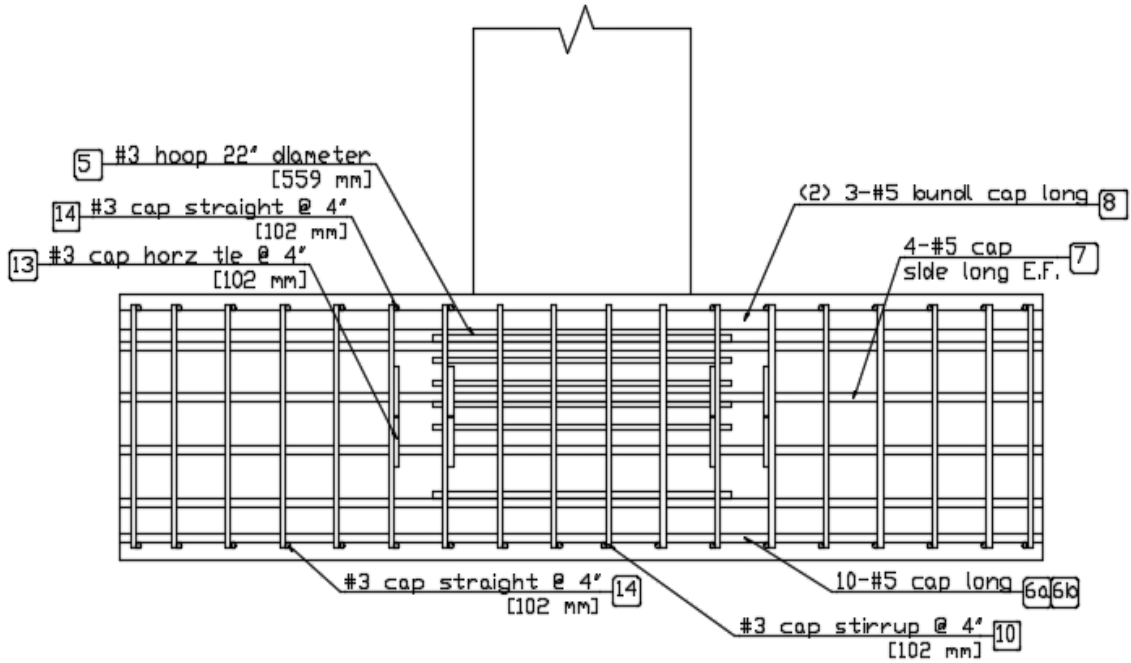
Figure 2.12 Elevation view of cap beam and joint reinforcement, flanges not shown for clarity
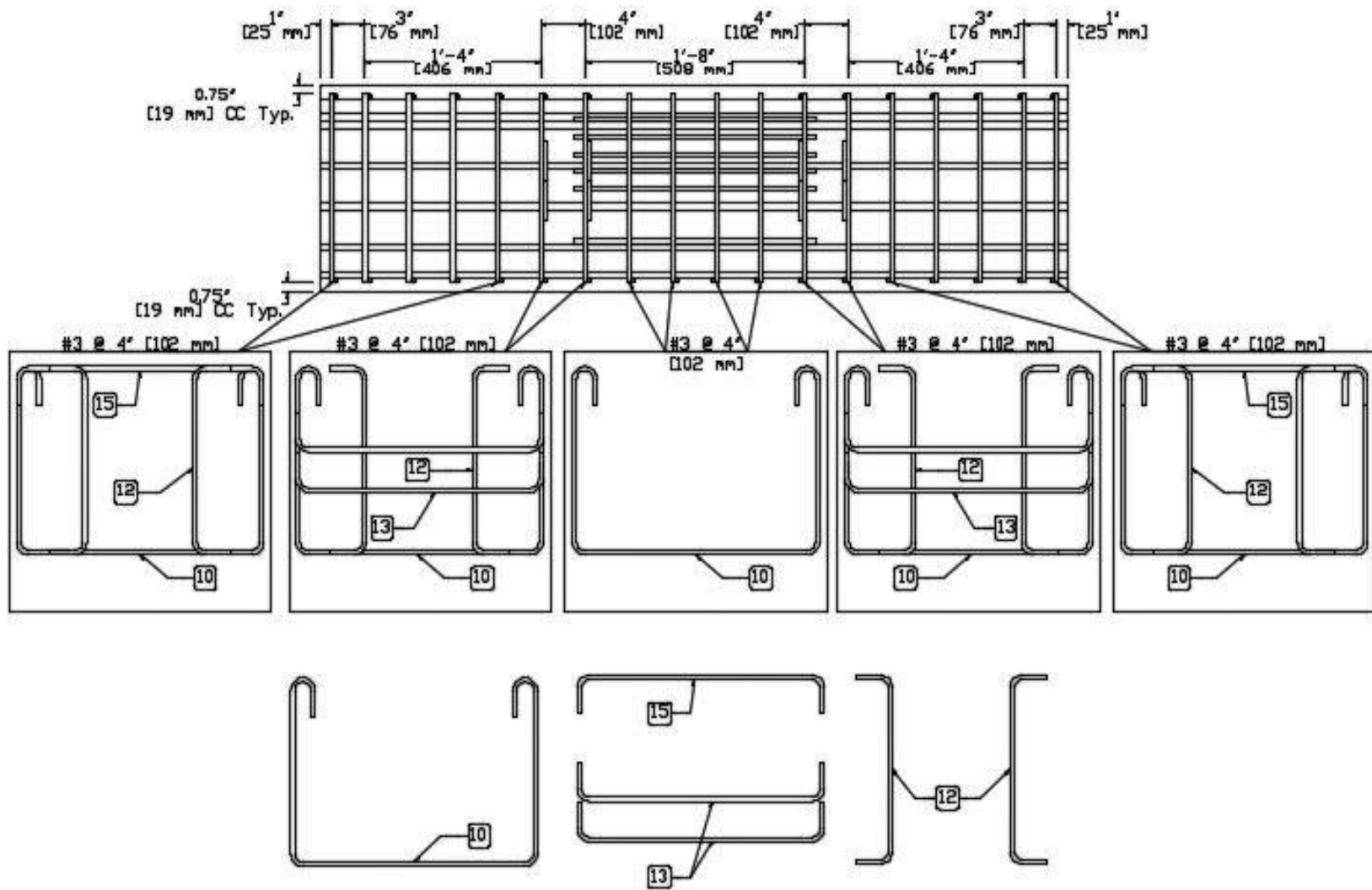
Figure 2.13 Cap beam and joint transverse reinforcement details
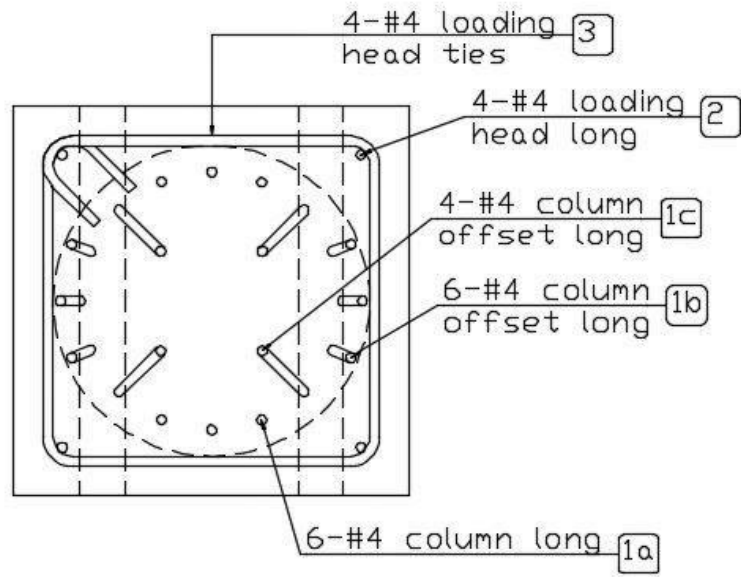
Figure 2.14 Plan view of loading head reinforcement
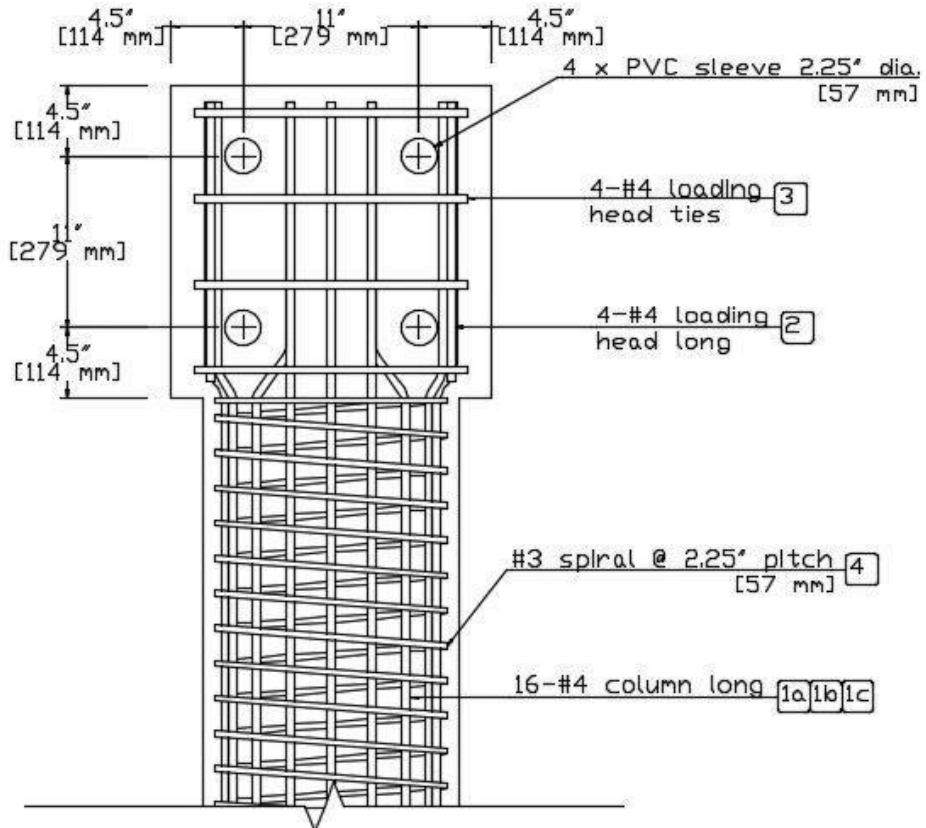
Figure 2.15 Elevation view of loading head reinforcement
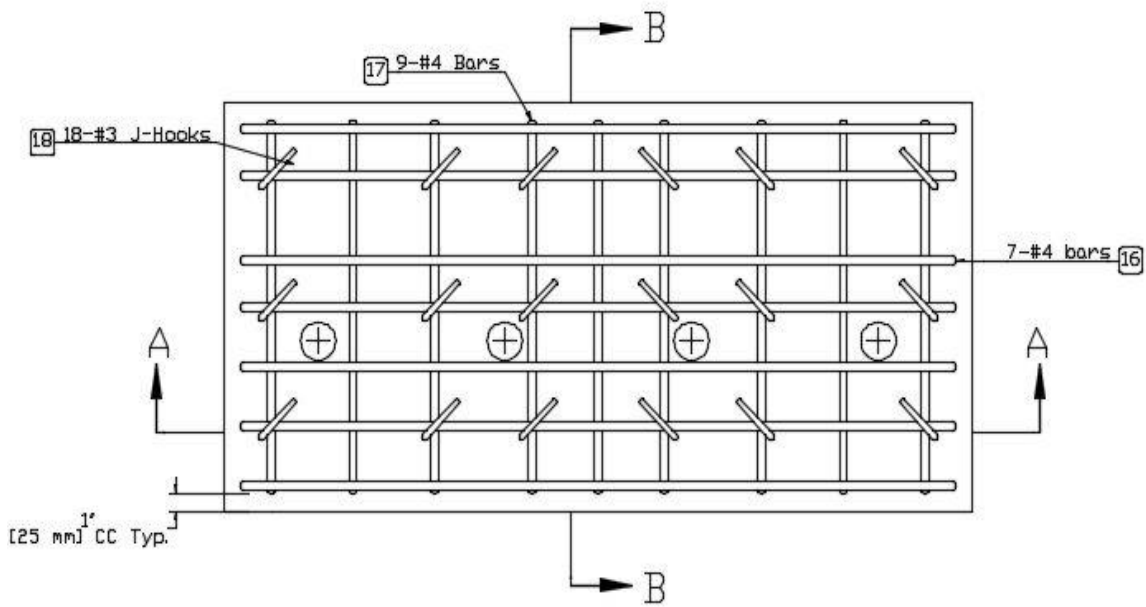
Figure 2.16 Plan view of end block reinforcement detail
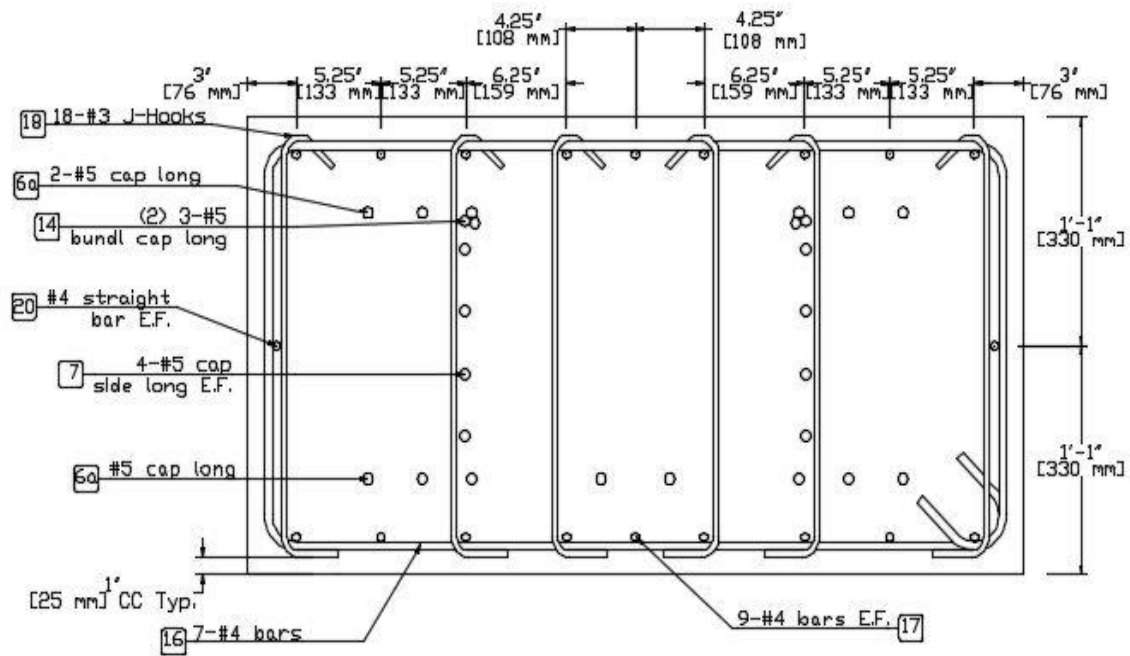
SECTION A-A

Figure 2.17 Section A-A of end block
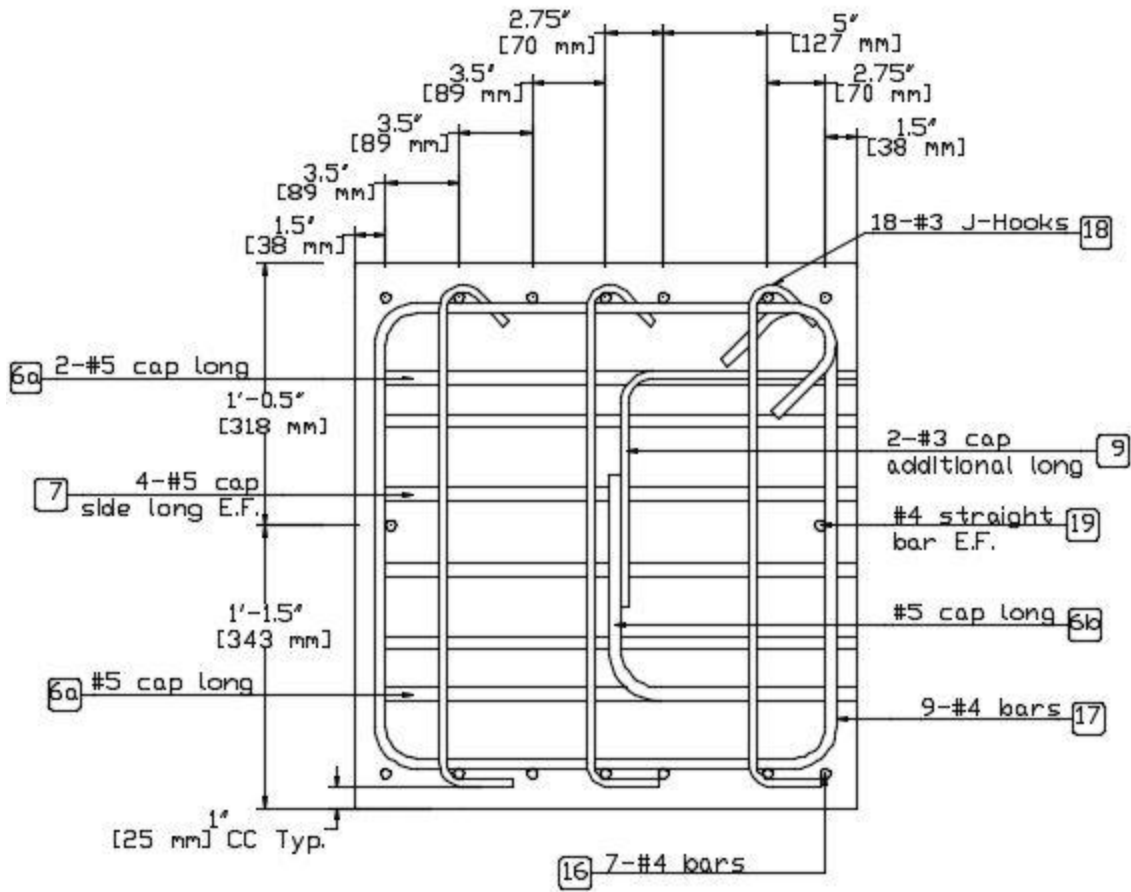
SECTION B-B

Figure 2.18 Section B-B of end block

79

Figure 2.19 Cap beam and end blocks reinforcement cages and forms

Figure 2.20 Joint reinforcement creating cast-in-place pocket

Figure 2.21 Column reinforcement cage placed in pocket

Figure 2.22 Clearance between column reinforcement cage and joint reinforcement
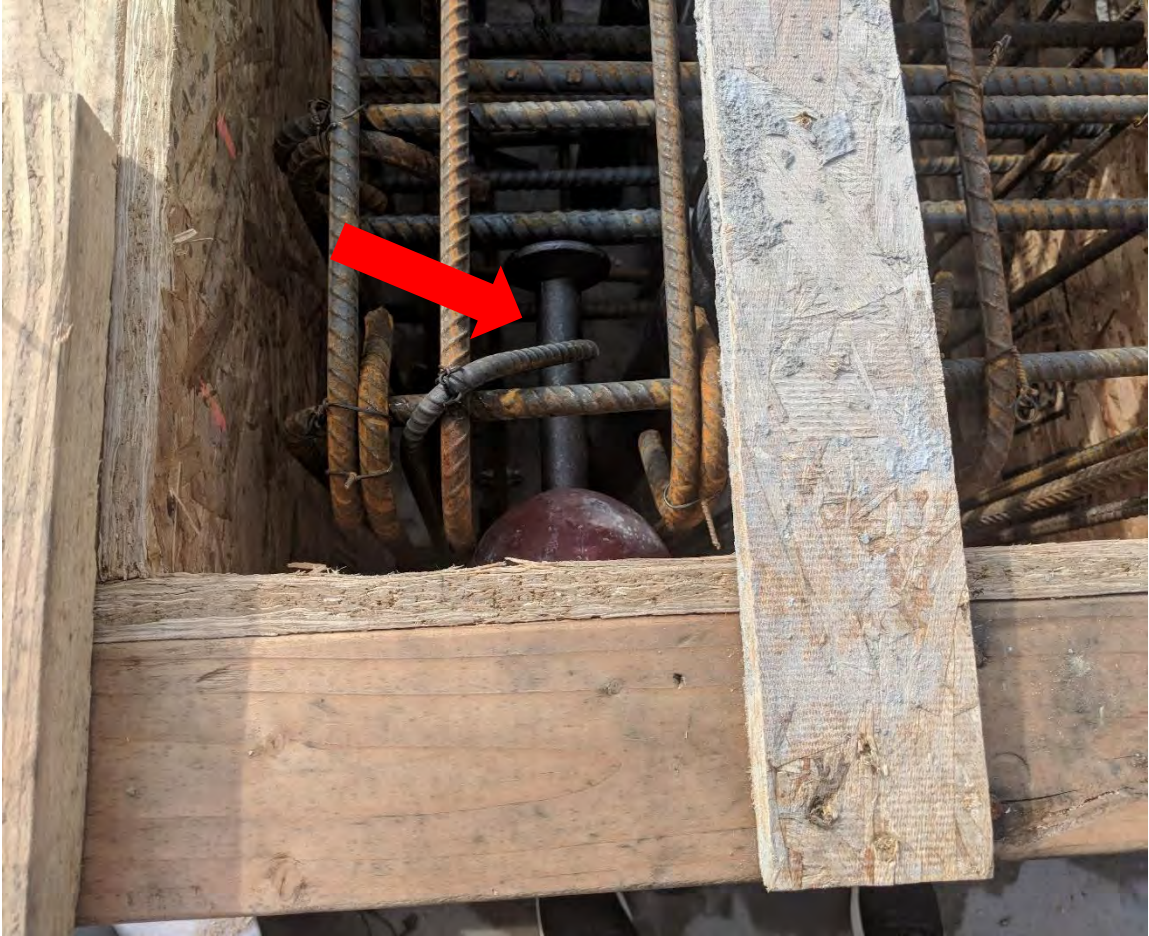
Figure 2.23 One of two lifting anchors placed in each end block

Figure 2.24 PVC pipes placed in an end block

Figure 2.25 Pouring and vibrating concrete in an end block

Figure 2.26 Vibrating cap beam concrete

Figure 2.27 Vibrating concrete around column to cap beam joint

Figure 2.28 Finishing concrete for the cap beam and end blocks

Figure 2.29 Finished concrete surface of the cap beam and end blocks

Figure 2.30 Cap beam and end blocks after stripping of formwork
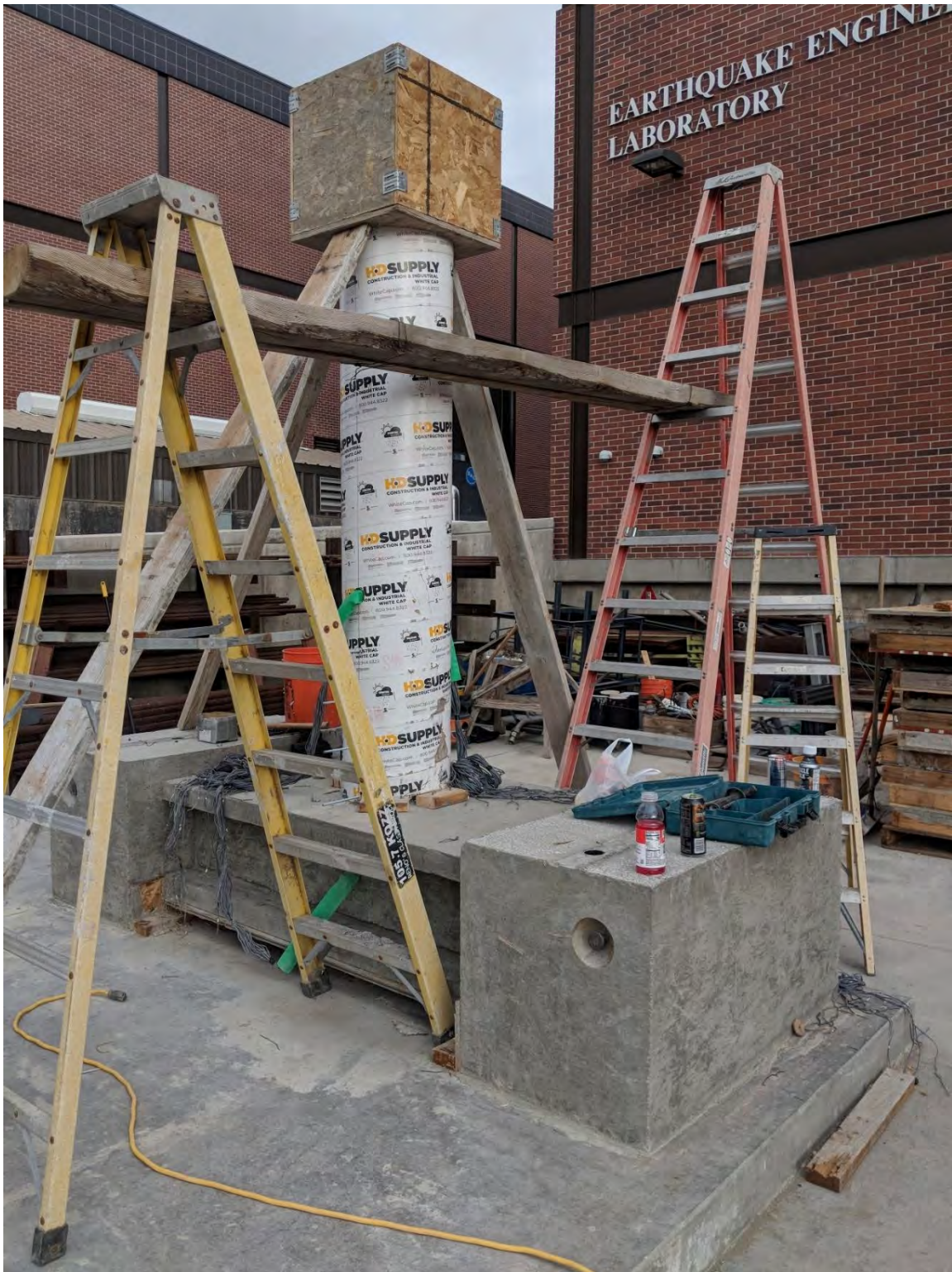
Figure 2.31 Column Sonotube and loading head form in place

Figure 2.32 Threaded rods for the placement of Novatechniks

Figure 2.33 Pouring concrete for the column and loading head
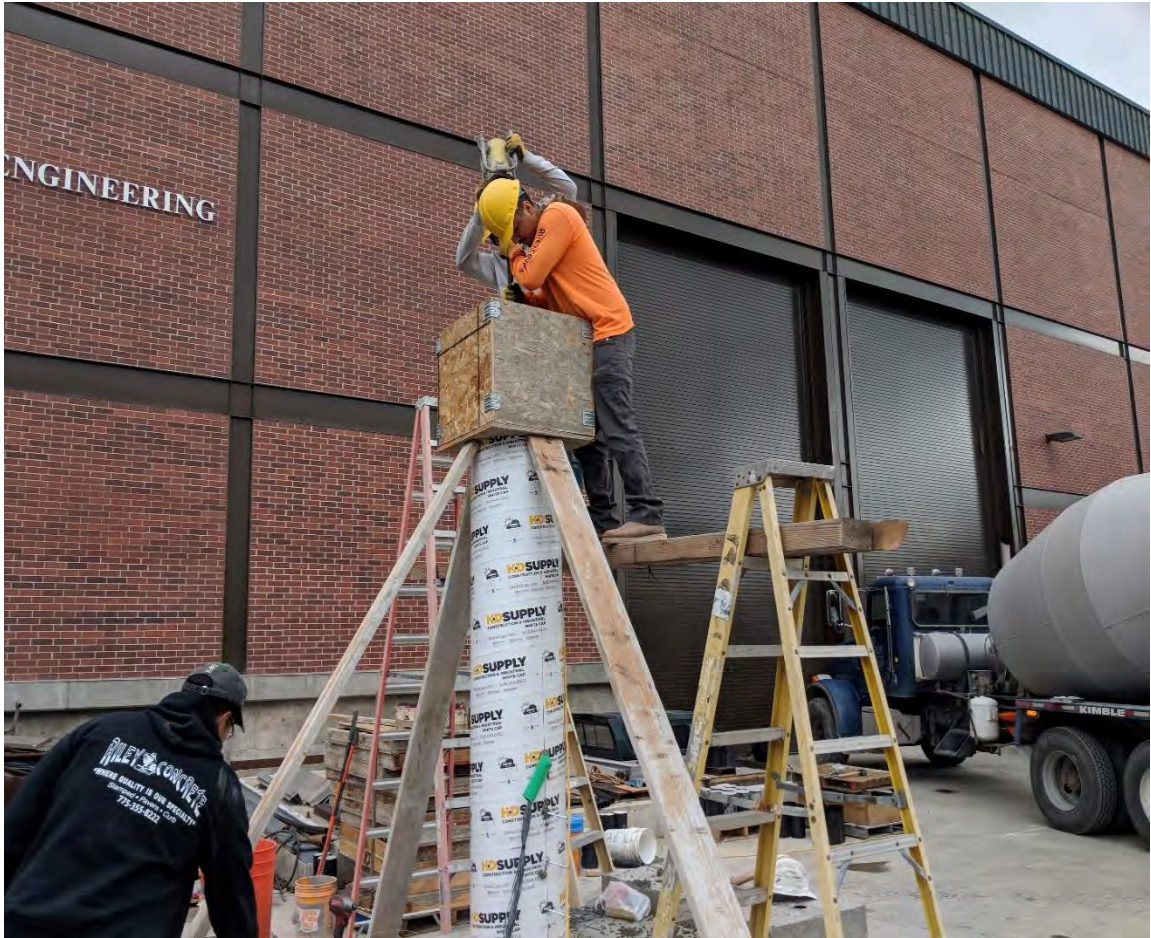
Figure 2.34 Vibrating column concrete

Figure 2.35 Finishing the surface of the loading head

Figure 2.36 Specimen after the removal of all formwork
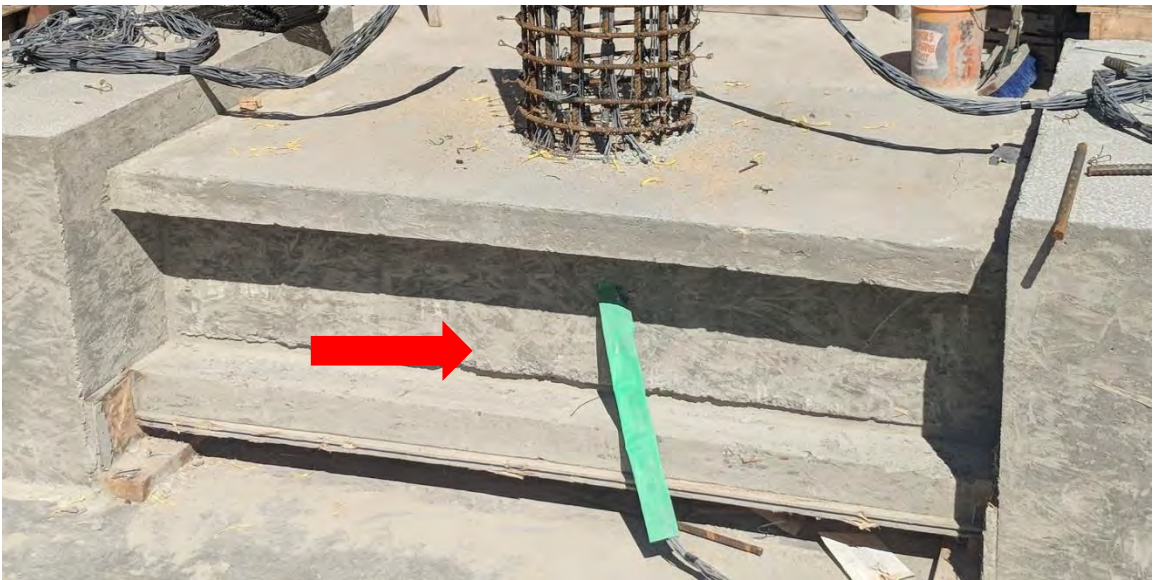
Figure 2.37 Increased cap beam web width due to formwork bulging

Figure 2.38 Deformed section of column due to Sonotube warping

Chapter 3 Figures

SOUTH ←——————→ NORTH

Axial Load

Lateral Load

Column: Force-Based
Beam/Column Element

A   A

SECTION A-A

6'-8"
[2032 mm]

Gauss-Lobatto
Integration Points
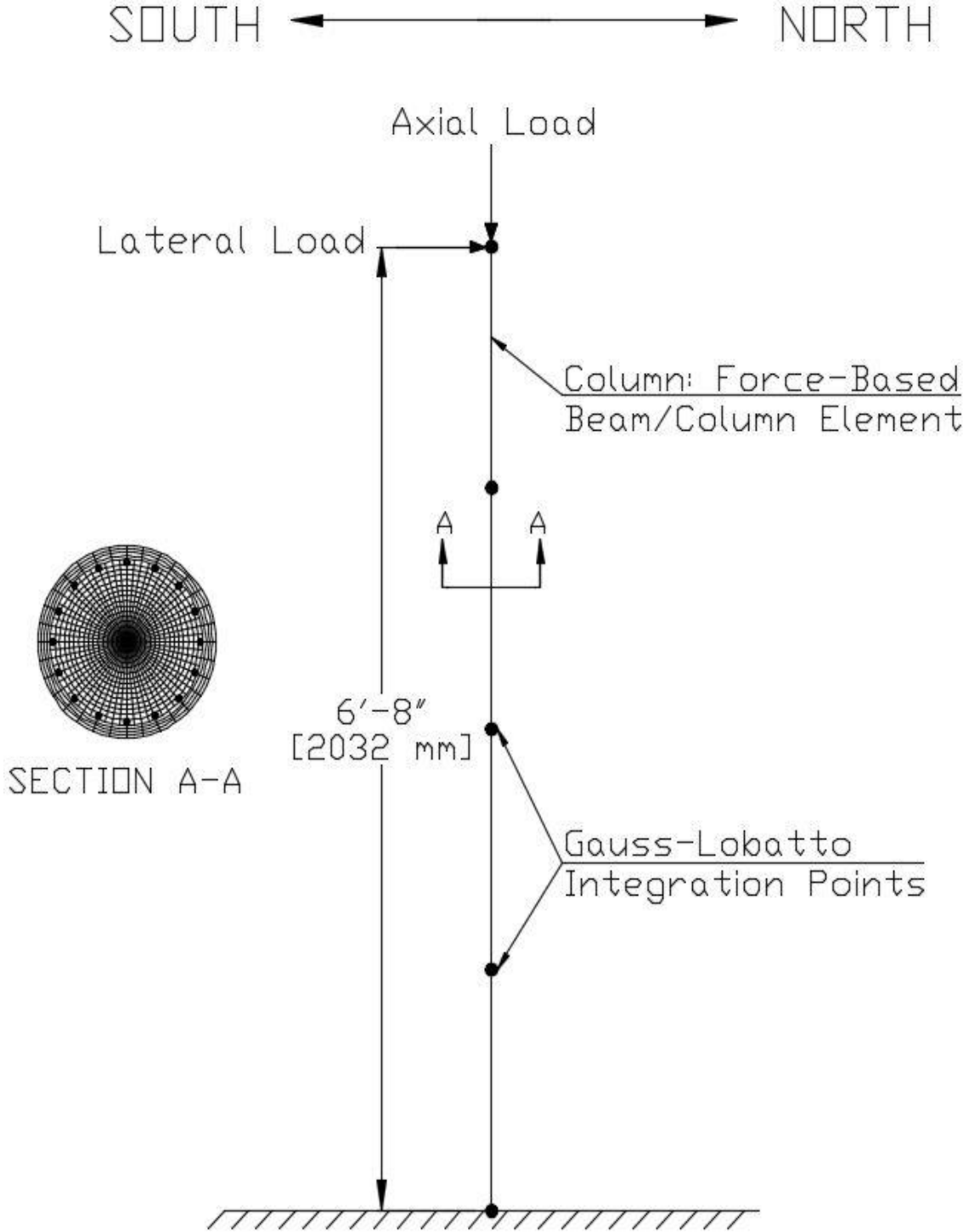
Figure 3.1 Two-Dimensional analytical model details
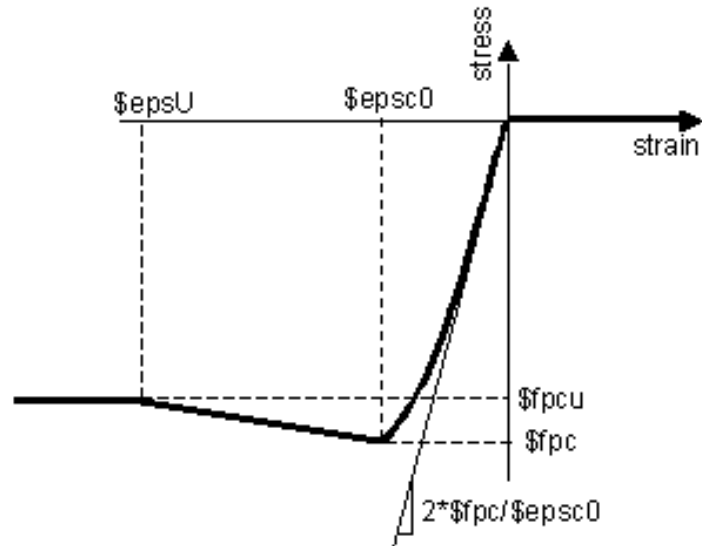
Figure 3.2 OpenSEES material Concrete01 stress-strain relationship
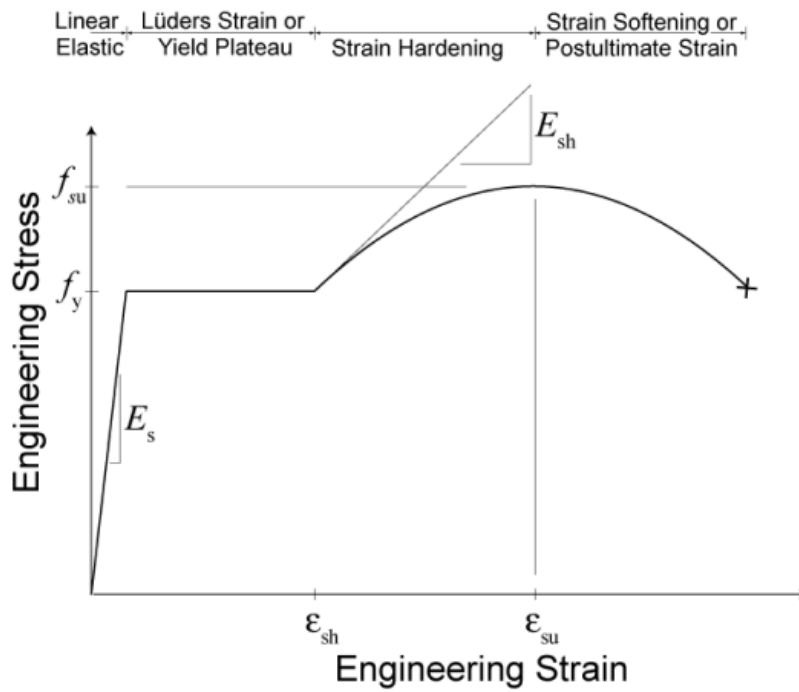
Figure 3.3 OpenSEES material ReinforcingSteel stress-strain relationship
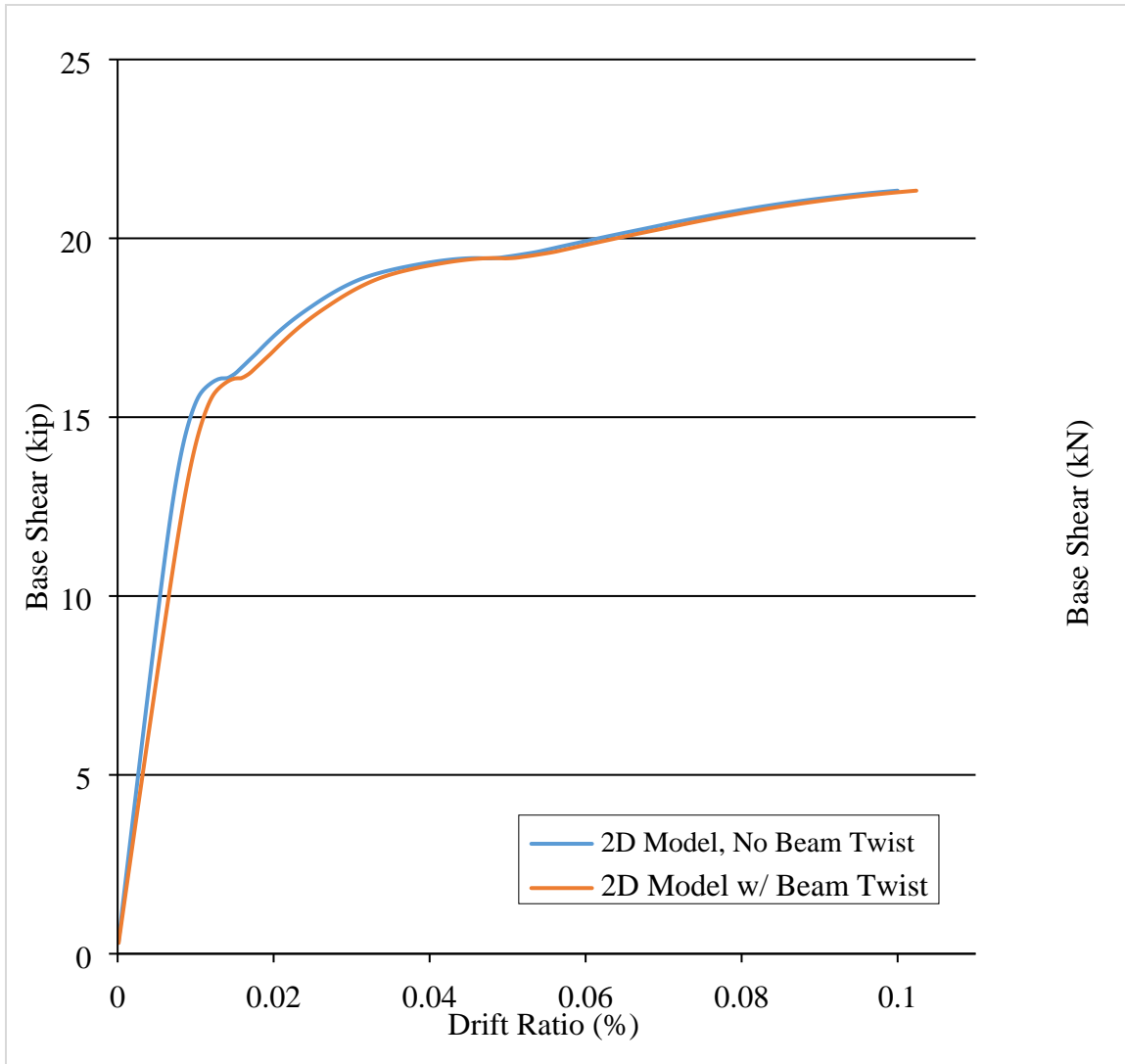
Figure 3.4 Pushover results for two-dimensional model with and without cap beam twist
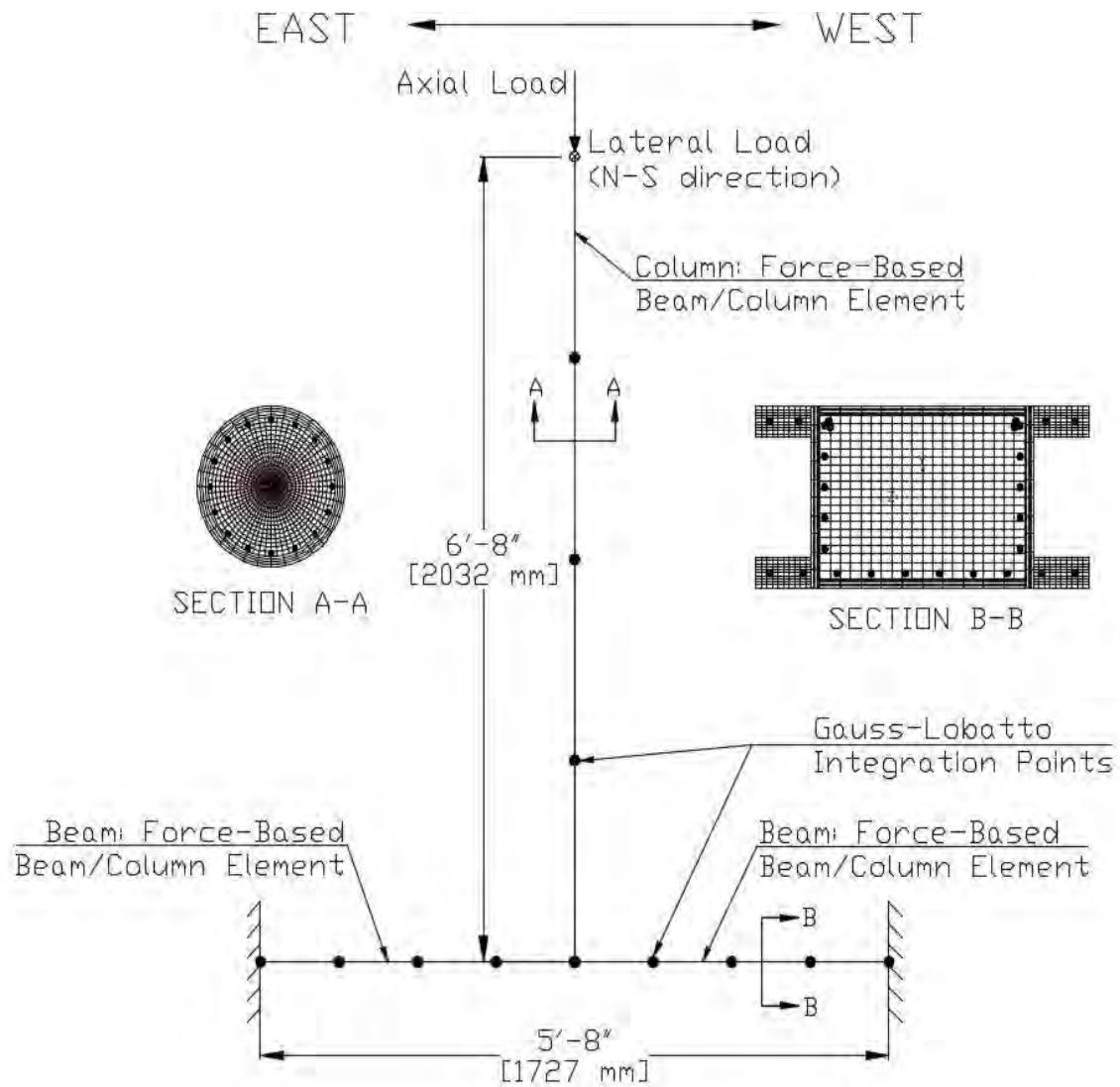
Figure 3.5 Three-dimensional analytical model details
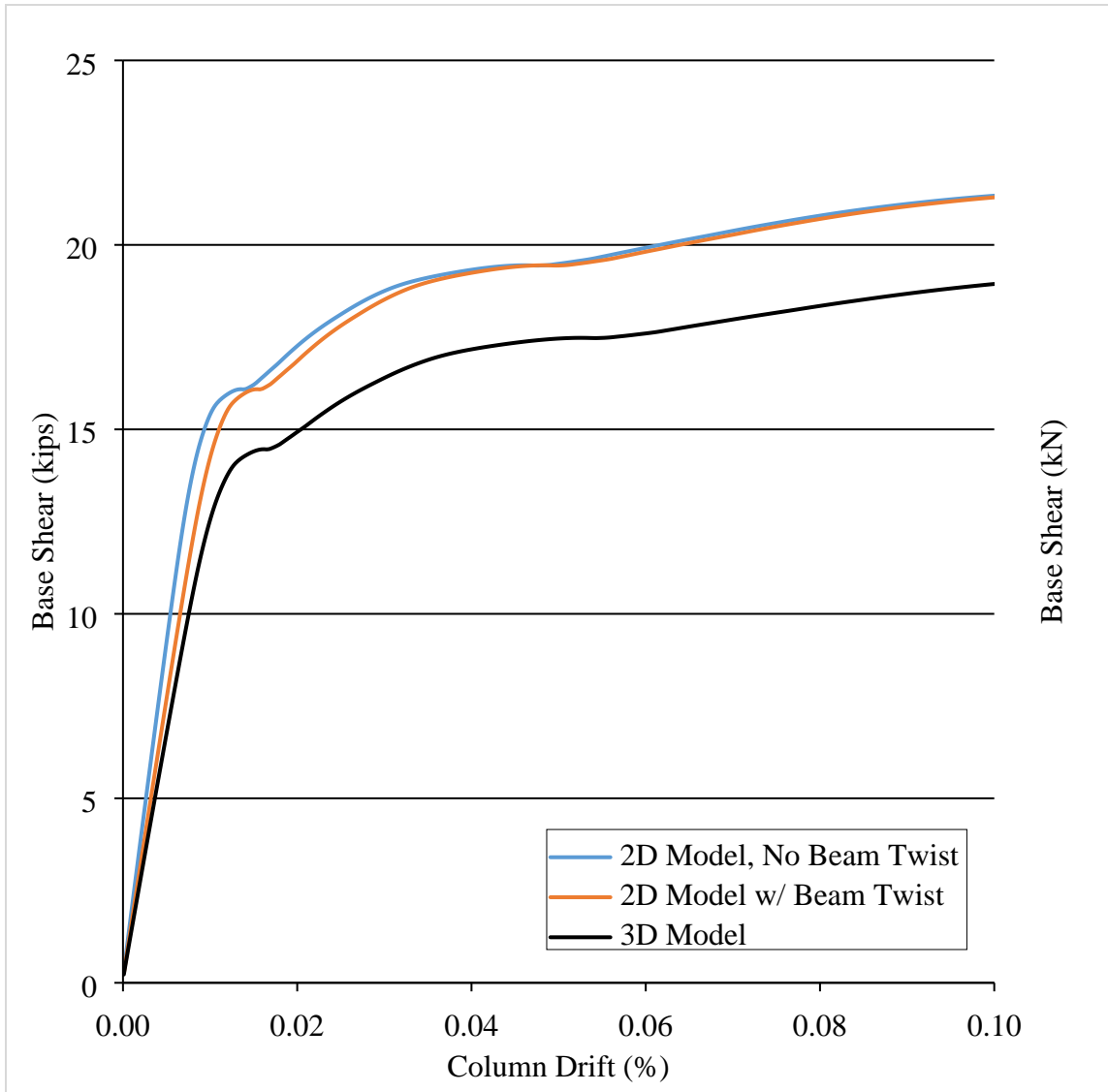
Figure 3.6 Comparison of pushover analyses for two- and three-dimensional models
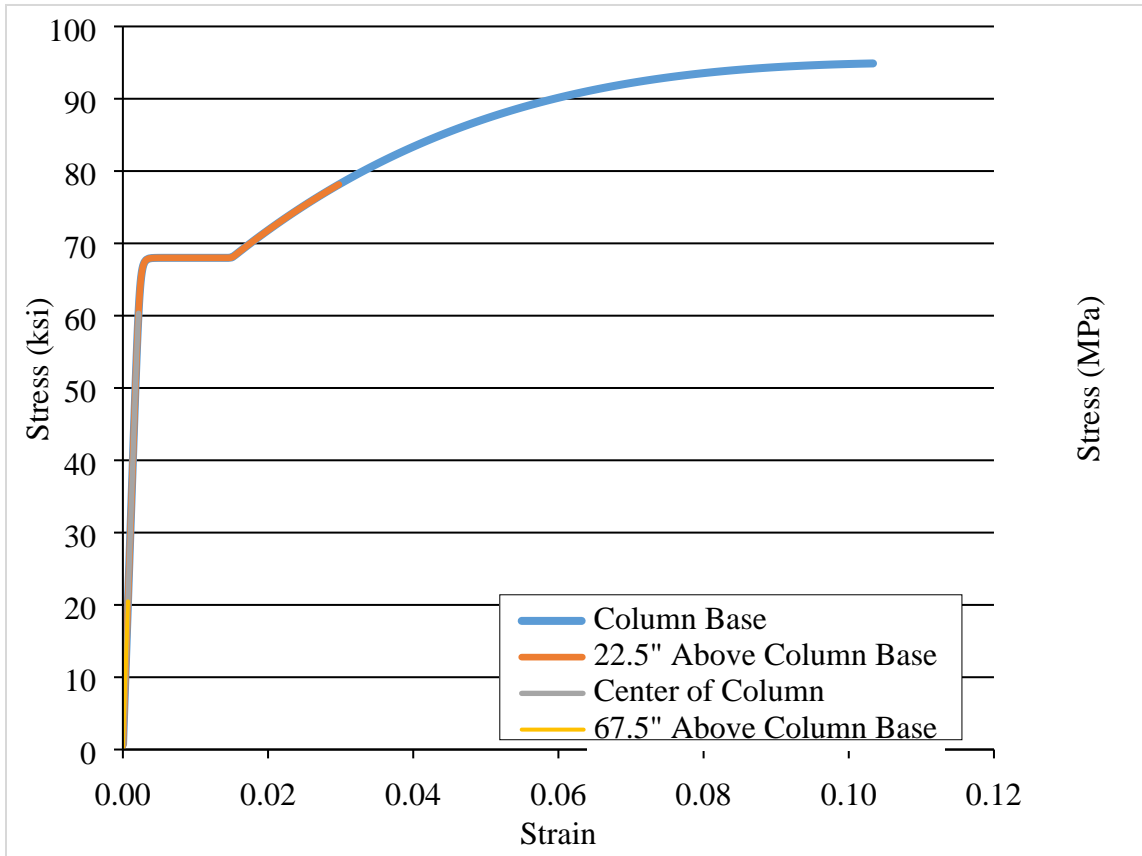
Figure 3.7 Stress-strain relationship in extreme tensile bar along column length
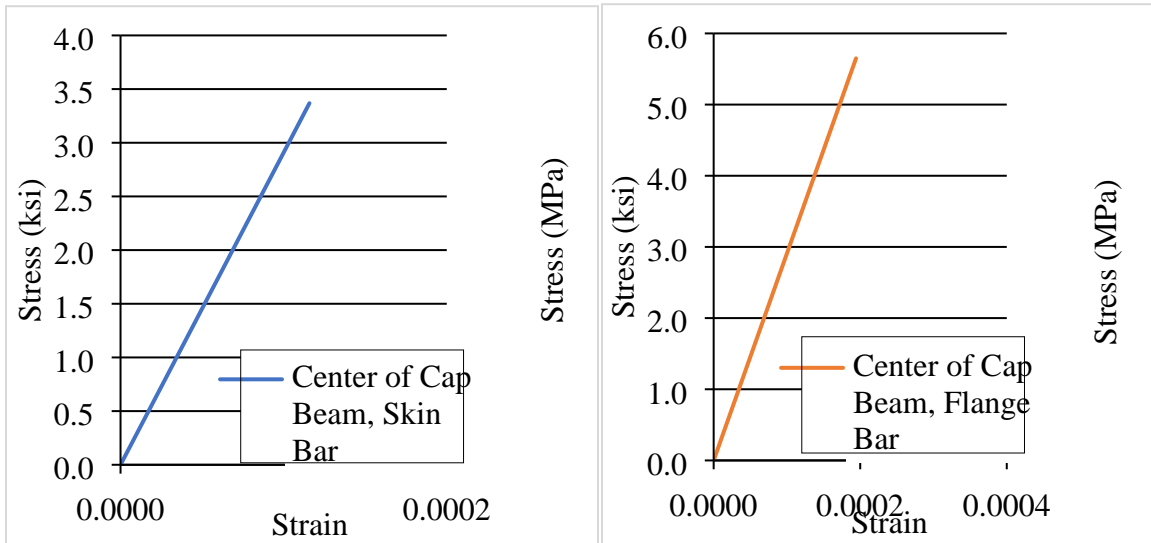
Figure 3.8 Stress-strain relationship in cap beam reinforcement
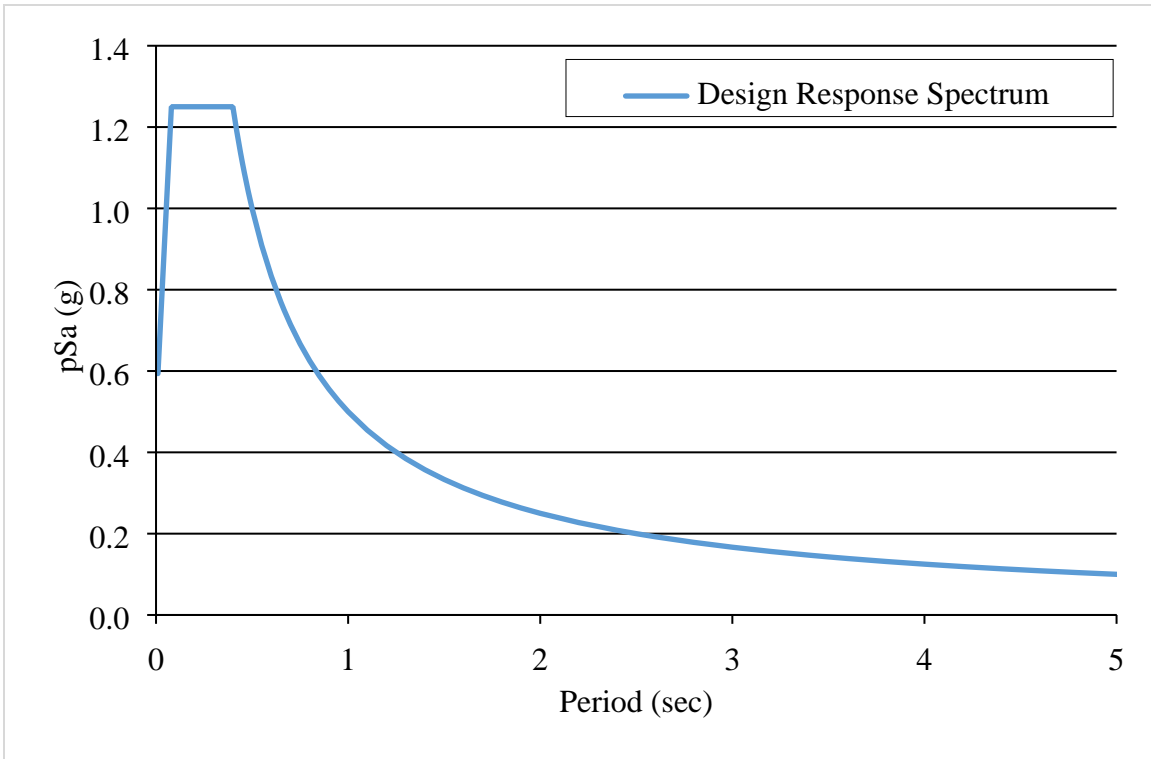
Figure 3.9 Prototype seismic design response spectrum
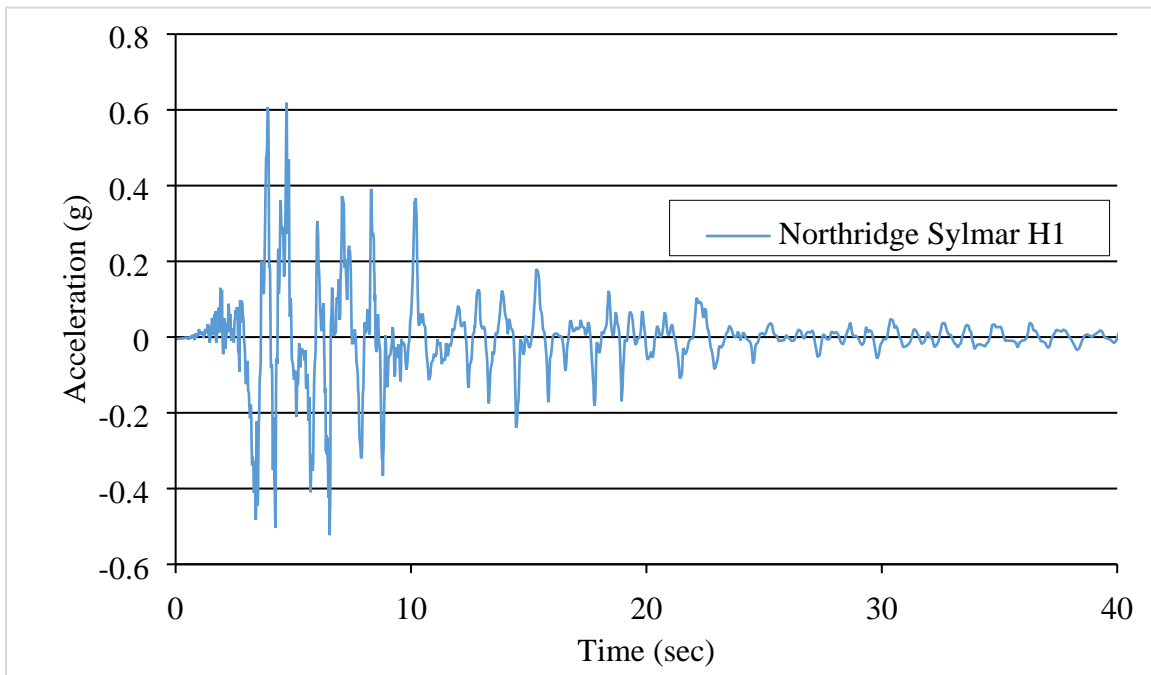
Figure 3.10 Northridge Sylmar H1 acceleration history, unscaled and uncompressed
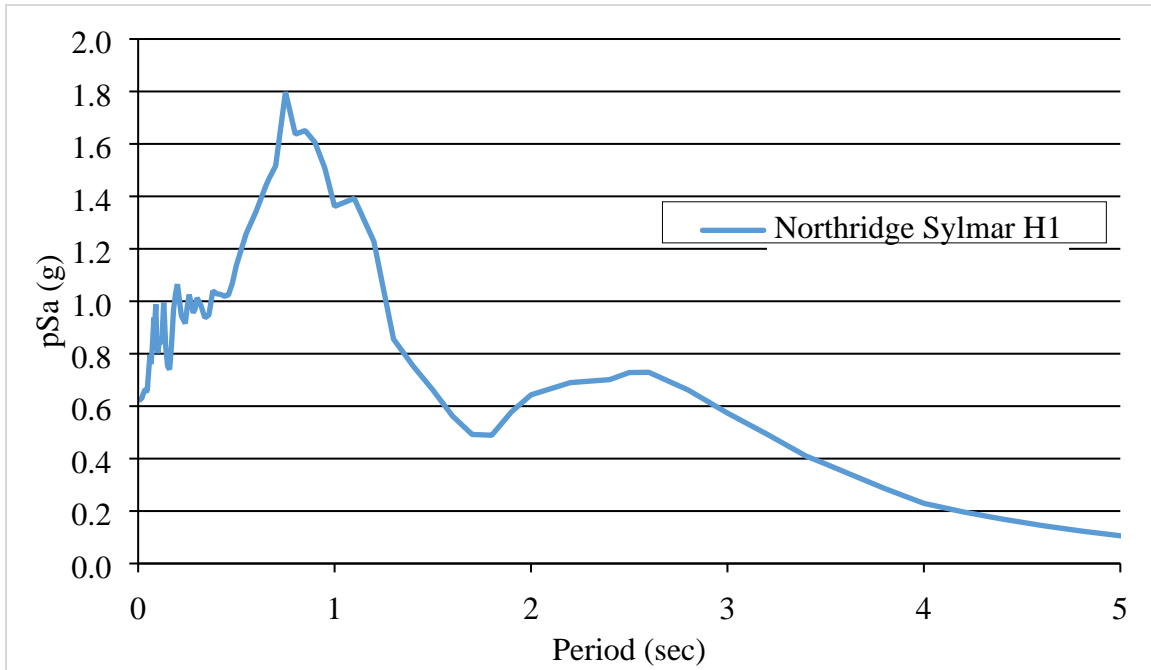
Figure 3.11 Response spectrum for Northridge Sylmar H1 component
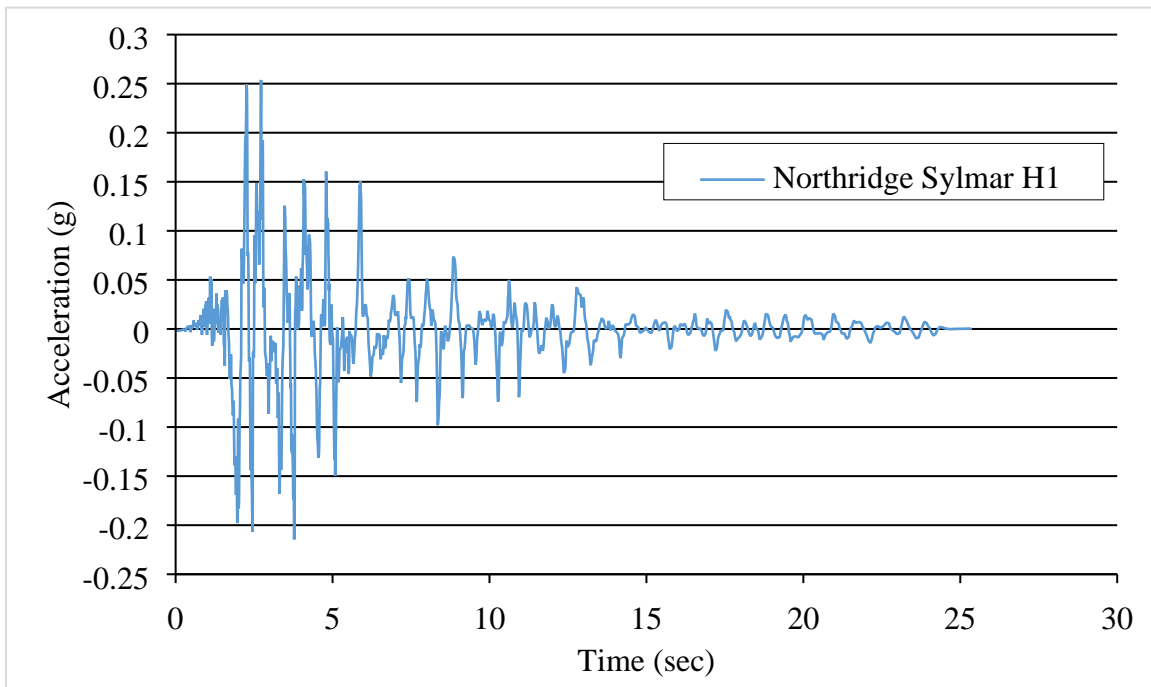
Figure 3.12 Northridge Sylmar H1 acceleration history, scaled and compressed

106
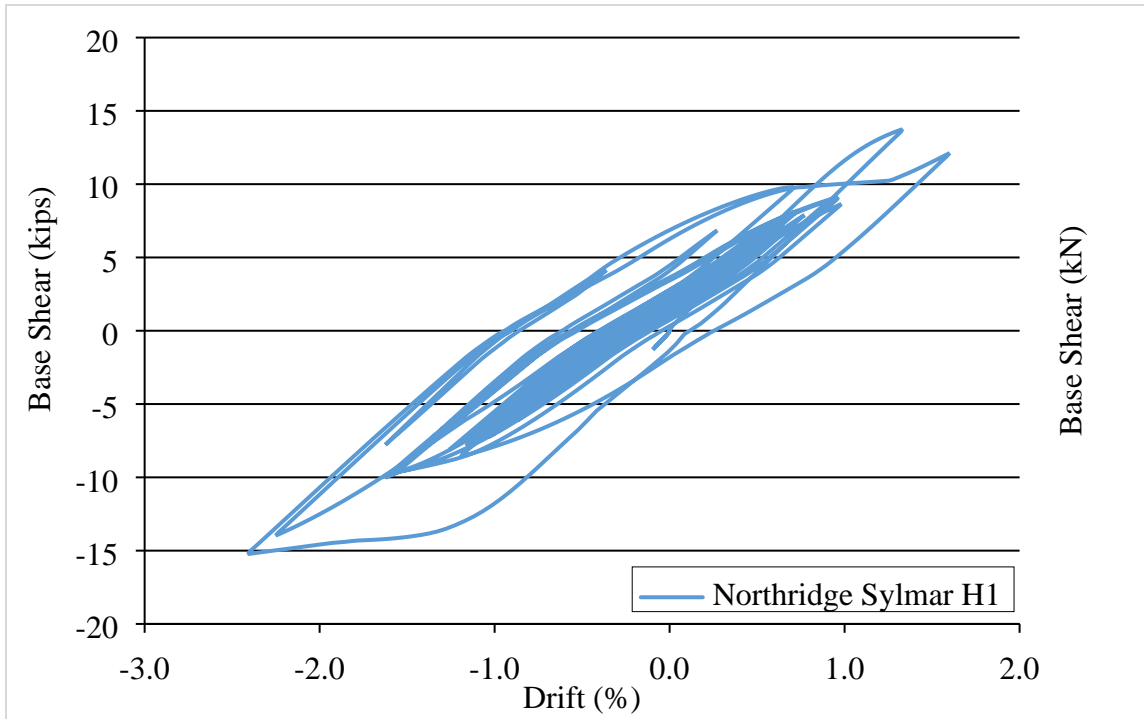
Figure 3.13 Force-displacement relationship for Northridge Sylmar H1 dynamic analysis
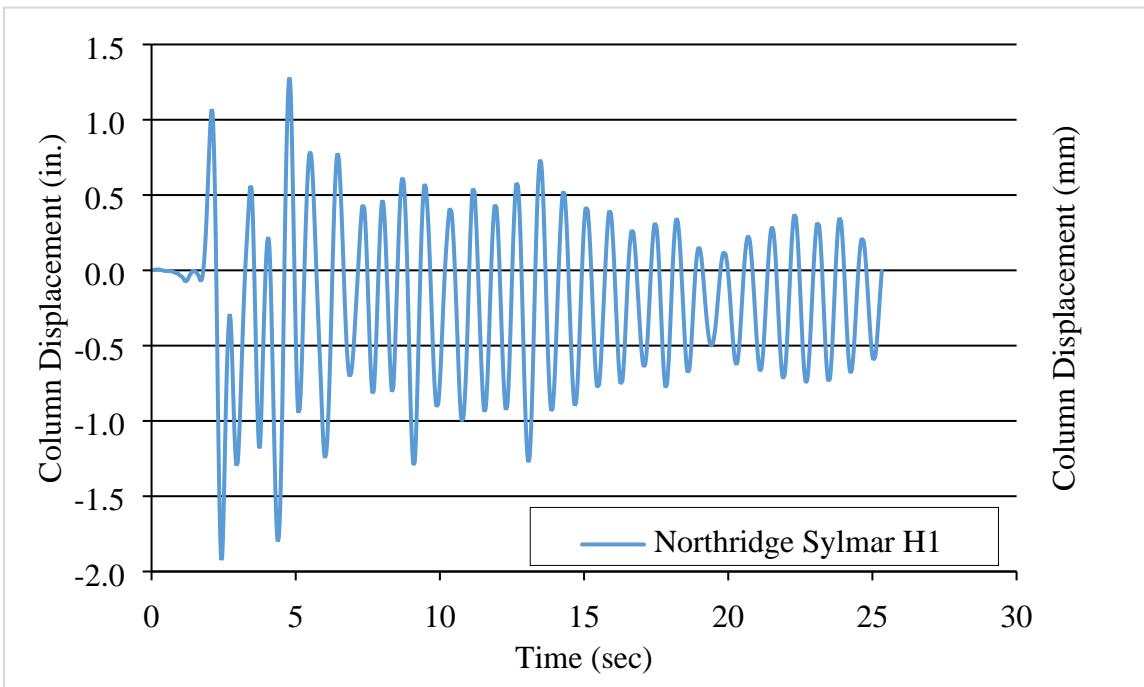
Figure 3.14 Displacement history for Northridge Sylmar H1 dynamic analysis
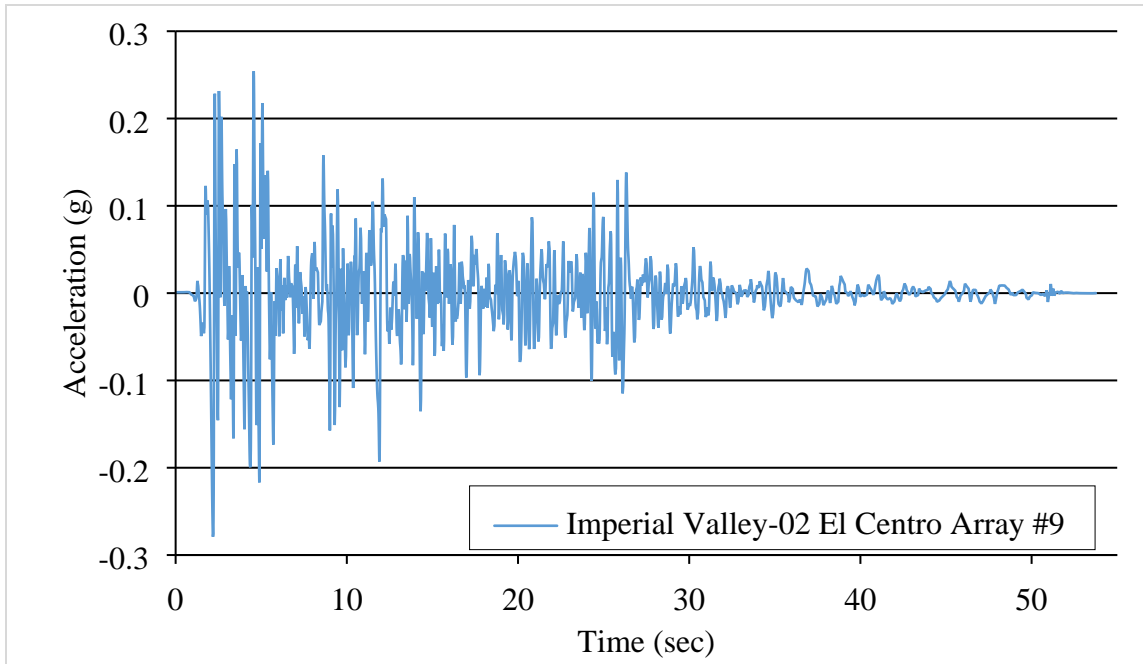
Figure 3.15 Acceleration history for Imperial Valley-02 event at El Centro Array #9
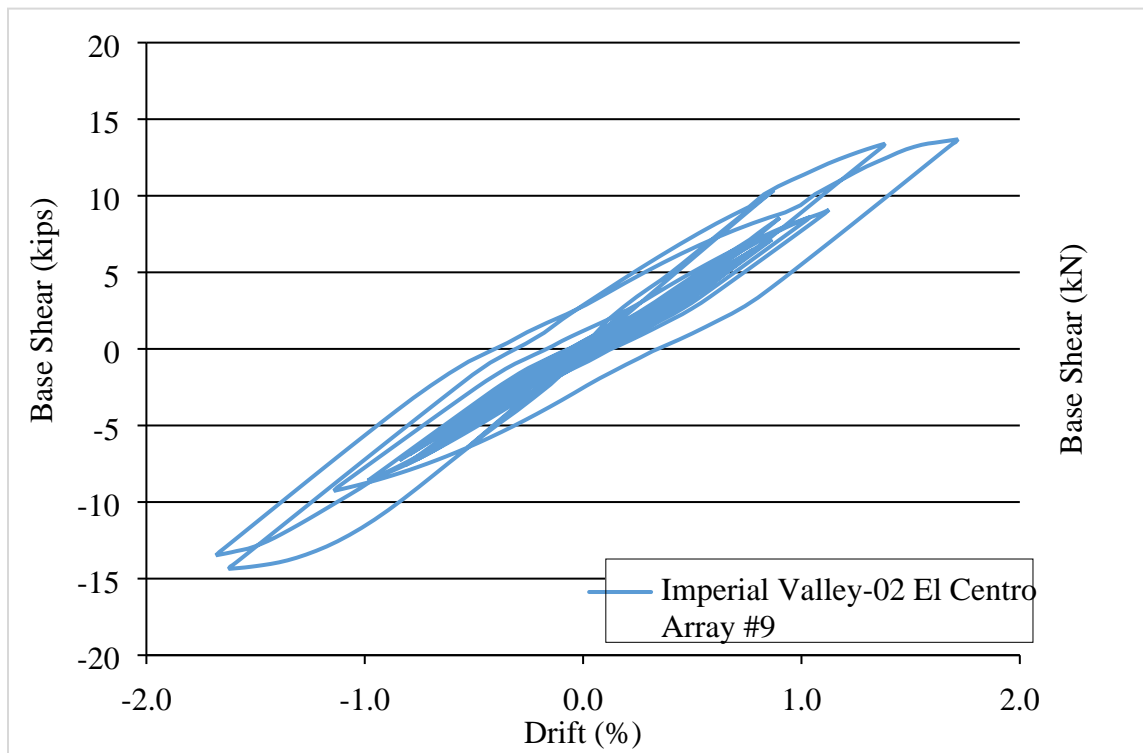
Figure 3.16 Force-displacement relationship for Imperial Valley El Centro dynamic analysis
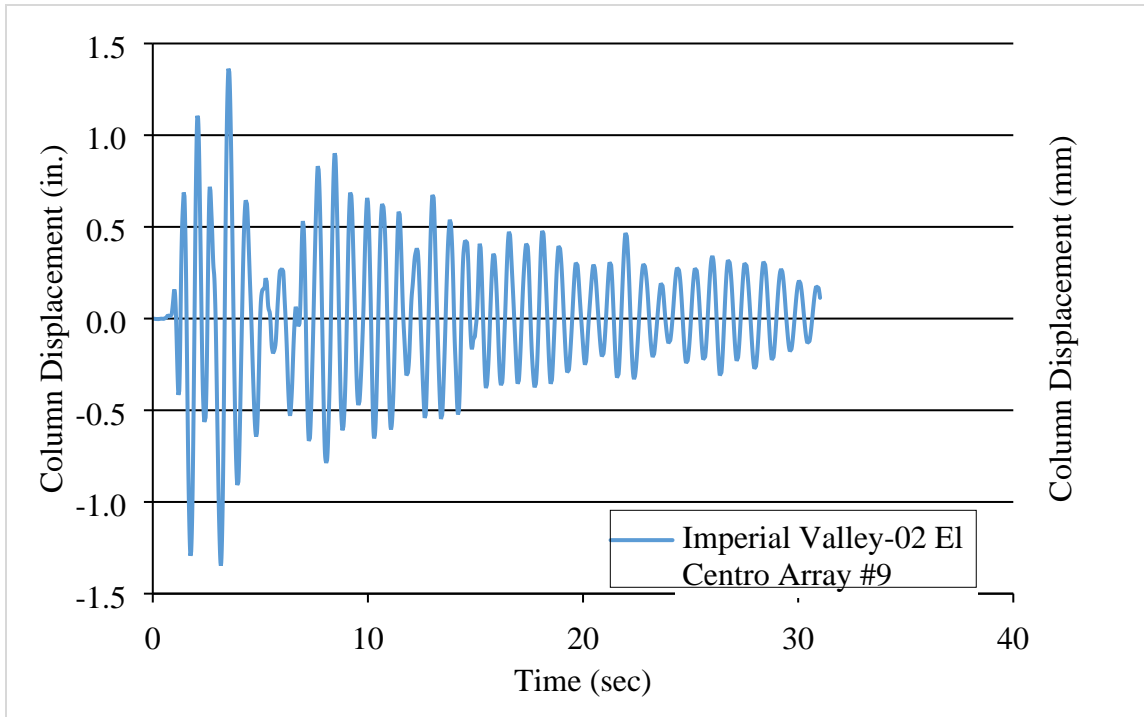
Figure 3.17 Displacement history for Imperial Valley El Centro dynamic analysis
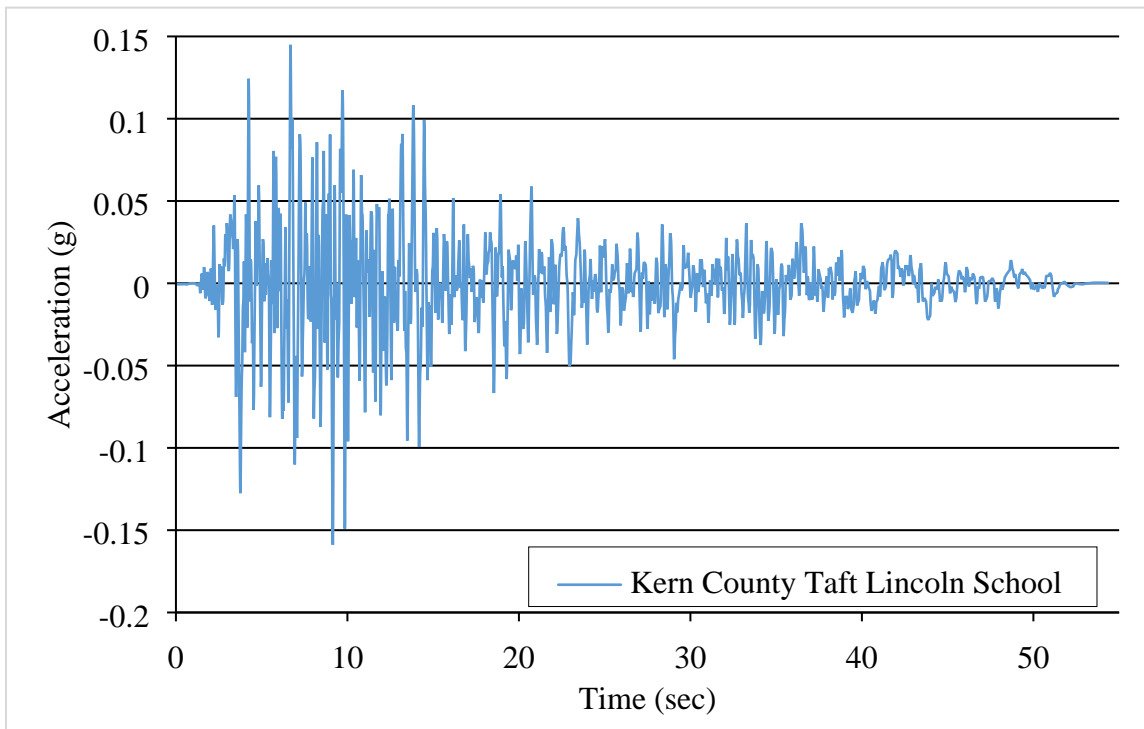
Figure 3.18 Acceleration history for Kern County Event at Taft Lincoln School

109
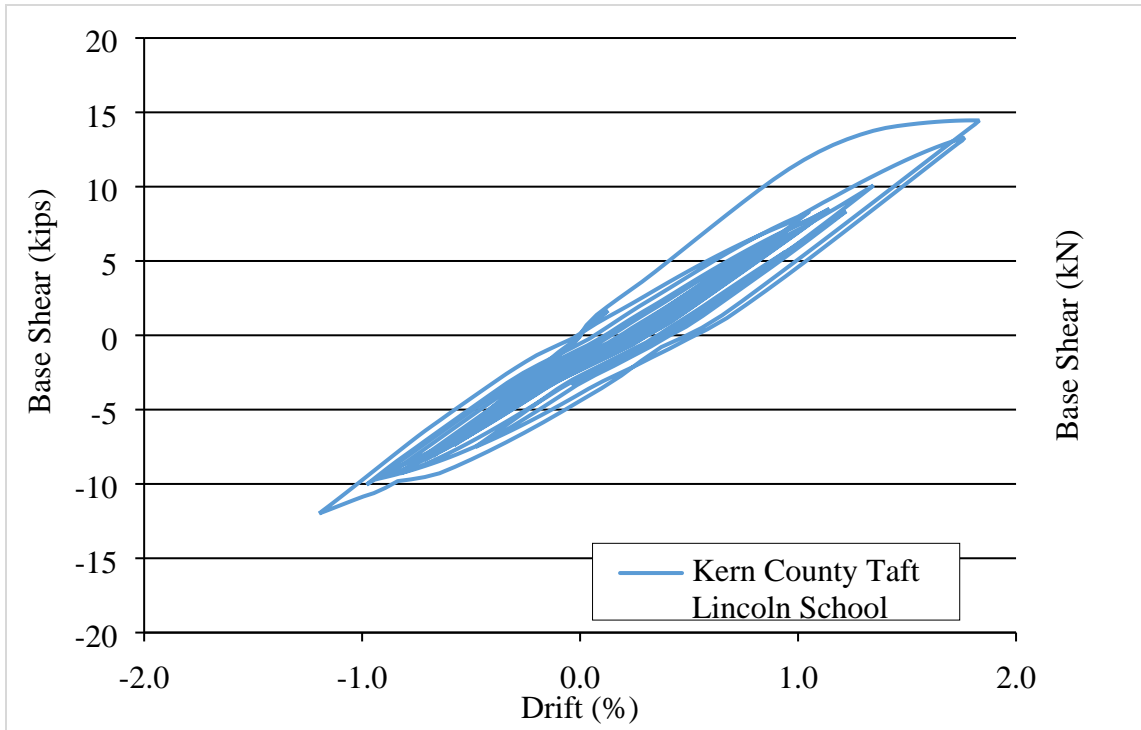
Figure 3.19 Force-displacement relationship for Kern County dynamic analysis
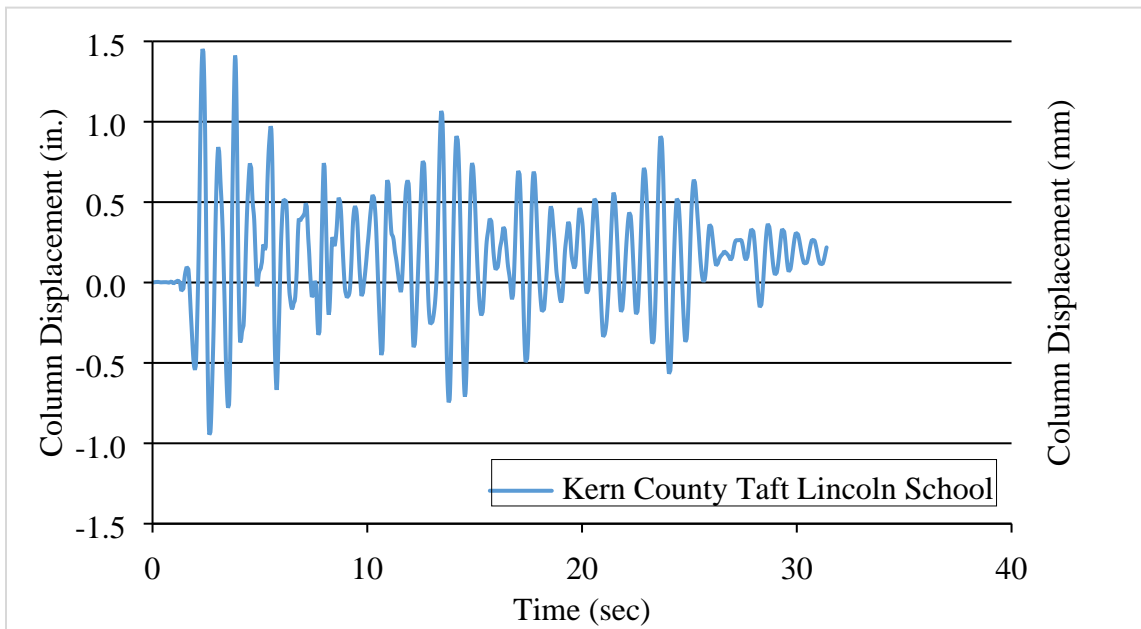
Figure 3.20 Displacement history for Kern County dynamic analysis
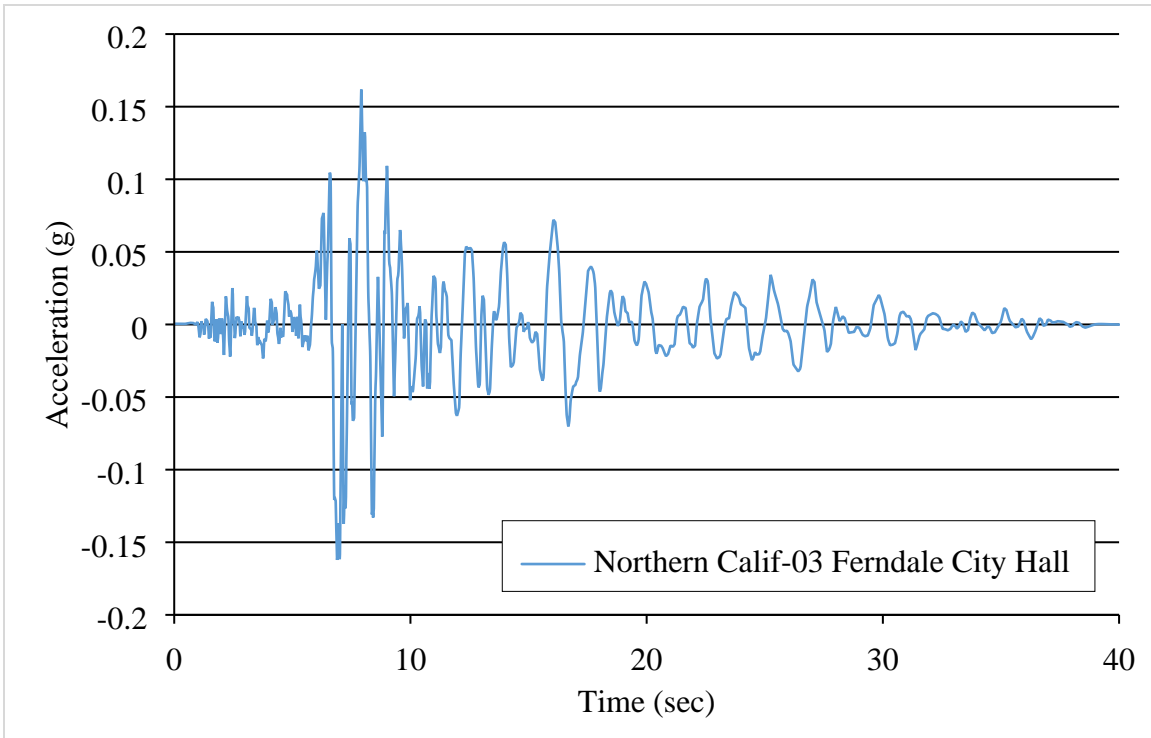
Figure 3.21 Acceleration history for Northern Calif-03 Event at Ferndale City Hall
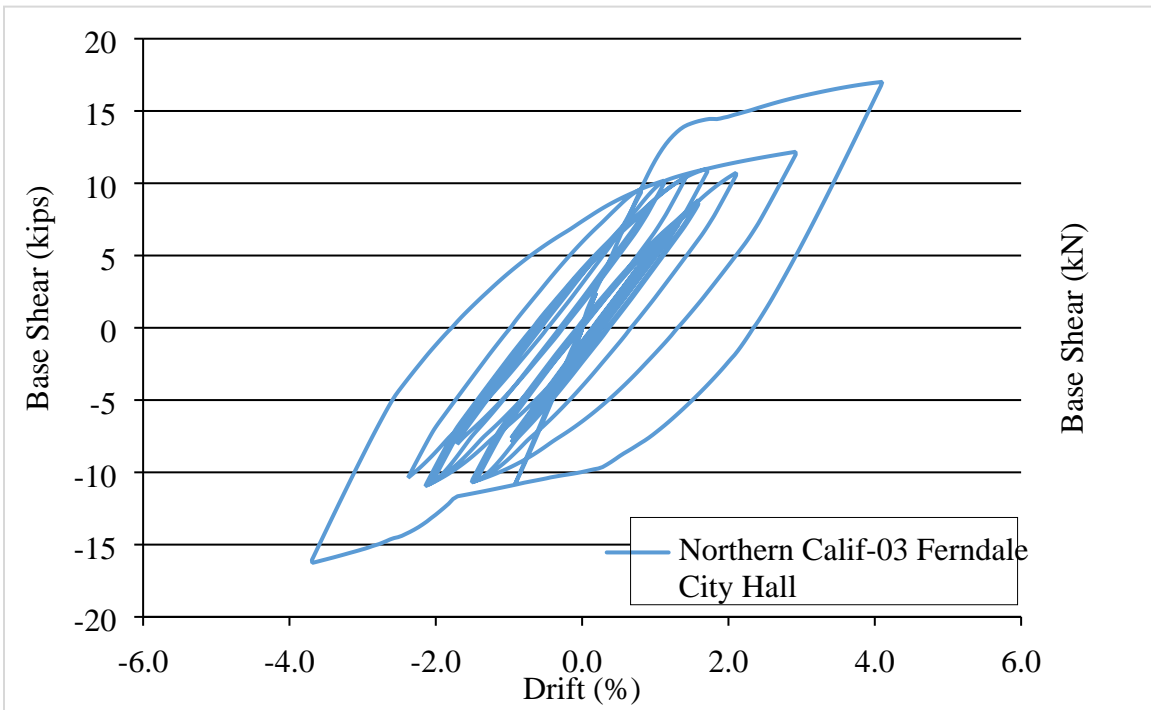
Figure 3.22 Force-displacement relationship for Northern Calif-03 dynamic analysis

111
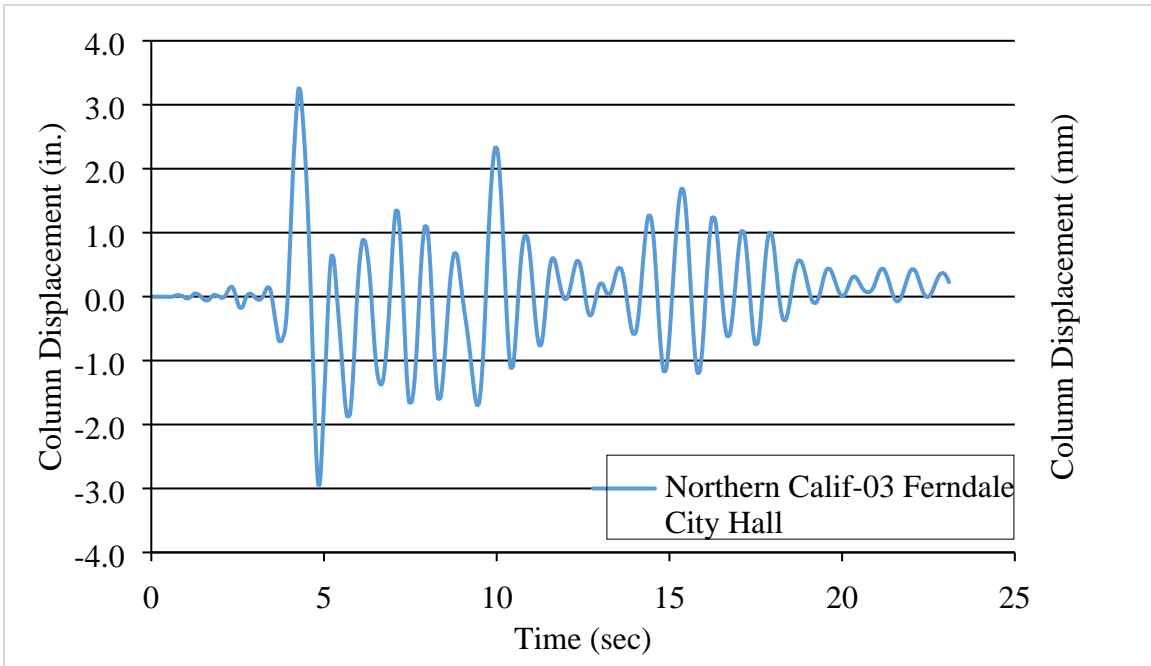
Figure 3.23 Displacement history for Northern Calif-03 dynamic analysis
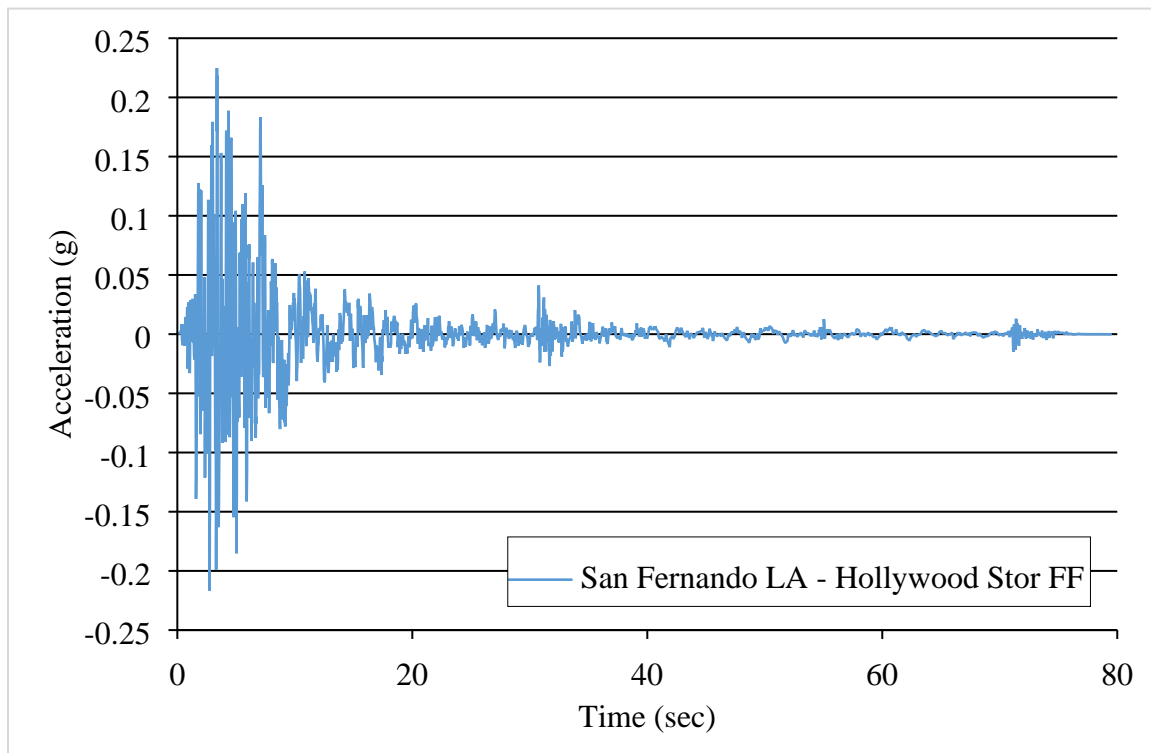
Figure 3.24 Acceleration history for San Fernando Event at LA – Hollywood Stor. FF
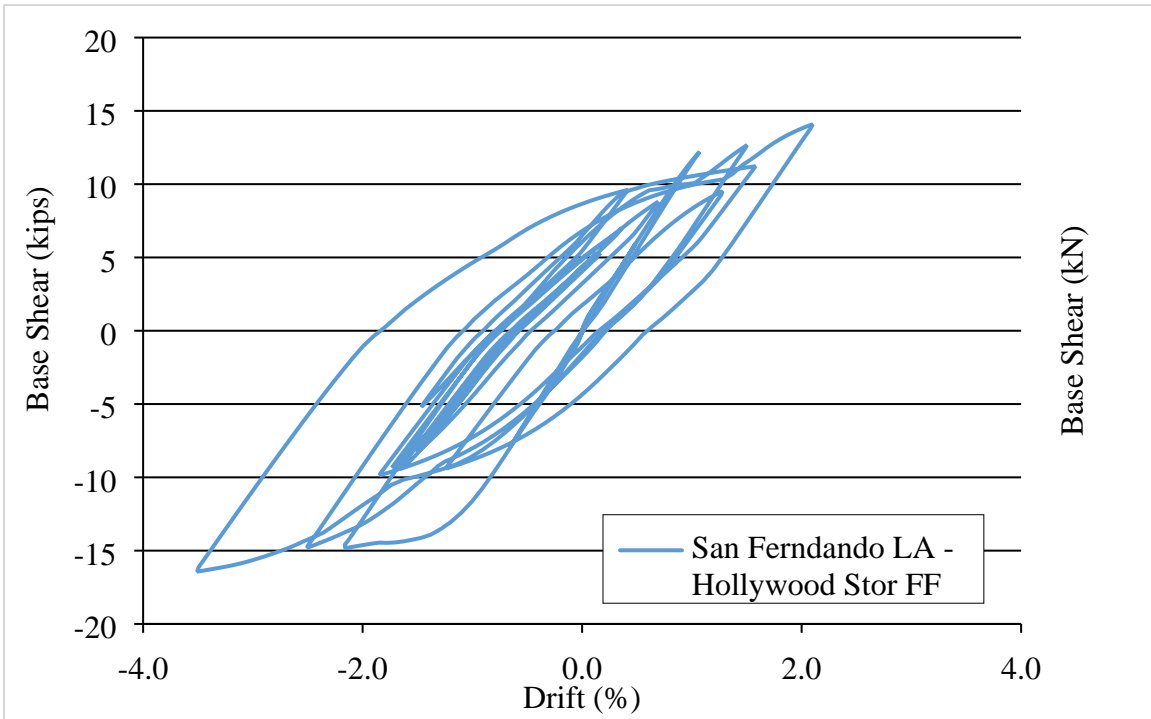
Figure 3.25 Force-displacement relationship for San Fernando dynamic analysis
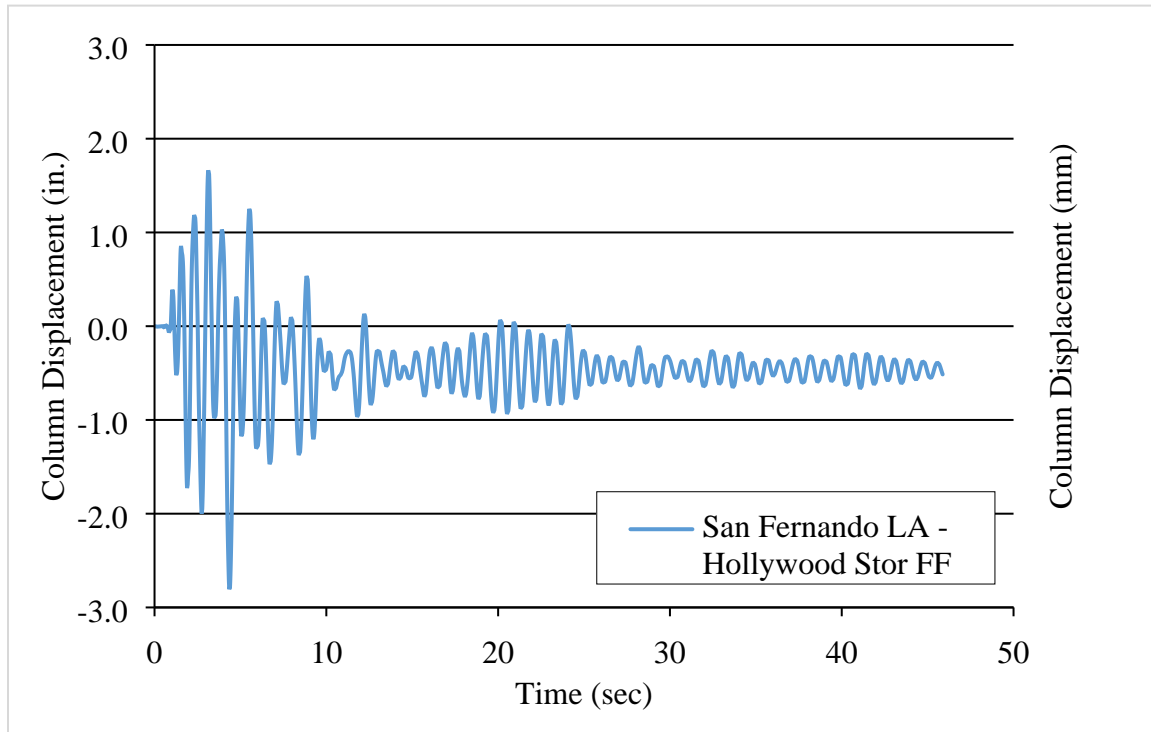
Figure 3.26 Displacement history for San Fernando dynamic analysis

113
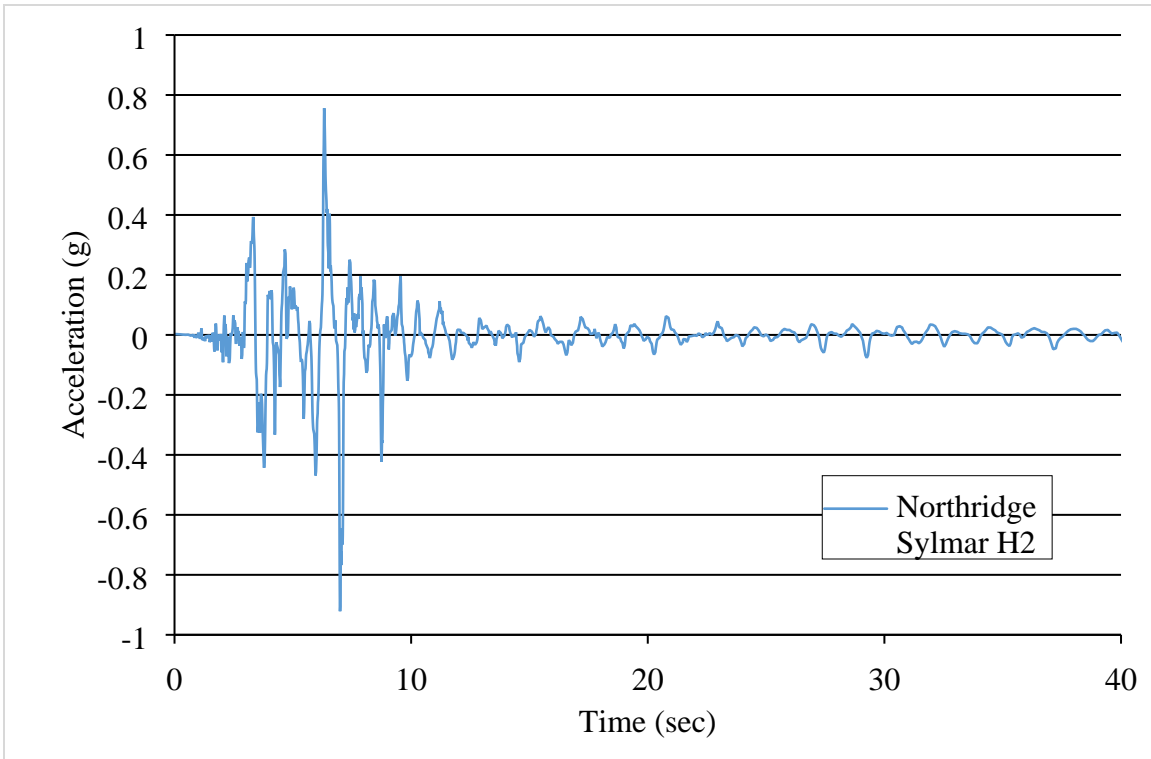
Figure 3.27 Acceleration history for Northridge event at Sylmar Converter Station, H2
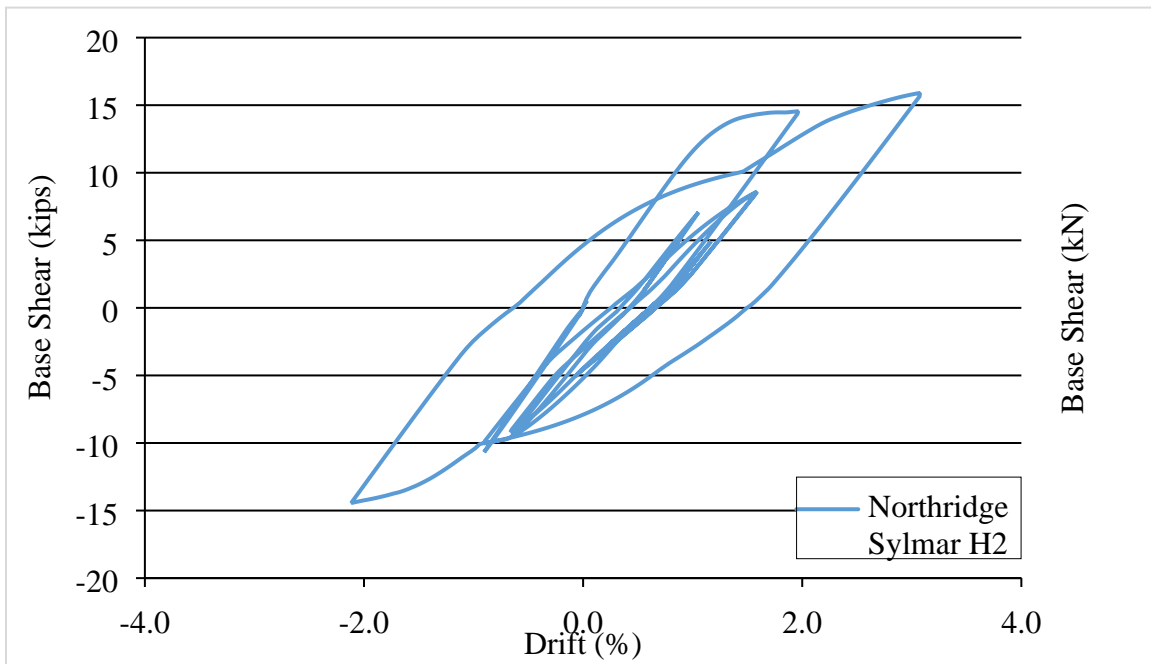
Figure 3.28 Force-displacement relationship for Northridge Sylmar H2 dynamic analysis
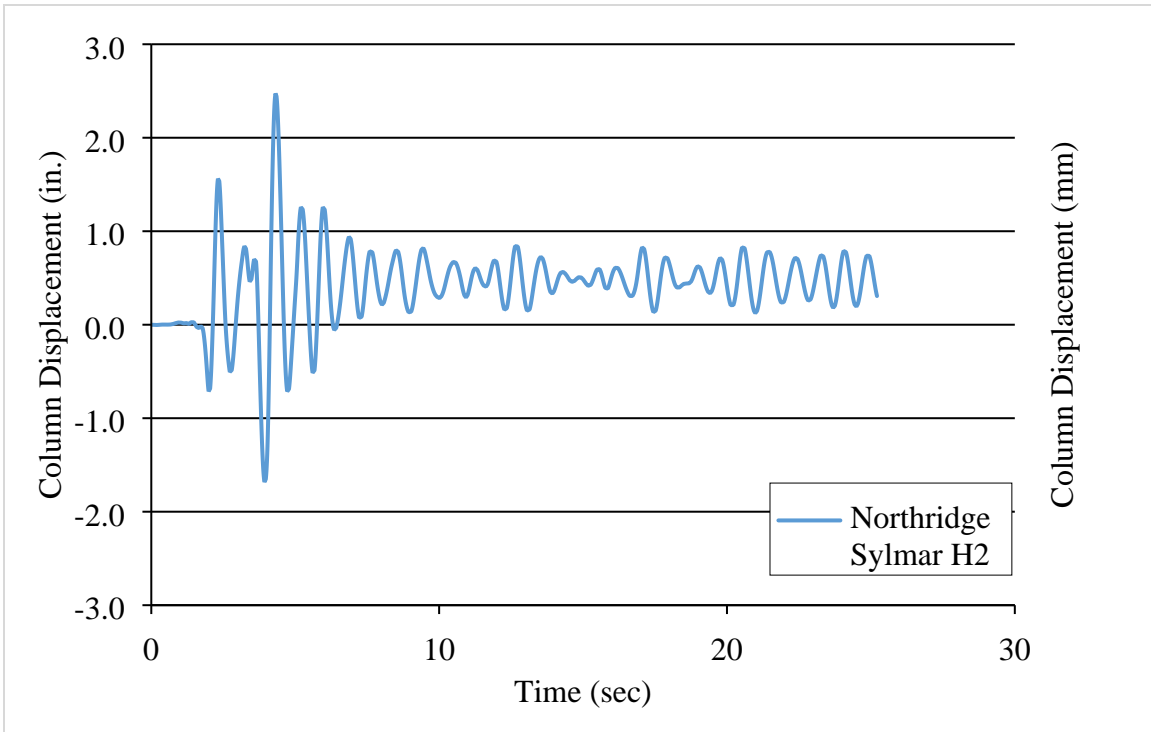
Figure 3.29 Displacement history for Northridge Sylmar H2 dynamic analysis
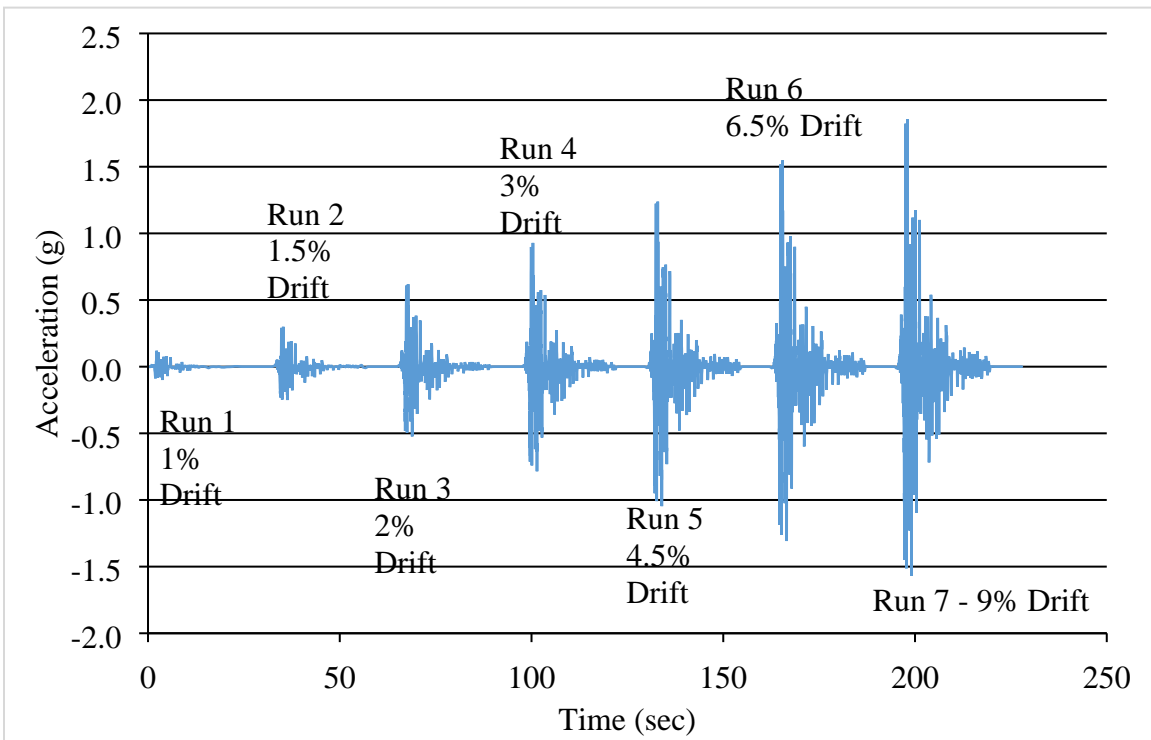
Figure 3.30 Loading protocol acceleration history
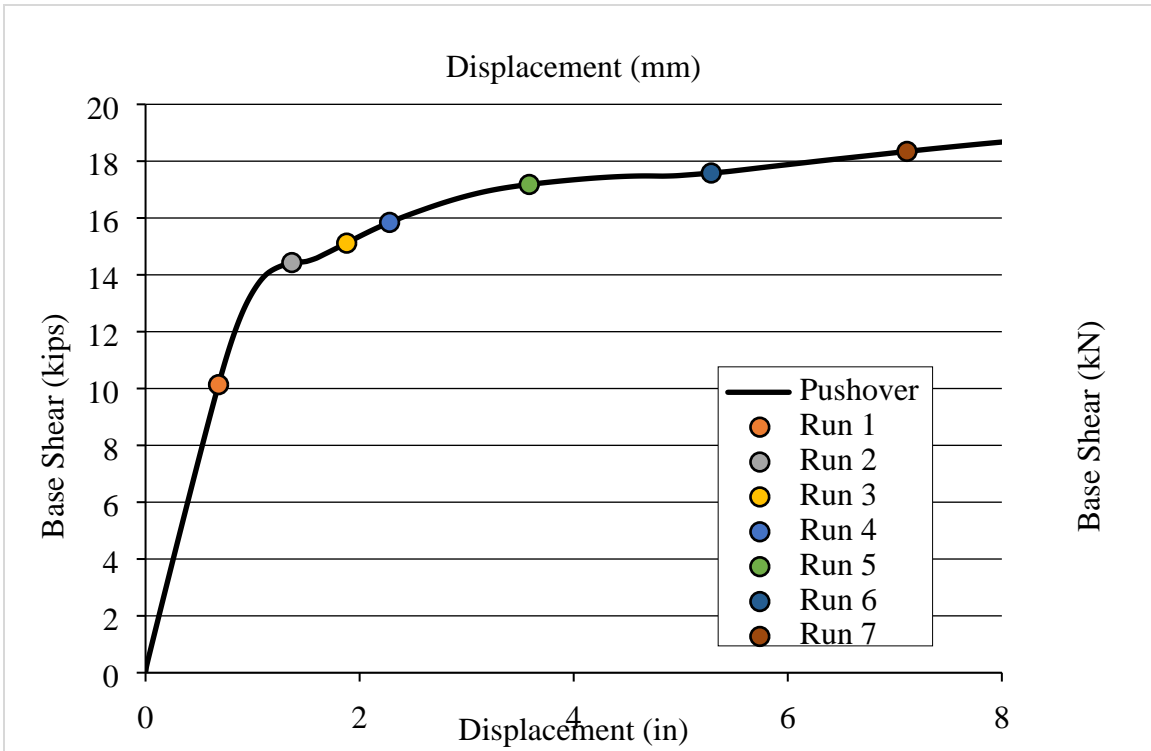
Figure 3.31 Points of pushover curve captured by loading protocol
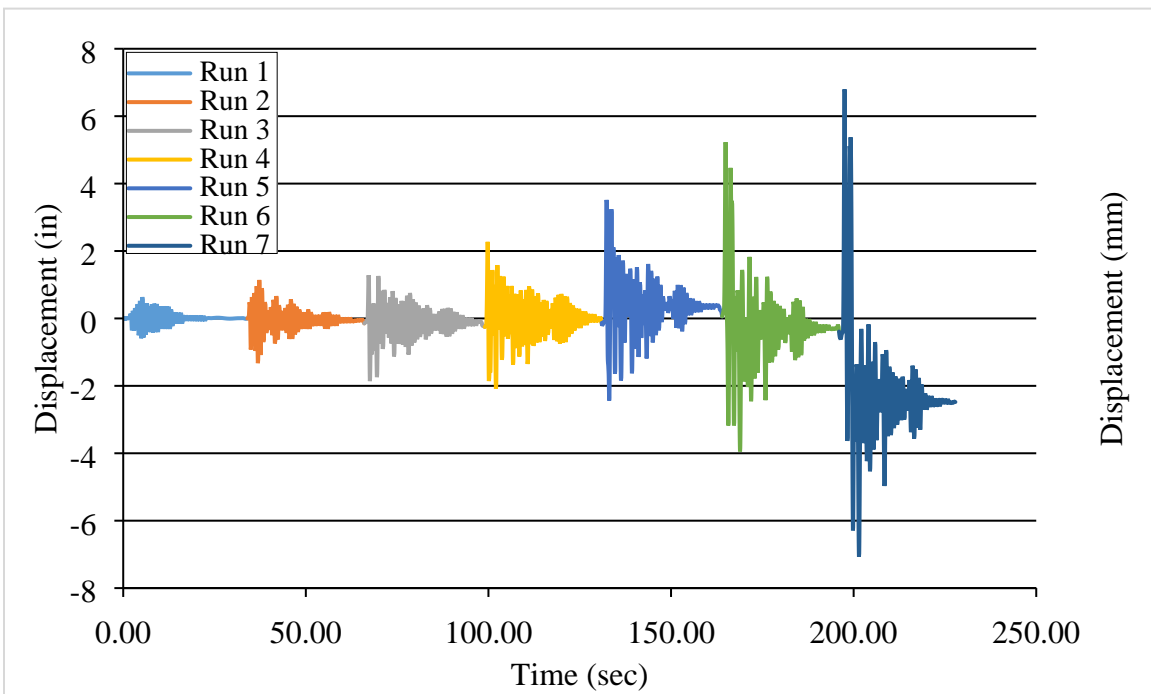
Figure 3.32 Predicted displacement history for all runs
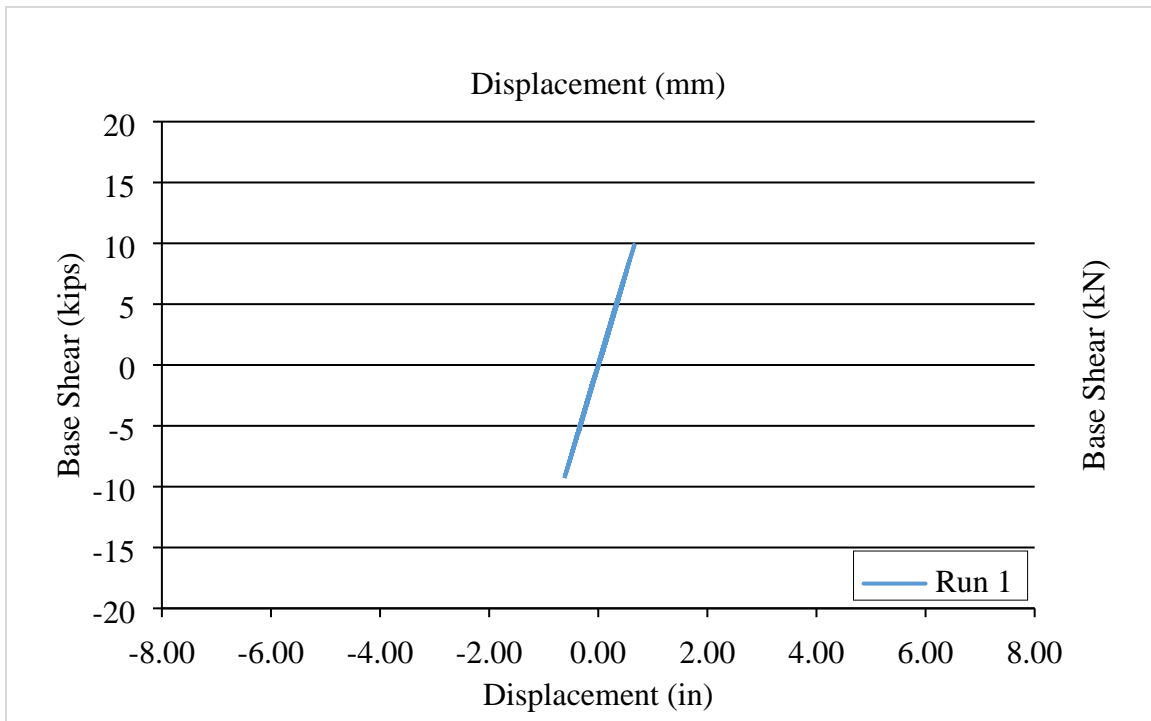
Figure 3.33 Force-displacement relationship for run 1
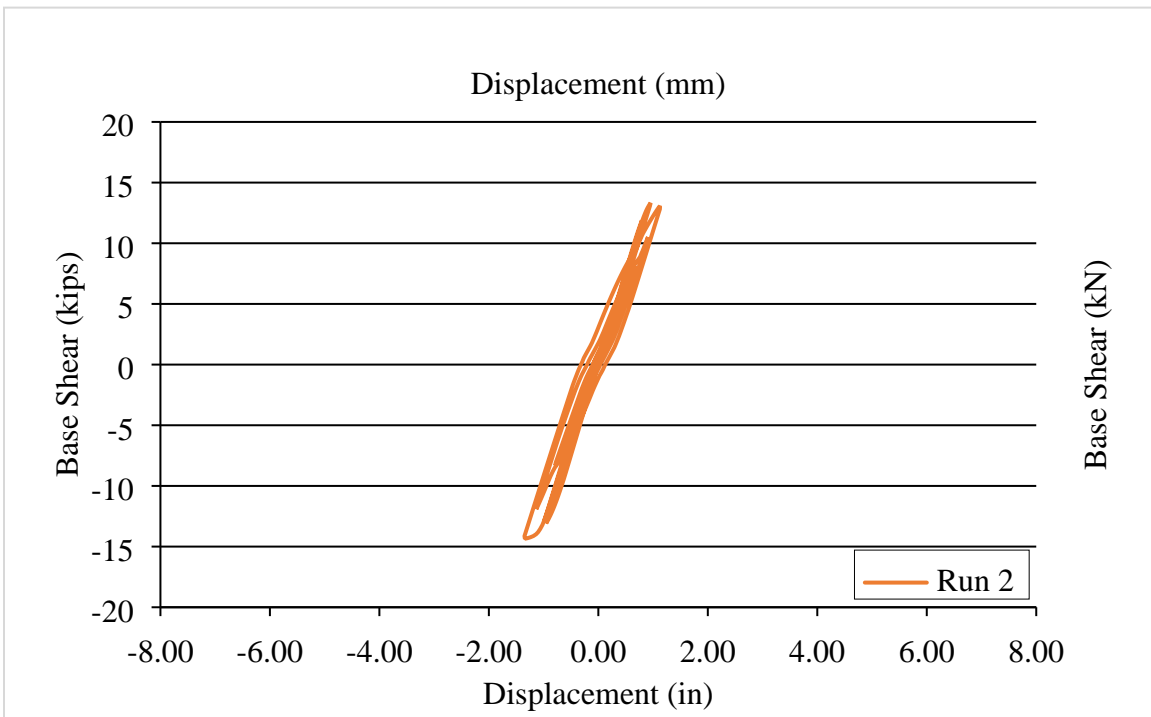
Figure 3.34 Force-displacement relationship for run 2
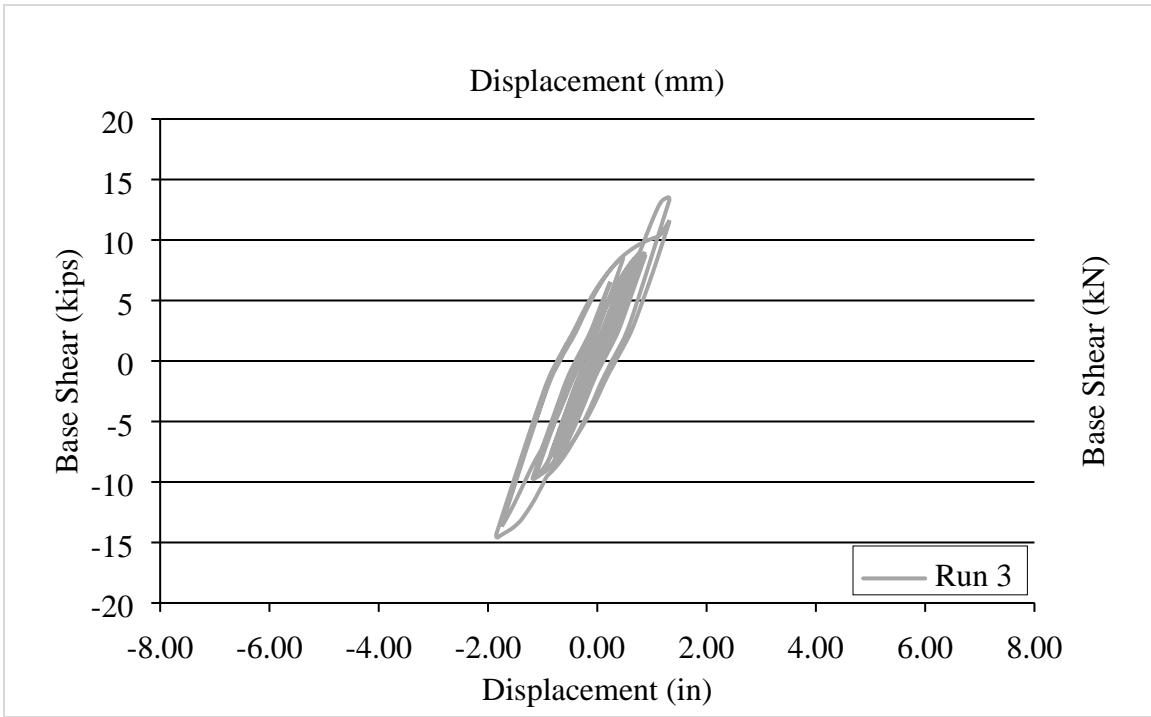
Figure 3.35 Force-displacement relationship for run 3
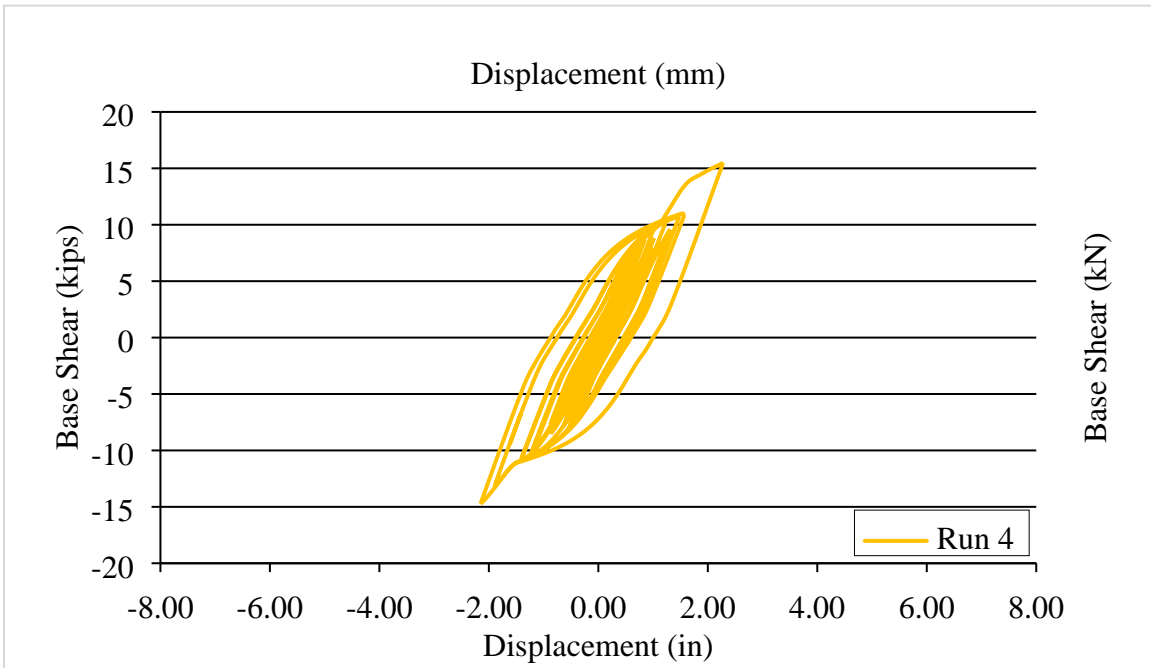
Figure 3.36 Force-displacement relationship for run 4
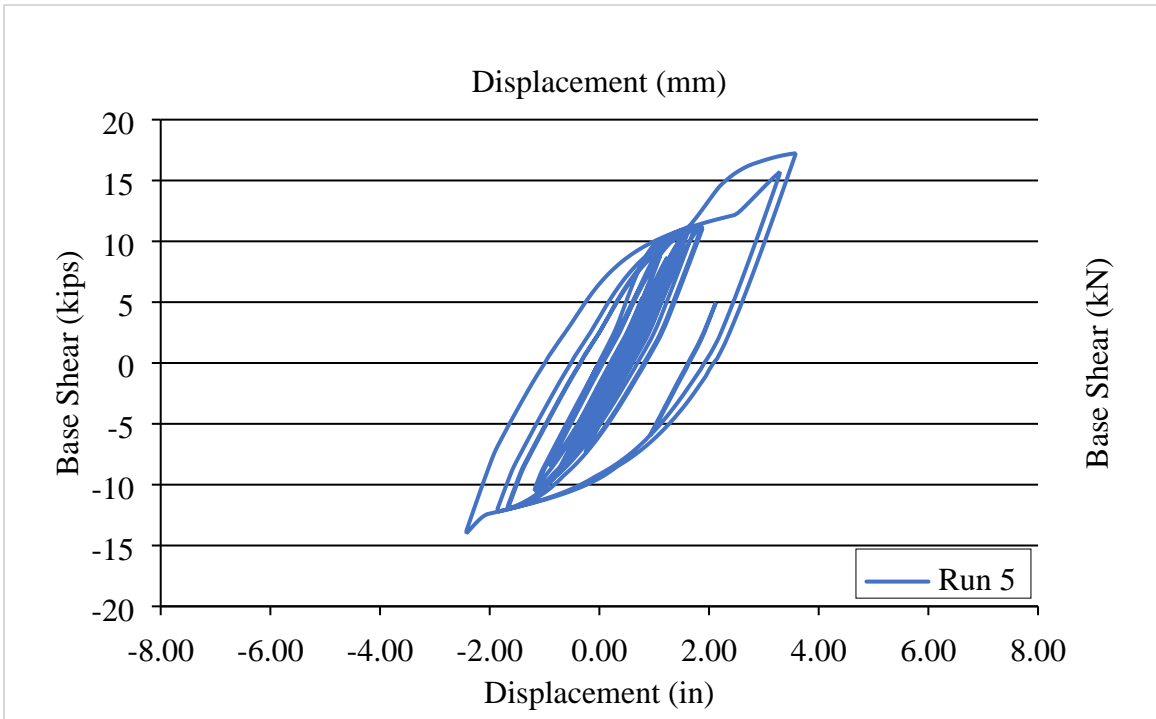
Figure 3.37 Force-displacement relationship for run 5
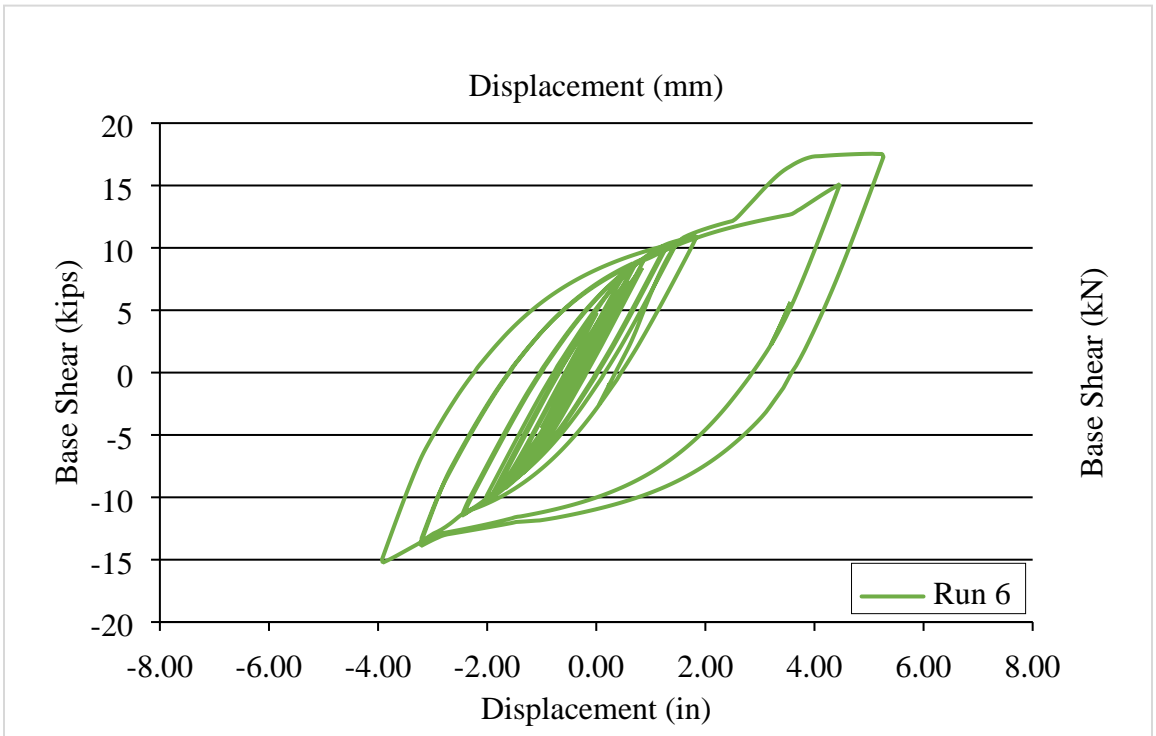
Figure 3.38 Force-displacement relationship for run 6
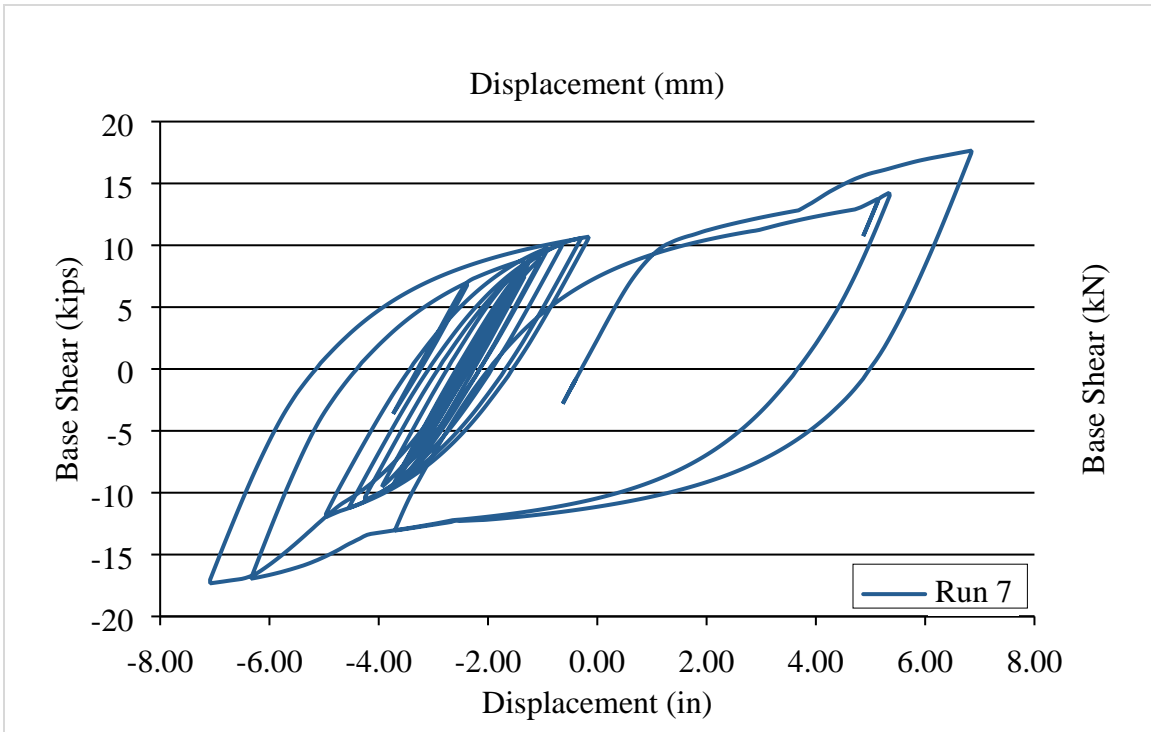
Figure 3.39 Force-displacement relationship for run 7
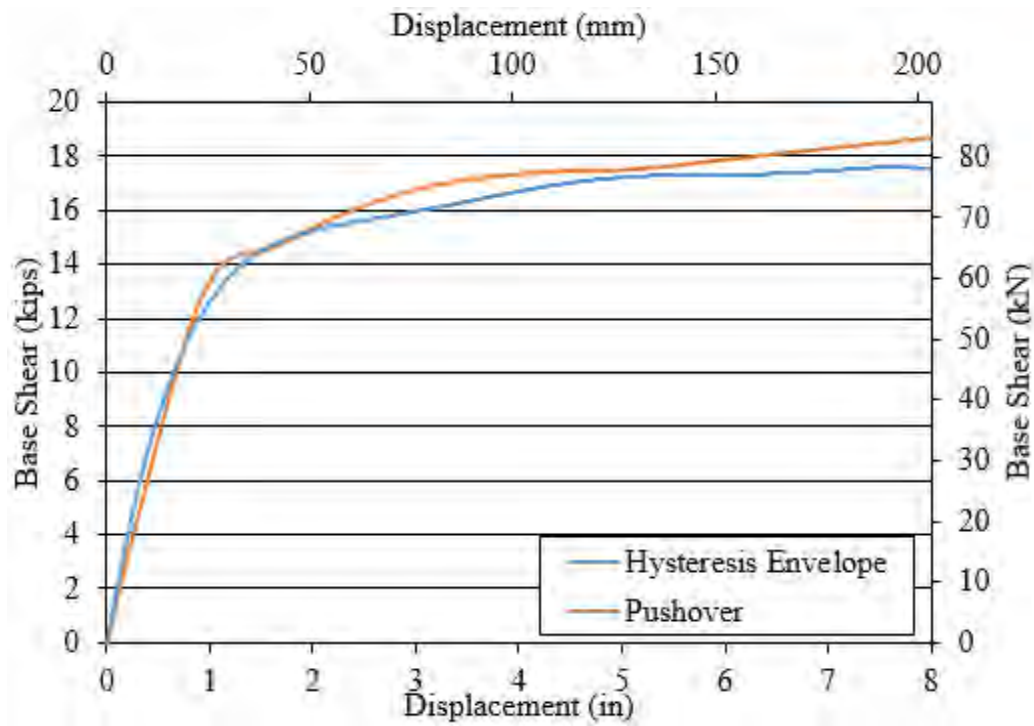
Figure 3.40 Hysteresis envelope compared to pushover curve

120

Chapter 4 Figures
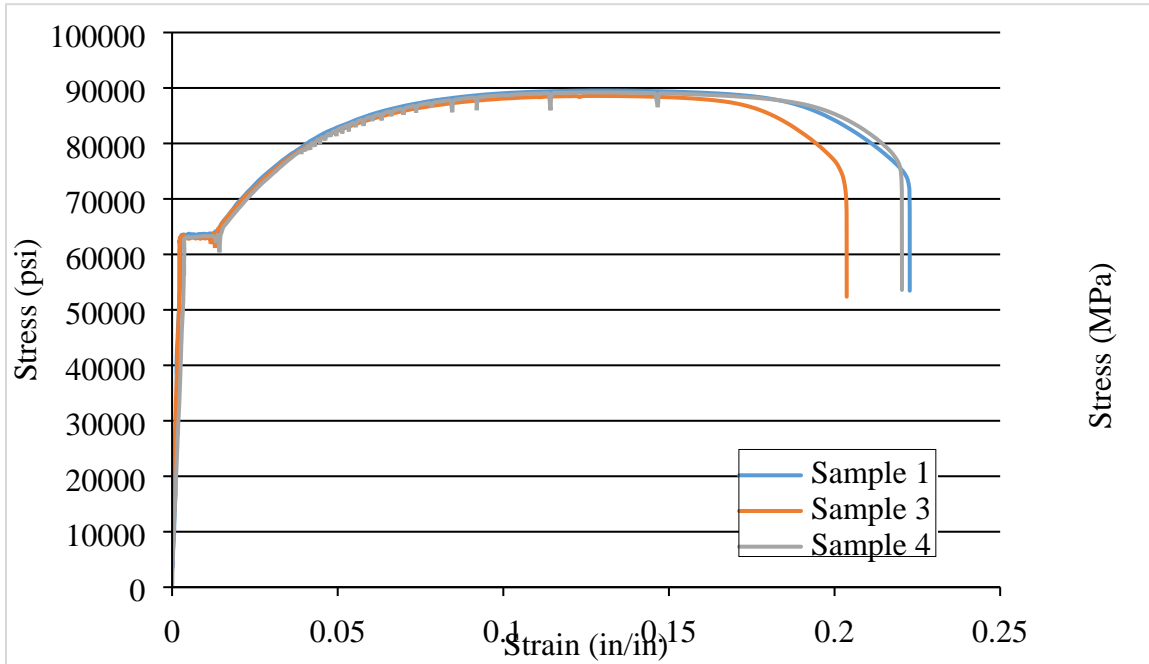
Figure 4.1 Measured stress-strain relationships for #3 bars
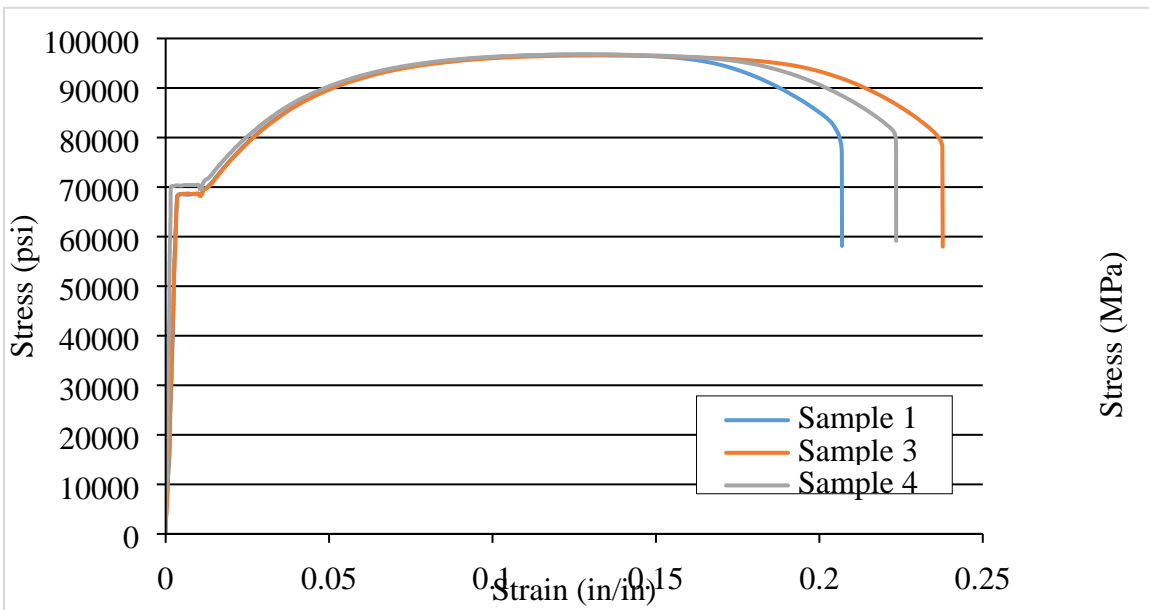
Figure 4.2 Measured stress-strain relationships for #4 bars
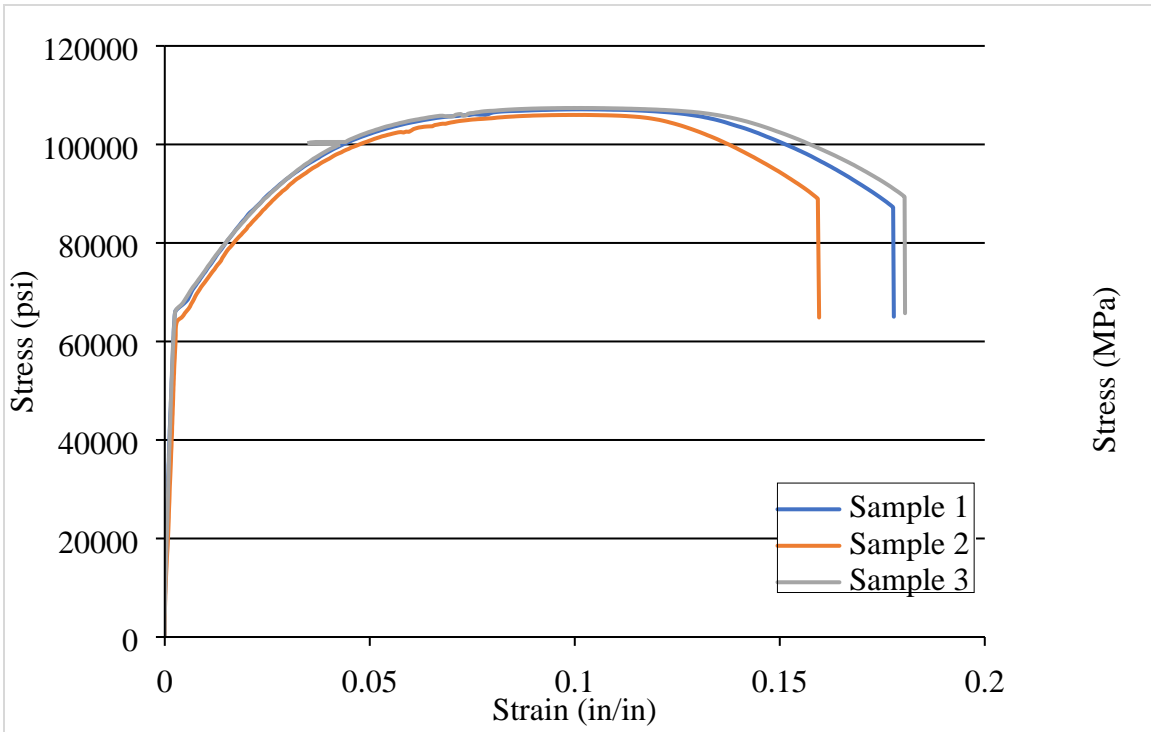
Figure 4.3 Measured stress-strain relationships for #5 bars
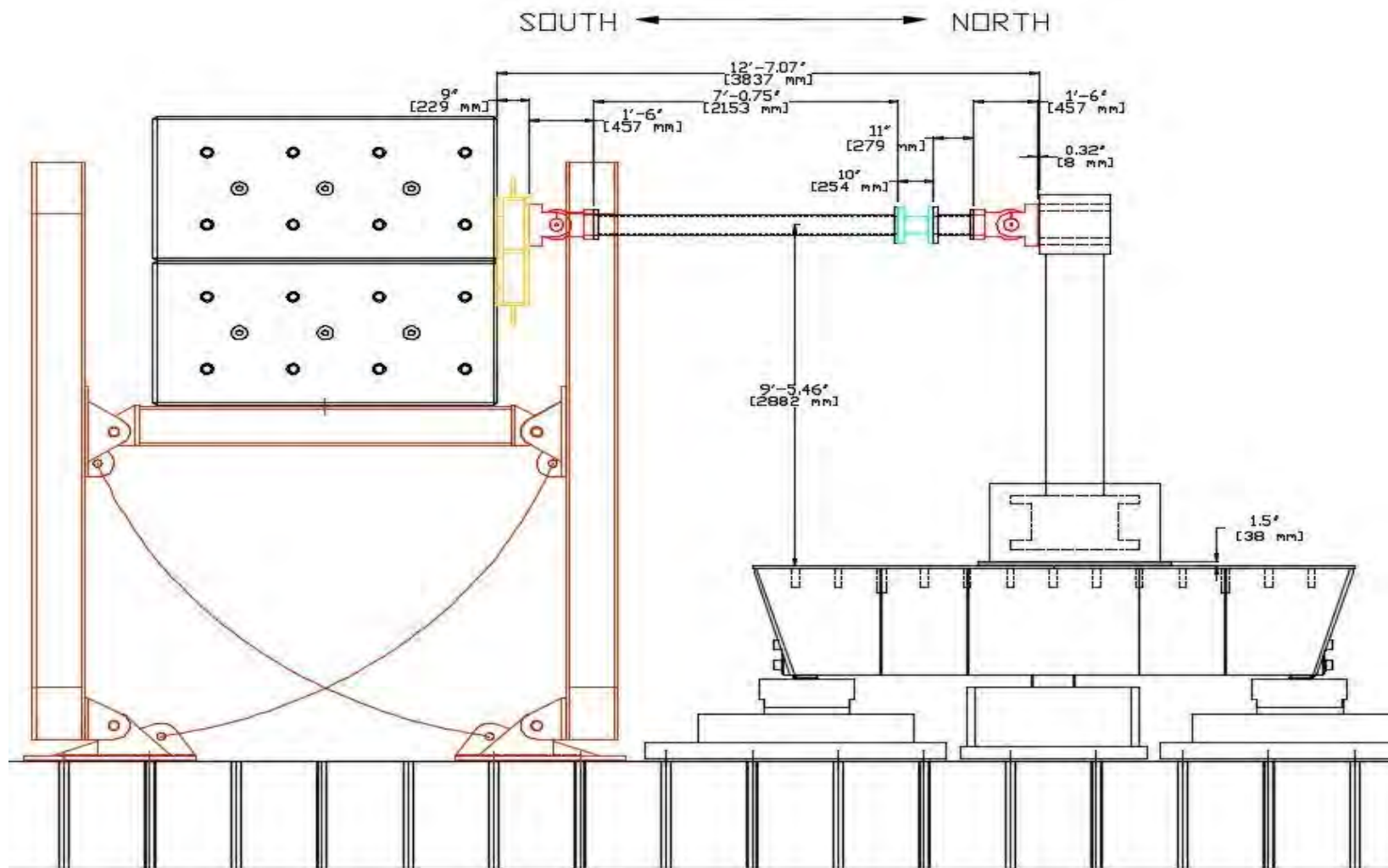
Figure 4.4 Elevation view of test setup
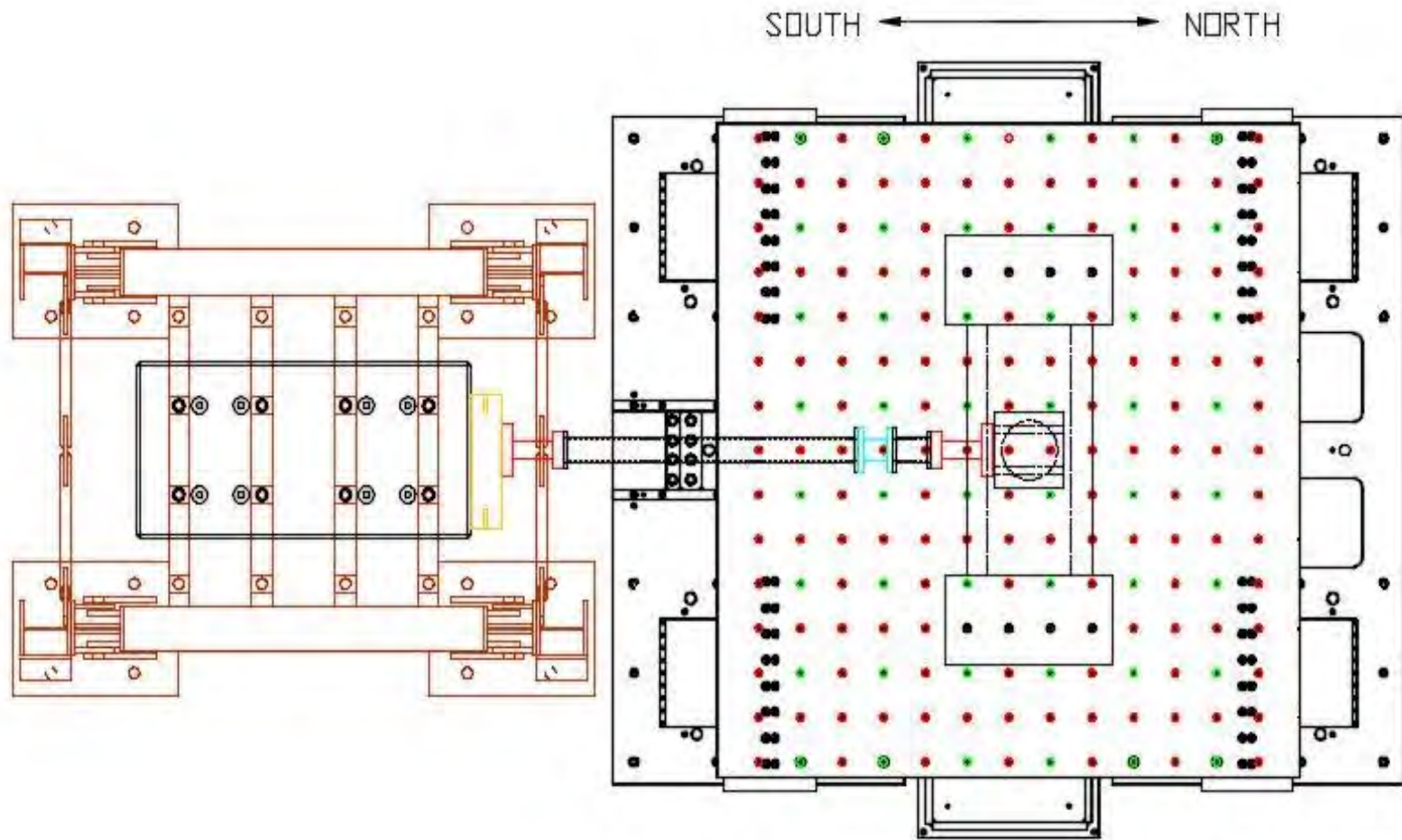
Figure 4.5 Plan view of test setup
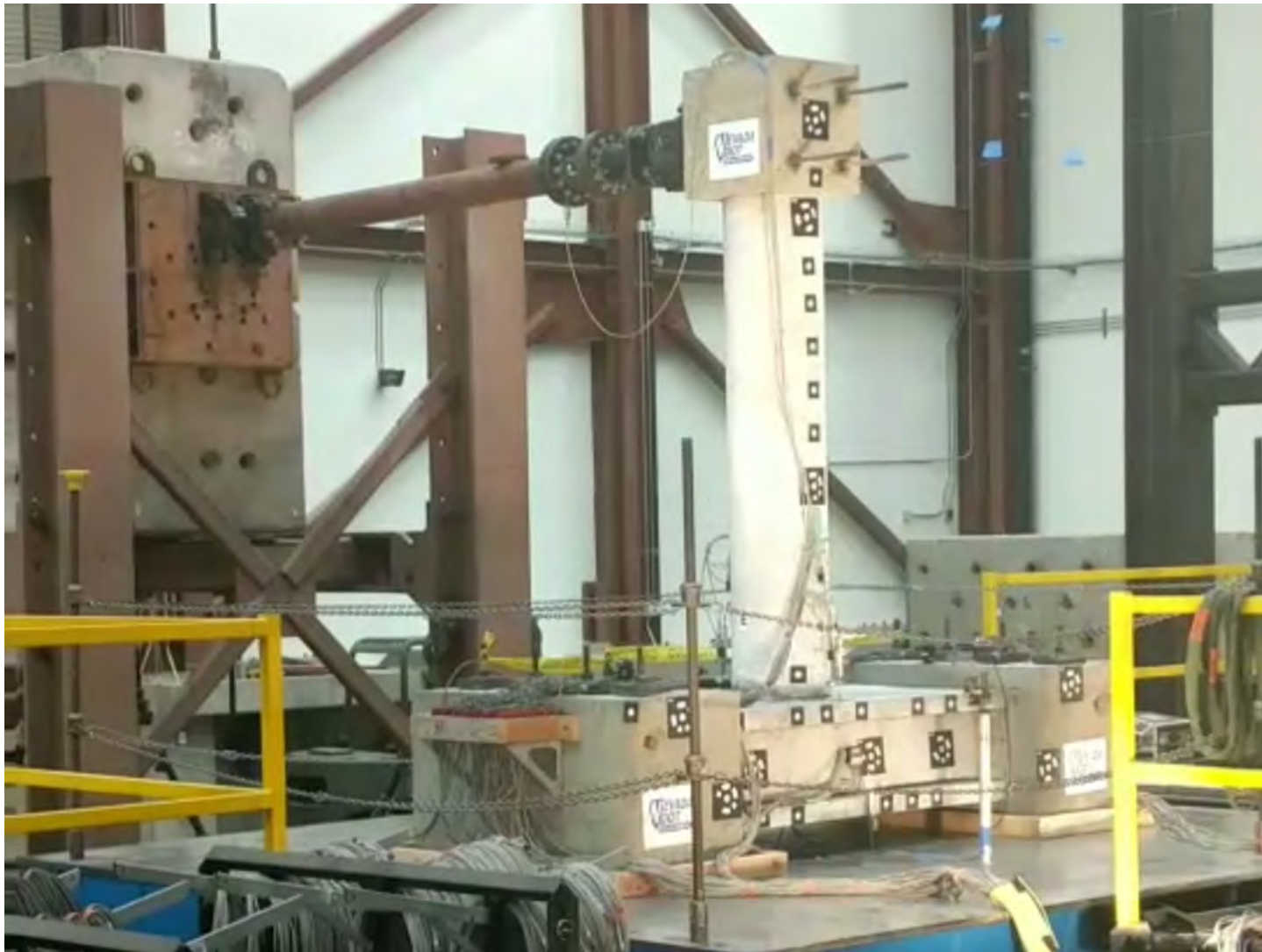
Figure 4.6 Photo of test setup
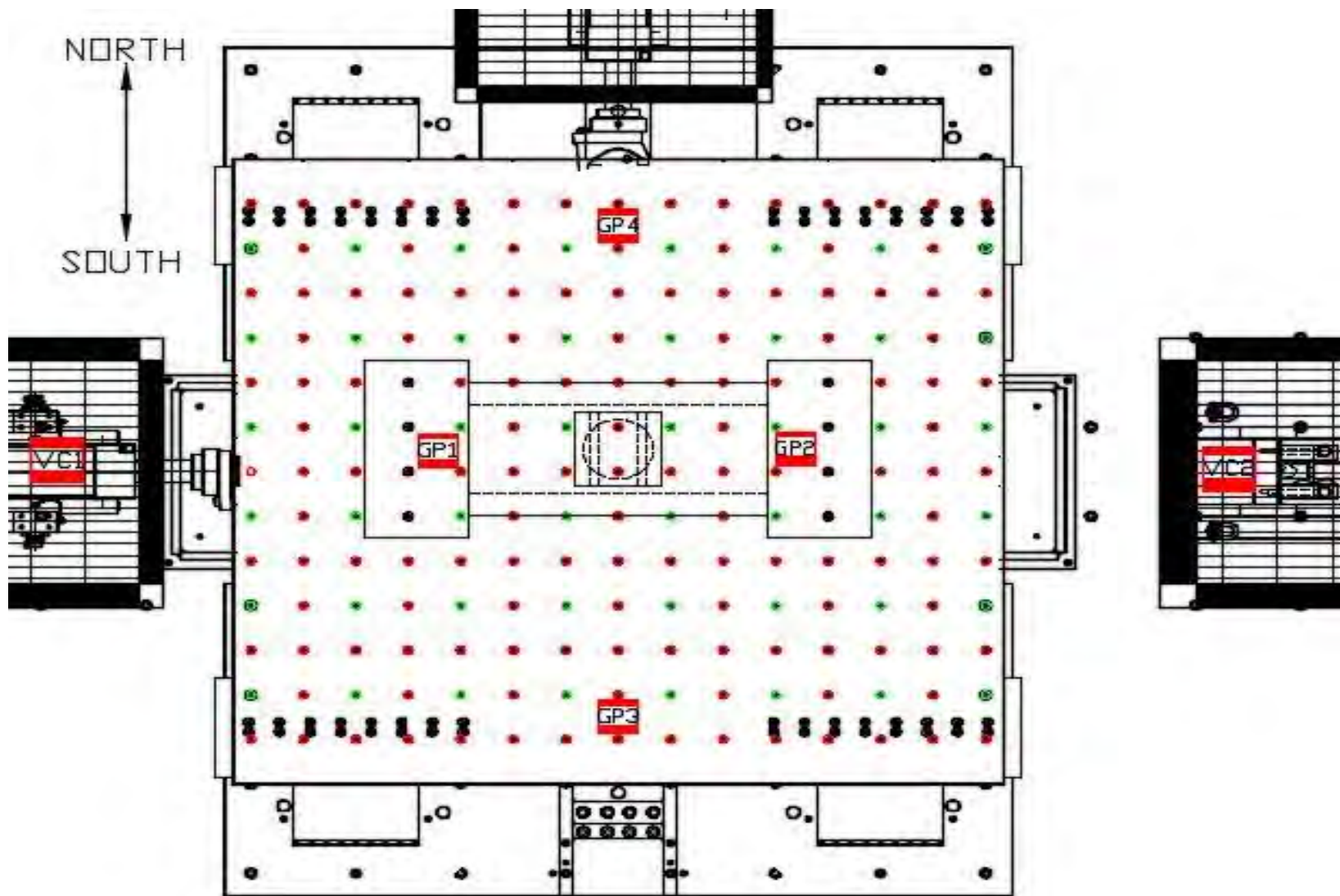
Figure 4.7 Video camera and GoPro locations
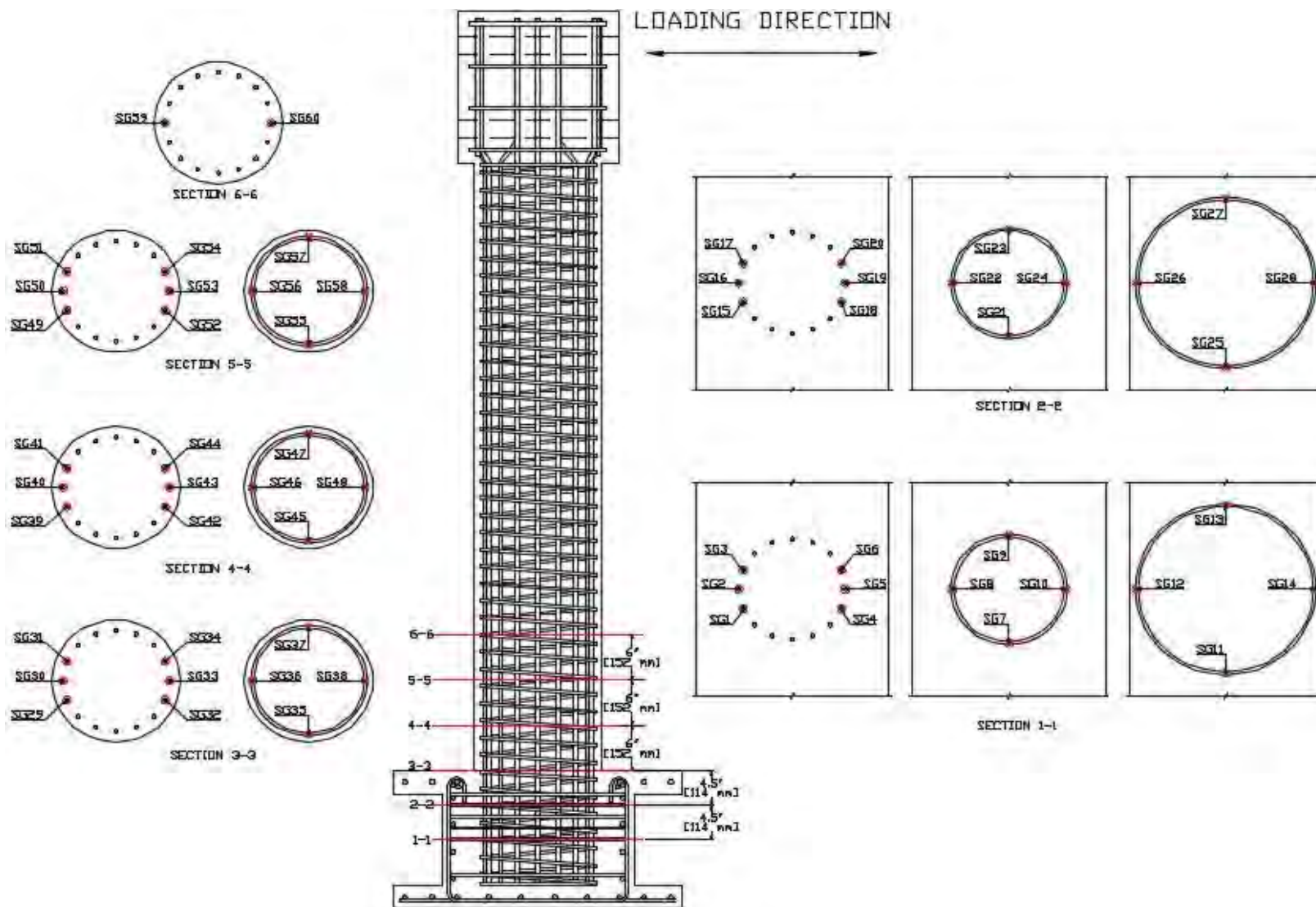
Figure 4.8 Strain gauge locations in column

Figure 4.9 Strain gauge locations around pocket connection
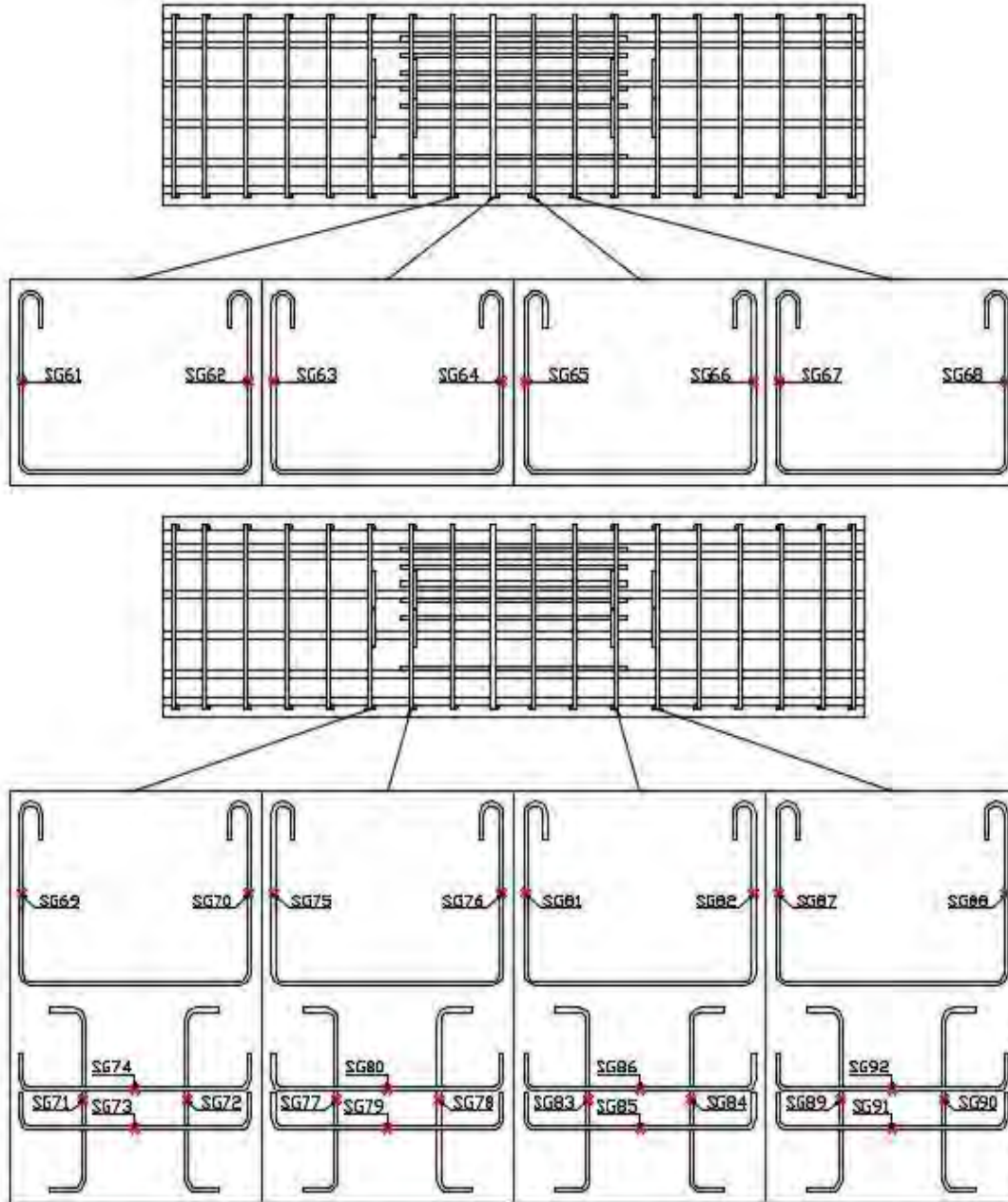
NOTE: ALL STRAIN GAUGES PLACED AT MID-HEIGHT/LENGTH OF STIRRUPS AND TIES

SECTION A-A
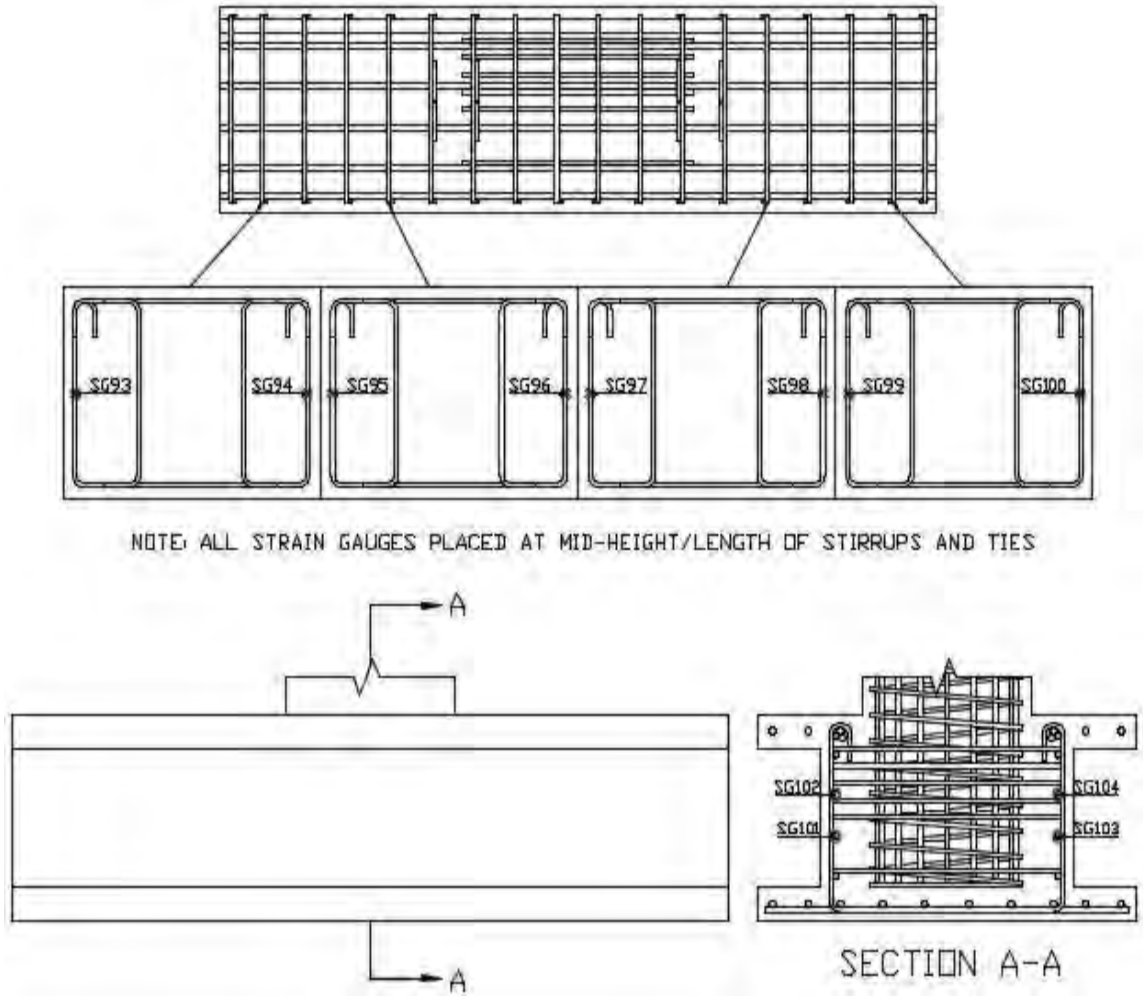
Figure 4.10 Strain gauge locations in cap beam
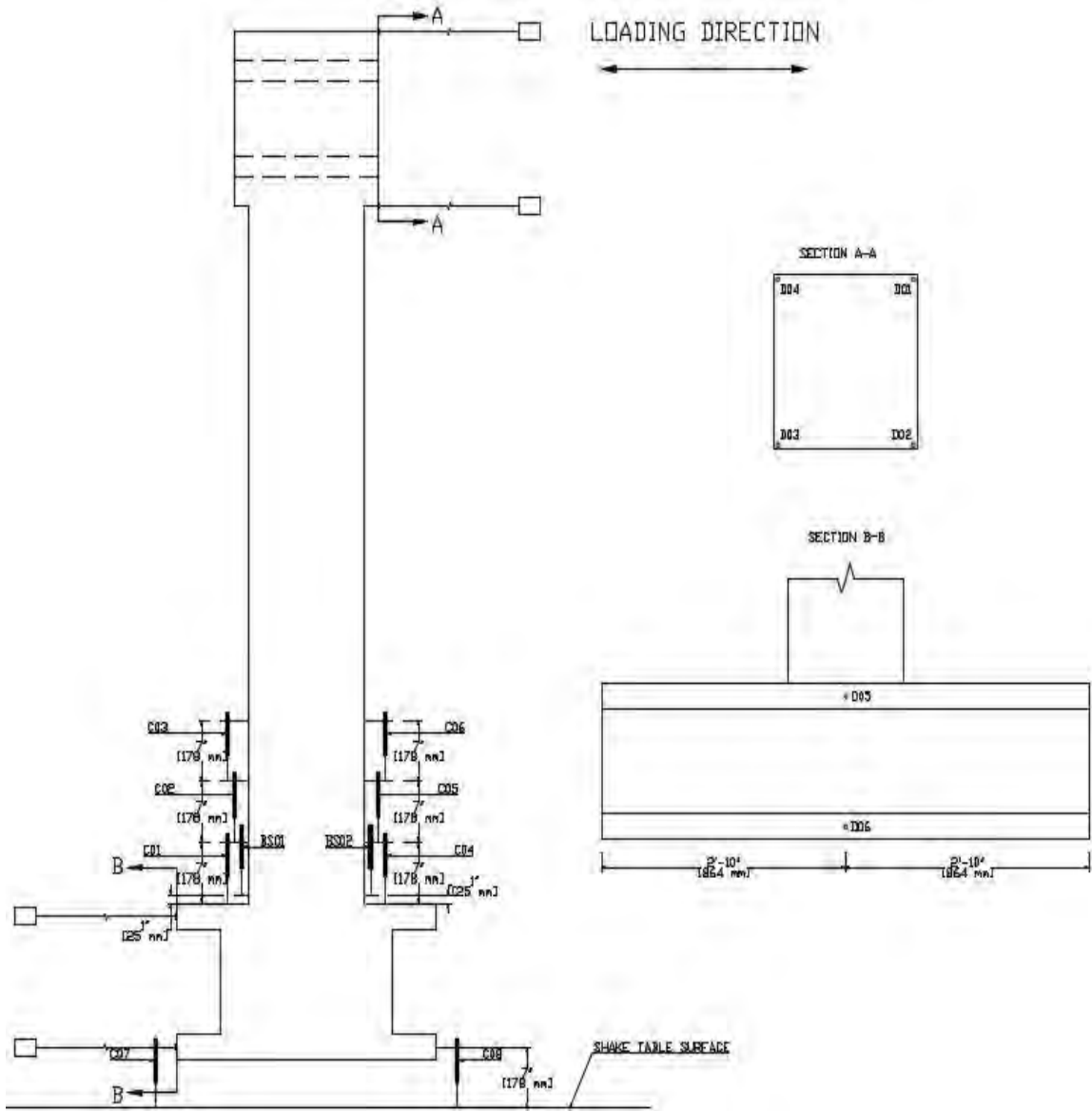
Figure 4.11 Locations of Novatechnik displacement transducers and string potentiometers
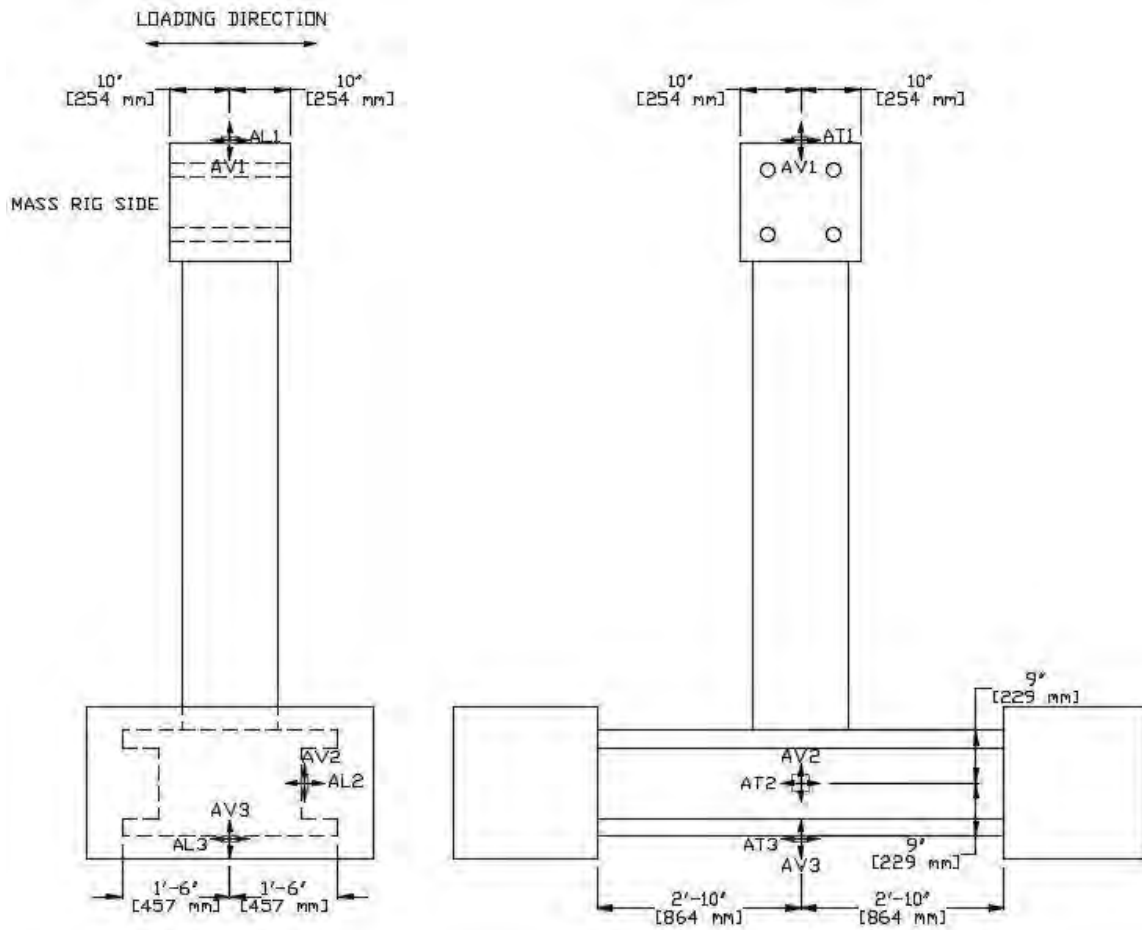
Figure 4.12 Accelerometer locations

Chapter 5 Figures

Figure 5.1 Shrinkage cracks in cap beam
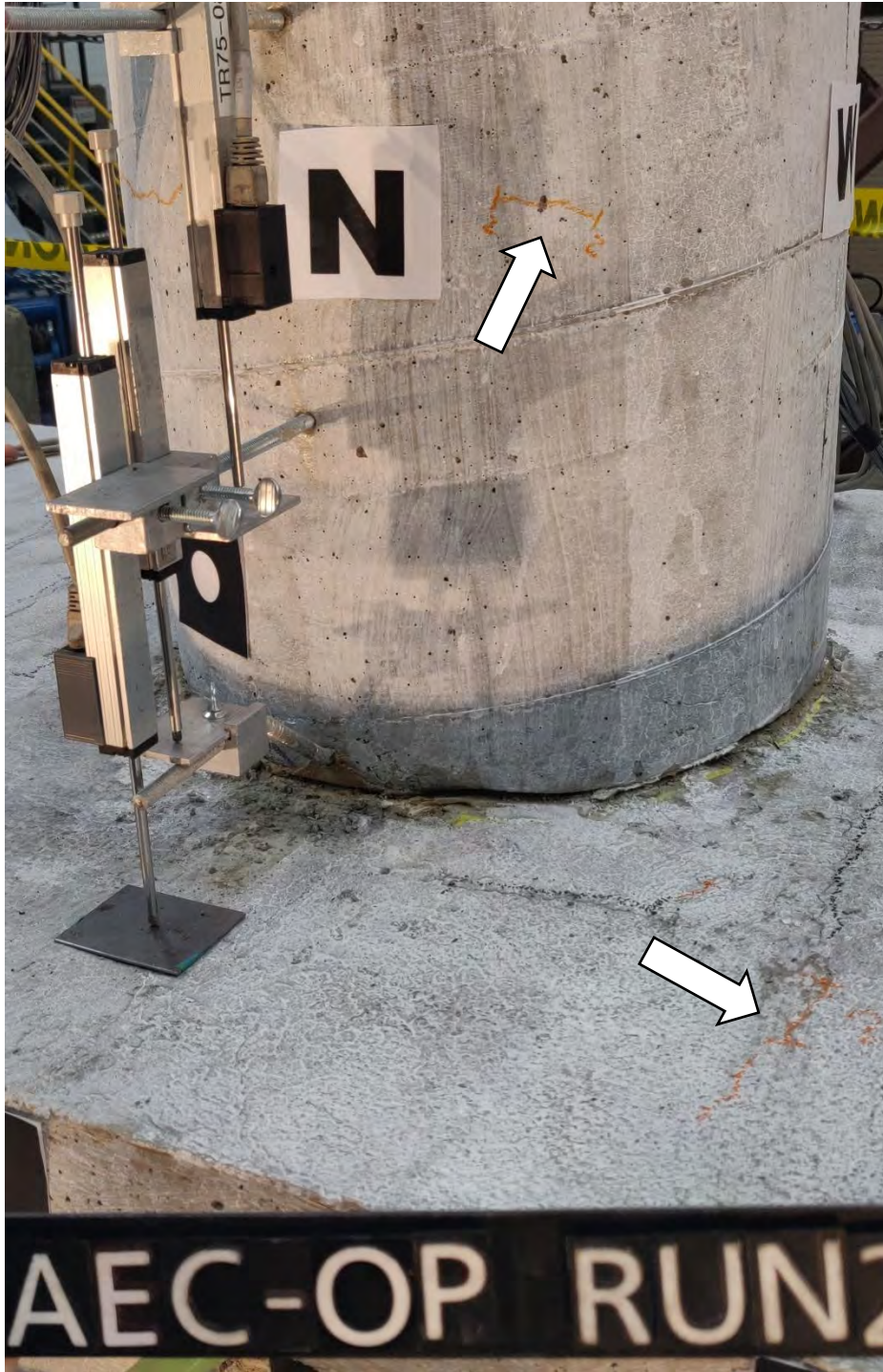
Figure 5.2 Column and cap beam damage after run 2

Figure 5.3 Flexural cracks on column north side after run 3

Figure 5.4 Shear and torsion cracks on cap beam south side after run 3

Figure 5.5 Flexural cracks on column north side after run 5
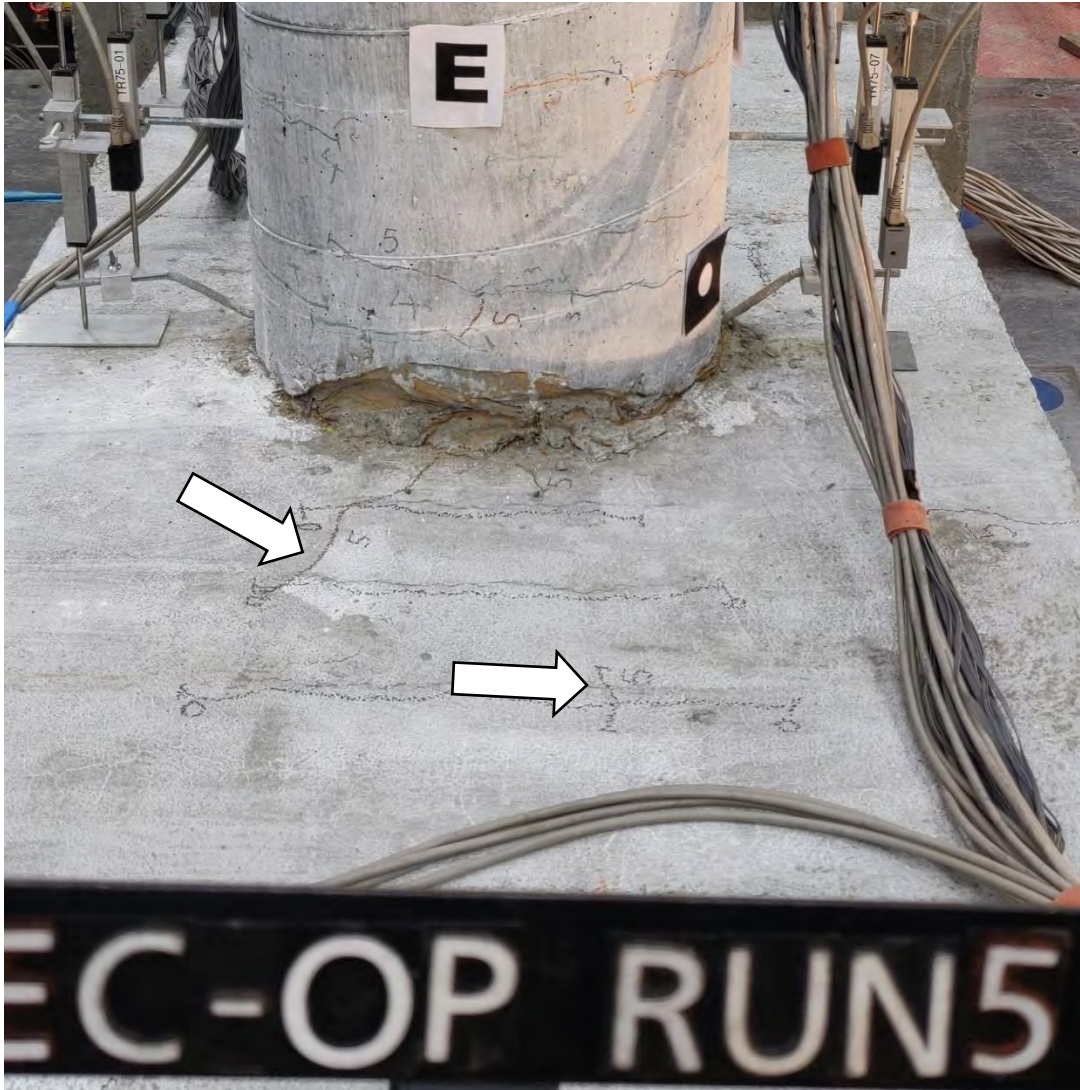
Figure 5.6 Torsion and shear cracks on cap beam east side after run 5

Figure 5.7 Concrete spalling on column south side after run 6

Figure 5.8 Concrete spalling on column south side after run 8

Figure 5.9 Torsion crack in cap beam flange after run 7
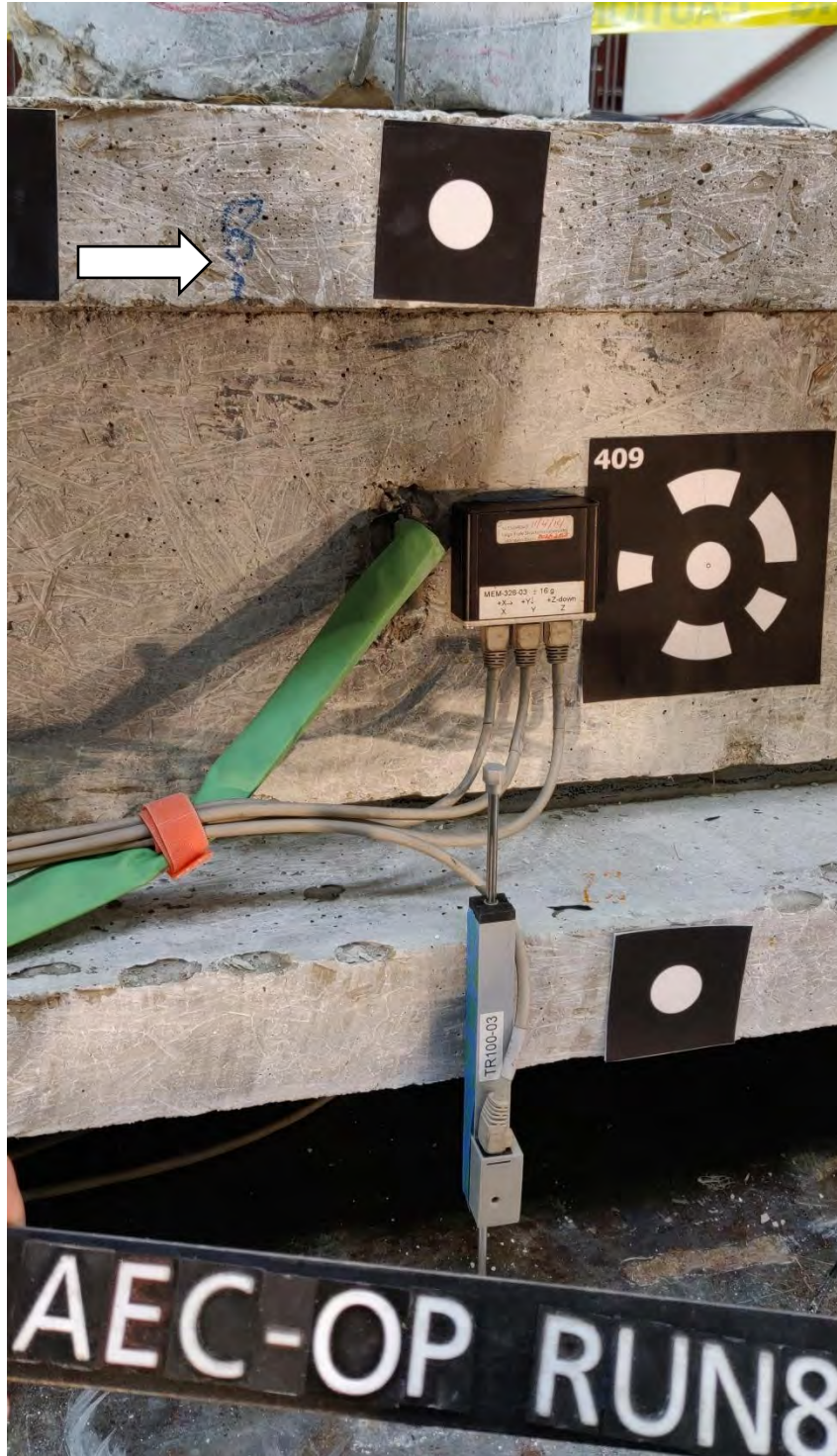
Figure 5.10 Torsion crack in cap beam flange after run 8

Figure 5.11 Shear crack on column north side after run 9
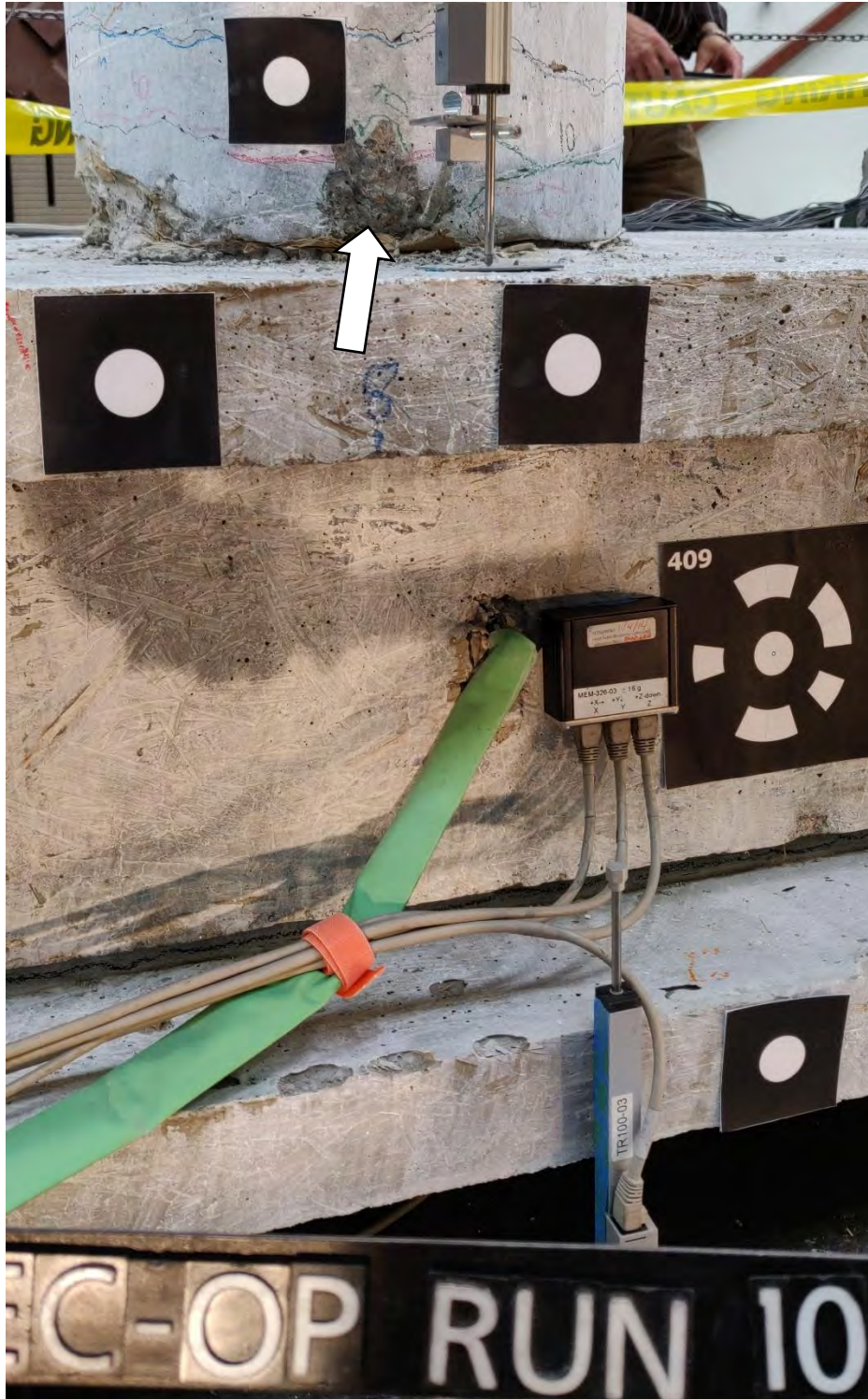
Figure 5.12 Concrete spalling on column north side after run 10

Figure 5.13 Flexural cracks widening after run 10

Figure 5.14 Concrete spalling on column north side after run 11 (final run)

Figure 5.15 Concrete spalling on column south side after run 11 (final run)

Figure 5.16 Widened flexural crack on column south side after run 11 (final run)
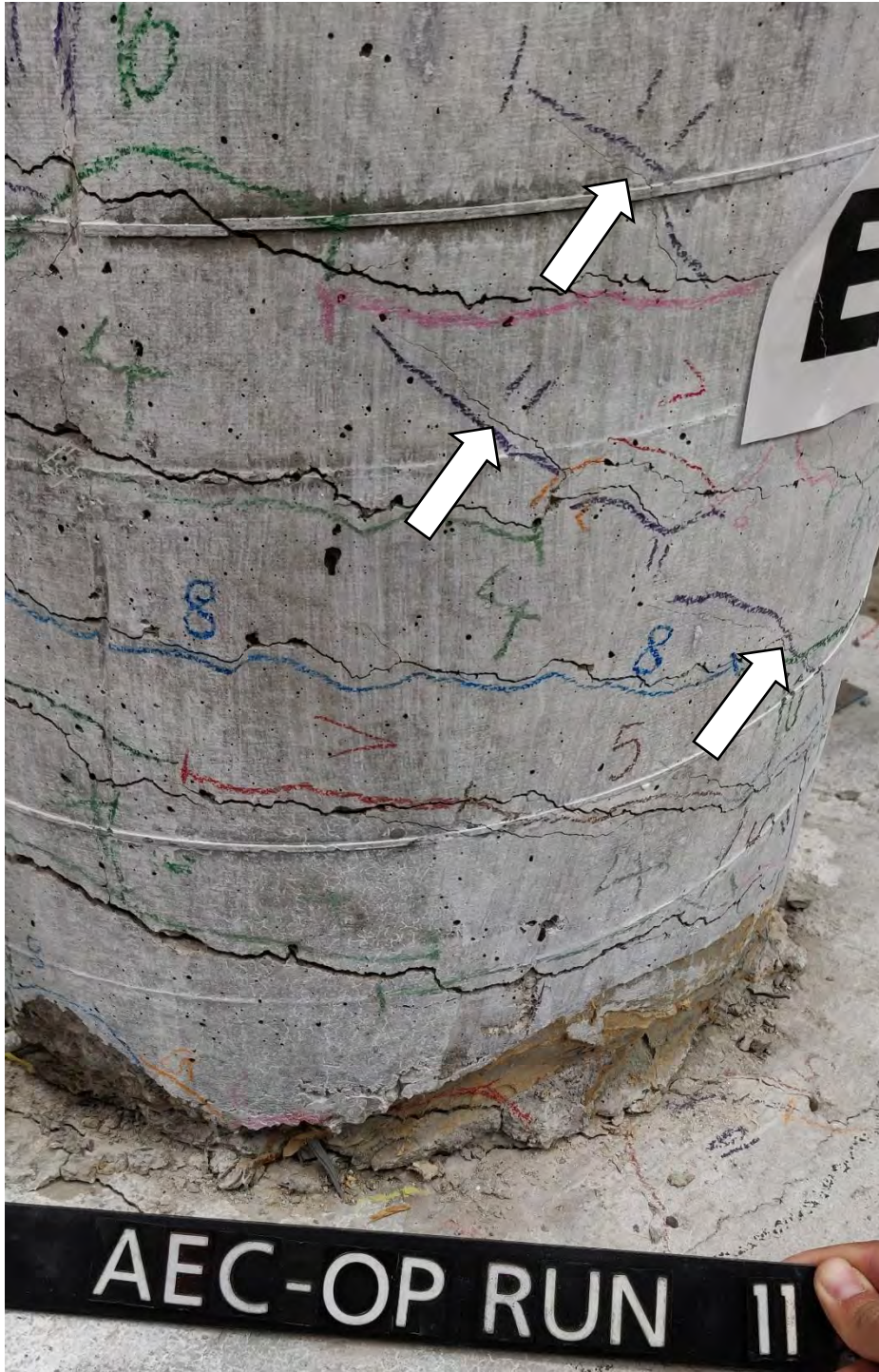
Figure 5.17 Shear cracks on column southeast side after run 11 (final run)
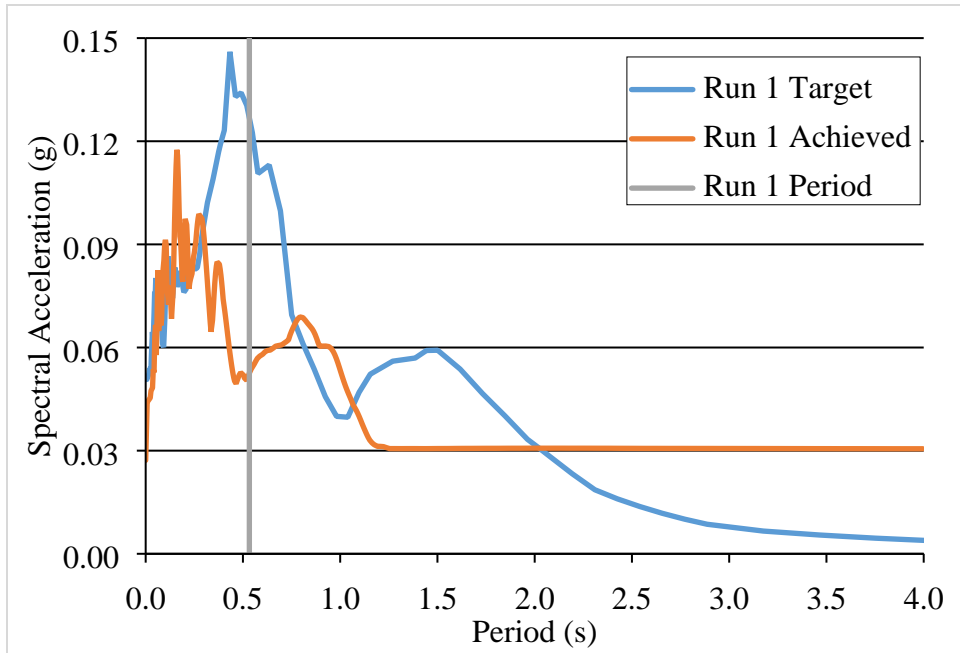
Figure 5.18 Target and achieved response spectra for run 1
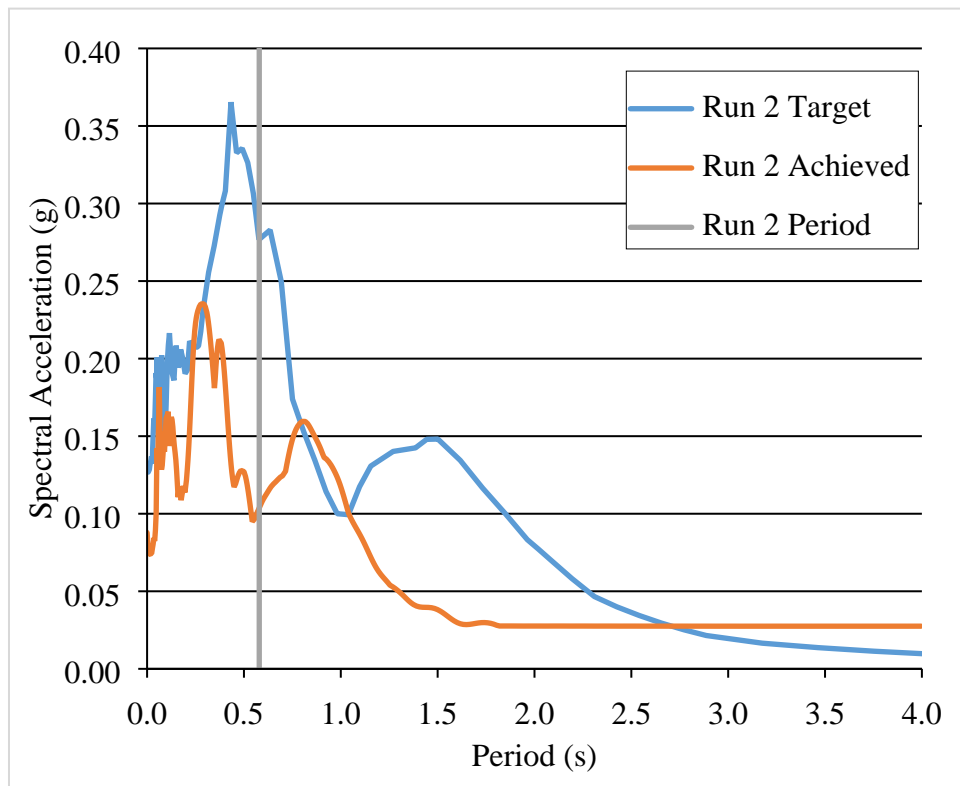
Figure 5.19 Target and achieved response spectra for run 2
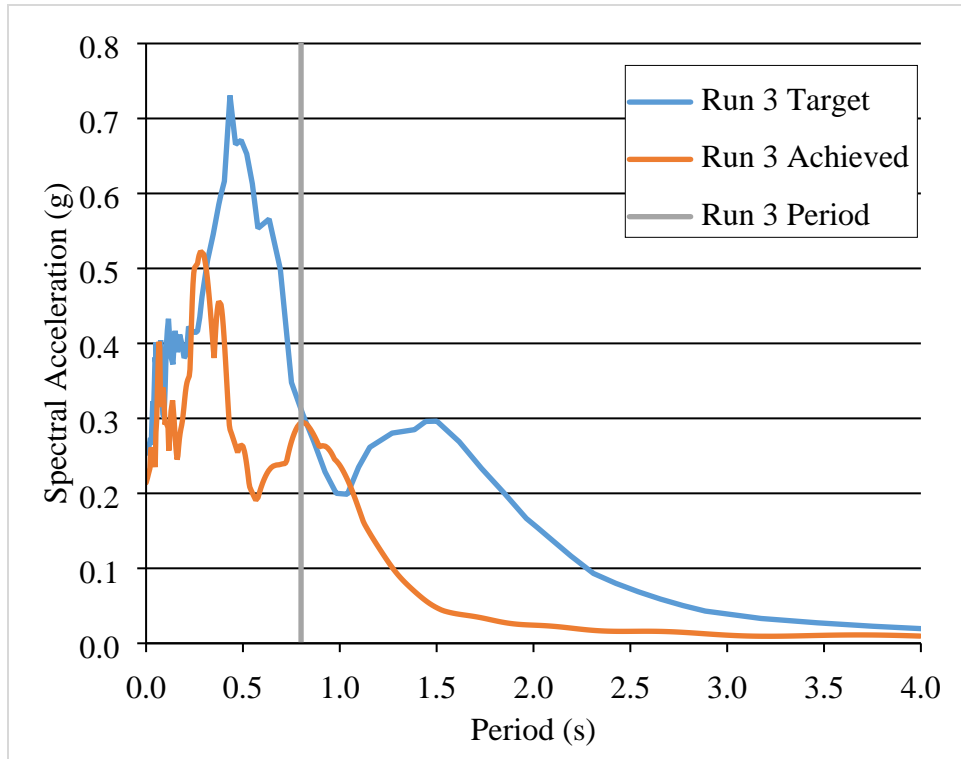
Figure 5.20 Target and achieved response spectra for run 3
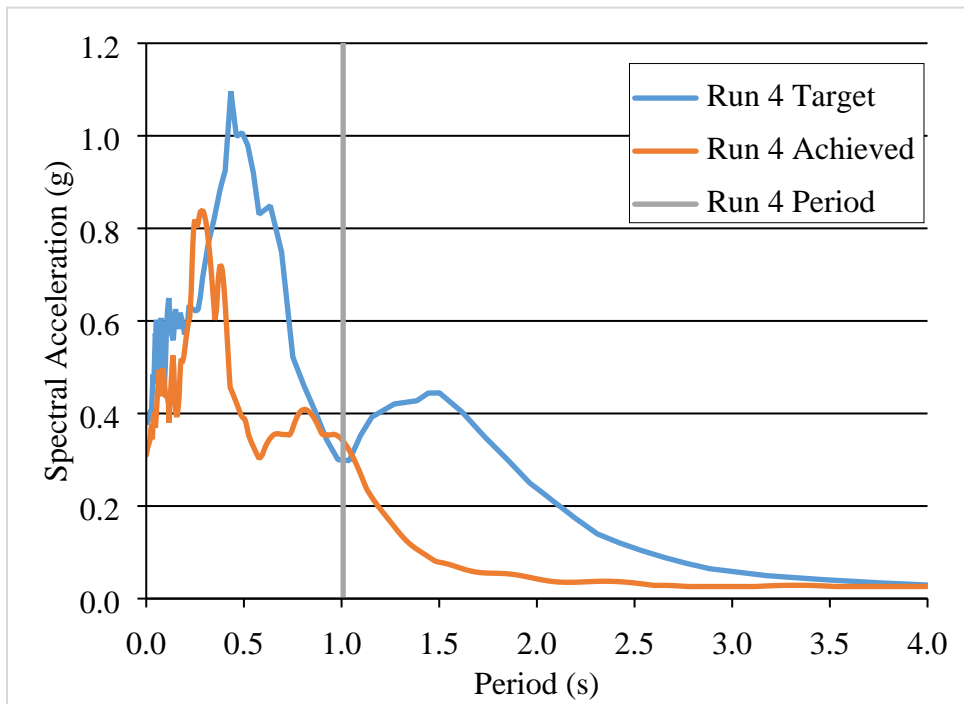
Figure 5.21 Target and achieved response spectra for run 4
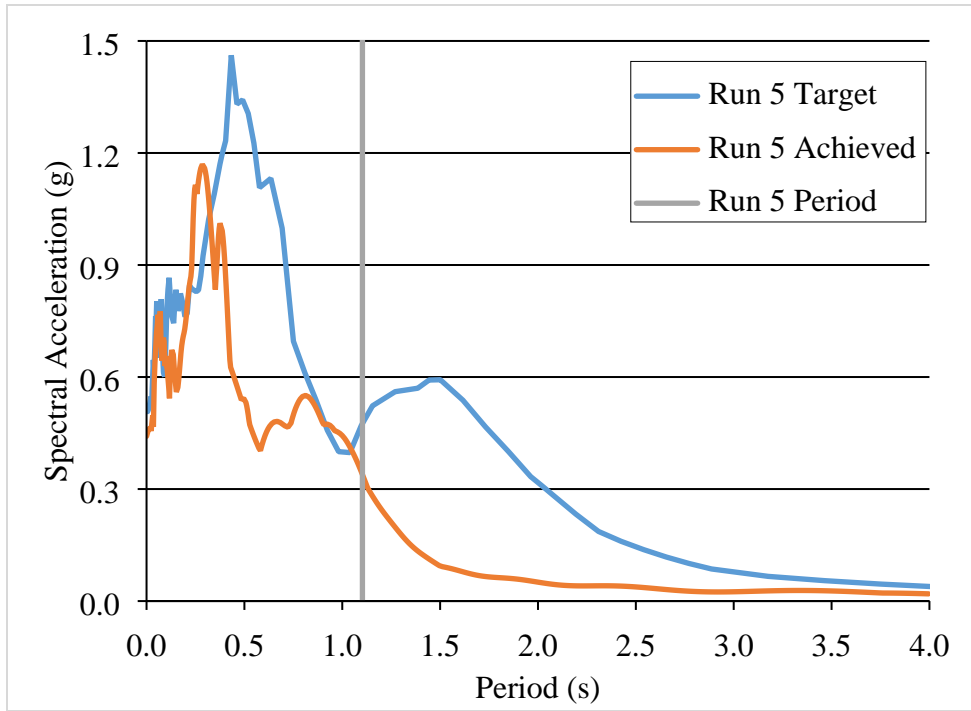
Figure 5.22 Target and achieved response spectra for run 5
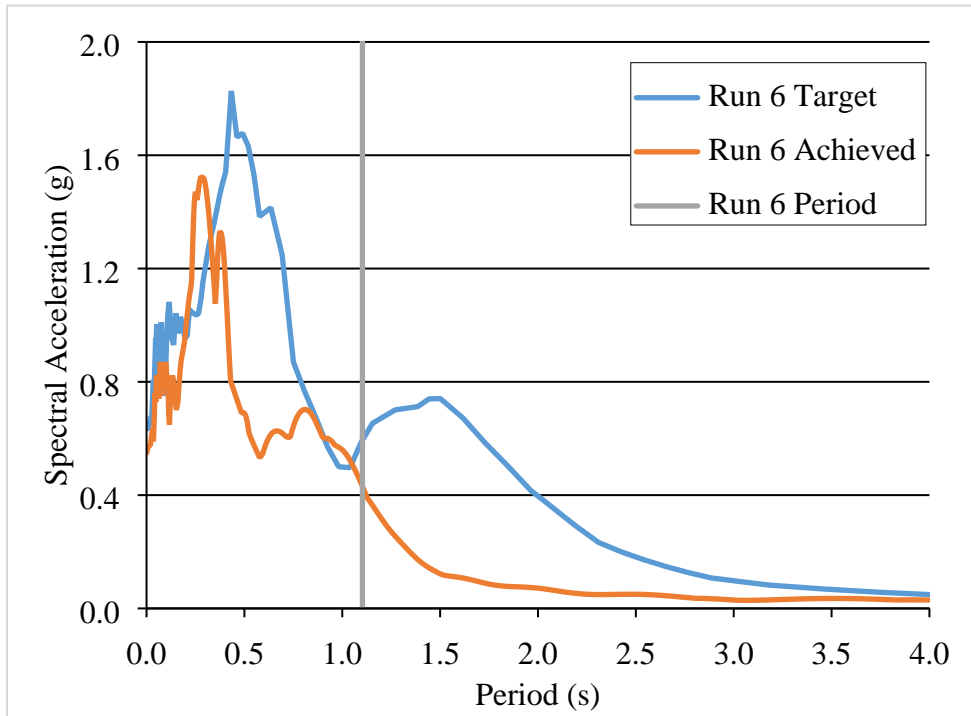
Figure 5.23 Target and achieved response spectra for run 6

150
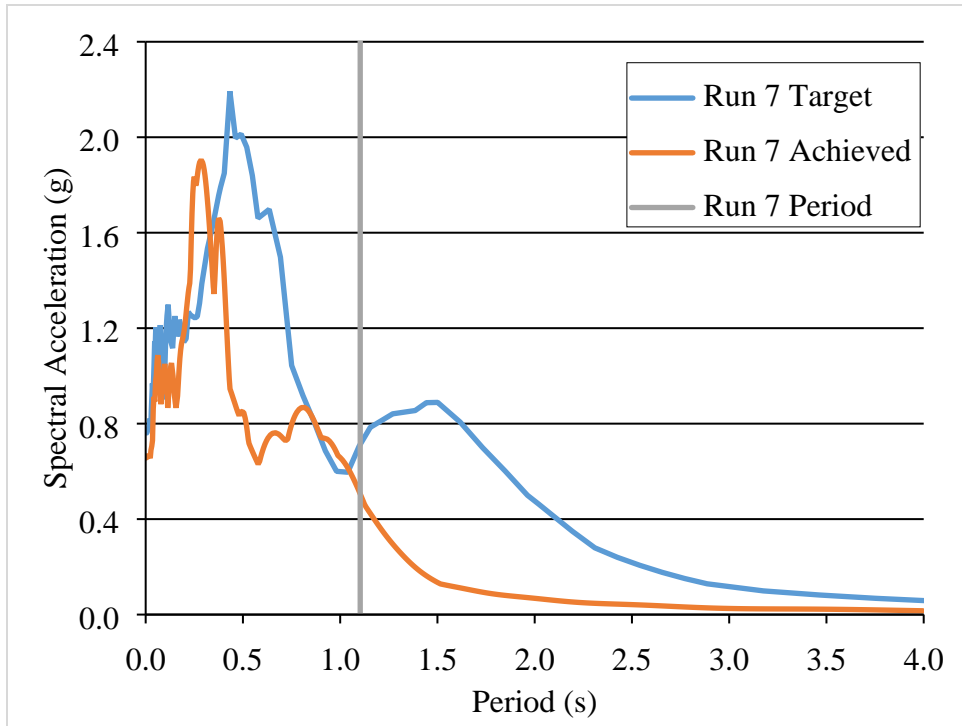
Figure 5.24 Target and achieved response spectra for run 7
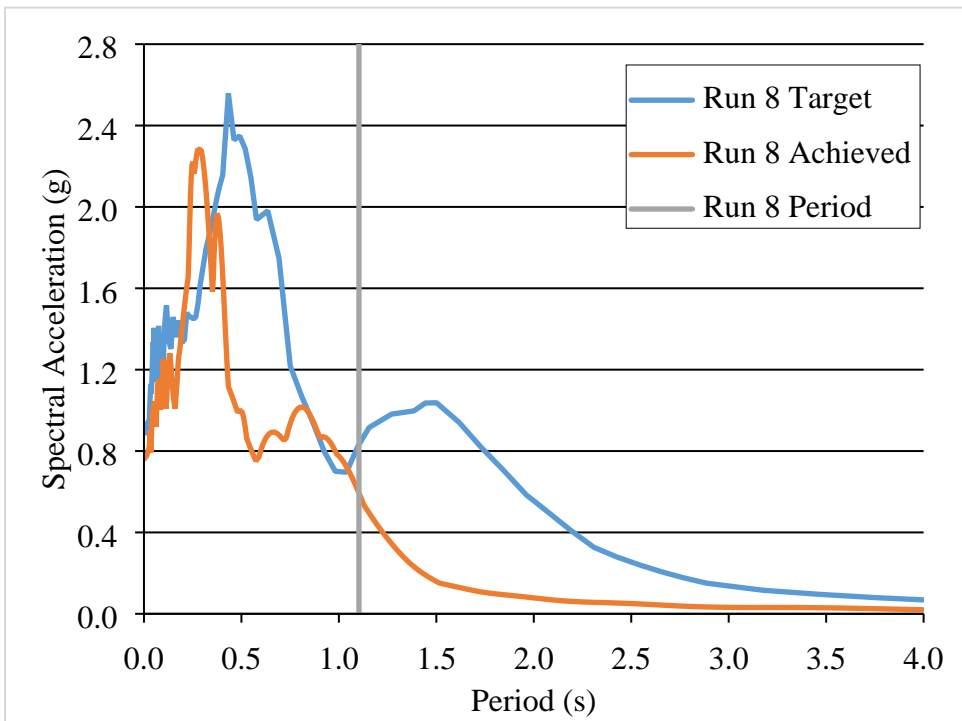
Figure 5.25 Target and achieved response spectra for run 8
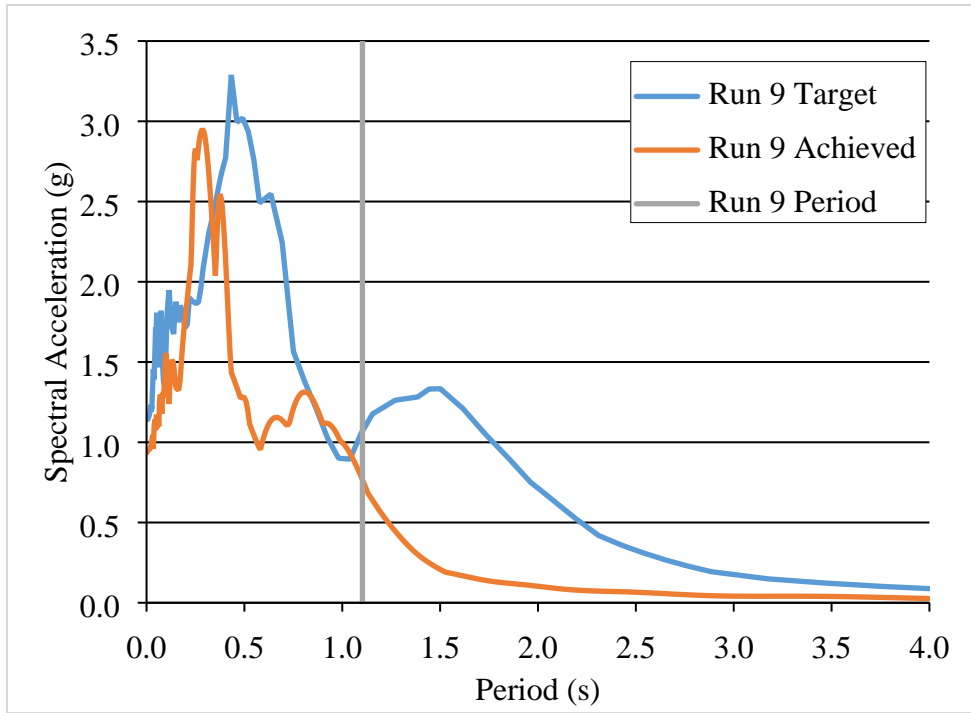
Figure 5.26 Target and achieved response spectra for run 9
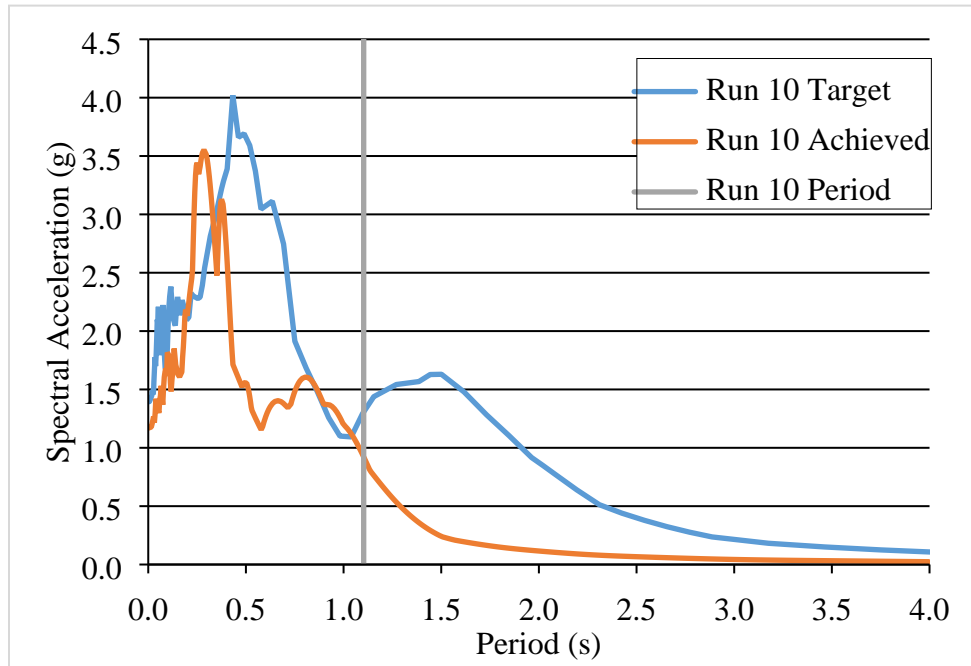
Figure 5.27 Target and achieved response spectra for run 10
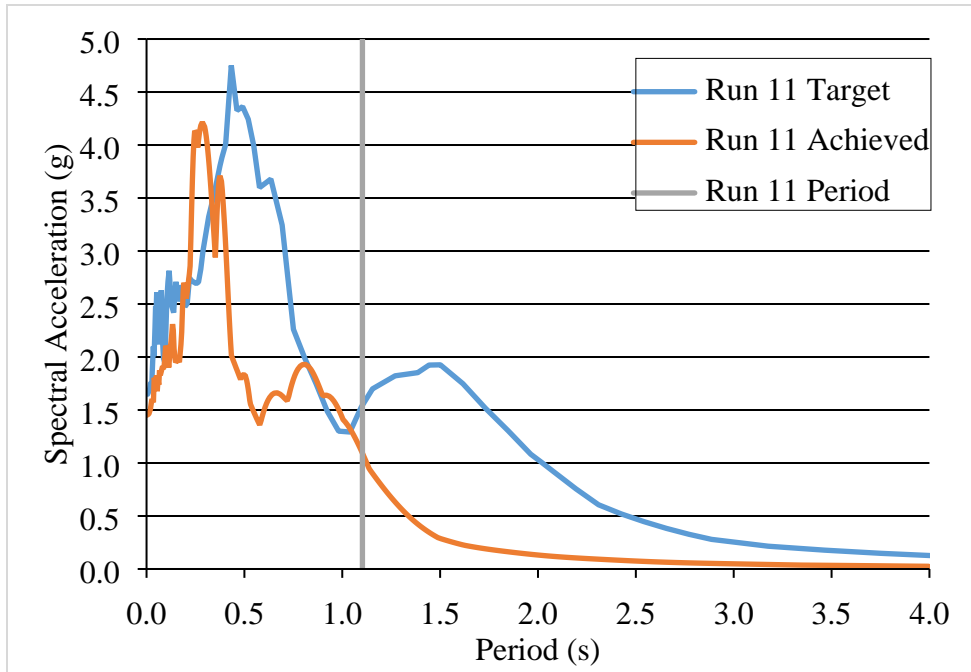
Figure 5.28 Target and achieved response spectra for run 11
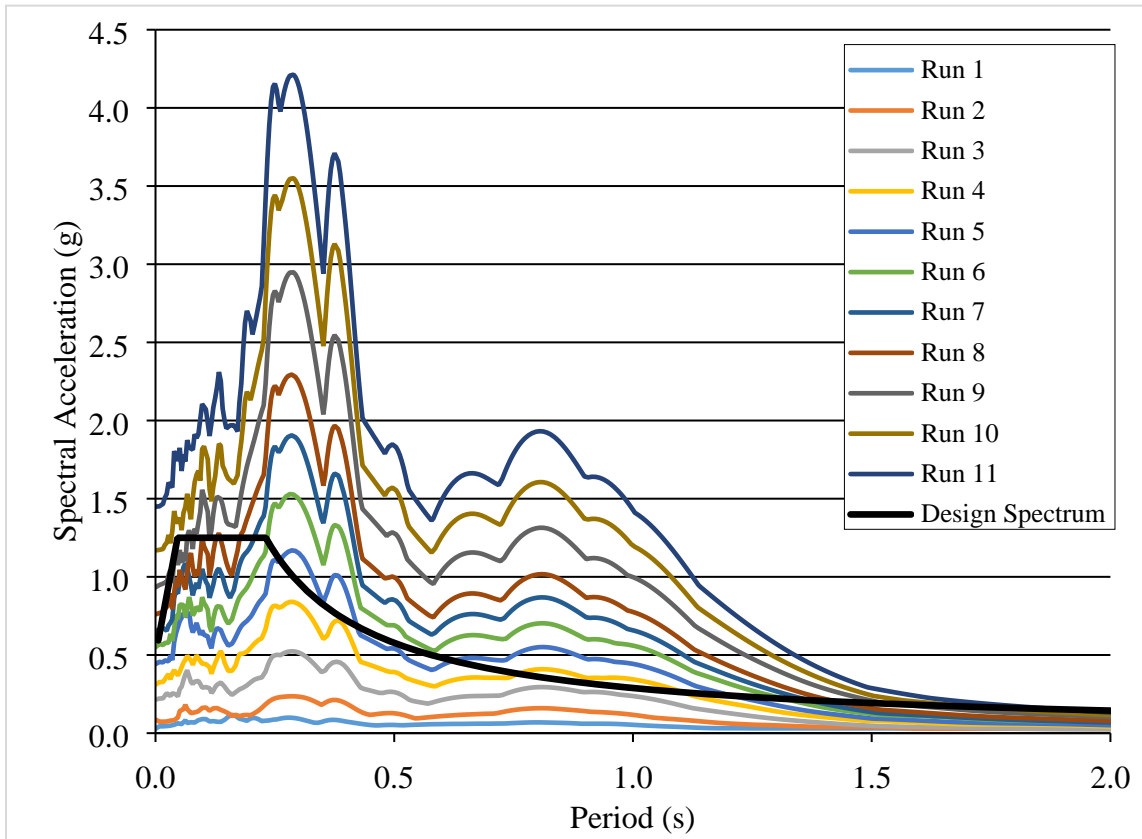
Figure 5.29 Achieved response spectra compared to seismic design response spectrum

153
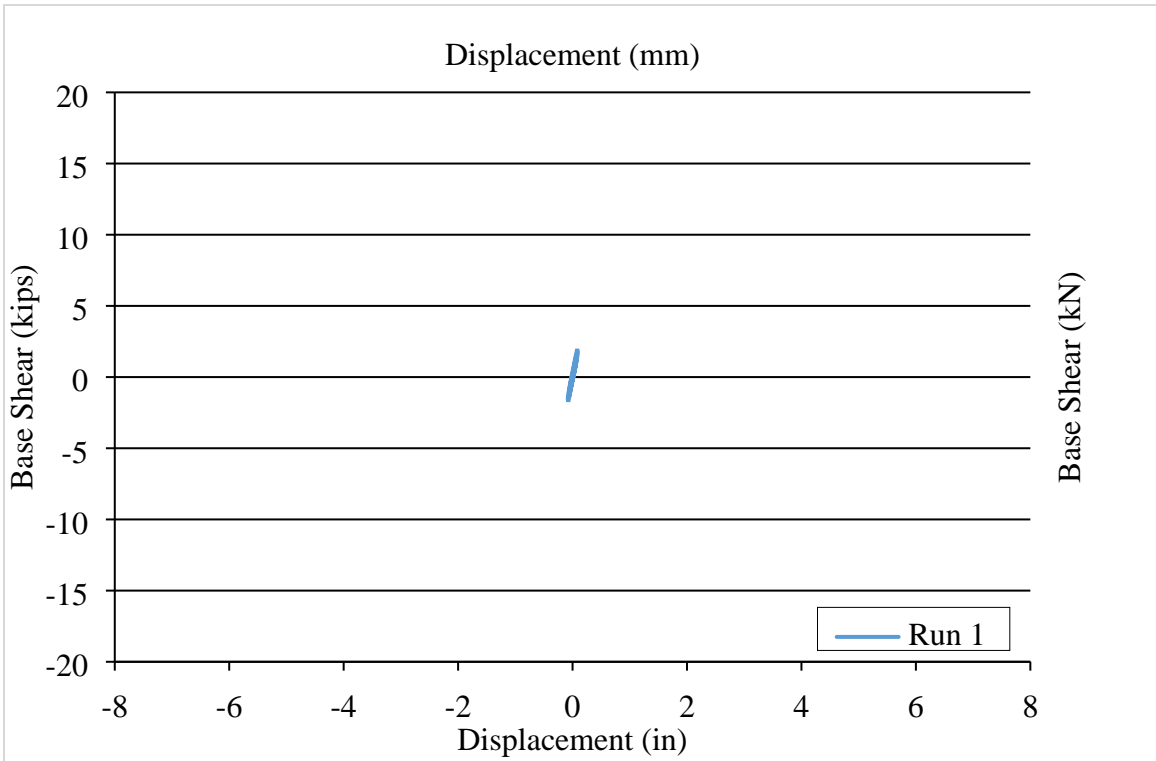
Figure 5.30 Force-displacement relationship for run 1
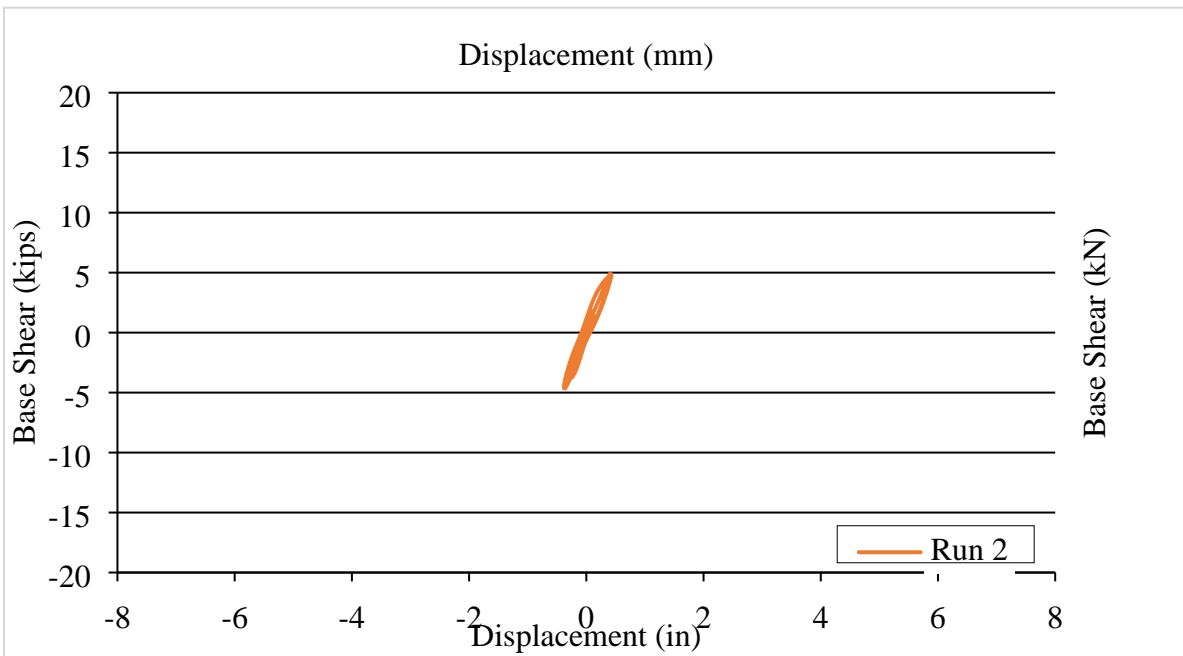
Figure 5.31 Force-displacement relationship for run 2

154
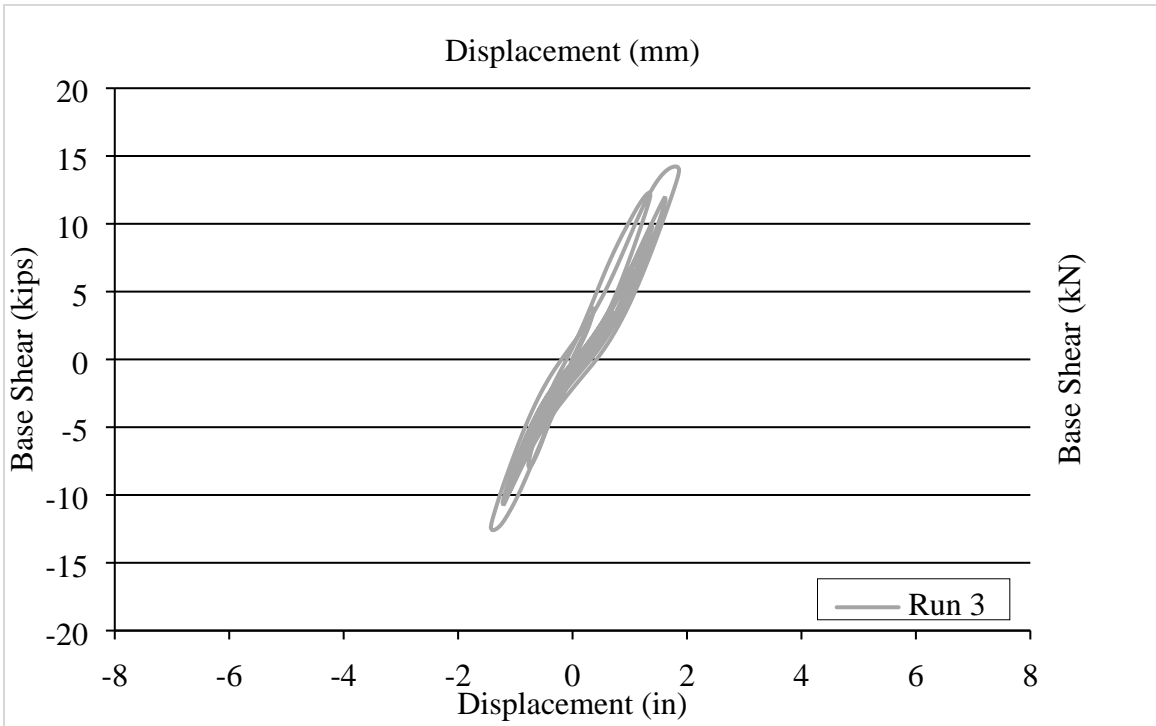
Figure 5.32 Force-displacement relationship for run 3
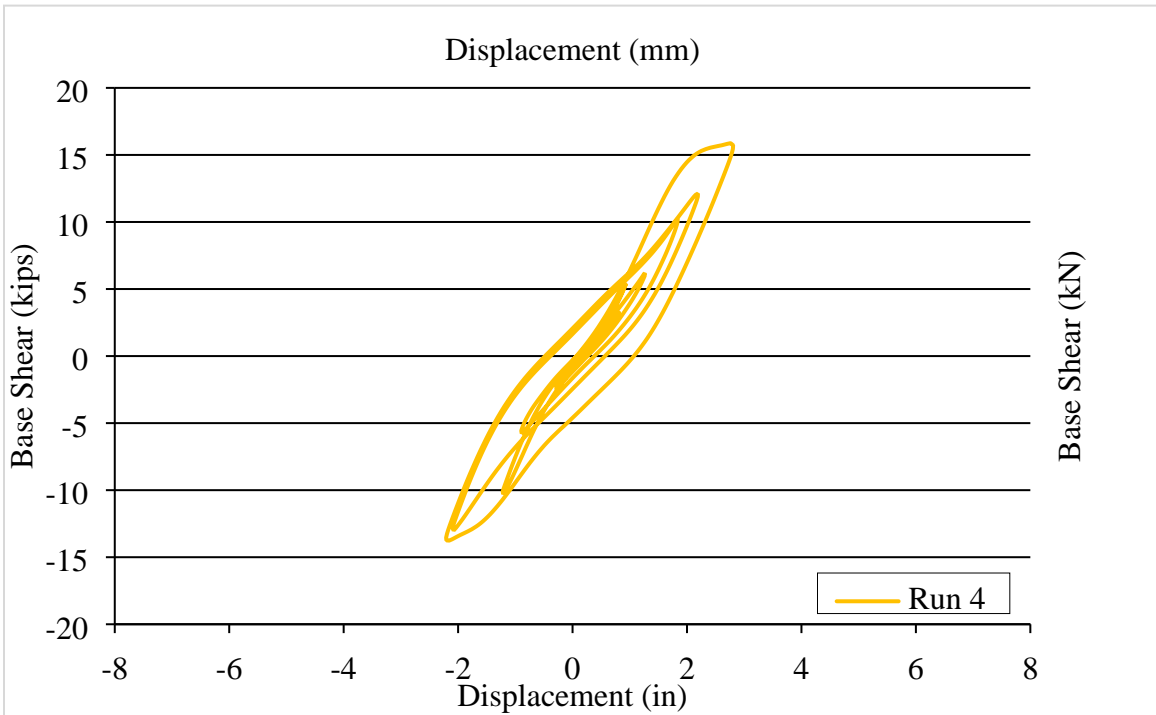
Figure 5.33 Force-displacement relationship for run 4
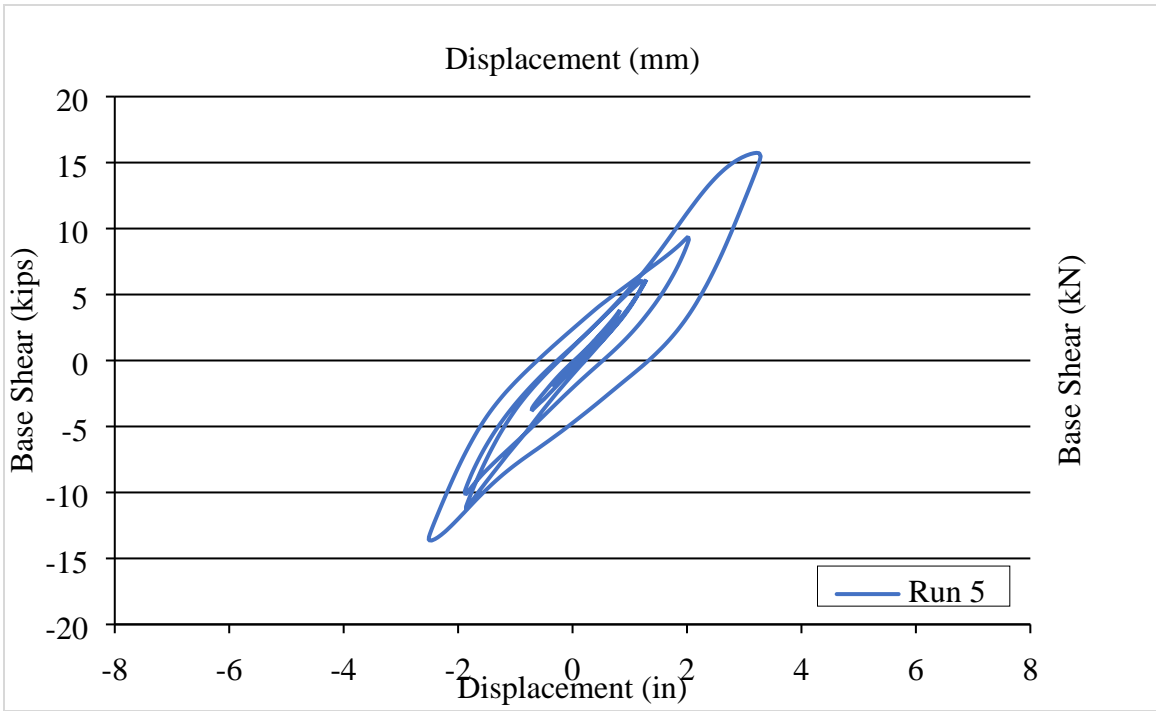
Figure 5.34 Force-displacement relationship for run 5
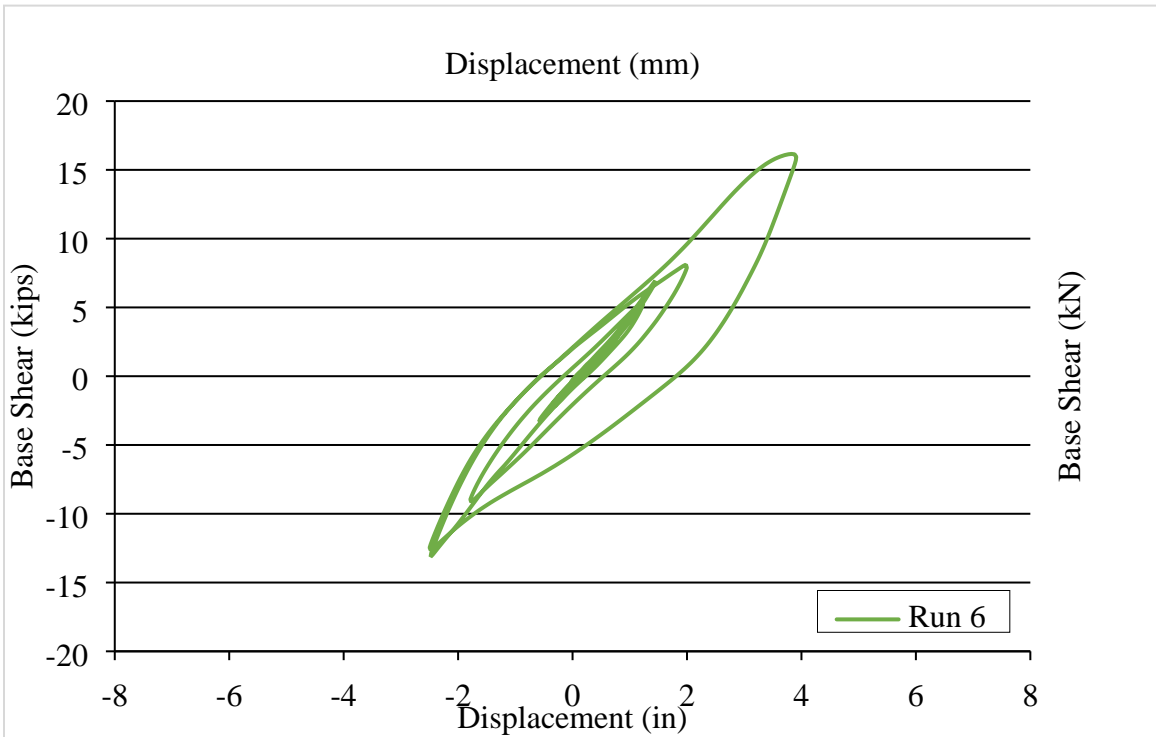
Figure 5.35 Force-displacement relationship for run 6
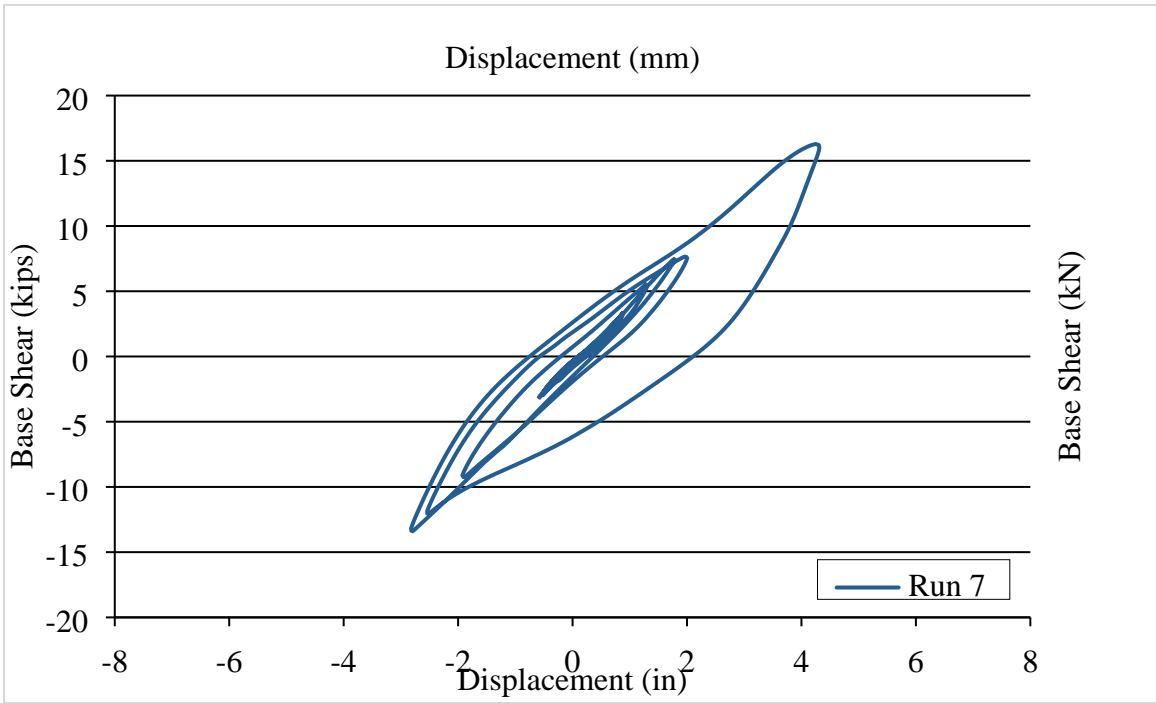
Figure 5.36 Force-displacement relationship for run 7
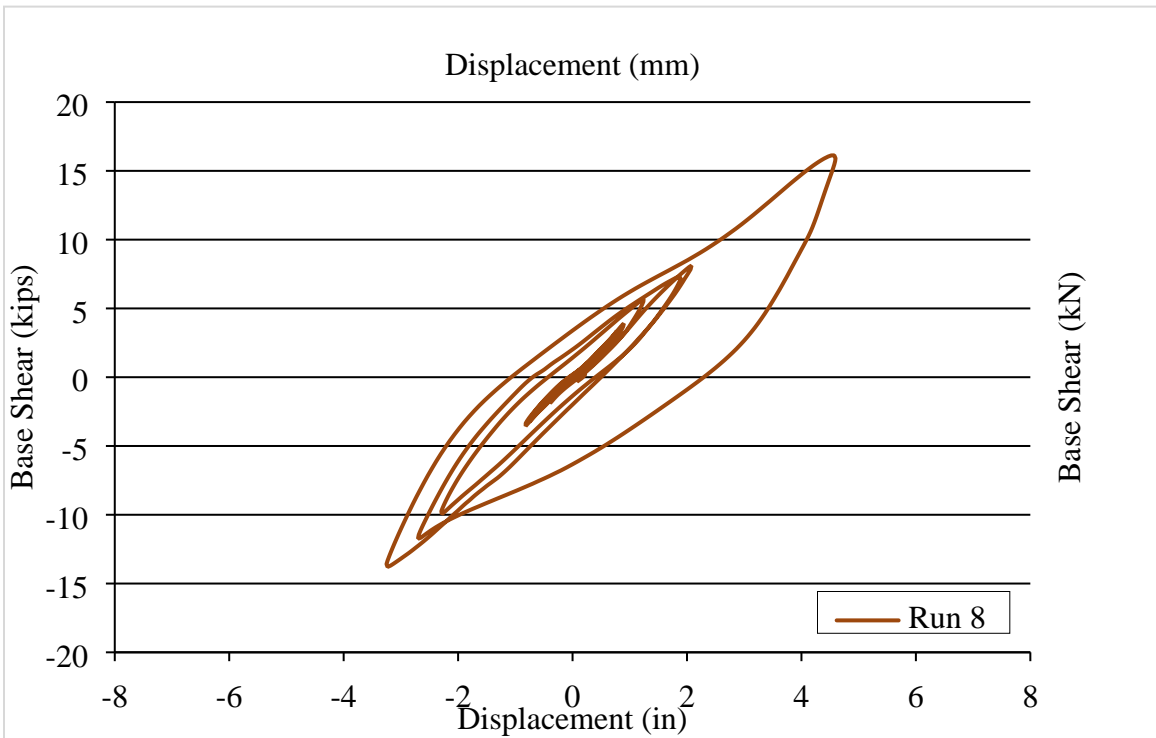
Figure 5.37 Force-displacement relationship for run 8
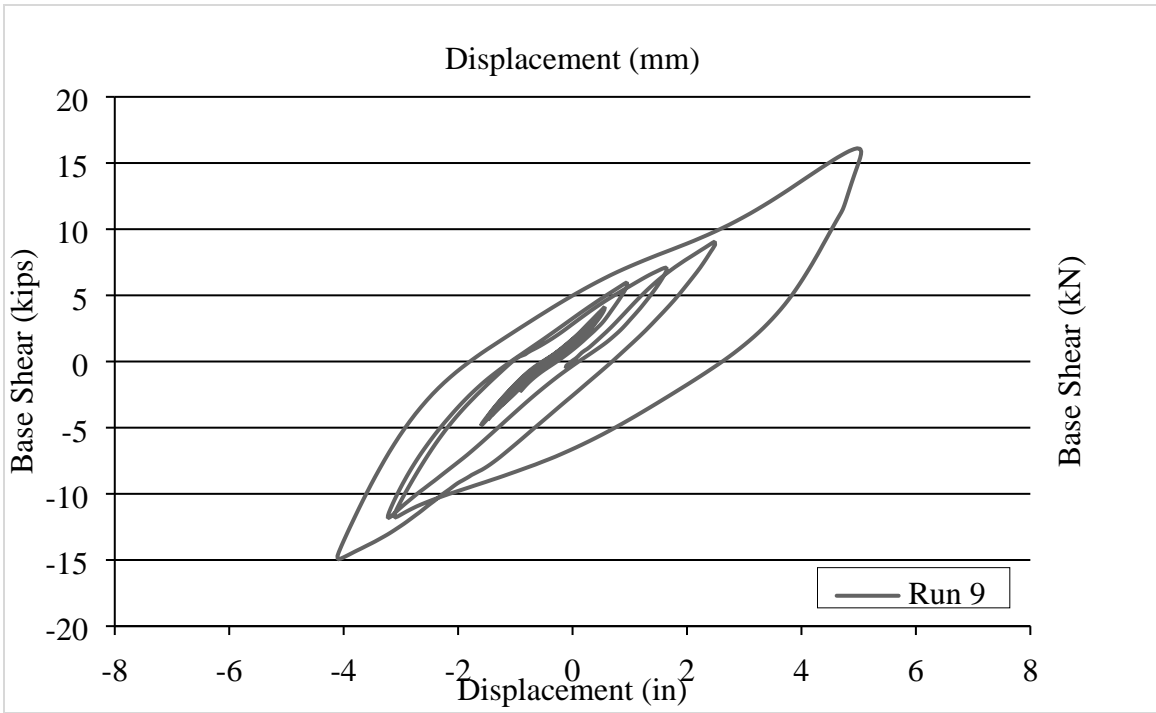
Figure 5.38 Force-displacement relationship for run 9
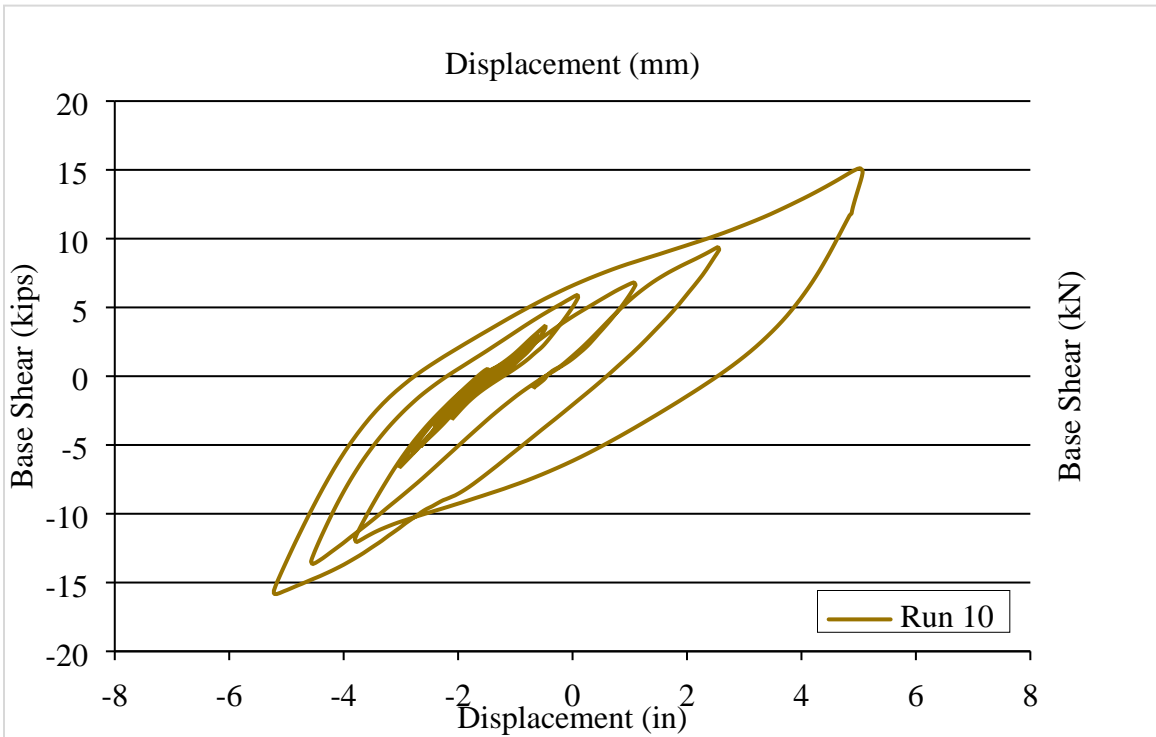
Figure 5.39 Force-displacement relationship for run 10
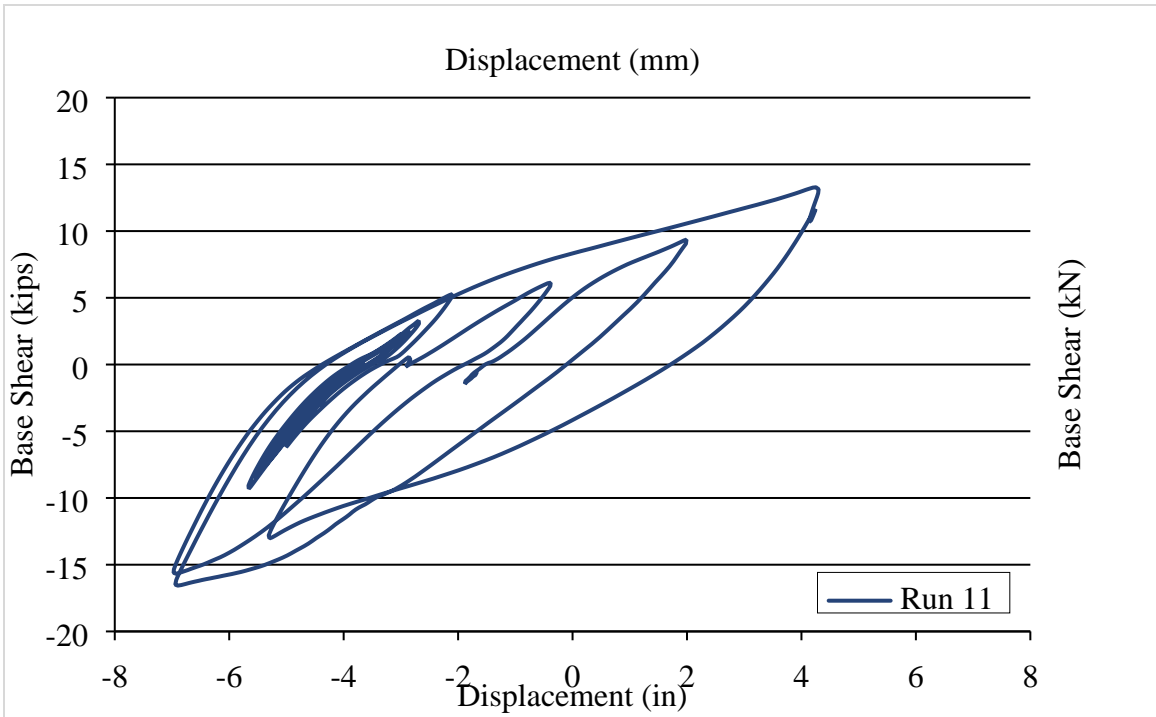
Figure 5.40 Force-displacement relationship for run 11
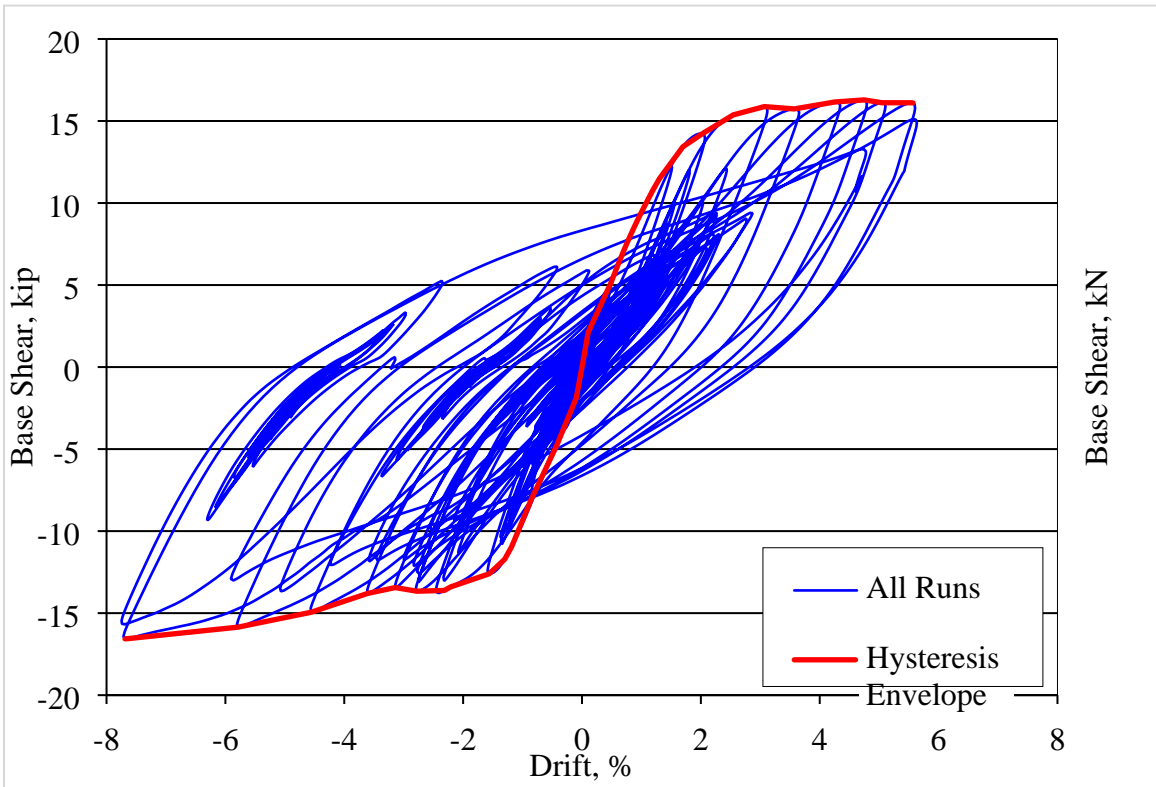
Figure 5.41 Hysteresis envelope for positive and negative sides
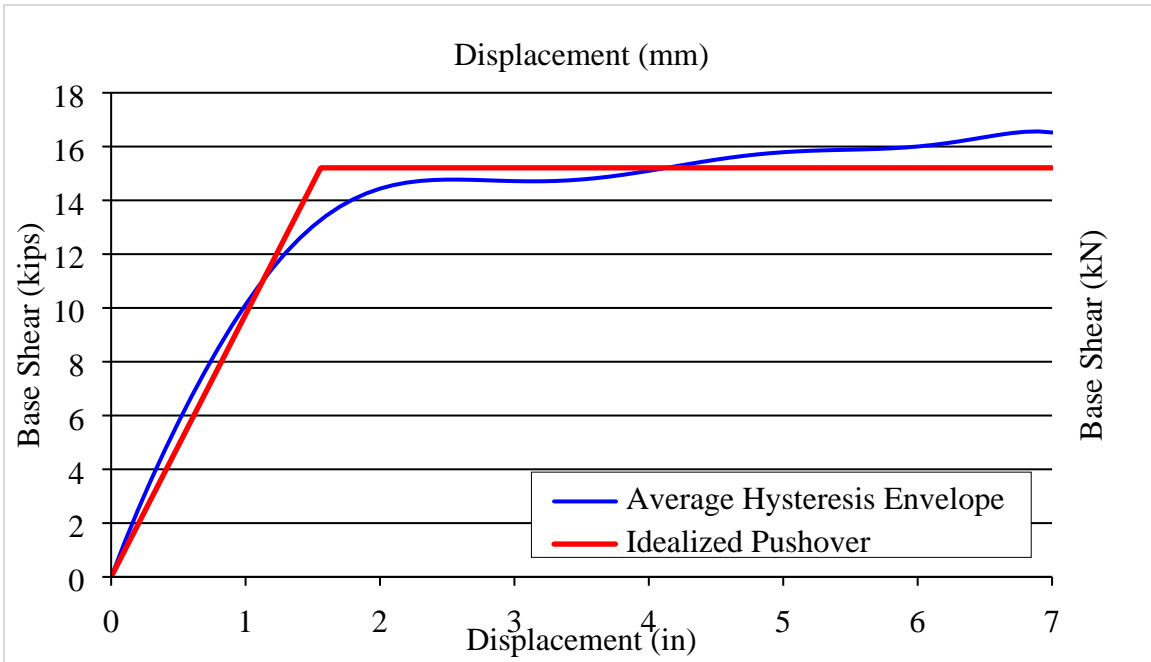
Figure 5.42 Actual and idealized pushover curves
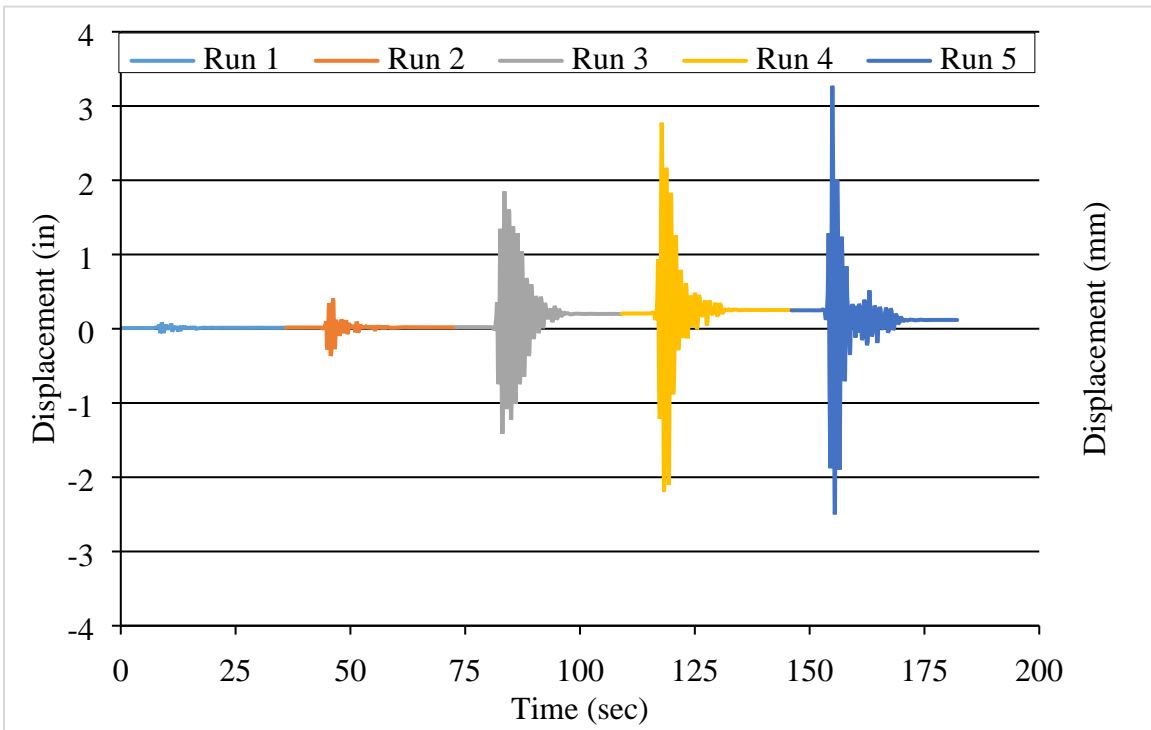
Figure 5.43 Measured displacement history for runs 1 through 5
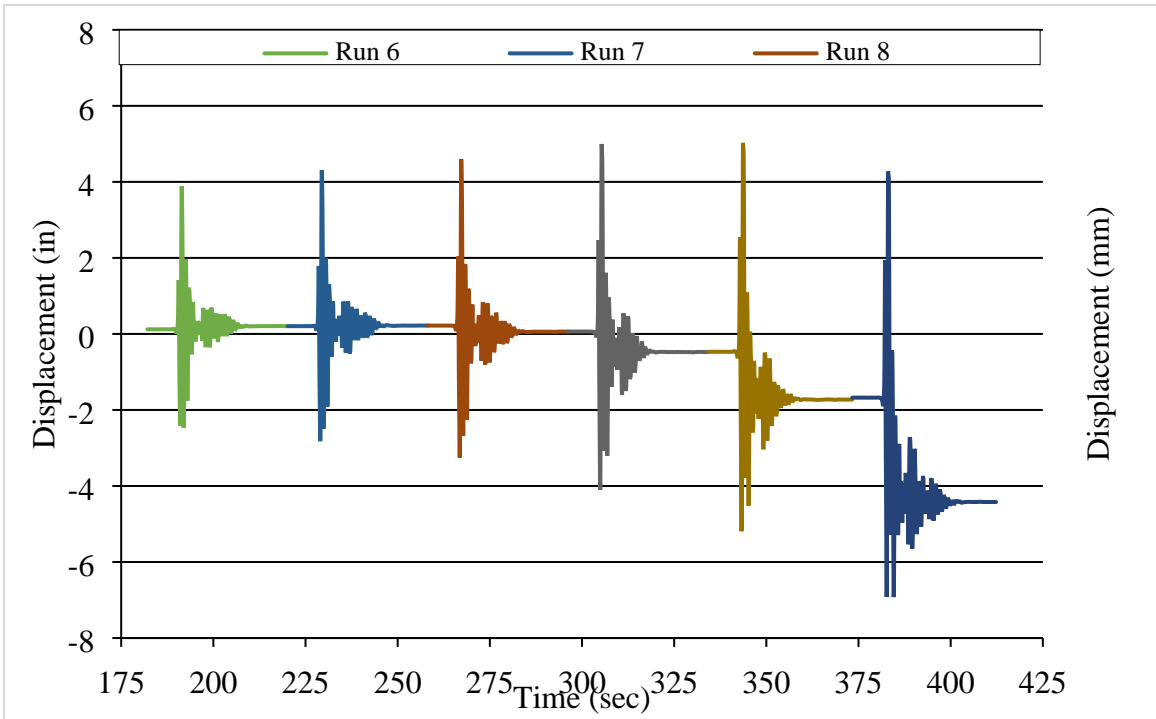
Figure 5.44 Measured displacement history for runs 6 through 11
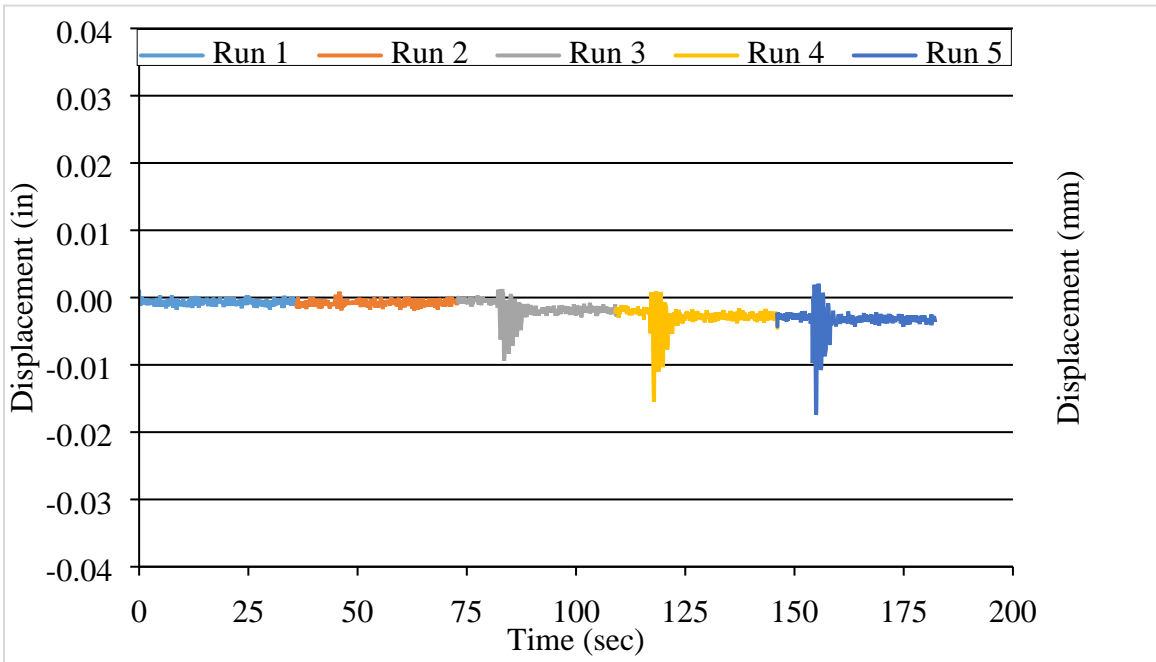
Figure 5.45 Measured cap beam displacement history for runs 1 through 5
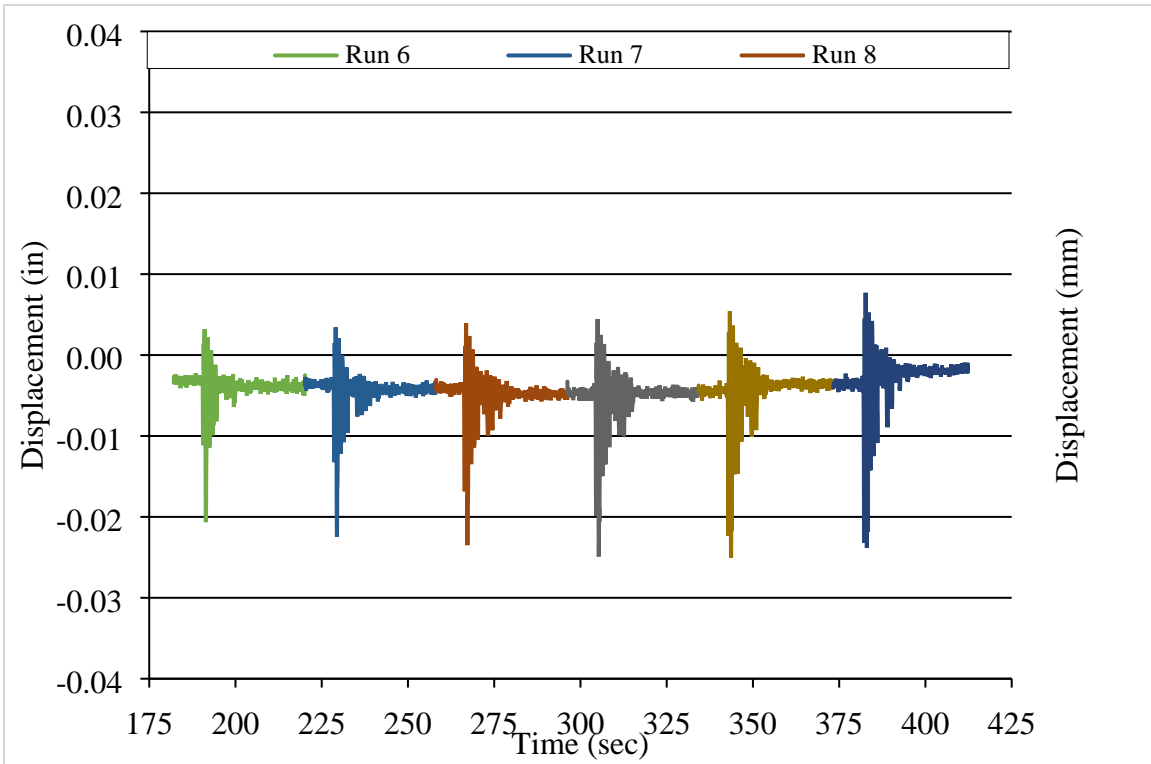
Figure 5.46 Measured cap beam displacement history for runs 6 through 11
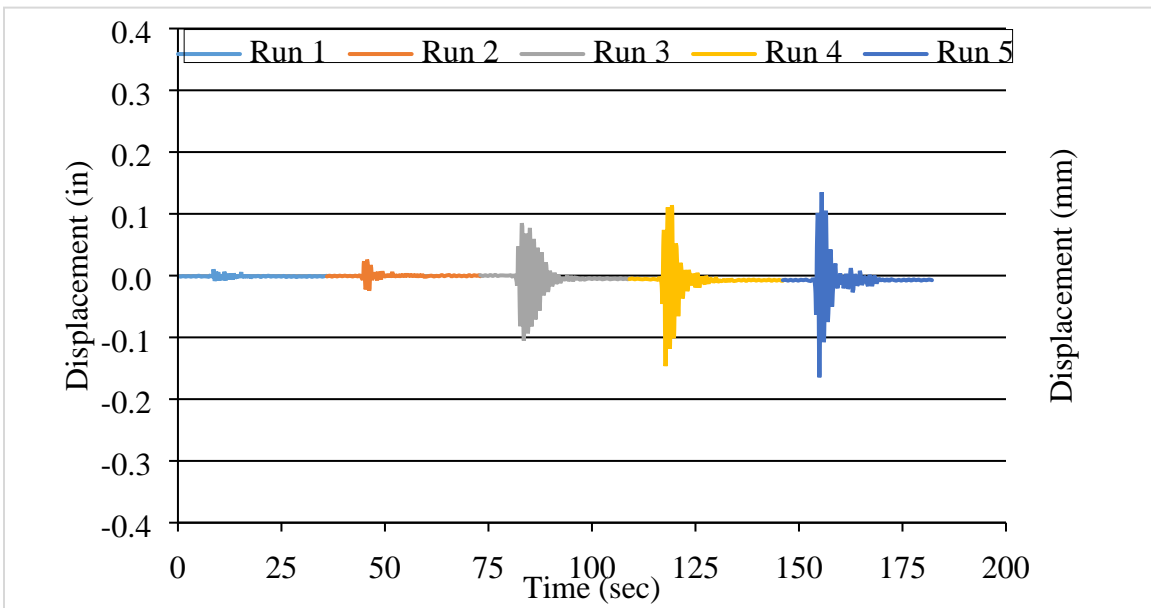
Figure 5.47 Measured displacement history at top of column due to cap beam twist for runs 1 through 5
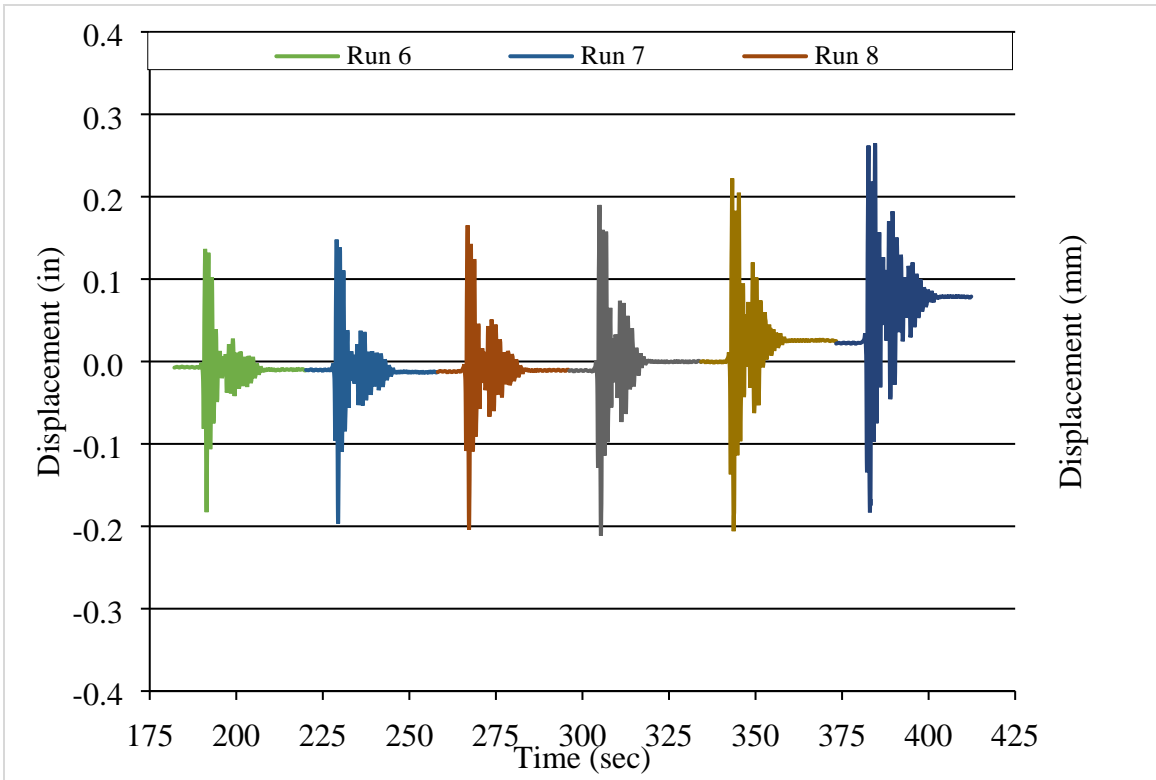
Figure 5.48 Measured displacement history at top of column due to cap beam twist for runs 6 through 11
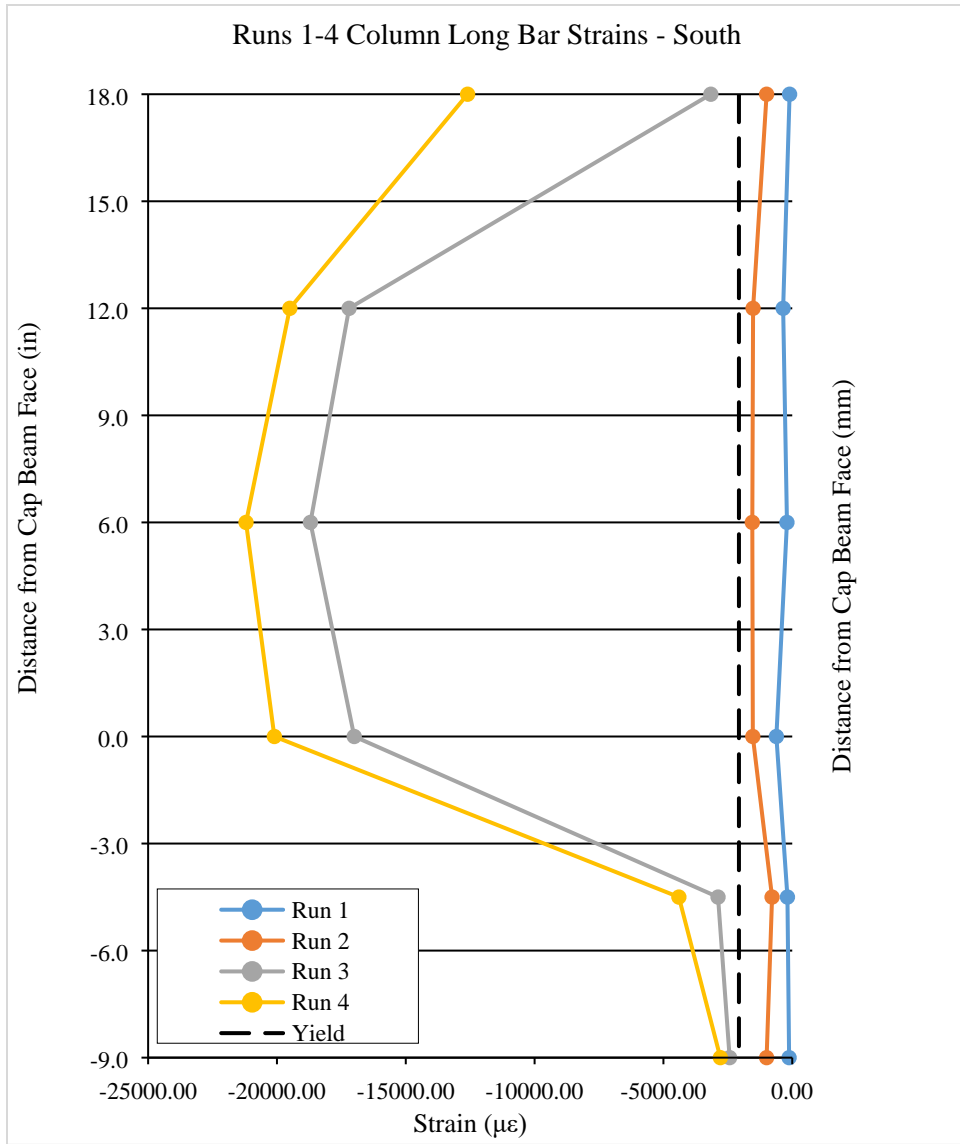
Figure 5.49 Column longitudinal reinforcement strains for runs 1 through 4
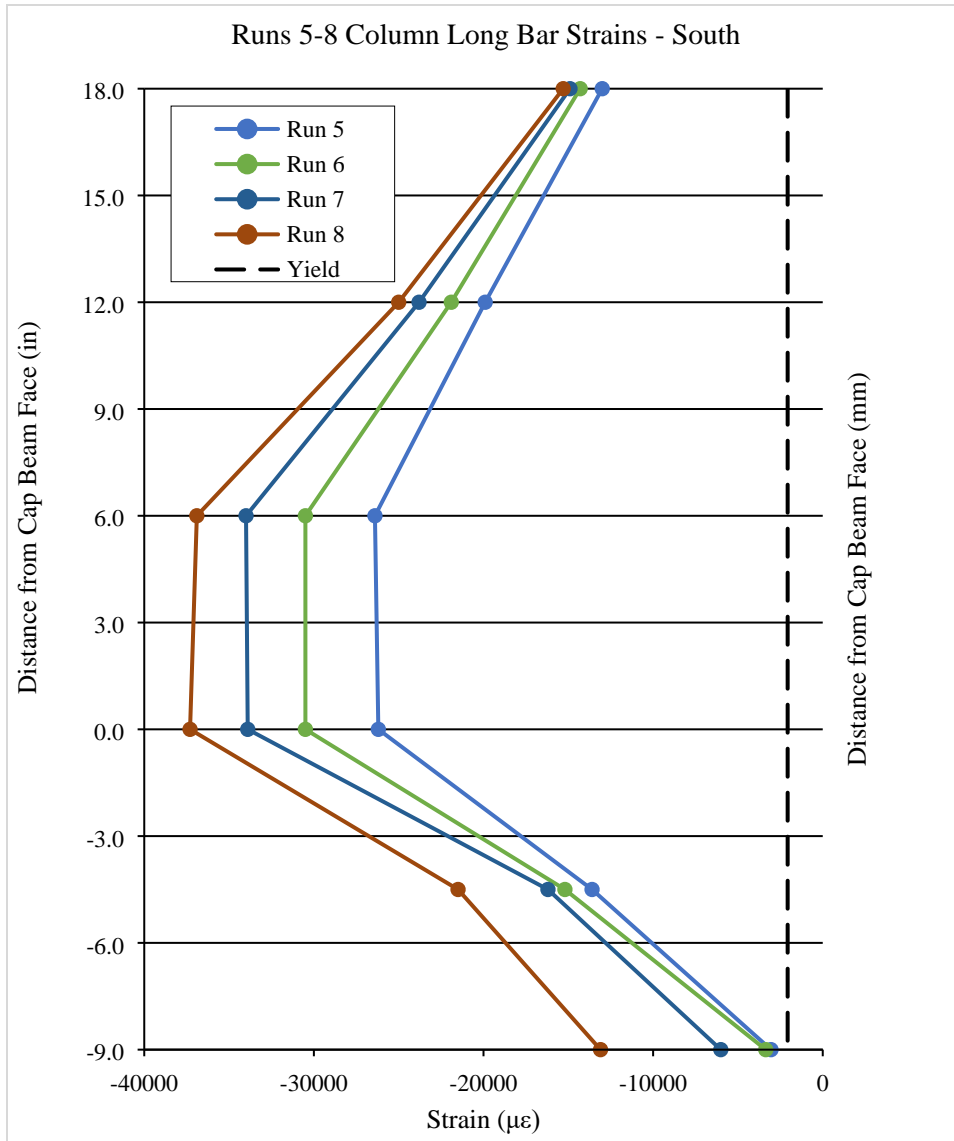
Figure 5.50 Column longitudinal reinforcement strains for runs 5 through 8
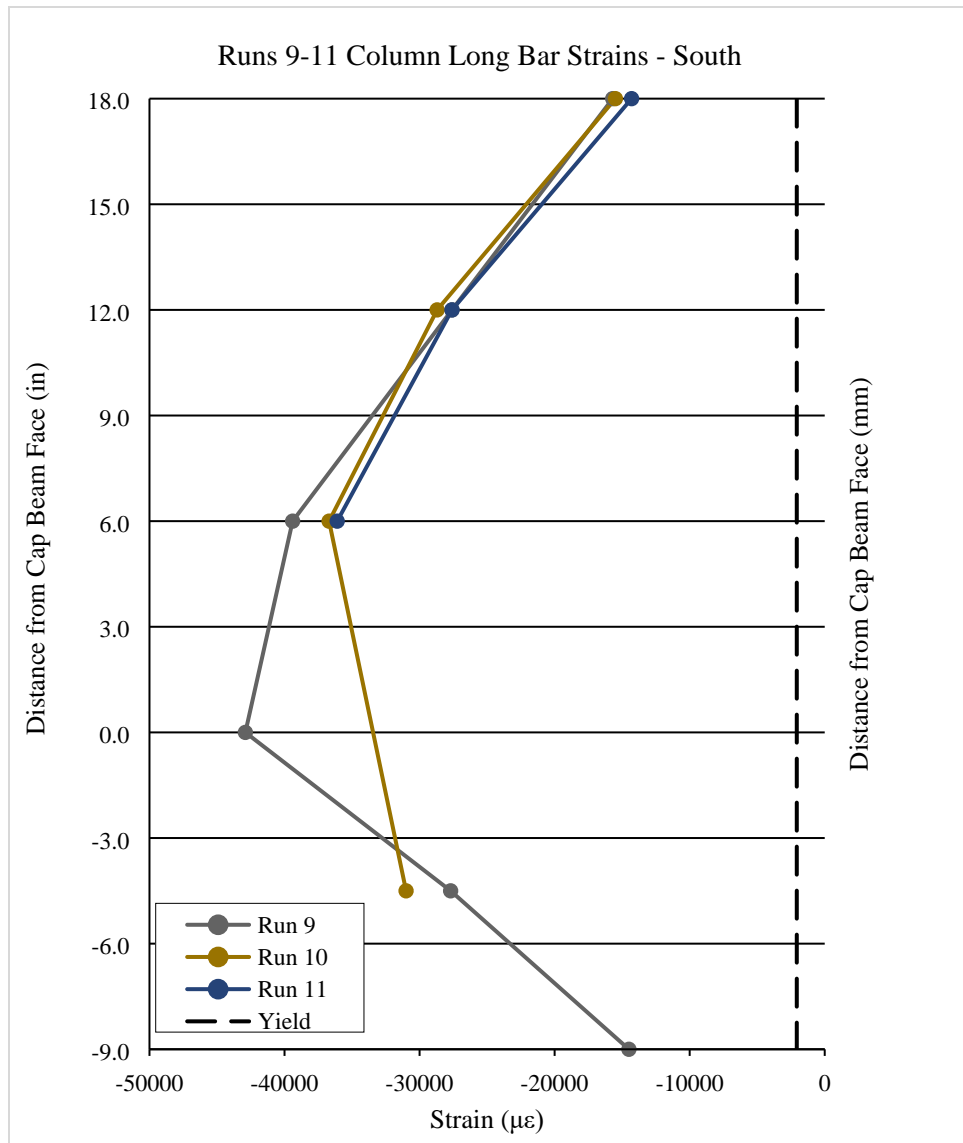
Figure 5.51 Column longitudinal reinforcement strains for runs 9 through 11
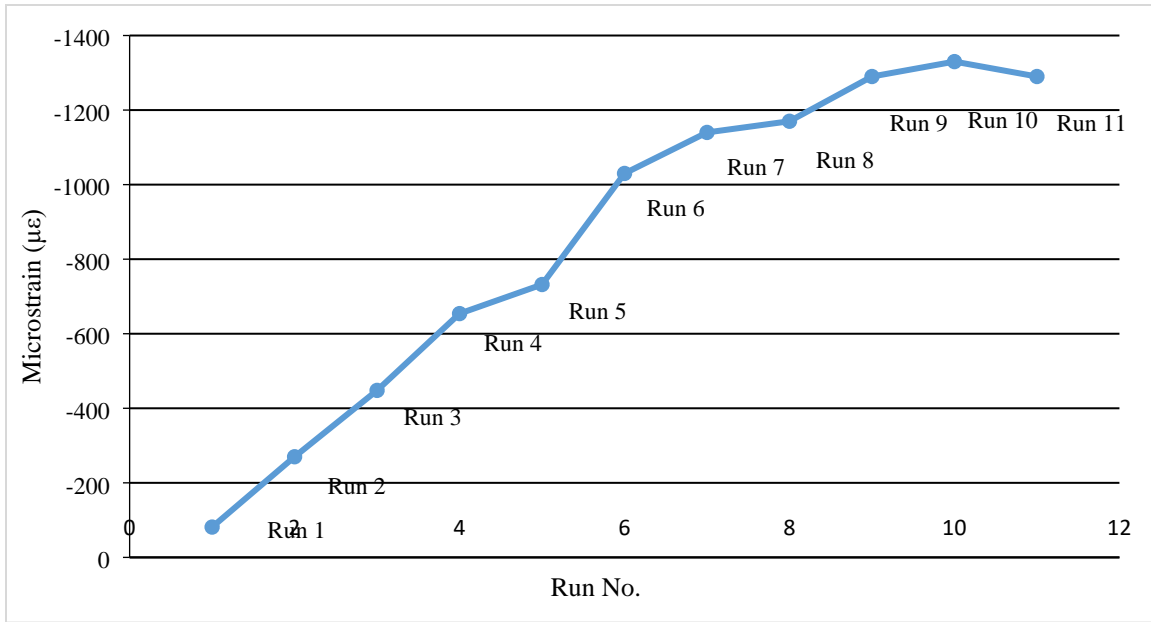
Figure 5.52 Maximum spiral strains due to confinement
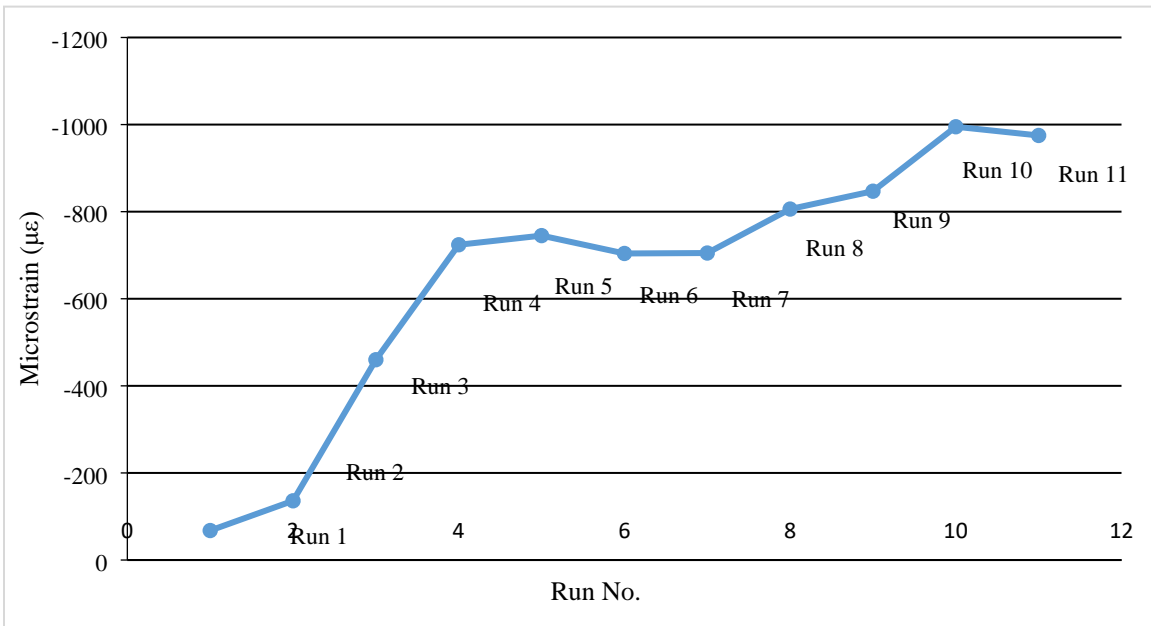
Figure 5.53 Maximum spiral strains due to shear

167
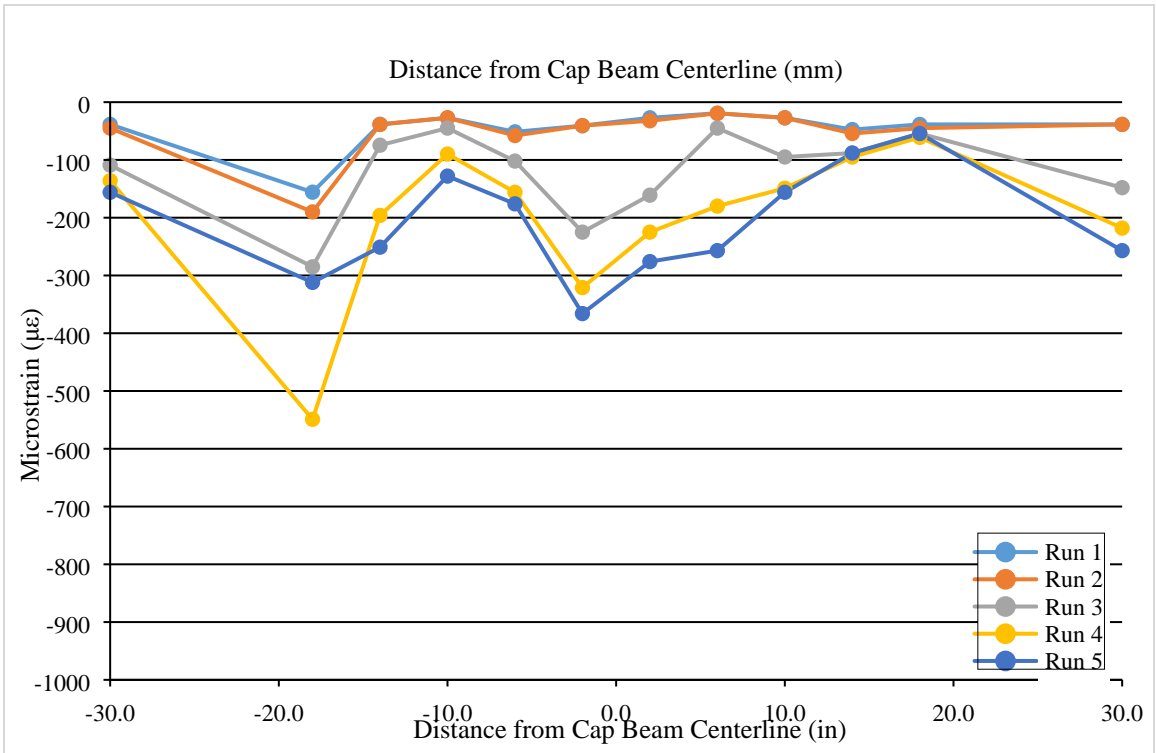
Figure 5.54 Strains in cap beam stirrups along cap beam length for runs 1 through 5
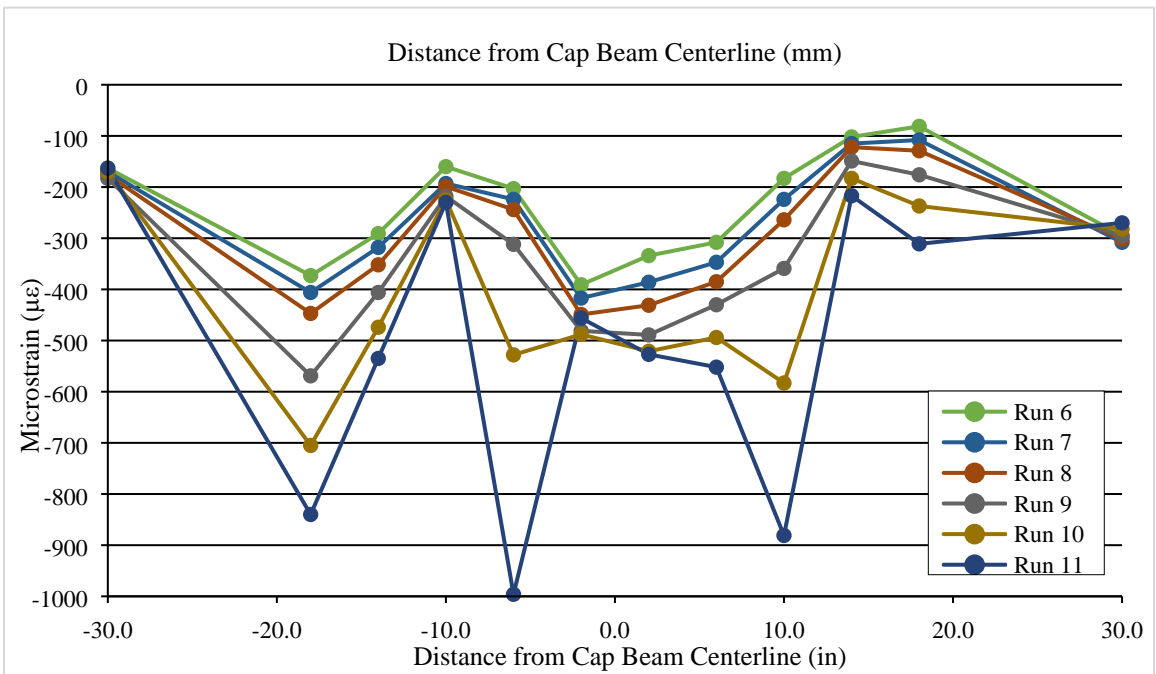
Figure 5.55 Strains in cap beam stirrups along cap beam length for runs 6 through 11

168
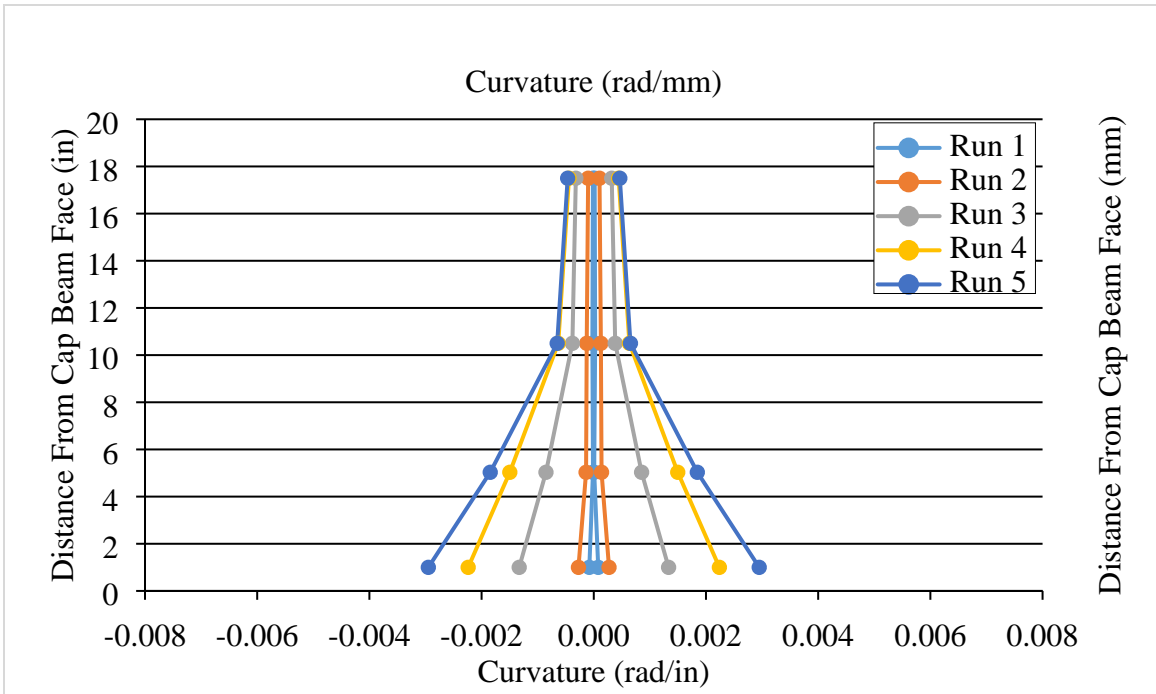
Figure 5.56 Measured curvatures for runs 1 through 5
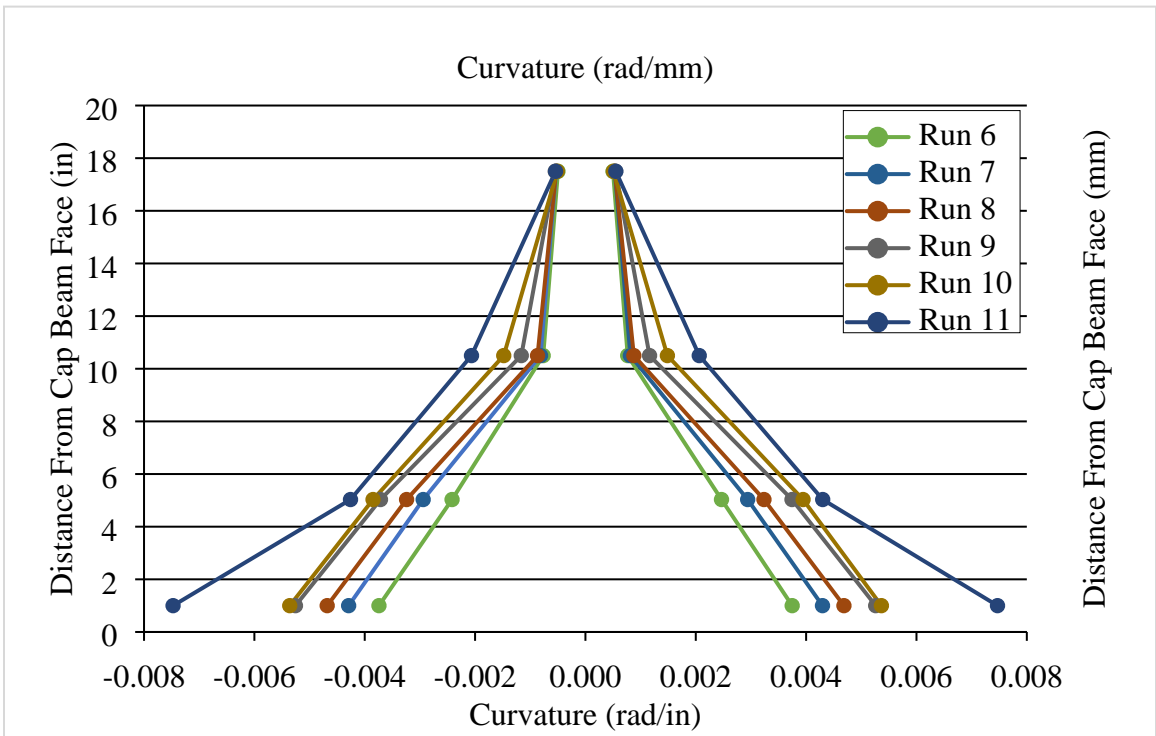
Figure 5.57 Measured curvatures for runs 6 through 11
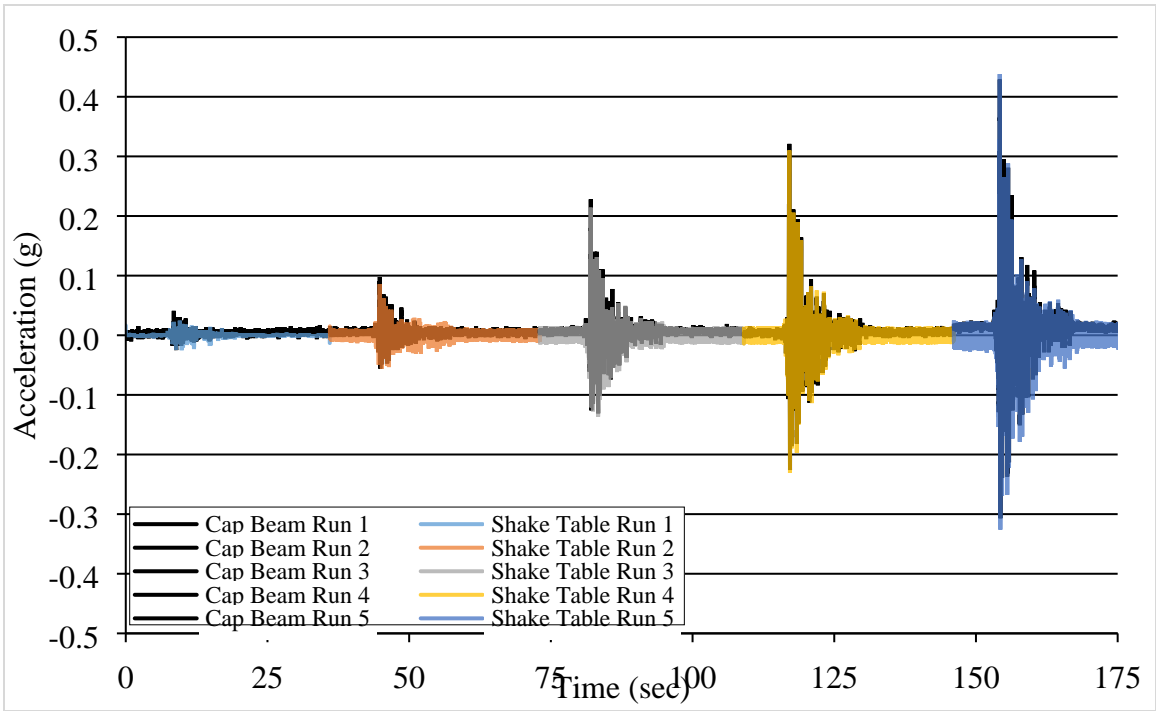
Figure 5.58 Comparison of cap beam and shake table accelerations for runs 1-5
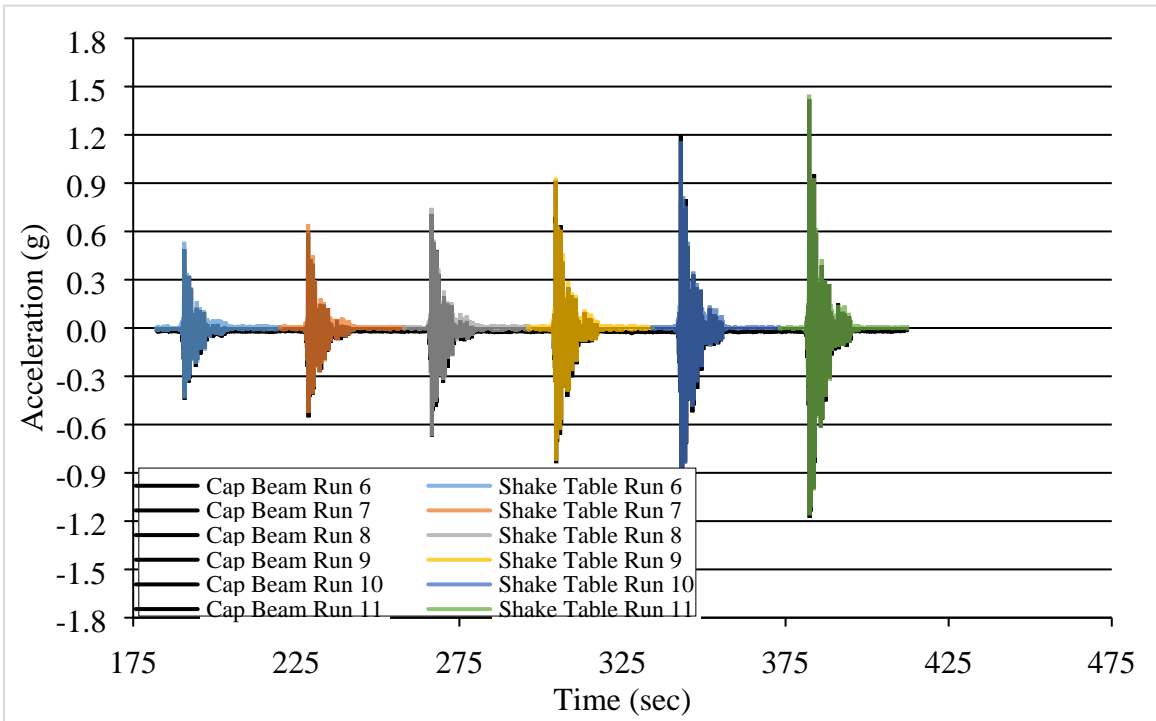
Figure 5.59 Comparison of cap beam and shake table accelerations for runs 6-11

170
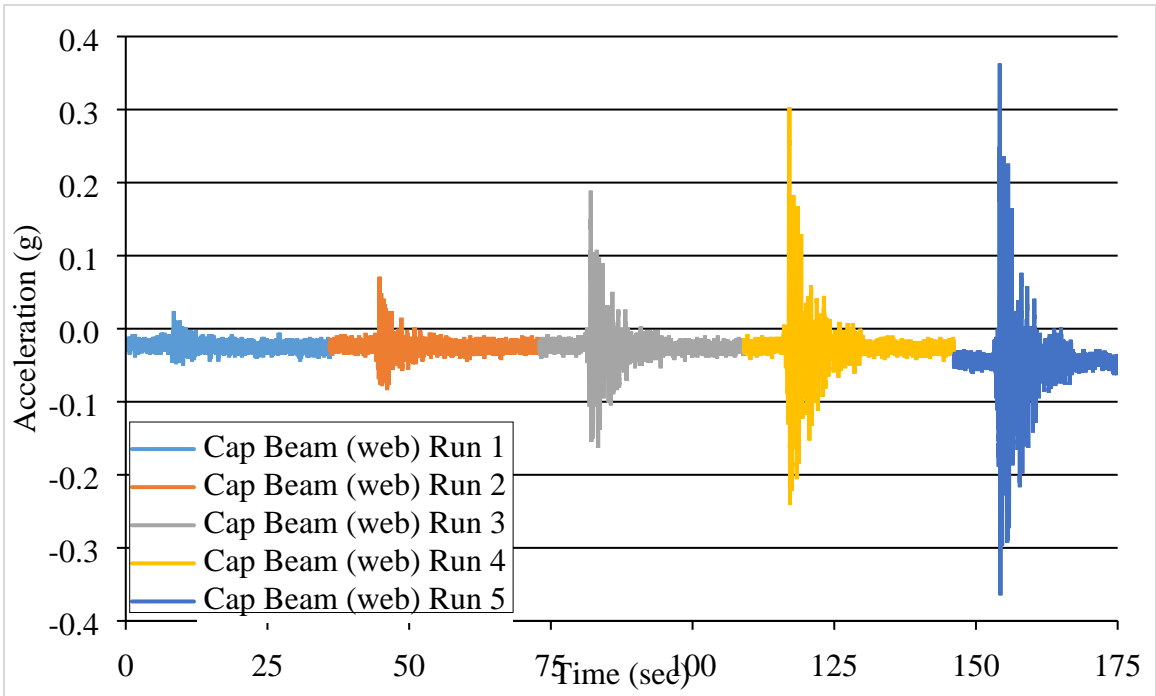
Figure 5.60 Accelerations on cap beam web for runs 1 through 5
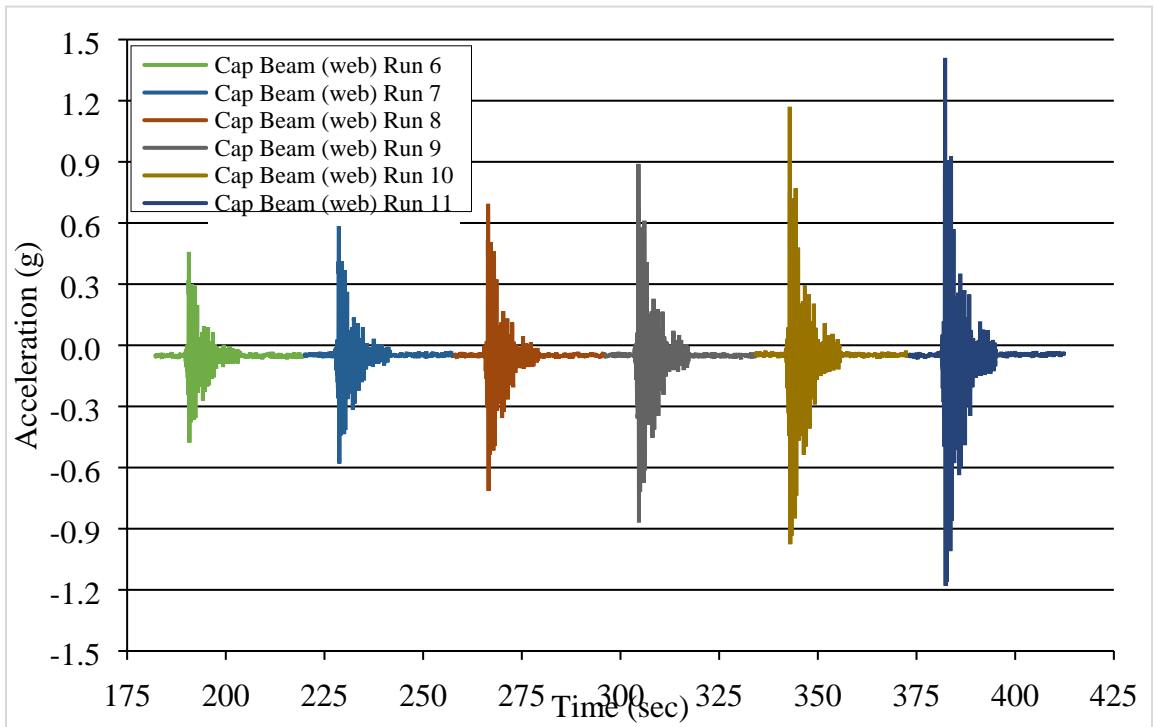
Figure 5.61 Accelerations on cap beam web for runs 6 through 11

171
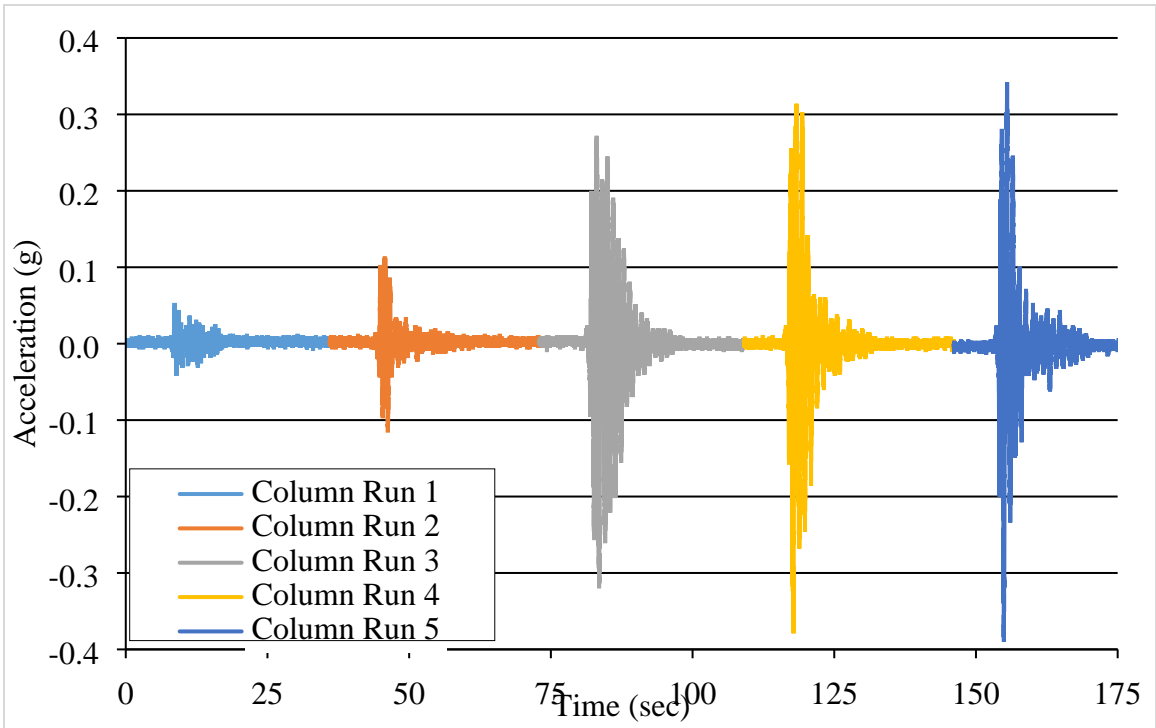
Figure 5.62 Accelerations at top of column for runs 1 through 5
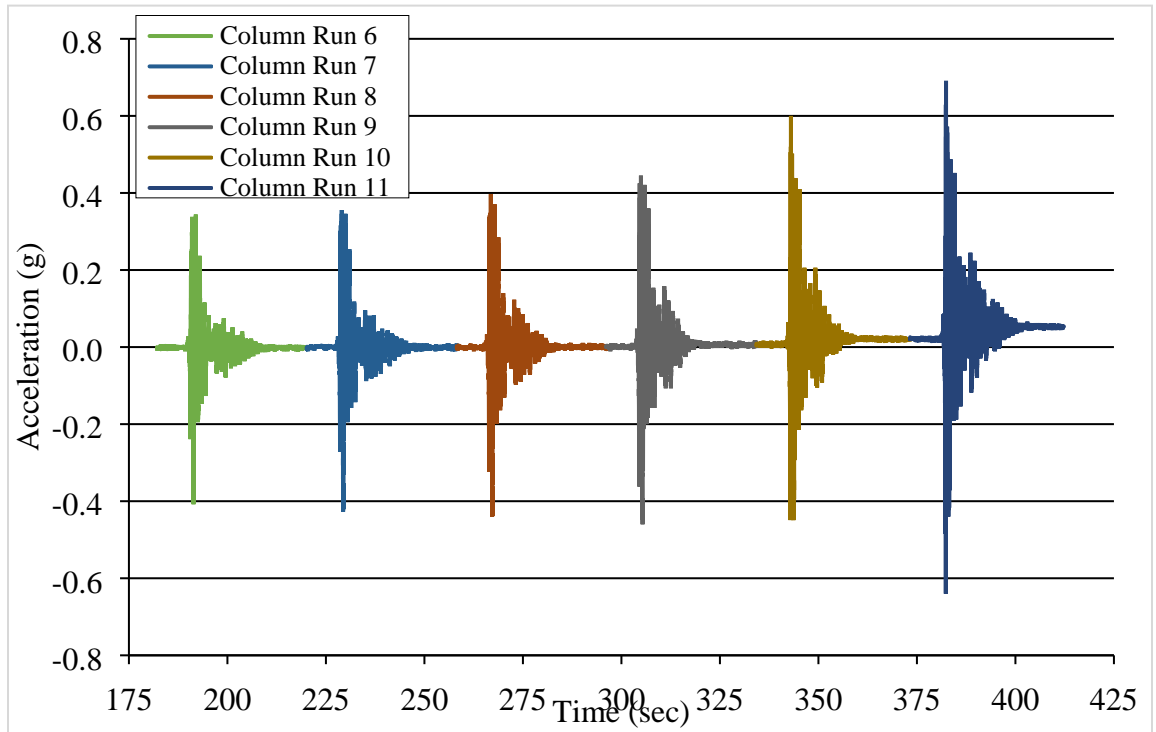
Figure 5.63 Accelerations at top of column for runs 6 through 11

172

Chapter 6 Figures
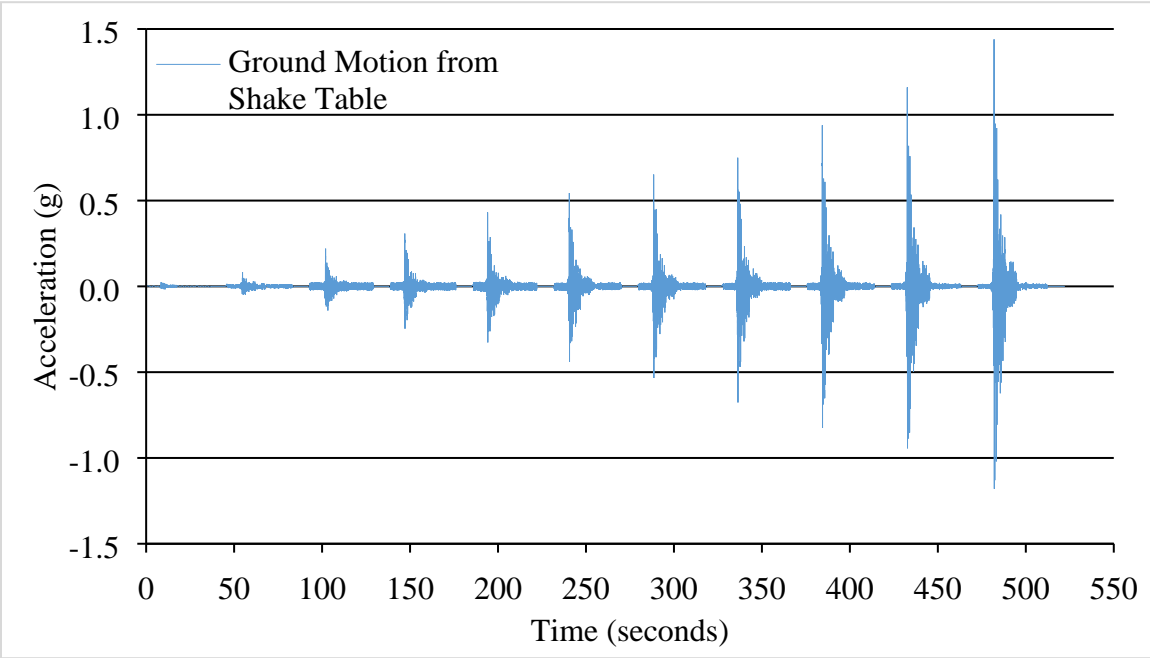
Figure 6.1 Ground motion applied to analytical model
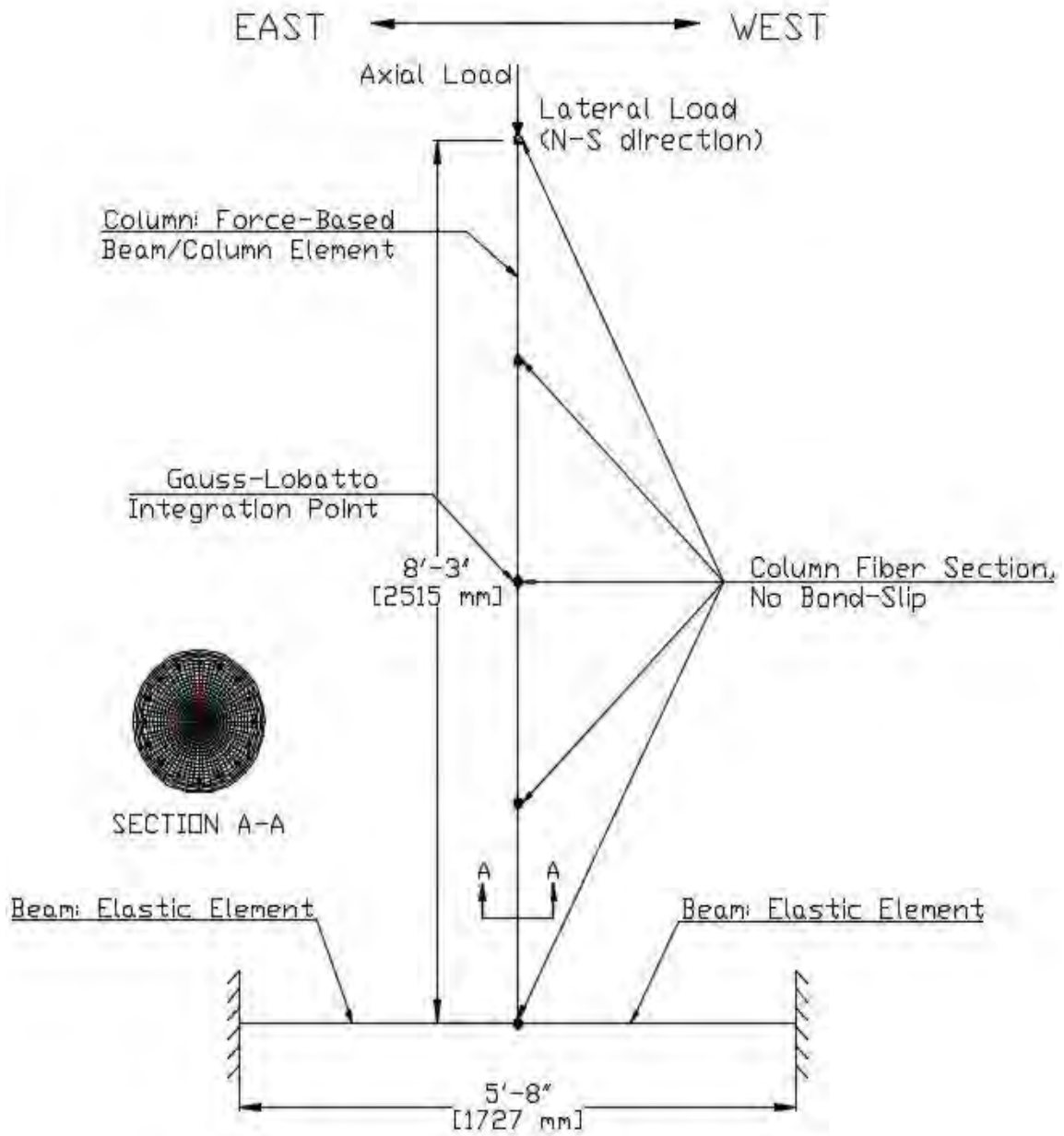
Figure 6.2 Post-test analytical model without bond-slip effects
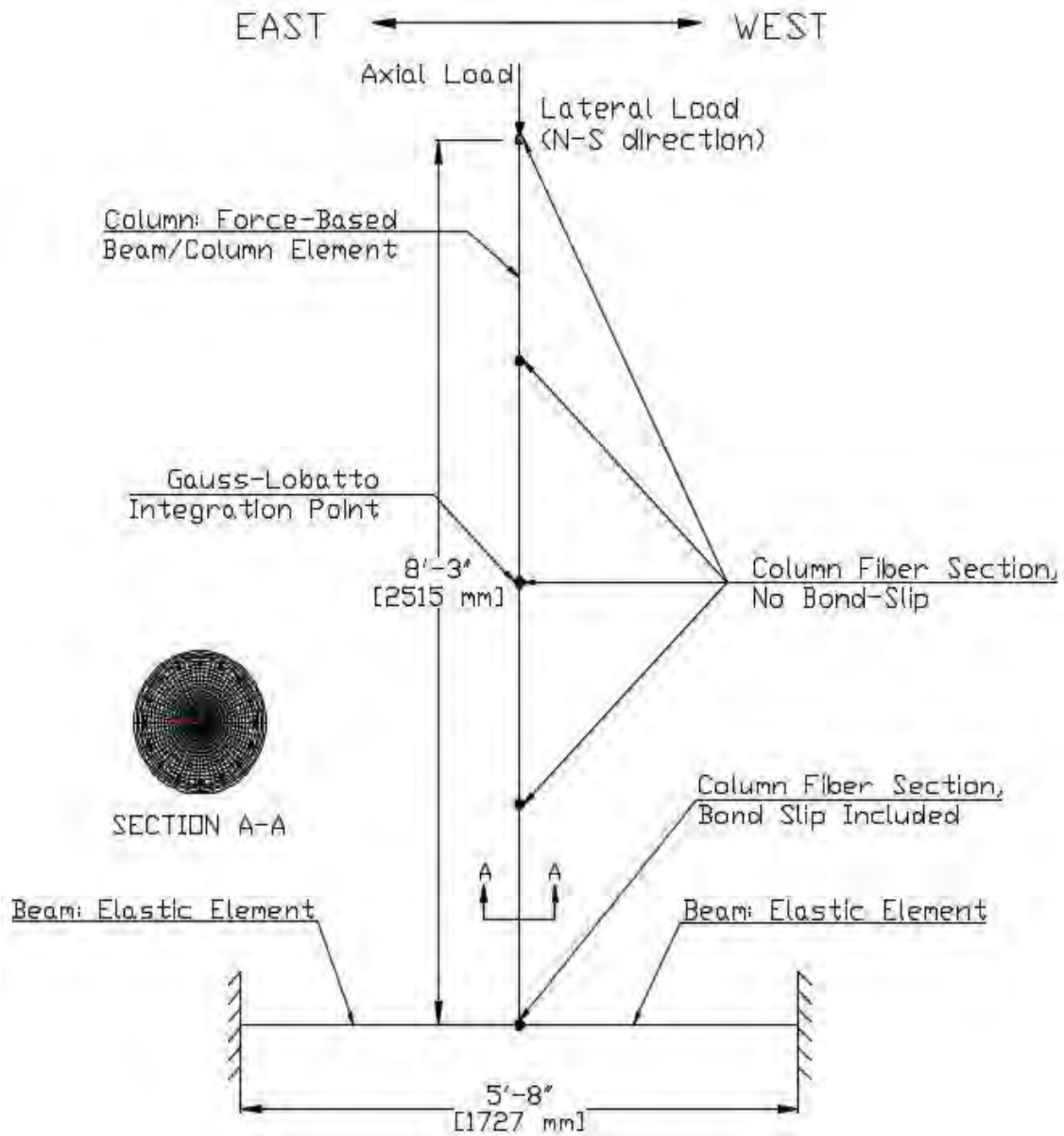
Figure 6.3 Post-test analytical model with bond-slip effects
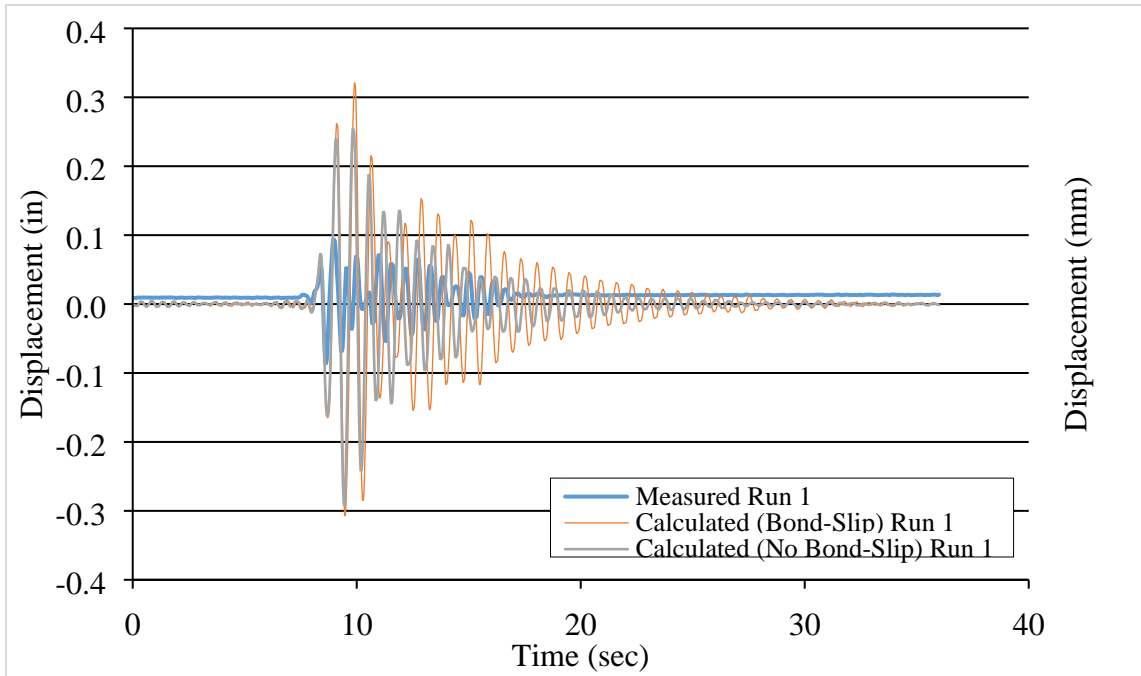
Figure 6.4 Measured and calculated displacement histories for run 1
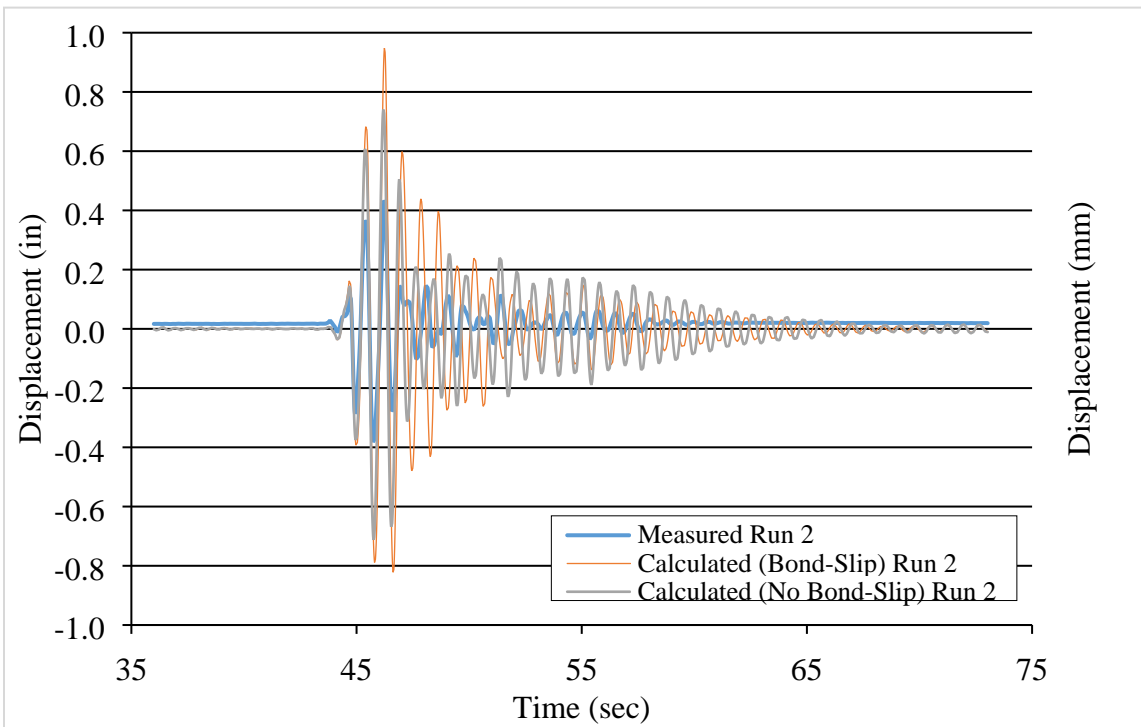
Figure 6.5 Measured and calculated displacement histories for run 2

176
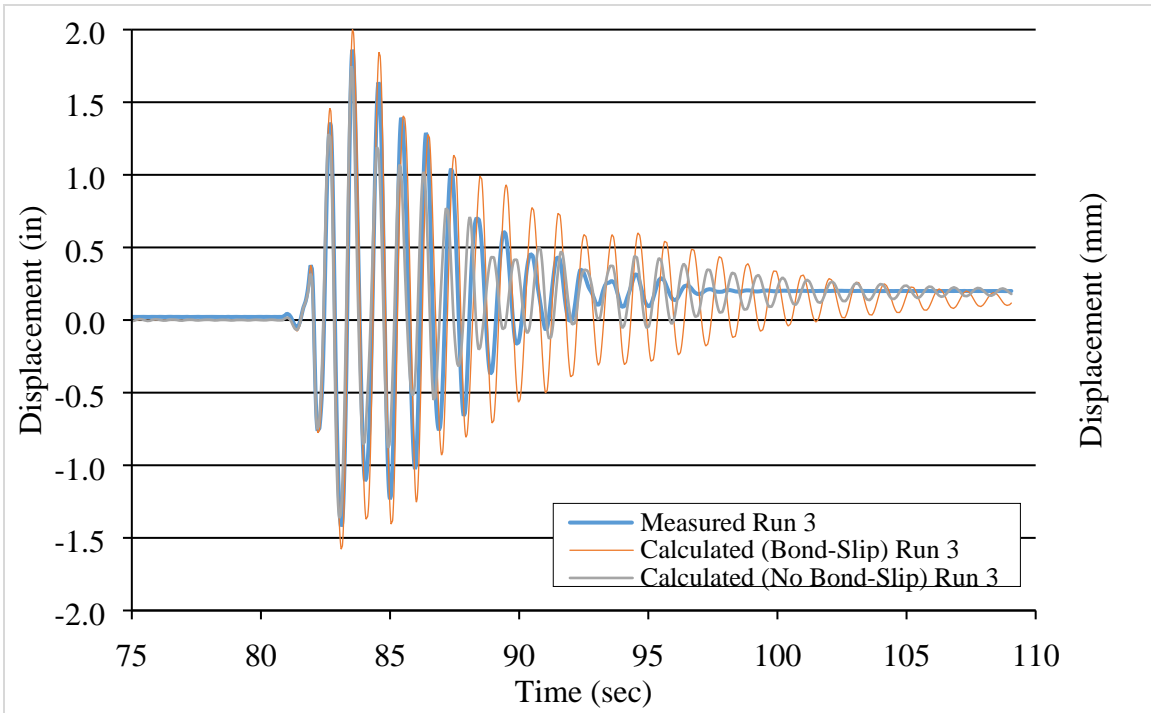
Figure 6.6 Measured and calculated displacement histories for run 3
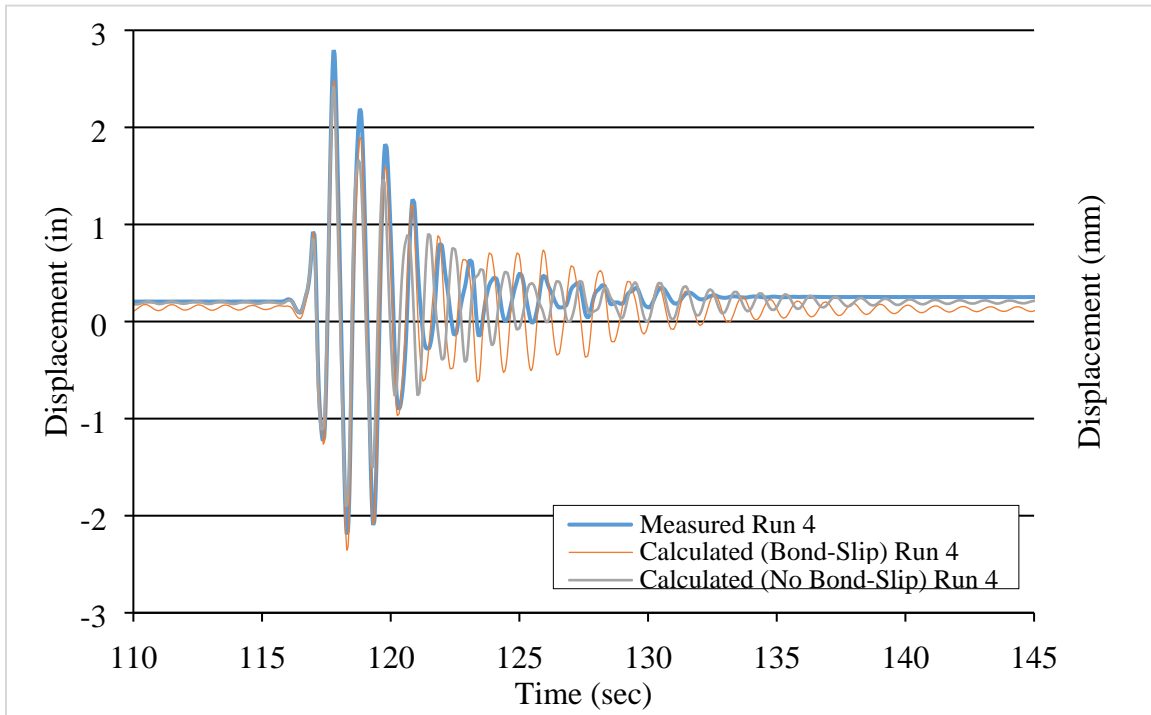
Figure 6.7 Measured and calculated displacement histories for run 4
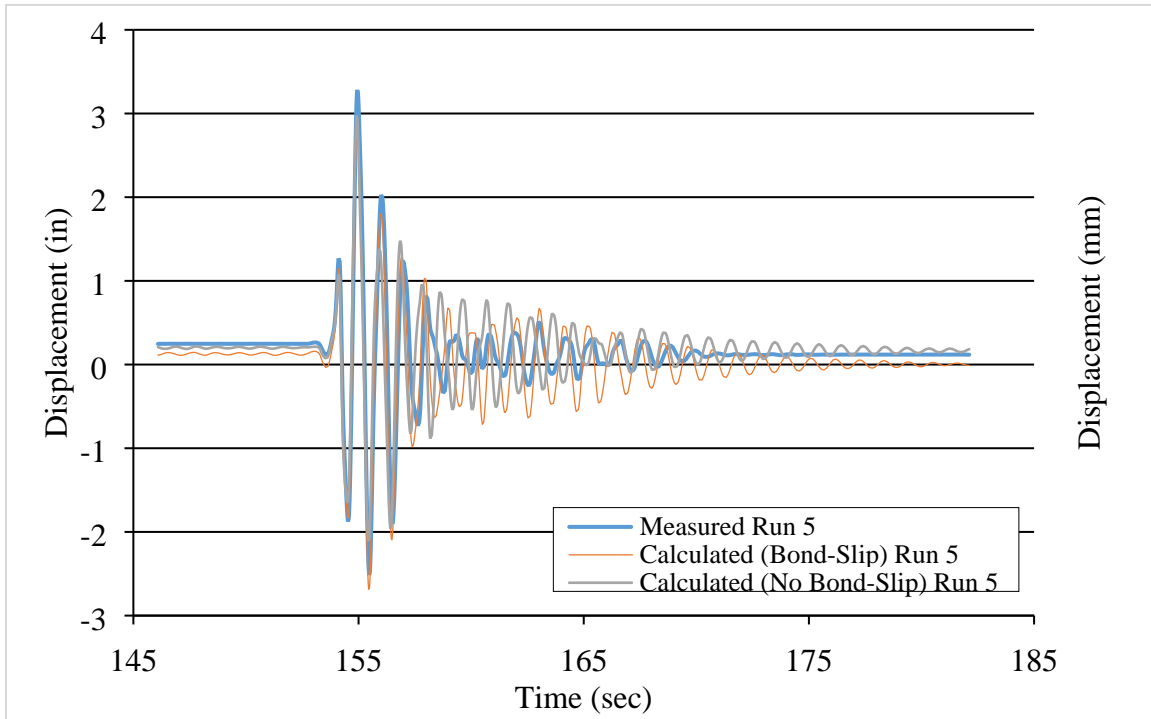
Figure 6.8 Measured and calculated displacement histories for run 5
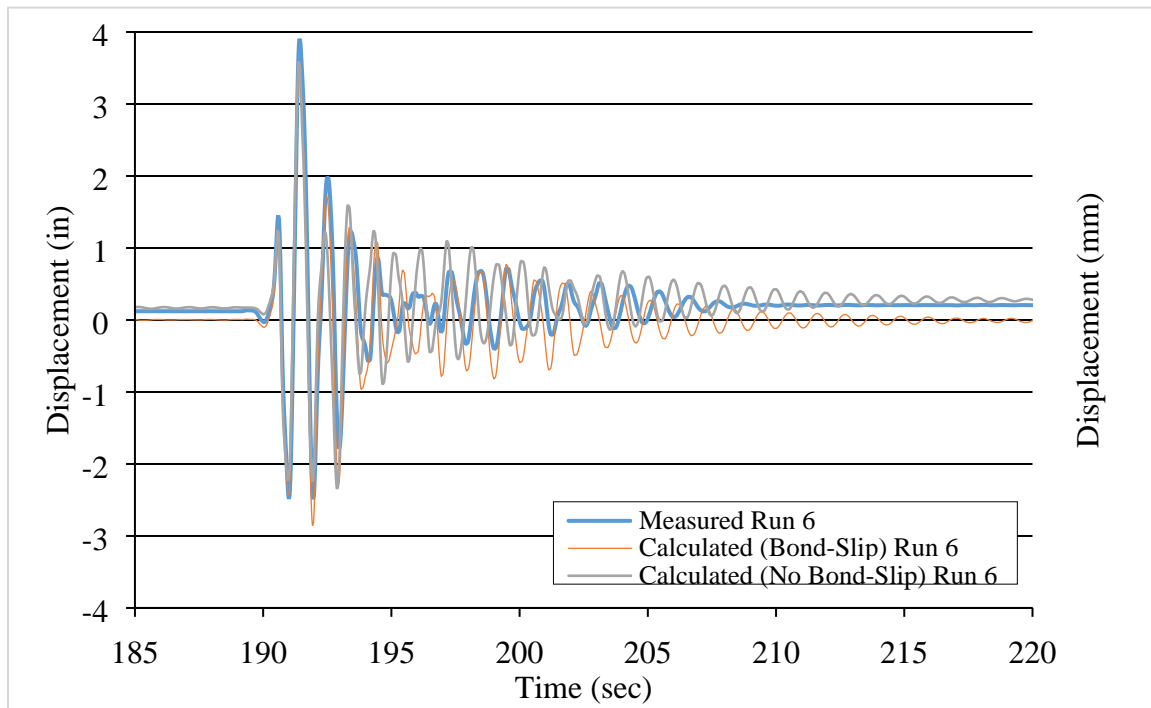
Figure 6.9 Measured and calculated displacement histories for run 6
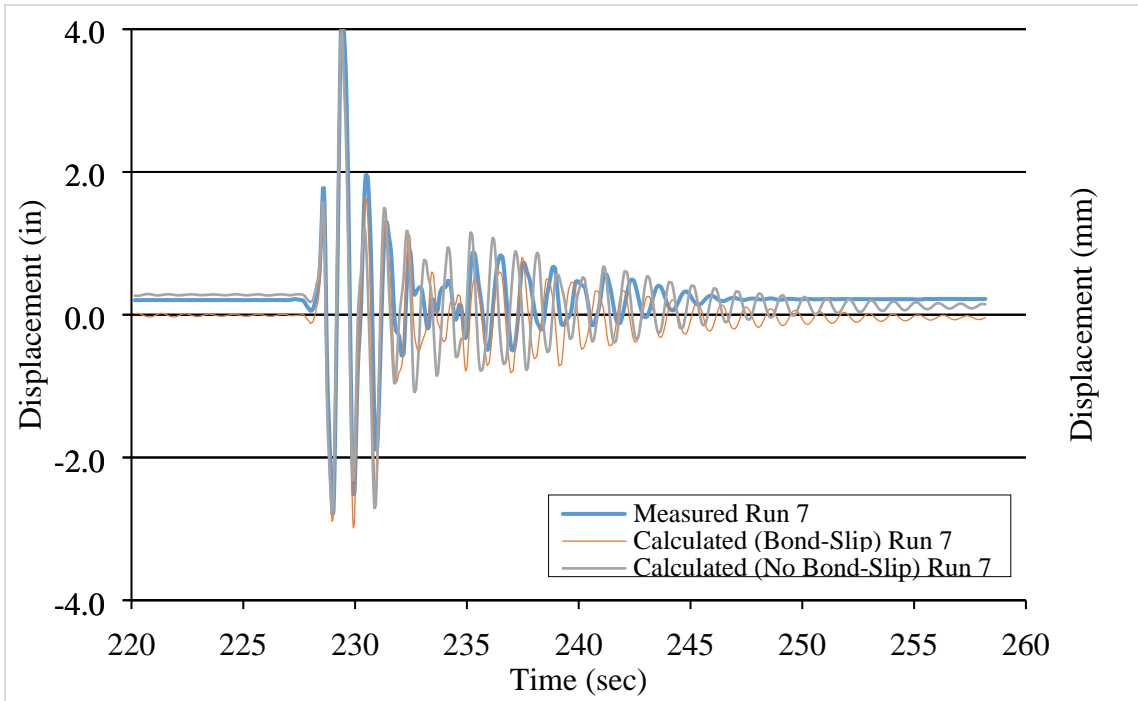
Figure 6.10 Measured and calculated displacement histories for run 7
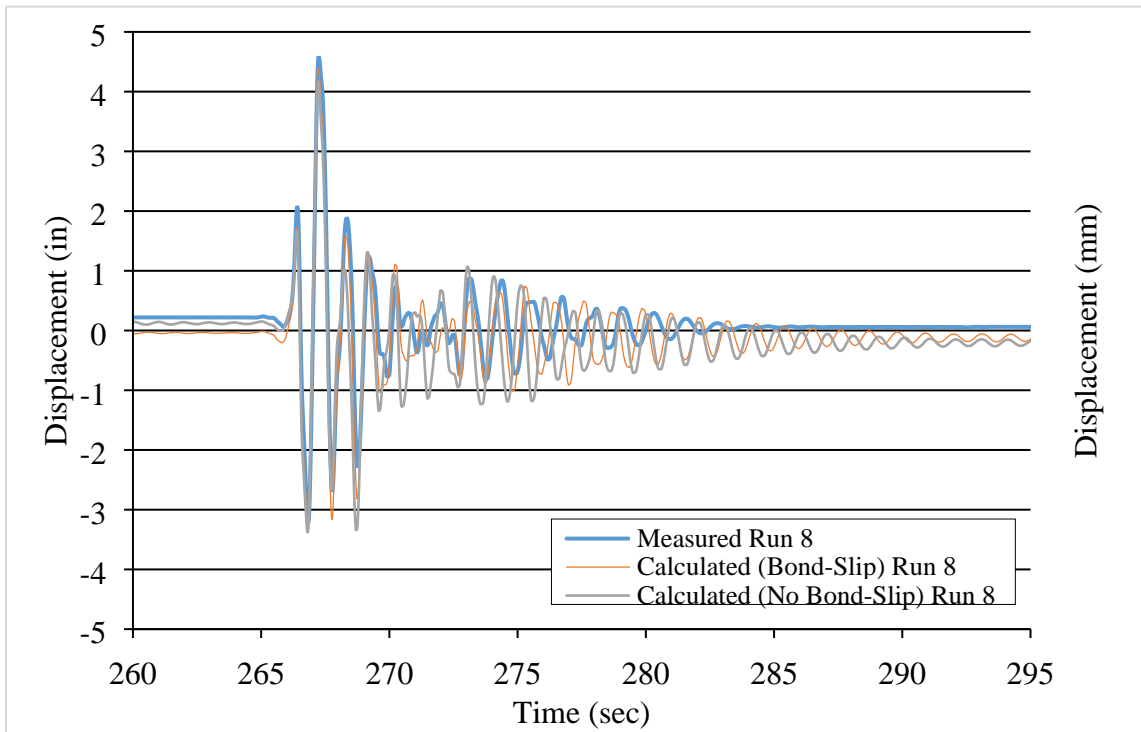
Figure 6.11 Measured and calculated displacement histories for run 8

179
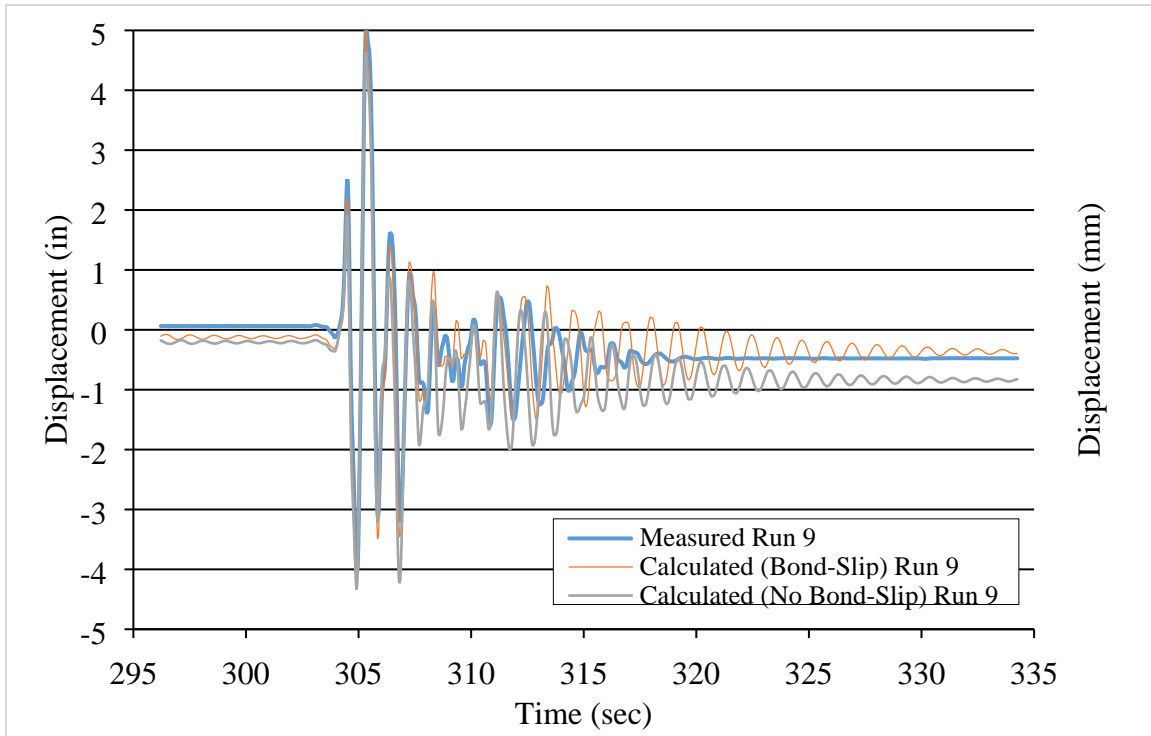
Figure 6.12 Measured and calculated displacement histories for run 9
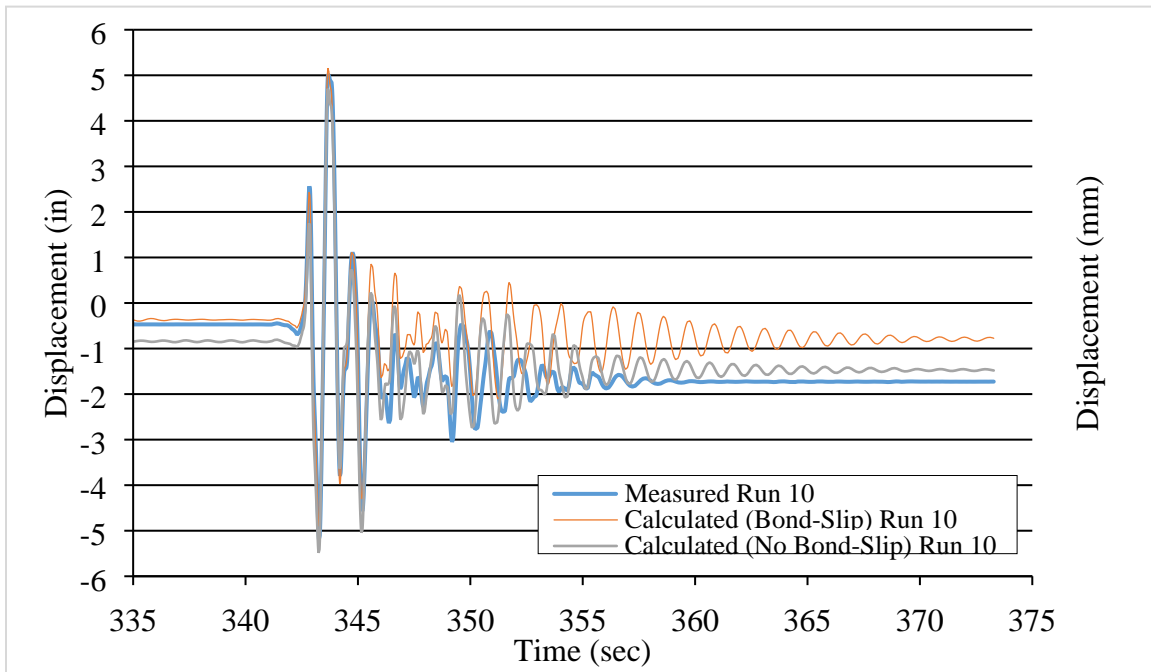
Figure 6.13 Measured and calculated displacement histories for run 10
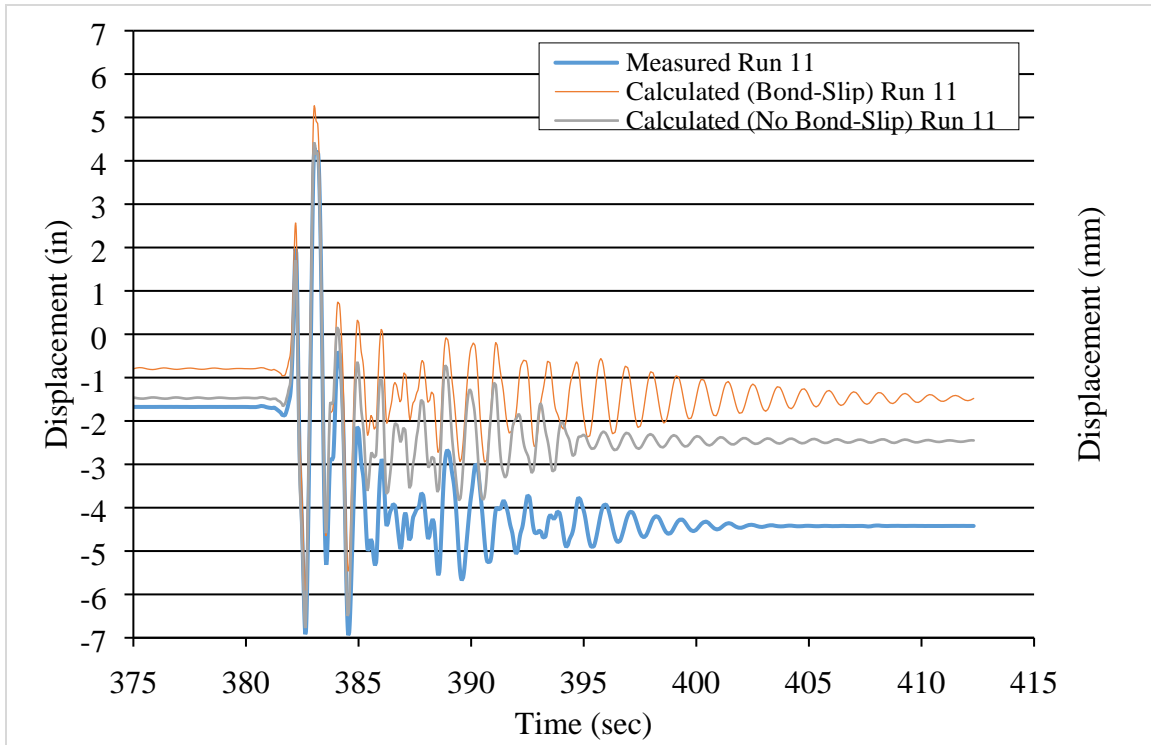
Figure 6.14 Measured and calculated displacement histories for run 11
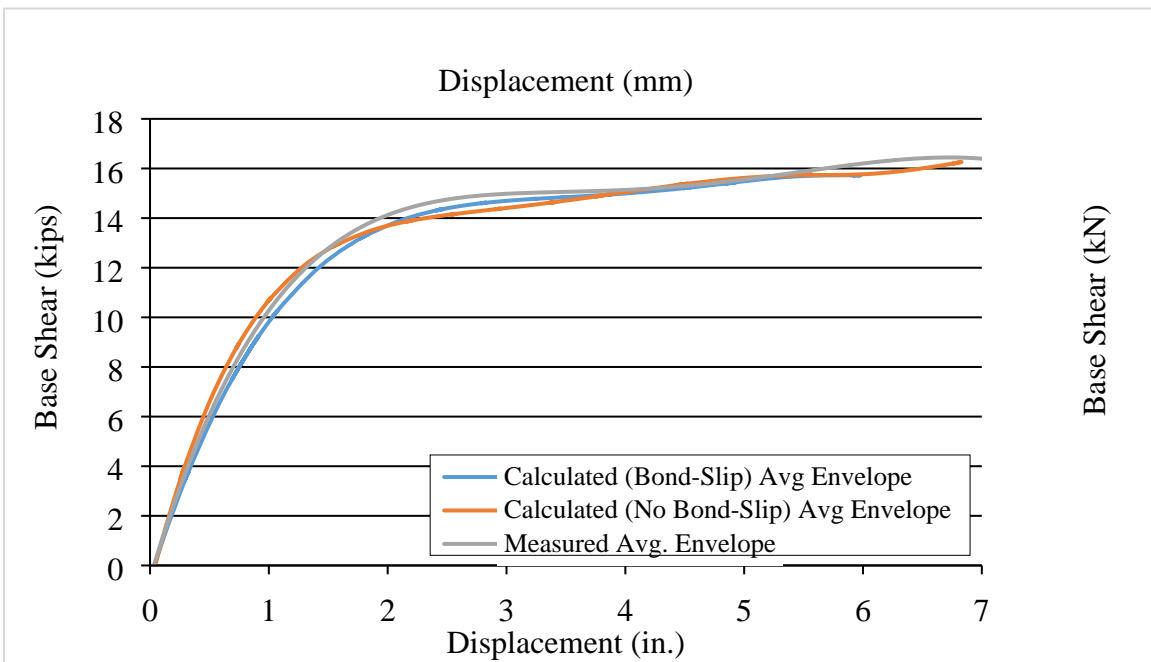
Figure 6.15 Measured and calculated envelope curves

181

LIST OF CCEER PUBLICATIONS

Report No.	Publication

CCEER-84-1   Saiidi, M., and R. Lawver, "User's Manual for LZAK-C64, A Computer Program to Implement the Q-Model on Commodore 64," Civil Engineering Department, Report No. CCEER-84-1, University of Nevada, Reno, January 1984.

CCEER-84-1   Douglas, B., Norris, G., Saiidi, M., Dodd, L., Richardson, J. and Reid, W., "Simple Bridge Models for Earthquakes and Test Data," Civil Engineering Department, Report No. CCEER-84-1 Reprint, University of Nevada, Reno, January 1984.

CCEER-84-2   Douglas, B. and T. Iwasaki, "Proceedings of the First USA-Japan Bridge Engineering Workshop," held at the Public Works Research Institute, Tsukuba, Japan, Civil Engineering Department, Report No. CCEER-84-2, University of Nevada, Reno, April 1984.

CCEER-84-3   Saiidi, M., J. Hart, and B. Douglas, "Inelastic Static and Dynamic Analysis of Short R/C Bridges Subjected to Lateral Loads," Civil Engineering Department, Report No. CCEER-84-3, University of Nevada, Reno, July 1984.

CCEER-84-4   Douglas, B., "A Proposed Plan for a National Bridge Engineering Laboratory," Civil Engineering Department, Report No. CCEER-84-4, University of Nevada, Reno, December 1984.

CCEER-85-1   Norris, G. and P. Abdollaholiaee, "Laterally Loaded Pile Response: Studies with the Strain Wedge Model," Civil Engineering Department, Report No. CCEER-85-1, University of Nevada, Reno, April 1985.

CCEER-86-1   Ghusn, G. and M. Saiidi, "A Simple Hysteretic Element for Biaxial Bending of R/C in NEABS-86," Civil Engineering Department, Report No. CCEER-86-1, University of Nevada, Reno, July 1986.

CCEER-86-2   Saiidi, M., R. Lawver, and J. Hart, "User's Manual of ISADAB and SIBA, Computer Programs for Nonlinear Transverse Analysis of Highway Bridges Subjected to Static and Dynamic Lateral Loads," Civil Engineering Department, Report No. CCEER-86-2, University of Nevada, Reno, September 1986.

CCEER-87-1   Siddharthan, R., "Dynamic Effective Stress Response of Surface and Embedded Footings in Sand," Civil Engineering Department, Report No. CCEER-86-2, University of Nevada, Reno, June 1987.

CCEER-87-2   Norris, G. and R. Sack, "Lateral and Rotational Stiffness of Pile Groups for Seismic Analysis of Highway Bridges," Civil Engineering Department, Report No. CCEER-87-2, University of Nevada, Reno, June 1987.

CCEER-88-1   Orie, J. and M. Saiidi, "A Preliminary Study of One-Way Reinforced Concrete Pier Hinges Subjected to Shear and Flexure," Civil Engineering Department, Report No. CCEER-88-1, University of Nevada, Reno, January 1988.

CCEER-88-2   Orie, D., M. Saiidi, and B. Douglas, "A Micro-CAD System for Seismic Design of Regular Highway Bridges," Civil Engineering Department, Report No. CCEER-88-2, University of Nevada, Reno, June 1988.

CCEER-88-3   Orie, D. and M. Saiidi, "User's Manual for Micro-SARB, a Microcomputer Program for

Seismic Analysis of Regular Highway Bridges," Civil Engineering Department, Report No. CCEER-88-3, University of Nevada, Reno, October 1988.

CCEER-89-1   Douglas, B., M. Saiidi, R. Hayes, and G. Holcomb, "A Comprehensive Study of the Loads and Pressures Exerted on Wall Forms by the Placement of Concrete," Civil Engineering Department, Report No. CCEER-89-1, University of Nevada, Reno, February 1989.

CCEER-89-2   Richardson, J. and B. Douglas, "Dynamic Response Analysis of the Dominion Road Bridge Test Data," Civil Engineering Department, Report No. CCEER-89-2, University of Nevada, Reno, March 1989.

CCEER-89-2   Vrontinos, S., M. Saiidi, and B. Douglas, "A Simple Model to Predict the Ultimate Response of R/C Beams with Concrete Overlays," Civil Engineering Department, Report NO. CCEER-89-2, University of Nevada, Reno, June 1989.

CCEER-89-3   Ebrahimpour, A. and P. Jagadish, "Statistical Modeling of Bridge Traffic Loads - A Case Study," Civil Engineering Department, Report No. CCEER-89-3, University of Nevada, Reno, December 1989.

CCEER-89-4   Shields, J. and M. Saiidi, "Direct Field Measurement of Prestress Losses in Box Girder Bridges," Civil Engineering Department, Report No. CCEER-89-4, University of Nevada, Reno, December 1989.

CCEER-90-1   Saiidi, M., E. Maragakis, G. Ghusn, Y. Jiang, and D. Schwartz, "Survey and Evaluation of Nevada's Transportation Infrastructure, Task 7.2 - Highway Bridges, Final Report," Civil Engineering Department, Report No. CCEER 90-1, University of Nevada, Reno, October 1990.

CCEER-90-2   Abdel-Ghaffar, S., E. Maragakis, and M. Saiidi, "Analysis of the Response of Reinforced Concrete Structures During the Whittier Earthquake 1987," Civil Engineering Department, Report No. CCEER 90-2, University of Nevada, Reno, October 1990.

CCEER-91-1   Saiidi, M., E. Hwang, E. Maragakis, and B. Douglas, "Dynamic Testing and the Analysis of the Flamingo Road Interchange," Civil Engineering Department, Report No. CCEER-91-1, University of Nevada, Reno, February 1991.

CCEER-91-2   Norris, G., R. Siddharthan, Z. Zafir, S. Abdel-Ghaffar, and P. Gowda, "Soil-Foundation-Structure Behavior at the Oakland Outer Harbor Wharf," Civil Engineering Department, Report No. CCEER-91-2, University of Nevada, Reno, July 1991.

CCEER-91-3   Norris, G., "Seismic Lateral and Rotational Pile Foundation Stiffnesses at Cypress," Civil Engineering Department, Report No. CCEER-91-3, University of Nevada, Reno, August 1991.

CCEER-91-4   O'Connor, D. and M. Saiidi, "A Study of Protective Overlays for Highway Bridge Decks in Nevada, with Emphasis on Polyester-Styrene Polymer Concrete," Civil Engineering Department, Report No. CCEER-91-4, University of Nevada, Reno, October 1991.

CCEER-91-5   O'Connor, D.N. and M. Saiidi, "Laboratory Studies of Polyester-Styrene Polymer Concrete Engineering Properties," Civil Engineering Department, Report No. CCEER-91-5, University of Nevada, Reno, November 1991.

CCEER-92-1   Straw, D.L. and M. Saiidi, "Scale Model Testing of One-Way Reinforced Concrete Pier Hinges Subject to Combined Axial Force, Shear and Flexure," edited by D.N. O'Connor, Civil Engineering Department, Report No. CCEER-92-1, University of Nevada, Reno, March 1992.

CCEER-92-2   Wehbe, N., M. Saiidi, and F. Gordaninejad, "Basic Behavior of Composite Sections Made of Concrete Slabs and Graphite Epoxy Beams," Civil Engineering Department, Report No. CCEER-92-2, University of Nevada, Reno, August 1992.

CCEER-92-3   Saiidi, M. and E. Hutchens, "A Study of Prestress Changes in A Post-Tensioned Bridge During the First 30 Months," Civil Engineering Department, Report No. CCEER-92-3, University of Nevada, Reno, April 1992.

CCEER-92-4   Saiidi, M., B. Douglas, S. Feng, E. Hwang, and E. Maragakis, "Effects of Axial Force on Frequency of Prestressed Concrete Bridges," Civil Engineering Department, Report No. CCEER-92-4, University of Nevada, Reno, August 1992.

CCEER-92-5   Siddharthan, R., and Z. Zafir, "Response of Layered Deposits to Traveling Surface Pressure Waves," Civil Engineering Department, Report No. CCEER-92-5, University of Nevada, Reno, September 1992.

CCEER-92-6   Norris, G., and Z. Zafir, "Liquefaction and Residual Strength of Loose Sands from Drained Triaxial Tests," Civil Engineering Department, Report No. CCEER-92-6, University of Nevada, Reno, September 1992.

CCEER-92-6-A   Norris, G., Siddharthan, R., Zafir, Z. and Madhu, R. "Liquefaction and Residual Strength of Sands from Drained Triaxial Tests," Civil Engineering Department, Report No. CCEER-92-6-A, University of Nevada, Reno, September 1992.

CCEER-92-7   Douglas, B., "Some Thoughts Regarding the Improvement of the University of Nevada, Reno's National Academic Standing," Civil Engineering Department, Report No. CCEER-92-7, University of Nevada, Reno, September 1992.

CCEER-92-8   Saiidi, M., E. Maragakis, and S. Feng, "An Evaluation of the Current Caltrans Seismic Restrainer Design Method," Civil Engineering Department, Report No. CCEER-92-8, University of Nevada, Reno, October 1992.

CCEER-92-9   O'Connor, D., M. Saiidi, and E. Maragakis, "Effect of Hinge Restrainers on the Response of the Madrone Drive Undercrossing During the Loma Prieta Earthquake," Civil Engineering Department, Report No. CCEER-92-9, University of Nevada, Reno, February 1993.

CCEER-92-10   O'Connor, D., and M. Saiidi, "Laboratory Studies of Polyester Concrete: Compressive Strength at Elevated Temperatures and Following Temperature Cycling, Bond Strength to Portland Cement Concrete, and Modulus of Elasticity," Civil Engineering Department, Report No. CCEER-92-10, University of Nevada, Reno, February 1993.

CCEER-92-11   Wehbe, N., M. Saiidi, and D. O'Connor, "Economic Impact of Passage of Spent Fuel Traffic on Two Bridges in Northeast Nevada," Civil Engineering Department, Report No. CCEER-92-11, University of Nevada, Reno, December 1992.

CCEER-93-1   Jiang, Y., and M. Saiidi, "Behavior, Design, and Retrofit of Reinforced Concrete One-way Bridge Column Hinges," edited by D. O'Connor, Civil Engineering Department, Report No. CCEER-93-1, University of Nevada, Reno, March 1993.

CCEER-93-2   Abdel-Ghaffar, S., E. Maragakis, and M. Saiidi, "Evaluation of the Response of the Aptos Creek Bridge During the 1989 Loma Prieta Earthquake," Civil Engineering Department, Report No. CCEER-93-2, University of Nevada, Reno, June 1993.

CCEER-93-3   Sanders, D.H., B.M. Douglas, and T.L. Martin, "Seismic Retrofit Prioritization of Nevada Bridges," Civil Engineering Department, Report No. CCEER-93-3, University of Nevada,

Reno, July 1993.

CCEER-93-4   Abdel-Ghaffar, S., E. Maragakis, and M. Saiidi, "Performance of Hinge Restrainers in the Huntington Avenue Overhead During the 1989 Loma Prieta Earthquake," Civil Engineering Department, Report No. CCEER-93-4, University of Nevada, Reno, June 1993.

CCEER-93-5   Maragakis, E., M. Saiidi, S. Feng, and L. Flournoy, "Effects of Hinge Restrainers on the Response of the San Gregorio Bridge during the Loma Prieta Earthquake," (in final preparation) Civil Engineering Department, Report No. CCEER-93-5, University of Nevada, Reno.

CCEER-93-6   Saiidi, M., E. Maragakis, S. Abdel-Ghaffar, S. Feng, and D. O'Connor, "Response of Bridge Hinge Restrainers during Earthquakes -Field Performance, Analysis, and Design," Civil Engineering Department, Report No. CCEER-93-6, University of Nevada, Reno, May 1993.

CCEER-93-7   Wehbe, N., Saiidi, M., Maragakis, E., and Sanders, D., "Adequacy of Three Highway Structures in Southern Nevada for Spent Fuel Transportation," Civil Engineering Department, Report No. CCEER-93-7, University of Nevada, Reno, August 1993.

CCEER-93-8   Roybal, J., Sanders, D.H., and Maragakis, E., "Vulnerability Assessment of Masonry in the Reno-Carson City Urban Corridor," Civil Engineering Department, Report No. CCEER-93-8, University of Nevada, Reno, May 1993.

CCEER-93-9   Zafir, Z. and Siddharthan, R., "MOVLOAD: A Program to Determine the Behavior of Nonlinear Horizontally Layered Medium Under Moving Load," Civil Engineering Department, Report No. CCEER-93-9, University of Nevada, Reno, August 1993.

CCEER-93-10   O'Connor, D.N., Saiidi, M., and Maragakis, E.A., "A Study of Bridge Column Seismic Damage Susceptibility at the Interstate 80/U.S. 395 Interchange in Reno, Nevada," Civil Engineering Department, Report No. CCEER-93-10, University of Nevada, Reno, October 1993.

CCEER-94-1   Maragakis, E., B. Douglas, and E. Abdelwahed, "Preliminary Dynamic Analysis of a Railroad Bridge," Report CCEER-94-1, January 1994.

CCEER-94-2   Douglas, B.M., Maragakis, E.A., and Feng, S., "Stiffness Evaluation of Pile Foundation of Cazenovia Creek Overpass," Civil Engineering Department, Report No. CCEER-94-2, University of Nevada, Reno, March 1994.

CCEER-94-3   Douglas, B.M., Maragakis, E.A., and Feng, S., "Summary of Pretest Analysis of Cazenovia Creek Bridge," Civil Engineering Department, Report No. CCEER-94-3, University of Nevada, Reno, April 1994.

CCEER-94-4   Norris, G.M., Madhu, R., Valceschini, R., and Ashour, M., "Liquefaction and Residual Strength of Loose Sands from Drained Triaxial Tests," Report 2, Vol. 1&2, Civil Engineering Department, Report No. CCEER-94-4, University of Nevada, Reno, August 1994.

CCEER-94-5   Saiidi, M., Hutchens, E., and Gardella, D., "Prestress Losses in a Post-Tensioned R/C Box Girder Bridge in Southern Nevada," Civil Engineering Department, CCEER-94-5, University of Nevada, Reno, August 1994.

CCEER-95-1   Siddharthan, R., El-Gamal, M., and Maragakis, E.A., "Nonlinear Bridge Abutment , Verification, and Design Curves," Civil Engineering Department, CCEER-95-1, University of Nevada, Reno, January 1995.

CCEER-95-2   Ashour, M. and Norris, G., "Liquefaction and Undrained Response Evaluation of Sands from Drained Formulation," Civil Engineering Department, Report No. CCEER-95-2, University of Nevada, Reno, February 1995.

CCEER-95-3   Wehbe, N., Saiidi, M., Sanders, D. and Douglas, B., "Ductility of Rectangular Reinforced Concrete Bridge Columns with Moderate Confinement," Civil Engineering Department, Report No. CCEER-95-3, University of Nevada, Reno, July 1995.

CCEER-95-4   Martin, T.., Saiidi, M. and Sanders, D., "Seismic Retrofit of Column-Pier Cap Connections in Bridges in Northern Nevada," Civil Engineering Department, Report No. CCEER-95-4, University of Nevada, Reno, August 1995.

CCEER-95-5   Darwish, I., Saiidi, M. and Sanders, D., "Experimental Study of Seismic Susceptibility Column-Footing Connections in Bridges in Northern Nevada," Civil Engineering Department, Report No. CCEER-95-5, University of Nevada, Reno, September 1995.

CCEER-95-6   Griffin, G., Saiidi, M. and Maragakis, E., "Nonlinear Seismic Response of Isolated Bridges and Effects of Pier Ductility Demand," Civil Engineering Department, Report No. CCEER-95-6, University of Nevada, Reno, November 1995.

CCEER-95-7   Acharya, S.., Saiidi, M. and Sanders, D., "Seismic Retrofit of Bridge Footings and Column-Footing Connections," Civil Engineering Department, Report No.   CCEER-95-7, University of Nevada, Reno, November 1995.

CCEER-95-8   Maragakis, E., Douglas, B., and Sandirasegaram, U., "Full-Scale Field Resonance Tests of a Railway Bridge," A Report to the Association of American Railroads, Civil Engineering Department, Report No. CCEER-95-8, University of Nevada, Reno, December 1995.

CCEER-95-9   Douglas, B., Maragakis, E. and Feng, S., "System Identification Studies on Cazenovia Creek Overpass," Report for the National Center for Earthquake Engineering Research, Civil Engineering Department, Report No. CCEER-95-9, University of Nevada, Reno, October 1995.

CCEER-96-1   El-Gamal, M.E. and Siddharthan, R.V., "Programs to Computer Translational Stiffness of Seat-Type Bridge Abutment," Civil Engineering Department, Report No. CCEER-96-1, University of Nevada, Reno, March 1996.

CCEER-96-2   Labia, Y., Saiidi, M. and Douglas, B., "Evaluation and Repair of Full-Scale Prestressed Concrete Box Girders," A Report to the National Science Foundation, Research Grant CMS-9201908, Civil Engineering Department, Report No. CCEER-96-2, University of Nevada, Reno, May 1996.

CCEER-96-3   Darwish, I., Saiidi, M. and Sanders, D., "Seismic Retrofit of R/C Oblong Tapered Bridge Columns with Inadequate Bar Anchorage in Columns and Footings," A Report to the Nevada Department of Transportation, Civil Engineering Department, Report No. CCEER-96-3, University of Nevada, Reno, May 1996.

CCEER-96-4   Ashour, M., Pilling, R., Norris, G. and Perez, H., "The Prediction of Lateral Load Behavior of Single Piles and Pile Groups Using the Strain Wedge Model," A Report to the California Department of Transportation, Civil Engineering Department, Report No. CCEER-96-4, University of Nevada, Reno, June 1996.

CCEER-97-1-A   Rimal, P. and Itani, A.   "Sensitivity Analysis of Fatigue Evaluations of Steel Bridges," Center for Earthquake Research, Department of Civil Engineering, University of Nevada, Reno, Nevada Report No. CCEER-97-1-A, September, 1997.

CCEER-97-1-B   Maragakis, E., Douglas, B., and Sandirasegaram, U. "Full-Scale Field Resonance Tests of a Railway Bridge," A Report to the Association of American Railroads, Civil Engineering Department, University of Nevada, Reno, May, 1996.

CCEER-97-2   Wehbe, N., Saiidi, M., and D. Sanders, "Effect of Confinement and Flares on the Seismic Performance of Reinforced Concrete Bridge Columns," Civil Engineering Department, Report No. CCEER-97-2, University of Nevada, Reno, September 1997.

CCEER-97-3   Darwish, I., M. Saiidi, G. Norris, and E. Maragakis, "Determination of In-Situ Footing Stiffness Using Full-Scale Dynamic Field Testing," A Report to the Nevada Department of Transportation, Structural Design Division, Carson City, Nevada, Report No. CCEER-97-3, University of Nevada, Reno, October 1997.

CCEER-97-4-A   Itani, A. "Cyclic Behavior of Richmond-San Rafael Tower Links," Center for Civil Engineering Earthquake Research, Department of Civil Engineering, University of Nevada, Reno, Nevada, Report No. CCEER-97-4, August 1997.

CCEER-97-4-B   Wehbe, N., and M. Saiidi, "User's Manual for RCMC v. 1.2 : A Computer Program for Moment-Curvature Analysis of Confined and Unconfined Reinforced Concrete Sections," Center for Civil Engineering Earthquake Research, Department of Civil Engineering, University of Nevada, Reno, Nevada, Report No. CCEER-97-4, November, 1997.

CCEER-97-5   Isakovic, T., M. Saiidi, and A. Itani, "Influence of new Bridge Configurations on Seismic Performance," Department of Civil Engineering, University of Nevada, Reno, Report No. CCEER-97-5, September, 1997.

CCEER-98-1   Itani, A., Vesco, T. and Dietrich, A., "Cyclic Behavior of "as Built" Laced Members With End Gusset Plates on the San Francisco Bay Bridge," Center for Civil Engineering Earthquake Research, Department of Civil Engineering, University of Nevada, Reno, Nevada Report No. CCEER-98-1, March, 1998.

CCEER-98-2   G. Norris and M. Ashour, "Liquefaction and Undrained Response Evaluation of Sands from Drained Formulation," Center for Civil Engineering Earthquake Research, Department of Civil Engineering, University of Nevada, Reno, Nevada, Report No. CCEER-98-2, May, 1998.

CCEER-98-3   Qingbin, Chen, B. M. Douglas, E. Maragakis, and I. G. Buckle, "Extraction of Nonlinear Hysteretic Properties of Seismically Isolated Bridges from Quick-Release Field Tests," Center for Civil Engineering Earthquake Research, Department of Civil Engineering, University of Nevada, Reno, Nevada, Report No. CCEER-98-3, June, 1998.

CCEER-98-4   Maragakis, E., B. M. Douglas, and C. Qingbin, "Full-Scale Field Capacity Tests of a Railway Bridge," Center for Civil Engineering Earthquake Research, Department of Civil Engineering, University of Nevada, Reno, Nevada, Report No. CCEER-98-4, June, 1998.

CCEER-98-5   Itani, A., Douglas, B., and Woodgate, J., "Cyclic Behavior of Richmond-San Rafael Retrofitted Tower Leg," Center for Civil Engineering Earthquake Research, Department of Civil Engineering, University of Nevada, Reno. Report No. CCEER-98-5, June 1998

CCEER-98-6   Moore, R., Saiidi, M., and Itani, A., "Seismic Behavior of New Bridges with Skew and Curvature," Center for Civil Engineering Earthquake Research, Department of Civil Engineering, University of Nevada, Reno. Report No. CCEER-98-6, October, 1998.

CCEER-98-7   Itani, A and Dietrich, A, "Cyclic Behavior of Double Gusset Plate Connections," Center for Civil Engineering Earthquake Research, Department of Civil Engineering, University of Nevada, Reno, Nevada, Report No. CCEER-98-5, December, 1998.

CCEER-99-1   Caywood, C., M. Saiidi, and D. Sanders, "Seismic Retrofit of Flared Bridge Columns with Steel Jackets," Civil Engineering Department, University of Nevada, Reno, Report No. CCEER-99-1, February 1999.

CCEER-99-2   Mangoba, N., M. Mayberry, and M. Saiidi, "Prestress Loss in Four Box Girder Bridges in Northern Nevada," Civil Engineering Department, University of Nevada, Reno, Report No. CCEER-99-2, March 1999.

CCEER-99-3   Abo-Shadi, N., M. Saiidi, and D. Sanders, "Seismic Response of Bridge Pier Walls in the Weak Direction," Civil Engineering Department, University of Nevada, Reno, Report No. CCEER-99-3, April 1999.

CCEER-99-4   Buzick, A., and M. Saiidi, "Shear Strength and Shear Fatigue Behavior of Full-Scale Prestressed Concrete Box Girders," Civil Engineering Department, University of Nevada, Reno, Report No. CCEER-99-4, April 1999.

CCEER-99-5   Randall, M., M. Saiidi, E. Maragakis and T. Isakovic, "Restrainer Design Procedures For Multi-Span Simply-Supported Bridges," Civil Engineering Department, University of Nevada, Reno, Report No. CCEER-99-5, April 1999.

CCEER-99-6   Wehbe, N. and M. Saiidi, "User's Manual for RCMC v. 1.2, A Computer Program for Moment-Curvature Analysis of Confined and Unconfined Reinforced Concrete Sections," Civil Engineering Department, University of Nevada, Reno, Report No. CCEER-99-6, May 1999.

CCEER-99-7   Burda, J. and A. Itani, "Studies of Seismic Behavior of Steel Base Plates," Civil Engineering Department, University of Nevada, Reno, Report No. CCEER-99-7, May 1999.

CCEER-99-8   Ashour, M. and G. Norris, "Refinement of the Strain Wedge Model Program," Civil Engineering Department, University of Nevada, Reno, Report No. CCEER-99-8, March 1999.

CCEER-99-9   Dietrich, A., and A. Itani, "Cyclic Behavior of Laced and Perforated Steel Members on the San Francisco-Oakland Bay Bridge," Civil Engineering Department, University, Reno, Report No. CCEER-99-9, December 1999.

CCEER 99-10   Itani, A., A. Dietrich, "Cyclic Behavior of Built Up Steel Members and their Connections," Civil Engineering Department, University of Nevada, Reno, Report No. CCEER-99-10, December 1999.

CCEER 99-10-A Itani, A., E. Maragakis and P. He, "Fatigue Behavior of Riveted Open Deck Railroad Bridge Girders," Civil Engineering Department, University of Nevada, Reno, Report No. CCEER-99-10-A, August 1999.

CCEER 99-11   Itani, A., J. Woodgate, "Axial and Rotational Ductility of Built Up Structural Steel Members," Civil Engineering Department, University of Nevada, Reno, Report No. CCEER-99-11, December 1999.

CCEER-99-12   Sgambelluri, M., Sanders, D.H., and Saiidi, M.S., "Behavior of One-Way Reinforced Concrete Bridge Column Hinges in the Weak Direction," Department of Civil Engineering, University of Nevada, Reno, Report No. CCEER-99-12, December 1999.

CCEER-99-13   Laplace, P., Sanders, D.H., Douglas, B, and Saiidi, M, "Shake Table Testing of Flexure Dominated Reinforced Concrete Bridge Columns", Department of Civil Engineering, University of Nevada, Reno, Report No. CCEER-99-13, December 1999.

CCEER-99-14   Ahmad M. Itani, Jose A. Zepeda, and Elizabeth A. Ware "Cyclic Behavior of Steel Moment Frame Connections for the Moscone Center Expansion," Department of Civil Engineering, University of Nevada, Reno, Report No. CCEER-99-14, December 1999.

CCEER 00-1   Ashour, M., and Norris, G. "Undrained Lateral Pile and Pile Group Response in Saturated Sand," Civil Engineering Department, University of Nevada, Reno, Report No. CCEER-00-1, May 1999. January 2000.

CCEER 00-2   Saiidi, M. and Wehbe, N., "A Comparison of Confinement Requirements in Different Codes for Rectangular, Circular, and Double-Spiral RC Bridge Columns," Civil Engineering Department, University of Nevada, Reno, Report No. CCEER-00-2, January 2000.

CCEER 00-3   McElhaney, B., M. Saiidi, and D. Sanders, "Shake Table Testing of Flared Bridge Columns With Steel Jacket Retrofit," Civil Engineering Department, University of Nevada, Reno, Report No. CCEER-00-3, January 2000.

CCEER 00-4   Martinovic, F., M. Saiidi, D. Sanders, and F. Gordaninejad, "Dynamic Testing of Non-Prismatic Reinforced Concrete Bridge Columns Retrofitted with FRP Jackets," Civil Engineering Department, University of Nevada, Reno, Report No. CCEER-00-4, January 2000.

CCEER 00-5   Itani, A., and M. Saiidi, "Seismic Evaluation of Steel Joints for UCLA Center for Health Science Westwood Replacement Hospital," Civil Engineering Department, University of Nevada, Reno, Report No. CCEER-00-5, February 2000.

CCEER 00-6   Will, J. and D. Sanders, "High Performance Concrete Using Nevada Aggregates," Civil Engineering Department, University of Nevada, Reno, Report No. CCEER-00-6, May 2000.

CCEER 00-7   French, C., and M. Saiidi, "A Comparison of Static and Dynamic Performance of Models of Flared Bridge Columns," Civil Engineering Department, University of Nevada, Reno, Report No. CCEER-00-7, October 2000.

CCEER 00-8   Itani, A., H. Sedarat, "Seismic Analysis of the AISI LRFD Design Example of Steel Highway Bridges," Civil Engineering Department, University of Nevada, Reno, Report No. CCEER 00-08, November 2000.

CCEER 00-9   Moore, J., D. Sanders, and M. Saiidi, "Shake Table Testing of 1960's Two Column Bent with Hinges Bases," Civil Engineering Department, University of Nevada, Reno, Report No. CCEER 00-09, December 2000.

CCEER 00-10   Asthana, M., D. Sanders, and M. Saiidi, "One-Way Reinforced Concrete Bridge Column Hinges in the Weak Direction," Civil Engineering Department, University of Nevada, Reno, Report No. CCEER 00-10, April 2001.

CCEER 01-1   Ah Sha, H., D. Sanders, M. Saiidi, "Early Age Shrinkage and Cracking of Nevada Concrete Bridge Decks," Civil Engineering Department, University of Nevada, Reno, Report No. CCEER 01-01, May 2001.

CCEER 01-2   Ashour, M. and G. Norris, "Pile Group program for Full Material Modeling a Progressive Failure," Civil Engineering Department, University of Nevada, Reno, Report No. CCEER 01-02, July 2001.

CCEER 01-3   Itani, A., C. Lanaud, and P. Dusicka, "Non-Linear Finite Element Analysis of Built-Up

Shear Links," Civil Engineering Department, University of Nevada, Reno, Report No. CCEER 01-03, July 2001.

CCEER 01-4   Saiidi, M., J. Mortensen, and F. Martinovic, "Analysis and Retrofit of Fixed Flared Columns with Glass Fiber-Reinforced Plastic Jacketing," Civil Engineering Department, University of Nevada, Reno, Report No. CCEER 01-4, August 2001

CCEER 01-5   Not Published

CCEER 01-6   Laplace, P., D. Sanders, and M. Saiidi, "Experimental Study and Analysis of Retrofitted Flexure and Shear Dominated Circular Reinforced Concrete Bridge Columns Subjected to Shake Table Excitation," Civil Engineering Department, University of Nevada, Reno, Report No. CCEER 01-6, June 2001.

CCEER 01-7   Reppi, F., and D. Sanders, "Removal and Replacement of Cast-in-Place, Post-tensioned, Box Girder Bridge," Civil Engineering Department, University of Nevada, Reno, Report No. CCEER 01-7, December 2001.

CCEER 02-1   Pulido, C., M. Saiidi, D. Sanders, and A. Itani, "Seismic Performance and Retrofitting of Reinforced Concrete Bridge Bents," Civil Engineering Department, University of Nevada, Reno, Report No. CCEER 02-1, January 2002.

CCEER 02-2   Yang, Q., M. Saiidi, H. Wang, and A. Itani, "Influence of Ground Motion Incoherency on Earthquake Response of Multi-Support Structures," Civil Engineering Department, University of Nevada, Reno, Report No. CCEER 02-2, May 2002.

CCEER 02-3   M. Saiidi, B. Gopalakrishnan, E. Reinhardt, and R. Siddharthan, "A Preliminary Study of Shake Table Response of A Two-Column Bridge Bent on Flexible Footings," Civil Engineering Department, University of Nevada, Reno, Report No. CCEER 02-03, June 2002.

CCEER 02-4   Not Published

CCEER 02-5   Banghart, A., Sanders, D., Saiidi, M., "Evaluation of Concrete Mixes for Filling the Steel Arches in the Galena Creek Bridge," Civil Engineering Department, University of Nevada, Reno, Report No. CCEER 02-05, June 2002.

CCEER 02-6   Dusicka, P., Itani, A., Buckle, I. G., "Cyclic Behavior of Shear Links and Tower Shaft Assembly of San Francisco – Oakland Bay Bridge Tower," Civil Engineering Department, University of Nevada, Reno, Report No. CCEER 02-06, July 2002.

CCEER 02-7   Mortensen, J., and M. Saiidi, "A Performance-Based Design Method for Confinement in Circular Columns," Civil Engineering Department, University of Nevada, Reno, Report No. CCEER 02-07, November 2002.

CCEER 03-1   Wehbe, N., and M. Saiidi, "User's manual for SPMC v. 1.0 : A Computer Program for Moment-Curvature Analysis of Reinforced Concrete Sections with Interlocking Spirals," Center for Civil Engineering Earthquake Research, Department of Civil Engineering, University of Nevada, Reno, Nevada, Report No. CCEER-03-1, May, 2003.

CCEER 03-2   Wehbe, N., and M. Saiidi, "User's manual for RCMC v. 2.0 : A Computer Program for Moment-Curvature Analysis of Confined and Unconfined Reinforced Concrete Sections," Center for Civil Engineering Earthquake Research, Department of Civil Engineering, University of Nevada, Reno, Nevada, Report No. CCEER-03-2, June, 2003.

CCEER 03-3 Nada, H., D. Sanders, and M. Saiidi, "Seismic Performance of RC Bridge Frames with Architectural-Flared Columns," Civil Engineering Department, University of Nevada, Reno, Report No. CCEER 03-3, January 2003.

CCEER 03-4 Reinhardt, E., M. Saiidi, and R. Siddharthan, "Seismic Performance of a CFRP/ Concrete Bridge Bent on Flexible Footings," Civil Engineering Department, University of Nevada, Reno, Report No. CCEER 03-4, August 2003.

CCEER 03-5 Johnson, N., M. Saiidi, A. Itani, and S. Ladkany, "Seismic Retrofit of Octagonal Columns with Pedestal and One-Way Hinge at the Base," Center for Civil Engineering Earthquake Research, Department of Civil Engineering, University of Nevada, Reno, Nevada, and Report No. CCEER-03-5, August 2003.

CCEER 03-6 Mortensen, C., M. Saiidi, and S. Ladkany, "Creep and Shrinkage Losses in Highly Variable Climates," Center for Civil Engineering Earthquake Research, Department of Civil Engineering, University of Nevada, Reno, Report No. CCEER-03-6, September 2003.

CCEER 03- 7 Ayoub, C., M. Saiidi, and A. Itani, "A Study of Shape-Memory-Alloy-Reinforced Beams and Cubes," Center for Civil Engineering Earthquake Research, Department of Civil Engineering, University of Nevada, Reno, Nevada, Report No. CCEER-03-7, October 2003.

CCEER 03-8 Chandane, S., D. Sanders, and M. Saiidi, "Static and Dynamic Performance of RC Bridge Bents with Architectural-Flared Columns," Center for Civil Engineering Earthquake Research, Department of Civil Engineering, University of Nevada, Reno, Nevada, Report No. CCEER-03-8, November 2003.

CCEER 04-1 Olaegbe, C., and Saiidi, M., "Effect of Loading History on Shake Table Performance of A Two-Column Bent with Infill Wall," Center for Civil Engineering Earthquake Research, Department of Civil Engineering, University of Nevada, Reno, Nevada, Report No. CCEER-04-1, January 2004.

CCEER 04-2 Johnson, R., Maragakis, E., Saiidi, M., and DesRoches, R., "Experimental Evaluation of Seismic Performance of SMA Bridge Restrainers," Center for Civil Engineering Earthquake Research, Department of Civil Engineering, University of Nevada, Reno, Nevada, Report No. CCEER-04-2, February 2004.

CCEER 04-3 Moustafa, K., Sanders, D., and Saiidi, M., "Impact of Aspect Ratio on Two-Column Bent Seismic Performance," Center for Civil Engineering Earthquake Research, Department of Civil Engineering, University of Nevada, Reno, Nevada, Report No. CCEER-04-3, February 2004.

CCEER 04-4 Maragakis, E., Saiidi, M., Sanchez-Camargo, F., and Elfass, S., "Seismic Performance of Bridge Restrainers At In-Span Hinges," Center for Civil Engineering Earthquake Research, Department of Civil Engineering, University of Nevada, Reno, Nevada, Report No. CCEER-04-4, March 2004.

CCEER 04-5 Ashour, M., Norris, G. and Elfass, S., "Analysis of Laterally Loaded Long or Intermediate Drilled Shafts of Small or Large Diameter in Layered Soil," Center for Civil Engineering Earthquake Research, Department of Civil Engineering, University of Nevada, Reno, Nevada, Report No. CCEER-04-5, June 2004.

CCEER 04-6   Correal, J., Saiidi, M. and Sanders, D., "Seismic Performance of RC Bridge Columns Reinforced with Two Interlocking Spirals," Center for Civil Engineering Earthquake Research, Department of Civil Engineering, University of Nevada, Reno, Nevada, Report No. CCEER-04-6, August 2004.

CCEER 04-7   Dusicka, P., Itani, A. and Buckle, I., "Cyclic Response and Low Cycle Fatigue Characteristics of Plate Steels," Center for Civil Engineering Earthquake Research, Department of Civil Engineering, University of Nevada, Reno, Nevada, Report No. CCEER-04-7, November 2004.

CCEER 04-8   Dusicka, P., Itani, A. and Buckle, I., "Built-up Shear Links as Energy Dissipaters for Seismic Protection of Bridges," Center for Civil Engineering Earthquake Research, Department of Civil Engineering, University of Nevada, Reno, Nevada, Report No. CCEER-04-8, November 2004.

CCEER 04-9   Sureshkumar, K., Saiidi, S., Itani, A. and Ladkany, S., "Seismic Retrofit of Two-Column Bents with Diamond Shape Columns," Center for Civil Engineering Earthquake Research, Department of Civil Engineering, University of Nevada, Reno, Nevada, Report No. CCEER-04-9, November 2004.

CCEER 05-1   Wang, H. and Saiidi, S., "A Study of RC Columns with Shape Memory Alloy and Engineered Cementitious Composites," Center for Civil Engineering Earthquake Research, Department of Civil Engineering, University of Nevada, Reno, Nevada, Report No. CCEER-05-1, January 2005.

CCEER 05-2   Johnson, R., Saiidi, S. and Maragakis, E., "A Study of Fiber Reinforced Plastics for Seismic Bridge Restrainers," Center for Civil Engineering Earthquake Research, Department of Civil Engineering, University of Nevada, Reno, Nevada, Report No. CCEER-05-2, January 2005.

CCEER 05-3   Carden, L.P., Itani, A.M., Buckle, I.G, "Seismic Load Path in Steel Girder Bridge Superstructures," Center for Civil Engineering Earthquake Research, Department of Civil Engineering, University of Nevada, Reno, Nevada, Report No. CCEER-05-3, January 2005.

CCEER 05-4   Carden, L.P., Itani, A.M., Buckle, I.G, "Seismic Performance of Steel Girder Bridge Superstructures with Ductile End Cross Frames and Seismic Isolation," Center for Civil Engineering Earthquake Research, Department of Civil Engineering, University of Nevada, Reno, Nevada, Report No. CCEER-05-4, January 2005.

CCEER 05-5   Goodwin, E., Maragakis, M., Itani, A. and Luo, S., "Experimental Evaluation of the Seismic Performance of Hospital Piping Subassemblies," Center for Civil Engineering Earthquake Research, Department of Civil Engineering, University of Nevada, Reno, Nevada, Report No. CCEER-05-5, February 2005.

CCEER 05-6   Zadeh M. S., Saiidi, S, Itani, A. and Ladkany, S., "Seismic Vulnerability Evaluation and Retrofit Design of Las Vegas Downtown Viaduct," Center for Civil Engineering Earthquake Research, Department of Civil Engineering, University of Nevada, Reno, Nevada, Report No. CCEER-05-6, February 2005.

CCEER 05-7   Phan, V., Saiidi, S. and Anderson, J., "Near Fault (Near Field) Ground Motion Effects on Reinforced Concrete Bridge Columns," Center for Civil Engineering Earthquake Research, Department of Civil Engineering, University of Nevada, Reno, Nevada, Report No. CCEER-05-7, August 2005.

CCEER 05-8   Carden, L., Itani, A. and Laplace, P., "Performance of Steel Props at the UNR Fire Science Academy subjected to Repeated Fire," Center for Civil Engineering Earthquake Research, Department of Civil Engineering, University of Nevada, Reno, Nevada, Report No. CCEER-05-8, August 2005.

CCEER 05-9   Yamashita, R. and Sanders, D., "Shake Table Testing and an Analytical Study of Unbonded Prestressed Hollow Concrete Column Constructed with Precast Segments," Center for Civil Engineering Earthquake Research, Department of Civil Engineering, University of Nevada, Reno, Nevada, Report No. CCEER-05-9, August 2005.

CCEER 05-10   Not Published

CCEER 05-11   Carden, L., Itani., A., and Peckan, G., "Recommendations for the Design of Beams and Posts in Bridge Falsework," Center for Civil Engineering Earthquake Research, Department of Civil Engineering, University of Nevada, Reno, Nevada, Report No. CCEER-05-11, October 2005.

CCEER 06-01   Cheng, Z., Saiidi, M., and Sanders, D., "Development of a Seismic Design Method for Reinforced Concrete Two-Way Bridge Column Hinges," Center for Civil Engineering Earthquake Research, Department of Civil Engineering, University of Nevada, Reno, Nevada, Report No. CCEER-06-01, February 2006.

CCEER 06-02   Johnson, N., Saiidi, M., and Sanders, D., "Large-Scale Experimental and Analytical Studies of a Two-Span Reinforced Concrete Bridge System," Center for Civil Engineering Earthquake Research, Department of Civil Engineering, University of Nevada, Reno, Nevada, Report No. CCEER-06-02, March 2006.

CCEER 06-03   Saiidi, M., Ghasemi, H. and Tiras, A., "Seismic Design and Retrofit of Highway Bridges," Proceedings, Second US-Turkey Workshop, Center for Civil Engineering Earthquake Research, Department of Civil Engineering, University of Nevada, Reno, Nevada, Report No. CCEER-06-03, May 2006.

CCEER 07-01   O'Brien, M., Saiidi, M. and Sadrossadat-Zadeh, M., "A Study of Concrete Bridge Columns Using Innovative Materials Subjected to Cyclic Loading," Center for Civil Engineering Earthquake Research, Department of Civil Engineering, University of Nevada, Reno, Nevada, Report No. CCEER-07-01, January 2007.

CCEER 07-02   Sadrossadat-Zadeh, M. and Saiidi, M., "Effect of Strain rate on Stress-Strain Properties and Yield Propagation in Steel Reinforcing Bars," Center for Civil Engineering Earthquake Research, Department of Civil Engineering, University of Nevada, Reno, Nevada, Report No. CCEER-07-02, January 2007.

CCEER 07-03   Sadrossadat-Zadeh, M. and Saiidi, M., "Analytical Study of NEESR-SG 4-Span Bridge Model Using OpenSees," Center for Civil Engineering Earthquake Research, Department of Civil Engineering, University of Nevada, Reno, Nevada, Report No. CCEER-07-03, January 2007.

CCEER 07-04   Nelson, R., Saiidi, M. and Zadeh, S., "Experimental Evaluation of Performance of Conventional Bridge Systems," Center for Civil Engineering Earthquake Research, Department of Civil Engineering, University of Nevada, Reno, Nevada, Report No. CCEER-07-04, October 2007.

CCEER 07-05   Bahen, N. and Sanders, D., "Strut-and-Tie Modeling for Disturbed Regions in Structural Concrete Members with Emphasis on Deep Beams," Center for Civil Engineering Earthquake Research, Department of Civil Engineering, University of Nevada, Reno, Nevada, Report No. CCEER-07-05, December 2007.

CCEER 07-06   Choi, H., Saiidi, M. and Somerville, P., "Effects of Near-Fault Ground Motion and Fault-Rupture on the Seismic Response of Reinforced Concrete Bridges," Center for Civil Engineering Earthquake Research, Department of Civil Engineering, University of Nevada, Reno, Nevada, Report No. CCEER-07-06, December 2007.

CCEER 07-07   Ashour M. and Norris, G., "Report and User Manual on Strain Wedge Model Computer Program for Files and Large Diameter Shafts with LRFD Procedure," Center for Civil Engineering Earthquake Research, Department of Civil Engineering, University of Nevada, Reno, Nevada, Report No. CCEER-07-07, October 2007.

CCEER 08-01   Doyle, K. and Saiidi, M., "Seismic Response of Telescopic Pipe Pin Connections," Center for Civil Engineering Earthquake Research, Department of Civil Engineering, University of Nevada, Reno, Nevada, Report No. CCEER-08-01, February 2008.

CCEER 08-02   Taylor, M. and Sanders, D., "Seismic Time History Analysis and Instrumentation of the Galena Creek Bridge," Center for Civil Engineering Earthquake Research, Department of Civil Engineering, University of Nevada, Reno, Nevada, Report No. CCEER-08-02, April 2008.

CCEER 08-03   Abdel-Mohti, A. and Pekcan, G., "Seismic Response Assessment and Recommendations for the Design of Skewed Post-Tensioned Concrete Box-Girder Highway Bridges," Center for Civil Engineering Earthquake Research, Department of Civil and Environmental Engineering, University of Nevada, Reno, Nevada, Report No. CCEER-08-03, September 2008.

CCEER 08-04   Saiidi, M., Ghasemi, H. and Hook, J., "Long Term Bridge Performance Monitoring, Assessment & Management," Proceedings, FHWA/NSF Workshop on Future Directions," Center for Civil Engineering Earthquake Research, Department of Civil and Environmental Engineering, University of Nevada, Reno, Nevada, Report No. CCEER 08-04, September 2008.

CCEER 09-01   Brown, A., and Saiidi, M., "Investigation of Near-Fault Ground Motion Effects on Substandard Bridge Columns and Bents," Center for Civil Engineering Earthquake Research, Department of Civil and Environmental Engineering, University of Nevada, Reno, Nevada, Report No. CCEER-09-01, July 2009.

CCEER 09-02   Linke, C., Pekcan, G., and Itani, A., "Detailing of Seismically Resilient Special Truss Moment Frames," Center for Civil Engineering Earthquake Research, Department of Civil and Environmental Engineering, University of Nevada, Reno, Nevada, Report No. CCEER-09-02, August 2009.

CCEER 09-03   Hillis, D., and Saiidi, M., "Design, Construction, and Nonlinear Dynamic Analysis of Three Bridge Bents Used in a Bridge System Test," Center for Civil Engineering Earthquake Research, Department of Civil and Environmental Engineering, University of Nevada, Reno, Nevada, Report No. CCEER-09-03, August 2009.

CCEER 09-04   Bahrami, H., Itani, A., and Buckle, I., "Guidelines for the Seismic Design of Ductile End Cross Frames in Steel Girder Bridge Superstructures," Center for Civil Engineering Earthquake Research, Department of Civil and Environmental Engineering, University of Nevada, Reno, Nevada, Report No. CCEER-09-04, September 2so009.

CCEER 10-01   Zaghi, A. E., and Saiidi, M., "Seismic Design of Pipe-Pin Connections in Concrete Bridges," Center for Civil Engineering Earthquake Research, Department of Civil and Environmental Engineering, University of Nevada, Reno, Nevada, Report No. CCEER-10-01, January 2010.

CCEER 10-02   Pooranampillai, S., Elfass, S., and Norris, G., "Laboratory Study to Assess Load Capacity Increase of Drilled Shafts through Post Grouting," Center for Civil Engineering Earthquake Research, Department of Civil and Environmental Engineering, University of Nevada, Reno, Nevada, Report No. CCEER-10-02, January 2010.

CCEER 10-03   Itani, A., Grubb, M., and Monzon, E, "Proposed Seismic Provisions and Commentary for Steel Plate Girder Superstructures," Center for Civil Engineering Earthquake Research, Department of Civil and Environmental Engineering, University of Nevada, Reno, Nevada, Report No. CCEER-10-03, June 2010.

CCEER 10-04   Cruz-Noguez, C., Saiidi, M., "Experimental and Analytical Seismic Studies of a Four-Span Bridge System with Innovative Materials," Center for Civil Engineering Earthquake Research, Department of Civil and Environmental Engineering, University of Nevada, Reno, Nevada, Report No. CCEER-10-04, September 2010.

CCEER 10-05   Vosooghi, A., Saiidi, M., "Post-Earthquake Evaluation and Emergency Repair of Damaged RC Bridge Columns Using CFRP Materials," Center for Civil Engineering Earthquake Research, Department of Civil and Environmental Engineering, University of Nevada, Reno, Nevada, Report No. CCEER-10-05, September 2010.

CCEER 10-06   Ayoub, M., Sanders, D., "Testing of Pile Extension Connections to Slab Bridges," Center for Civil Engineering Earthquake Research, Department of Civil and Environmental Engineering, University of Nevada, Reno, Nevada, Report No. CCEER-10-06, October 2010.

CCEER 10-07   Builes-Mejia, J. C. and Itani, A., "Stability of Bridge Column Rebar Cages during Construction," Center for Civil Engineering Earthquake Research, Department of Civil and Environmental Engineering, University of Nevada, Reno, Nevada, Report No. CCEER-10-07, November 2010.

CCEER 10-08   Monzon, E.V., "Seismic Performance of Steel Plate Girder Bridges with Integral Abutments," Center for Civil Engineering Earthquake Research, Department of Civil and Environmental Engineering, University of Nevada, Reno, Nevada, Report No. CCEER-10-08, November 2010.

CCEER 11-01   Motaref, S., Saiidi, M., and Sanders, D., "Seismic Response of Precast Bridge Columns with Energy Dissipating Joints," Center for Civil Engineering Earthquake Research, Department of Civil and Environmental Engineering, University of Nevada, Reno, Nevada, Report No. CCEER-11-01, May 2011.

CCEER 11-02   Harrison, N. and Sanders, D., "Preliminary Seismic Analysis and Design of Reinforced Concrete Bridge Columns for Curved Bridge Experiments," Center for Civil Engineering Earthquake Research, Department of Civil and Environmental Engineering, University of Nevada, Reno, Nevada, Report No. CCEER-11-02, May 2011.

CCEER 11-03   Vallejera, J. and Sanders, D., "Instrumentation and Monitoring the Galena Creek Bridge," Center for Civil Engineering Earthquake Research, Department of Civil and Environmental Engineering, University of Nevada, Reno, Nevada, Report No. CCEER-11-03, September 2011.

CCEER 11-04   Levi, M., Sanders, D., and Buckle, I., "Seismic Response of Columns in Horizontally Curved Bridges," Center for Civil Engineering Earthquake Research, Department of Civil and Environmental Engineering, University of Nevada, Reno, Nevada, Report No. CCEER-11-04, December 2011.

CCEER 12-01   Saiidi, M., "NSF International Workshop on Bridges of the Future – Wide Spread Implementation of Innovation," Center for Civil Engineering Earthquake Research, Department of Civil and Environmental Engineering, University of Nevada, Reno, Nevada, Report No. CCEER-12-01, January 2012.

CCEER 12-02   Larkin, A.S., Sanders, D., and Saiidi, M., "Unbonded Prestressed Columns for Earthquake Resistance," Center for Civil Engineering Earthquake Research, Department of Civil and Environmental Engineering, University of Nevada, Reno, Nevada, Report No. CCEER-12-02, January 2012.

CCEER 12-03   Arias-Acosta, J. G., Sanders, D., "Seismic Performance of Circular and Interlocking Spirals RC Bridge Columns under Bidirectional Shake Table Loading Part 1," Center for Civil Engineering Earthquake Research, Department of Civil and Environmental Engineering, University of Nevada, Reno, Nevada, Report No. CCEER-12-03, September 2012.

CCEER 12-04   Cukrov, M.E., Sanders, D., "Seismic Performance of Prestressed Pile-To-Bent Cap Connections," Center for Civil Engineering Earthquake Research, Department of Civil and Environmental Engineering, University of Nevada, Reno, Nevada, Report No. CCEER-12-04, September 2012.

CCEER 13-01   Carr, T. and Sanders, D., "Instrumentation and Dynamic Characterization of the Galena Creek Bridge," Center for Civil Engineering Earthquake Research, Department of Civil and Environmental Engineering, University of Nevada, Reno, Nevada, Report No. CCEER-13-01, January 2013.

CCEER 13-02   Vosooghi, A. and Buckle, I., "Evaluation of the Performance of a Conventional Four-Span Bridge During Shake Table Tests," Center for Civil Engineering Earthquake Research, Department of Civil and Environmental Engineering, University of Nevada, Reno, Nevada, Report No. CCEER-13-02, January 2013.

CCEER 13-03   Amirihormozaki, E. and Pekcan, G., "Analytical Fragility Curves for Horizontally Curved Steel Girder Highway Bridges," Center for Civil Engineering Earthquake Research, Department of Civil and Environmental Engineering, University of Nevada, Reno, Nevada, Report No. CCEER-13-03, February 2013.

CCEER 13-04   Almer, K. and Sanders, D., "Longitudinal Seismic Performance of Precast Bridge Girders Integrally Connected to a Cast-in-Place Bentcap," Center for Civil Engineering Earthquake Research, Department of Civil and Environmental Engineering, University of Nevada, Reno, Nevada, Report No. CCEER-13-04, April 2013.

CCEER 13-05   Monzon, E.V., Itani, A.I., and Buckle, I.G., "Seismic Modeling and Analysis of Curved Steel Plate Girder Bridges," Center for Civil Engineering Earthquake Research, Department of Civil and Environmental Engineering, University of Nevada, Reno, Nevada, Report No. CCEER-13-05, April 2013.

CCEER 13-06   Monzon, E.V., Buckle, I.G., and Itani, A.I., "Seismic Performance of Curved Steel Plate Girder Bridges with Seismic Isolation," Center for Civil Engineering Earthquake Research, Department of Civil and Environmental Engineering, University of Nevada, Reno, Nevada, Report No. CCEER-13-06, April 2013.

CCEER 13-07   Monzon, E.V., Buckle, I.G., and Itani, A.I., "Seismic Response of Isolated Bridge Superstructure to Incoherent Ground Motions," Center for Civil Engineering Earthquake Research, Department of Civil and Environmental Engineering, University of Nevada, Reno, Nevada, Report No. CCEER-13-07, April 2013.

CCEER 13-08   Haber, Z.B., Saiidi, M.S., and Sanders, D.H., "Precast Column-Footing Connections for Accelerated Bridge Construction in Seismic Zones," Center for Civil Engineering Earthquake Research, Department of Civil and Environmental Engineering, University of Nevada, Reno, Nevada, Report No. CCEER-13-08, April 2013.

CCEER 13-09   Ryan, K.L., Coria, C.B., and Dao, N.D., "Large Scale Earthquake Simulation of a Hybrid Lead Rubber Isolation System Designed under Nuclear Seismicity Considerations," Center for Civil Engineering Earthquake Research, Department of Civil and Environmental Engineering, University of Nevada, Reno, Nevada, Report No. CCEER-13-09, April 2013.

CCEER 13-10   Wibowo, H., Sanford, D.M., Buckle, I.G., and Sanders, D.H., "The Effect of Live Load on the Seismic Response of Bridges," Center for Civil Engineering Earthquake Research, Department of Civil and Environmental Engineering, University of Nevada, Reno, Nevada, Report No. CCEER-13-10, May 2013.

CCEER 13-11   Sanford, D.M., Wibowo, H., Buckle, I.G., and Sanders, D.H., "Preliminary Experimental Study on the Effect of Live Load on the Seismic Response of Highway Bridges," Center for Civil Engineering Earthquake Research, Department of Civil and Environmental Engineering, University of Nevada, Reno, Nevada, Report No. CCEER-13-11, May 2013.

CCEER 13-12   Saad, A.S., Sanders, D.H., and Buckle, I.G., "Assessment of Foundation Rocking Behavior in Reducing the Seismic Demand on Horizontally Curved Bridges," Center for Civil Engineering Earthquake Research, Department of Civil and Environmental Engineering, University of Nevada, Reno, Nevada, Report No. CCEER-13-12, June 2013.

CCEER 13-13   Ardakani, S.M.S. and Saiidi, M.S., "Design of Reinforced Concrete Bridge Columns for Near-Fault Earthquakes," Center for Civil Engineering Earthquake Research, Department of Civil and Environmental Engineering, University of Nevada, Reno, Nevada, Report No. CCEER-13-13, July 2013.

CCEER 13-14   Wei, C. and Buckle, I., "Seismic Analysis and Response of Highway Bridges with Hybrid Isolation," Center for Civil Engineering Earthquake Research, Department of Civil and Environmental Engineering, University of Nevada, Reno, Nevada, Report No. CCEER-13-14, August 2013.

CCEER 13-15   Wibowo, H., Buckle, I.G., and Sanders, D.H., "Experimental and Analytical Investigations on the Effects of Live Load on the Seismic Performance of a Highway Bridge," Center for Civil Engineering Earthquake Research, Department of Civil and Environmental Engineering, University of Nevada, Reno, Nevada, Report No. CCEER-13-15, August 2013.

CCEER 13-16   Itani, A.M., Monzon, E.V., Grubb, M., and Amirihormozaki, E. "Seismic Design and Nonlinear Evaluation of Steel I-Girder Bridges with Ductile End Cross-Frames," Center for Civil Engineering Earthquake Research, Department of Civil and Environmental Engineering, University of Nevada, Reno, Nevada, Report No. CCEER-13-16, September 2013.

CCEER 13-17   Kavianipour, F. and Saiidi, M.S., "Experimental and Analytical Seismic Studies of a Four-span Bridge System with Composite Piers," Center for Civil Engineering Earthquake Research, Department of Civil and Environmental Engineering, University of Nevada, Reno, Nevada, Report No. CCEER-13-17, September 2013.

CCEER 13-18   Mohebbi, A., Ryan, K., and Sanders, D., "Seismic Response of a Highway Bridge with Structural Fuses for Seismic Protection of Piers," Center for Civil Engineering Earthquake Research, Department of Civil and Environmental Engineering, University of Nevada, Reno, Nevada, Report No. CCEER-13-18, December 2013.

CCEER 13-19   Guzman Pujols, Jean C., Ryan, K.L., "Development of Generalized Fragility Functions for Seismic Induced Content Disruption," Center for Civil Engineering Earthquake Research, Department of Civil and Environmental Engineering, University of Nevada, Reno, Nevada, Report No. CCEER-13-19, December 2013.

CCEER 14-01   Salem, M. M. A., Pekcan, G., and Itani, A., "Seismic Response Control Of Structures Using Semi-Active and Passive Variable Stiffness Devices," Center for Civil Engineering Earthquake Research, Department of Civil and Environmental Engineering, University of Nevada, Reno, Nevada, Report No. CCEER-14-01, May 2014.

CCEER 14-02   Saini, A. and Saiidi, M., "Performance-Based Probabilistic Damage Control Approach for Seismic Design of Bridge Columns," Center For Civil Engineering Earthquake Research, Department Of Civil and Environmental Engineering, University of Nevada, Reno, Nevada, Report No. CCEER-14-02, May 2014.

CCEER 14-03   Saini, A. and Saiidi, M., "Post Earthquake Damage Repair of Various Reinforced Concrete Bridge Components," Center For Civil Engineering Earthquake Research, Department Of Civil and Environmental Engineering, University of Nevada, Reno, Nevada, Report No. CCEER-14-03, May 2014.

CCEER 14-04   Monzon, E.V., Itani, A.M., and Grubb, M.A., "Nonlinear Evaluation of the Proposed Seismic Design Procedure for Steel Bridges with Ductile End Cross Frames," Center For Civil Engineering Earthquake Research, Department Of Civil and Environmental Engineering, University of Nevada, Reno, Nevada, Report No. CCEER-14-04, July 2014.

CCEER 14-05   Nakashoji, B. and Saiidi, M.S., "Seismic Performance of Square Nickel-Titanium Reinforced ECC Columns with Headed Couplers," Center For Civil Engineering Earthquake Research, Department Of Civil and Environmental Engineering, University of Nevada, Reno, Nevada, Report No. CCEER-14-05, July 2014.

CCEER 14-06   Tazarv, M. and Saiidi, M.S., "Next Generation of Bridge Columns for Accelerated Bridge Construction in High Seismic Zones," Center For Civil Engineering Earthquake Research, Department Of Civil and Environmental Engineering, University of Nevada, Reno, Nevada, Report No. CCEER-14-06, August 2014.

CCEER 14-07   Mehrsoroush, A. and Saiidi, M.S., "Experimental and Analytical Seismic Studies of Bridge Piers with Innovative Pipe Pin Column-Footing Connections and Precast Cap Beams," Center For Civil Engineering Earthquake Research, Department Of Civil and Environmental Engineering, University of Nevada, Reno, Nevada, Report No. CCEER-14-07, December 2014.

CCEER 15-01   Dao, N.D. and Ryan, K.L., "Seismic Response of a Full-scale 5-story Steel Frame Building Isolated by Triple Pendulum Bearings under 3D Excitations," Center For Civil Engineering Earthquake Research, Department Of Civil and Environmental Engineering, University of Nevada, Reno, Nevada, Report No. CCEER-15-01, January 2015.

CCEER 15-02   Allen, B.M. and Sanders, D.H., "Post-Tensioning Duct Air Pressure Testing Effects on Web Cracking," Center For Civil Engineering Earthquake Research, Department Of Civil and Environmental Engineering, University of Nevada, Reno, Nevada, Report No. CCEER-15-02, January 2015.

CCEER 15-03   Akl, A. and Saiidi, M.S., "Time-Dependent Deflection of In-Span Hinges in Prestressed Concrete Box Girder Bridges," Center For Civil Engineering Earthquake Research, Department Of Civil and Environmental Engineering, University of Nevada, Reno, Nevada, Report No. CCEER-15-03, May 2015.

CCEER 15-04   Zargar Shotorbani, H. and Ryan, K., "Analytical and Experimental Study of Gap Damper System to Limit Seismic Isolator Displacements in Extreme Earthquakes," Center For Civil Engineering Earthquake Research, Department Of Civil and Environmental Engineering, University of Nevada, Reno, Nevada, Report No. CCEER-15-04, June 2015.

CCEER 15-05   Wieser, J., Maragakis, E.M., and Buckle, I., "Experimental and Analytical Investigation of Seismic Bridge-Abutment Interaction in a Curved Highway Bridge," Center For Civil Engineering Earthquake Research, Department Of Civil and Environmental Engineering, University of Nevada, Reno, Nevada, Report No. CCEER-15-05, July 2015.

CCEER 15-06   Tazarv, M. and Saiidi, M.S., "Design and Construction of Precast Bent Caps with Pocket Connections for High Seismic Regions," Center For Civil Engineering Earthquake Research, Department Of Civil and Environmental Engineering, University of Nevada, Reno, Nevada, Report No. CCEER-15-06, August 2015.

CCEER 15-07   Tazarv, M. and Saiidi, M.S., "Design and Construction of Bridge Columns Incorporating Mechanical Bar Splices in Plastic Hinge Zones," Center For Civil Engineering Earthquake Research, Department Of Civil and Environmental Engineering, University of Nevada, Reno, Nevada, Report No. CCEER-15-07, August 2015.

CCEER 15-08   Sarraf Shirazi, R., Pekcan, G., and Itani, A.M., "Seismic Response and Analytical Fragility Functions for Curved Concrete Box-Girder Bridges," Center For Civil Engineering Earthquake Research, Department Of Civil and Environmental Engineering, University of Nevada, Reno, Nevada, Report No. CCEER-15-08, December 2015.

CCEER 15-09   Coria, C.B., Ryan, K.L., and Dao, N.D., "Response of Lead Rubber Bearings in a Hybrid Isolation System During a Large Scale Shaking Experiment of an Isolated Building," Center For Civil Engineering Earthquake Research, Department Of Civil and Environmental Engineering, University of Nevada, Reno, Nevada, Report No. CCEER-15-09, December 2015.

CCEER 16-01   Mehraein, M and Saiidi, M.S., "Seismic Performance of Bridge Column-Pile-Shaft Pin Connections for Application in Accelerated Bridge Construction," Center For Civil Engineering Earthquake Research, Department Of Civil and Environmental Engineering, University of Nevada, Reno, Nevada, Report No. CCEER-16-01, May 2016.

CCEER 16-02   Varela Fontecha, S. and Saiidi, M.S., "Resilient Earthquake-Resistant Bridges Designed For Disassembly," Center For Civil Engineering Earthquake Research, Department Of Civil and Environmental Engineering, University of Nevada, Reno, Nevada, Report No. CCEER-16-02, May 2016.

CCEER 16-03   Mantawy, I. M, and Sanders, D. H., "Assessment of an Earthquake Resilient Bridge with Pretensioned, Rocking Columns," Center For Civil Engineering Earthquake Research, Department Of Civil and Environmental Engineering, University of Nevada, Reno, Nevada, Report No. CCEER-16-03, May 2016.

CCEER 16-04   Mohammed, M, Biasi, G., and Sanders, D., "Post-earthquake Assessment of Nevada Bridges using ShakeMap/ShakeCast," Center For Civil Engineering Earthquake Research, Department Of Civil and Environmental Engineering, University of Nevada, Reno, Nevada, Report No. CCEER-16-04, May 2016.

CCEER 16-05   Jones, J, Ryan, K., and Saiidi, M, "Toward Successful Implementation of Prefabricated Deck Panels to Accelerate the Bridge Construction Process," Center For Civil Engineering Earthquake Research, Department Of Civil and Environmental Engineering, University of Nevada, Reno, Nevada, Report No. CCEER-16-05, August 2016.

CCEER 16-06   Mehrsoroush, A. and Saiidi, M., "Probabilistic Seismic Damage Assessment for Sub-standard Bridge Columns," Center For Civil Engineering Earthquake Research, Department Of Civil and Environmental Engineering, University of Nevada, Reno, Nevada, Report No. CCEER-16-06, November 2016.

CCEER 16-07   Nielsen, T., Maree, A., and Sanders, D., "Experimental Investigation into the Long-Term Seismic Performance of Dry Storage Casks," Center For Civil Engineering Earthquake Research, Department Of Civil and Environmental Engineering, University of Nevada, Reno, Nevada, Report No. CCEER-16-07, December 2016.

CCEER 16-08   Wu, S., Buckle, I., and Itani, A., "Effect of Skew on Seismic Performance of Bridges with Seat-Type Abutments," Center For Civil Engineering Earthquake Research, Department Of Civil and Environmental Engineering, University of Nevada, Reno, Nevada, Report No. CCEER-16-08, December 2016.

CCEER 16-09   Mohammed, M., and Sanders, D., "Effect of Earthquake Duration on Reinforced Concrete Bridge Columns," Center For Civil Engineering Earthquake Research, Department Of Civil and Environmental Engineering, University of Nevada, Reno, Nevada, Report No. CCEER-16-09, December 2016.

CCEER 16-10   Guzman Pujols, J., and Ryan, K., "Slab Vibration and Horizontal-Vertical Coupling in the Seismic Response of Irregular Base-Isolated and Conventional Buildings," Center For Civil Engineering Earthquake Research, Department Of Civil and Environmental Engineering, University of Nevada, Reno, Nevada, Report No. CCEER-16-10, December 2016.

CCEER 17-01   White, L., Ryan, K., and Buckle, I., "Thermal Gradients in Southwestern United States and the Effect on Bridge Bearing Loads," Center For Civil Engineering Earthquake Research, Department Of Civil and Environmental Engineering, University of Nevada, Reno, Nevada, Report No. CCEER-17-01, May 2017.

CCEER 17-02   Mohebbi, A., Saiidi, M., and Itani, A., "Development and Seismic Evaluation of Pier Systems w/Pocket Connections, CFRP Tendons, and ECC/UHPC Columns," Center For Civil Engineering Earthquake Research, Department Of Civil and Environmental Engineering, University of Nevada, Reno, Nevada, Report No. CCEER-17-02, May 2017.

CCEER 17-03   Mehrsoroush, A., Saiidi, M., and Ryan, K., "Development of Earthquake-resistant Precast Pier Systems for Accelerated Bridge Construction in Nevada," Center For Civil Engineering Earthquake Research, Department Of Civil and Environmental Engineering, University of Nevada, Reno, Nevada, Report No. CCEER-17-03, June 2017.

CCEER 17-04   Abdollahi, B., Saiidi, M., Siddharthan, R., and Elfass, S., "Shake Table Studies on Soil-Abutment-Structure Interaction in Skewed Bridges," Center For Civil Engineering Earthquake Research, Department Of Civil and Environmental Engineering, University of Nevada, Reno, Nevada, Report No. CCEER-17-04, July 2017.

CCEER 17-05   Shrestha, G., Itani, A., and Saiidi, M., "Seismic Performance of Precast Full-Depth Decks in Accelerated Bridge Construction," Center for Civil Engineering Earthquake Research, Department of Civil and Environmental Engineering, University of Nevada, Reno, Nevada, Report No. CCEER-17-05, September 2017.

CCEER 17-06   Wu, S., Buckle, I., and Ryan, K., "Large-Scale Experimental Verification of an Optically-Based Sensor System for Monitoring Structural Response," Center for Civil Engineering Earthquake Research, Department of Civil and Environmental Engineering, University of Nevada, Reno, Nevada, Report No. CCEER-17-06, October 2017.

CCEER 17-07   Nada, H., and Sanders, D., "Analytical Investigation into Bridge Column Innovations for Mitigating Earthquake Damage," Center For Civil Engineering Earthquake Research, Department Of Civil and Environmental Engineering, University of Nevada, Reno, Nevada, Report No. CCEER-17-07, October 2017.

CCEER 18-01   Maree, A. F., and Sanders, D., "Performance and Design of Anchorage Zones for Post-Tensioned Box Girder Bridges," Center for Civil Engineering Earthquake Research, Department of Civil and Environmental Engineering, University of Nevada, Reno, Nevada, Report No. CCEER-18-01, January 2018.

CCEER 18-02   Mostafa, K., and Sanders, D., "Improving the Long-Term Performance of Bridge Decks using Deck and Crack Sealers," Center for Civil Engineering Earthquake Research, Department of Civil and Environmental Engineering, University of Nevada, Reno, Nevada, Report No. CCEER-18-02, March 2018.

CCEER 18-03   Blount, S., Ryan, K., Henry, R., Lu, Y., and Elwood, K., "Evaluation of lower damage concepts for enhanced repairability of reinforced concrete walls," Center for Civil Engineering Earthquake Research, Department of Civil and Environmental Engineering, University of Nevada, Reno, Nevada, Report No. CCEER-18-03, June 2018.

CCEER 18-04   Mohebbi, A., Jordan, E., and Saiidi, M., "Exploratory Experimental Studies of Spliced Cam Shape Memory Alloy Bars for Seismic Application," Center for Civil Engineering Earthquake Research, Department Of Civil and Environmental Engineering, University of Nevada, Reno, Nevada, Report No. CCEER-18-04, September 2018.

CCEER 19-01   Saint Pierre, E., Elfass, S., Watters, R., Norris, G., and Ashour, M. "Improving Strain Wedge Model Capabilities in Analyzing Laterally Loaded Drilled Shafts in Cemented Soils," Center for Civil Engineering Earthquake Research, Department of Civil and Environmental Engineering, University of Nevada, Reno, Nevada, Report No. CCEER-19-01, March 2019.

CCEER 19-02   Benjumea, J., Saiidi, M., and Itani, A., "Experimental and Analytical Seismic Studies of a Two-Span Bridge System with Precast Concrete Elements and ABC Connections," Center for Civil Engineering Earthquake Research, Department of Civil and Environmental Engineering, University of Nevada, Reno, Nevada, Report No. CCEER-19-02, May 2019.

CCEER 19-03   Subedi, D., Moustafa, M., and Saiidi, M., "Non-Proprietary UHPC for Anchorage of Large Diameter Column Bars in Grouted Ducts," Center for Civil Engineering Earthquake Research, Department of Civil and Environmental Engineering, University of Nevada, Reno, Nevada, Report No. CCEER-19-03, May 2019.

CCEER 19-04   Shoushtari, E, D., Saiidi, M., Itani, A., and Moustafa, M., "Shake Table Studies of a Steel Girder Bridge System with ABC Connections," Center for Civil Engineering Earthquake Research, Department of Civil and Environmental Engineering, University of Nevada, Reno, Nevada, Report No. CCEER-19-04, June 2019.

CCEER 19-05   Wu, S., Miah, M., and McCallen, D., "Four Canonical Steel Moment Frame Buildings and Inter-Code Comparisons of Nonlinear Building Response," Center for Civil Engineering Earthquake Research, Department of Civil and Environmental Engineering, University of Nevada, Reno, Nevada, Report No. CCEER-19-05, September 2019.

CCEER 20-01   Schwartz, T., Saiidi, M., and Moustafa, M., "Simplifying Cast-in-Place Joint Design Using ABC Pocket Connection Details in High Seismic Regions," Center for Civil Engineering Earthquake Research, Department of Civil and Environmental Engineering, University of Nevada, Reno, Nevada, Report No. CCEER-20-01, January 2020.

Nevada Department of Transportation
Kristina L. Swallow, P.E. Director
Ken Chambers, Research Division Chief
(775) 888-7220
kchambers@dot.nv.gov
1263 South Stewart Street
Carson City, Nevada 89712